

**KERNFORSCHUNGSZENTRUM
KARLSRUHE**

August 1973

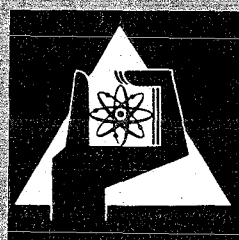
KFK-1632
EACRP-U-46

Institut für Neutronenphysik und Reaktortechnik
Institut für Angewandte Systemtechnik und Reaktorphysik
INTERATOM
Belgonucléaire

**Progress in Fast Reactor Physics in the
Federal Republic of Germany**

compiled by

H. Küsters



**GESELLSCHAFT
FÜR
KERNFORSCHUNG M.B.H.**

KARLSRUHE

Als Manuskript vervielfältigt

Für diesen Bericht behalten wir uns alle Rechte vor

**GESELLSCHAFT FÜR KERNFORSCHUNG M. B. H.
KARLSRUHE**

KERNFORSCHUNGSZENTRUM KARLSRUHE

KFK-1632

EACRP-U-46

Institut für Neutronenphysik und Reaktortechnik
Institut für Angewandte Systemtechnik und Reaktorphysik
INTERATOM
Belgonucléaire

Progress in Fast Reactor Physics in the

Federal Republic of Germany

compiled

by

H. Küsters

with contributions

from

H.J. Bluhm, R. Böhme, H. Bogensberger, H. Borgwaldt, G. Buckel,
H. Doerfel, G. Durance, E. Eisemann, P. Fehsenfeld, G. Fieg,
E.A. Fischer, R. Fröhlich, W. Gebhardt, B. Goel, P.E. McGrath,
C. Günther, F. Helm, H. Henssen, W. Höbel, H. Huschke, G. Jacobs,
F. Kappler, E. Kiefhaber, H. Küsters, J. Lieberoth, D. Luigs, L. Mayer,
W.J. Oosterkamp, R. Papp, N. Pieroni, S. Pilate, M. Pinter, D. Rusch,
B. Schatz, W. Scholtyssek, B. Stehle, D. Struwe, W. Terney,
E. Wattecamps, U. Wehmann, H. Werle, D. Wintzer.

Gesellschaft für Kernforschung m.b.H., Karlsruhe

Juli 1973

KFK 1632

Progress in Fast Reactor Physics in the
Federal Republic of Germany

compiled

by

H. Küsters

Summary

This report summarizes the progress in fast reactor physics in the Federal Republik of Germany during the years 1969 to 1972/73. It comprises mainly the work done in the Nuclear Research Center of Karlsruhe, which was partly supplemented by investigations at INTERATOM, Bensberg and BELGONUCLEAIRE, Brussels.

The document contains:

- Assessment of target accuracies in the prediction of physical quantities of fast prototype power reactors.
- Status of experimental and calculational techniques in fast reactor physics in 1969.
- Improvements in theoretical fast reactor physics
- Improvements in experimental fast reactor physics
- Check of improved methods in integral experiments.
- Results obtained in zero power facilities and their extrapolation for use in fast power reactors.
- Status of the prediction of physics quantities in 1972/73 and general conclusions.

Zusammenfassung

Dieser Bericht faßt die in der Bundesrepublik Deutschland erzielten Fortschritte der Physik Schneller Reaktoren von 1969 bis 1972/73 zusammen. Er enthält hauptsächlich Arbeiten aus dem Kernforschungszentrum Karlsruhe, die teilweise durch Untersuchungen bei INTERATOM, Bensberg und BELGONUCLEAIRE, Brüssel ergänzt wurden.

Im einzelnen werden folgende Punkte detailliert dargestellt:

- Aufstellen der Zielgenauigkeiten für die Vorhersage physikalischer Kenngrößen von schnellen Prototypreaktoren.
- Stand der experimentellen und theoretischen Verfahren der Physik Schneller Reaktoren im Jahre 1969.
- Verbesserungen der Berechnung Schneller Reaktoren.
- Verbesserungen der experimentellen Methoden zur Untersuchung Schneller Reaktoren.
- Überprüfung der verbesserten Verfahren in integralen Nullenergie-Experimenten.
- Extrapolation der Ergebnisse auf die Vorhersagegenauigkeit von physikalischen Kenngrößen in Leistungsreaktoren.
- Stand der Vorhersagegenauigkeit 1972/73 und Schlußfolgerungen.

LIST OF CONTENTS

	Page
Introduction	II-13
1. ASSESSMENT OF TARGET ACCURACIES IN THE PREDICTION OF PHYSICAL QUANTITIES OF FAST PROTOTYPE POWER REACTORS	1.1-1.14
1.1 Criticality and plutonium inventory	1.3
1.2 Power distribution	1.6
1.3 Breeding ratio	1.8
1.4 Control rod worth	1.9
1.5 Reactivity effects	1.10
1.6 Theoretical Models, necessary for a reliable prediction of physics quantities of fast prototype reactors	1.11
1.7 Summary of target accuracies for physics quantities of a fast prototype reactor	1.13
References for chapter 1	1.14
2. STATUS OF EXPERIMENTAL AND CALCULATIONAL TECHNIQUES IN FAST REACTOR PHYSICS IN 1969	2.1-2.6
2.1 Experimental fast reactor physics in 1969	2.2
2.2 Theoretical fast reactor physics in 1969	2.3
2.3 Prediction of fast reactor quantities in 1969	2.5
References for chapter 2	2.6

	Page
3. IMPROVEMENTS IN THEORETICAL FAST REACTOR PHYSICS	3.1-3.86
3.1 Evaluation and processing of nuclear cross sections	3.2
3.1.1 The nuclear data file KEDAK	3.3
3.1.2 Procedures for the calculation of group constants	3.5
3.1.3 Group constant libraries and codes	3.6
3.1.4 The MOXTOT- and KFKINR-Sets	3.7
Fig. 3.1 - 3.3	3.11-3.13
3.2 Development of diffusion and transport theory methods	3.14
3.2.1 Diffusion codes	3.14
3.2.2 Transport codes	3.18
3.2.3 Monte Carlo techniques	3.20
3.3 Theoretical foundation, code development and application of flux synthesis methods	3.25
3.3.1 Problem definition and introduction of general flux synthesis methods for the diffusion theory model	3.26
3.3.2 State of the art for various flux synthesis methods in different physics situations	3.27
3.3.3 Development of the computer program KASY	3.31
3.3.4 Comparison of the results of the flux synthesis method with those obtained by iterated solution methods of fine mesh difference equations	3.34
3.3.5 Half-range expansion for approximately solving the neutron transport equation for slabs	3.38
Fig. 3.4 - 3.6	3.42-3.44
3.4 Development of codes for the treatment of special physical problems in fast reactors	3.45
3.4.1 KAPER, A computer program for the analysis of experiments performed in heterogeneous critical facilities	3.45

	Page
3.4.2 The use of a probability table method in calculating reaction rates	3.50
3.4.3 Many group perturbation calculations for the determination of reactivity coefficients	3.52
3.4.4 Resonance phenomena near interfaces and boundaries	3.55
3.4.5 Calculation of neutron streaming effects in gas cooled fast reactors	3.56
3.4.6 Improvement in the theoretical treatment of the Doppler effect	3.60
Fig. 3.7 - 3.9	3.61-3.63
3.5 Burnup code developments for fast reactors	3.64
3.6 Development of kinetics and safety analysis codes	3.67
3.6.1 The improved synthesis code RADYVAR 2 and its feedback parts	3.68
3.6.2 The quasi-static approach KINTIC	3.70
3.6.3 Investigation on group collapsing schemes and energy synthesis	3.71
3.7 The development of modern modular code systems	3.74
3.7.1 The Karlsruhe program system KAPROS	3.74
3.7.2 The INTERATOM modular code system IANUS	3.78
Fig. 3.10	3.82
References for chapter 3	3.83
4. IMPROVEMENTS IN EXPERIMENTAL FAST REACTOR PHYSICS	4.1-4.41
4.1 Reaction rate measurements	4.3
4.1.1 Measurement of fission and capture rates by activation techniques	4.4

	Page
4.1.2 Calibration of fission rate measurements	4.8
4.1.3 Fission track recording	4.10
4.1.4 Fission rate mapping by the whole platelet method	4.13
4.1.5 Measurement of the γ heating with RPL-glasses	4.16
4.1.6 Activities to improve the reliability and accuracy of reaction rate measurements	4.17
Fig. 4.1 - 4.8	4.19-4.26
4.2 Spectrum measurements	4.27
4.2.1 Proton recoil proportional counters	4.27
4.2.2 ³ He-Semiconductor-sandwich-spectrometer	4.28
4.2.3 Time-of-flight spectroscopy	4.30
4.2.4 Intercomparison of techniques and accuracy of spectrum measurement	4.33
Fig. 4.9 - 4.11	4.36-4.38
References for chapter 4	4.39
5. CHECK OF IMPROVED METHODS IN INTEGRAL EXPERIMENTS	5.1-5.98
5.1 Criticality and reaction rate ratios	5.2
5.2 Evaluation of power density measurements in SNEAK 2 and 6	5.5
5.2.1 Measurements performed	5.5
5.2.2 Methods of calculation	5.6
5.2.3 Evaluation of fission ratios	5.7
5.2.4 Evaluation of power traverses in the clean core	5.8
5.2.5 Influence of control rods	5.9
5.2.6 Power distributions in the blanket	5.10
Fig. 5.1 - 5.8	5.12-5.19
5.3 Analysis of buckling measurements	5.20

	Page
5.4 Analysis of central material worth measurements	5.23
5.4.1 The problem of the reactivity scale	5.23
5.4.2 Heterogeneity effects in the reactivity worth determination	5.26
5.4.3 Present status of the interpretation of material worth measurements	5.26
5.5. Prediction of control rod worth	5.28
5.5.1 Methods and data used for the interpretation of the experiments	5.28
5.5.2 Interpretation of experiments	5.30
Fig. 5.9 - 5.11	5.36-5.38
5.6 Analysis of Doppler experiments in SNEAK and SEFOR	5.39
5.6.1 SEFOR experiments and check of nuclear data	5.39
5.6.2 The Doppler experiment in SNEAK-9B	5.42
5.6.3 Comparison of the SEFOR and SNEAK results	5.42
5.6.4 SEFOR transient power excursions and comparison with experiment	5.43
Fig. 5.12 - 5.13	5.44-5.46
5.7 Measurements and calculations of sodium void coefficients	5.47
5.7.1 Survey of the measurements	5.48
5.7.2 Calculational methods and cross section sets	5.49
5.7.3 Evaluation of axial traverses	5.52
5.7.4 Measurements with different orientation of the platelets	5.52
5.7.5 Evaluation of radial traverses	5.54
5.7.6 Central voids of increasing radius	5.55
5.7.7 The Na-void effect in test zones with high ^{240}Pu contents and with B_4C poisoning	5.57
5.7.8 The cavity experiment in SNEAK-6A	5.59
Fig. 5.14 - 5.18	5.62-5.66

	Page
5.8. Information from supporting spectrum measurements	5.67
5.8.1 Measurements in a depleted uranium system	5.68
5.8.2 The small natural uranium system "UNAT"	5.71
5.8.3 Applications of the adjusted ^{238}U cross section sets	5.73
5.8.4 Spectrum investigations in the fast thermal facility STARK	5.77
Fig. 5.19 - 5.26	5.80-5.87
5.9. Measurements of prompt fission neutron spectra	5.88
Fig. 5.27	5.90
5.10 Measurement of delayed fission neutron spectra	5.91
Fig. 5.28 - 5.29	5.93-5.94
5.11 Typical deviations for predicted physics parameters in integral experiments, status 1972	5.95
References for chapter 5	5.96
6. RESULTS OBTAINED IN ZERO POWER FACILITIES AND THEIR EXTRAPOLATION FOR USE IN FAST POWER REACTORS	6.1-6.14
6.1 Criticality	6.5
6.2 Reactivity worth of absorber rods	6.9
6.3 Power distribution	6.11
6.4 Breeding ratio	6.12
6.5 Power and energy coefficients	6.13
6.6 Sodium void reactivity	6.13
7. GENERAL CONCLUSIONS	7.1-7.4

PROGRESS IN FAST REACTOR PHYSICS IN THE FEDERAL REPUBLIC
OF GERMANY

INTRODUCTION

In the framework of the German Fast Reactor Project a large effort was spent since 1960 to develop experimental and theoretical methods in order to provide a reliable basis for the prediction of physics parameters of fast power reactors under consideration. This review summarizes the progress in the field since the past few years. It comprises mainly the work done at the Gesellschaft für Kernforschung, Karlsruhe (GfK), which was partly supplemented by investigations at INTERATOM, Bensberg near Köln, and at BELGONUCLEAIRE, Brussels, which form together with the Dutch NERATOM firm and LUXATOM from Luxembourg the international KONSORTIUM of parties responsible for the design of the prototype reactor SNR 300 ("Schneller Natriumgekühlter Reaktor").

Besides the goal to have a rather comprehensive document on the fast reactor physics effort in the past years, this report is also aimed to give a clear status of the art, thus providing a basis for further investigations. This latter aspect is not fully covered in this review.

In chapter 1 the target accuracies for a fast prototype reactor of about 300 MWe are discussed. This is based mainly on the experience obtained during the design work for SNR 300 and is concerned with the prediction of:

- a) criticality and enrichment, power profile and reaction rates, initial conversion and breeding, material and control rod worth, reactivity coefficients as Doppler-effect and Na-Void effect.
- b) time-dependent reactor characteristics, including burnup aspects as well as a discussion of necessary tools for the description of the dynamic behaviour of the reactor.

Regarding the above mentioned topics, in chapter 2 the state of the art as it appeared at the 1969 BNES-Conference on Fast Reactor Physics is given.

Chapter 3 comprises the developments in fast reactor theory. It deals with

- a) the evaluation and processing of nuclear data
- b) improved calculational procedures as for instance two or three dimensional static diffusion and transport codes, special developments for the analysis of zero power facilities, codes for the appropriate treatment of burn-up processes and reloading operations, investigations with respect to reactor dynamics based on an improved synthesis technique and on the quasi-static approach. Both methods include elaborate feedback parts.
- c) the main characteristics of modern modularly organized code systems.

In chapter 4 our improvements in experimental techniques are discussed for reaction rate and spectrum measurements. Emphasis is put on the present accuracies obtained with different techniques, covering for example fission chamber measurements, foil activation methods, new techniques for the determination of the power distribution and on automatic evaluation of track records. Various methods for the measurement of the neutron spectrum are discussed and a comparison of these methods, used at different laboratories, is given.

Chapter 5 summarizes the most important checks of improved theoretical and experimental methods in integral experiments. The accuracies for the prediction of criticality and reaction rate ratios, power profile,

material worth and control rod worth, Doppler- and sodium void reactivity coefficients are evaluated.

The uncertainty, connected with the extrapolation of the results and experience obtained in the prediction of physics quantities of zero power facilities, to a prototype fast power reactor, is assessed in chapter 6. Besides chapter 5, this chapter indicates the main basis for future investigations.

Reading this report, one should be aware of the fact that, due to the many contributions from various persons and places, sometimes the impression of inhomogeneity might arise. We hope, however, that this never leads to a misunderstanding of physical facts.

In order to give the reader of this document some assistance, it should be noted that all tables are presented within the written text; the figures are found at the end of each section, for instance the related figures to the topic of improvements in reaction rate measurements, section 4.1., are placed at the end of this section, that is between the end of subsection 4.1.6. and the beginning of section 4.2. All references and the numeration of figures and tables have as a first character the number of the corresponding chapter, the second character being a current index. Figure 4.3. thus means the third figure in chapter 4. The references are listed at the end of each chapter. The list of contents may provide further help for easy orientation.

1. ASSESSMENT OF TARGET ACCURACIES IN THE PREDICTION
OF PHYSICAL QUANTITIES OF FAST PROTOTYPE POWER REACTORS

In 1970, when the second series of critical experiments, directly related to the SNR 300 project, was planned for the Karlsruhe zero-power facility SNEAK, the requirements on the accuracy of various reactor physics parameters were estimated, especially those regarding the design of this prototype reactor core. The results of this assessment served as some guide for the planning of further research activities in reactor physics. The required accuracies have been under discussion since and may be revised according to new requests of the safety authorities, or changes in design, or fuel management of the SNR.

The designer must guarantee safe and economic operation of the reactor under all possible conditions, before constructions starts or operation can be licensed. This can only be done if physics parameters can be predicted with reasonable accuracy. It is furthermore essential to have sound knowledge about possible deviations between theoretical prediction and reality. To compensate for possible errors, proper margins or back up solutions must be provided, for instance additional absorber rod worth, or excess reactivity, or safety margin in power density.

These provisions usually cause additional expenses and therefore there are strong economic reasons to attain high accuracies in reactor physics. Unfortunately expenditures, necessary for improving the accuracy, rise very strongly with increasing accuracy goals. Examples for this relationship may be the number of experiments needed for a given goal, or computation time in reactor calculations, or the number of fabricated parts ruled out because they do not fit into tolerance requirements. On the other hand the economic penalties are roughly proportional to the expected error (a special case will be discussed below). Therefore an optimum target accuracy can be defined in principle from the minimum total cost, which considers the "research"-expenditures and design penalties. Although a detailed optimization as indicated here would be difficult and elaborate, the current superficial knowledge of the costs

involved is sufficient to arrive at a reasonable first set of target accuracies, which may serve as a guide for physics research.

In estimating the design penalty one must consider possible feedback of knowledge from reactor operation, such that uncertainty penalties pertain only the first few loadings of the core. This is especially true for the critical mass and most of the reactivity effects.

The "research" expenditures on the other hand usually are rather "cheap" as long as existing facilities, staff and methods are available and can be used, but they may rise very sharply when new buildings, machines, research groups or methods are required. In consequence target accuracies are very often those values, which can be reached with the existing potential.

In some cases target accuracies are actually determined by comparison to other sources of uncertainty, like tolerances in fabrication, which were not questioned at this point.

It should be pointed out that the analysis of this chapter considers one fast prototype reactor project only. Costs and benefits of other orders of magnitude are involved if large commercial reactors in an entire reactor generation and corresponding research activities are reviewed.

1.1. Criticality and plutonium inventory

In order to insure criticality for the full power core at the end of guaranteed operational period, the uncertainties in predicting k_{eff} under this condition must be compensated by a corresponding surplus in the nominal value of the excess reactivity. This surplus of excess reactivity must be obtained by a corresponding higher plutonium inventory.

As can be seen from the detailed analysis in chapter 6 (also see Table 6.3), in the various contributions of the total uncertainty in k_{eff} at the end of the core life, the uncertainty due to reactor physics is still considerable larger than that expected from fuel fabrication. Part of the contributions, which are caused by the extrapolation from the small SNEAK core to the larger SNR core, could actually be eliminated by a one to one mock up of the SNR 300 core. However, this would only remove a partial uncertainty of 4 % from a total of 1.8 %. The quoted uncertainties are given as values with a 90 % confidence level, the various contributions are combined statistically, i.e. small possible correlations between some contributions are neglected.

Since only about one third of the required fissile inventory for SNR 300 was available as platelets with nearly clean ^{239}Pu for experiments in SNEAK, an investigation was conducted to determine, how much additional plutonium (with a larger content of the higher isotopes) was to be acquired to yield an economically justified improved prediction of the fissile inventory of SNR. From the experience in predicting k_{eff} for partially Pu-fuelled SNEAK assemblies, an estimate of the related error for a corresponding full Pu-fuelled core has been made, based on substitution experiments /1.2./. This error decreases with increasing Pu amount. The cost of additional Pu as a function of the error reduction is shown in Fig. 1.1. based upon the total uncertainty of 1.8 % (Table 6.3). The cost penalty of uncertainties in k_{eff} has also been estimated for the SNR 300. It was assumed, that the second reloading could

be corrected with the knowledge from operating the first core. The cost penalty, shown in Fig. 1.1., divides about equally into the following contributions:

- higher inventory,
- lower breeding ratio,
- higher absorber worth.

Concerning the last item it should be mentioned that most of the k_{eff} uncertainties (excluding the temperature and the burnup effect) have to be included twice in the requirements for shut down potential, since the net error can be either positive or negative.

There are several ways of compensating for this additional excess reactivity other than by more absorber, for instance replacing fuel elements by blanket or dummy elements. A detailed discussion of these strategies was given by Billaux et al. /1.1./. If such policies are employed the cost penalty in the SNR 300 may even be reduced to some extent.

This very rough analysis shows, that it is indeed economically not reasonable to buy larger amounts of additional plutonium for the critical experiment in order to obtain a better accuracy for the prediction of criticality of SNR 300.

Considering all possible improvements, especially reductions of the uncertainty in the burn up effects, a target accuracy in k_{eff} of about 1.3 % (90 % confidence) seems reasonable at this time.

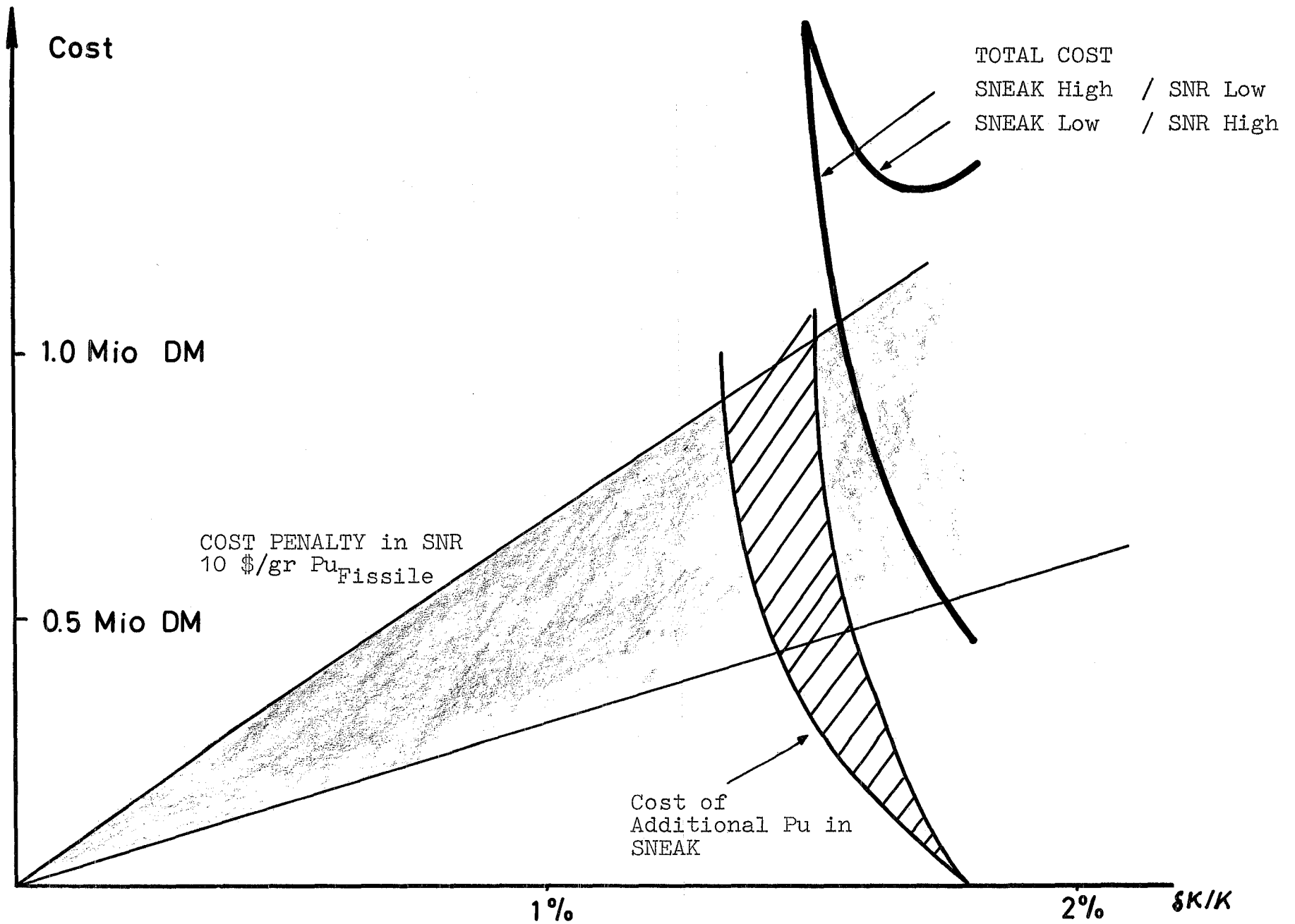


FIG.1.1. Cost benefit analysis of additional Pu in SNEAK for Criticality Prediction SNR 300

1.2. Power distribution

The benefits of high accuracy on the power distribution come primarily from a higher average power density, where the essential physics parameter is the overall power peaking factor, and from a higher core exit temperature of the coolant by avoiding overcooling. The power distribution is also the basis for determining the local burn up and may be used for fuel management optimization. Furthermore flux and power distributions are used in calculating bowing effects.

The situation for fast breeders is different from that in light water reactors, in that more accurate knowledge of the power distribution is not expected today, by the use of incore measurements during operation compared with the accuracy of theoretical prediction. There are several inherent differences between both reactor types which facilitate theoretical treatment of power distribution in fast cores: The change of the infinite medium multiplication k_{inf} , during burn up is much higher in light water reactors than in fast reactors. Also in light water reactors, especially BWR's, there are strong local changes of the diffusion coefficient depending on the coolant density. This means however that there will be no substantial feedback of knowledge from the operation of fast reactors, if not post irradiation analysis of the fuel is considered.

The largest penalty results from unnecessary safety margins in the power peaking factor, required to insure operation of all pins below the maximum allowable linear power rating. The actual value of this penalty depends heavily on parameters like Pu-prices, out-of-core inventory and fabrication cost which are quite uncertain themselves. Again there are other sources of uncertainty outside of the reactor physics area to be considered:

- inhomogeneity of fuel density and composition,
- variations in pellet diameter,
- calibration of total reactor power,
- error in the flux detector signal,
- uncertainties in absorber positioning.

All these effects combine together statistically to an uncertainty of about 5 %, with a 90 % confidence level.

It is useful to separate uncertainty of the total power peaking factor into two parts, one related to the flux distribution in the core, and another related to that in the blanket. It seems reasonable to require a target accuracy of about 3-5% for the total power peaking too.

As will be seen in chapter 6, an accuracy of 5 % is thought to be realistic for the core. In the blanket relative errors of 10 % in the first row, 20 % and 30 % respectively in the following rows of blanket assemblies, result in an additional net uncertainty of less than 2 % in the total power peaking factor.

The corresponding accuracy of the calculated flux- and power maps meets any needs concerning the other uses of these quantities mentioned at the beginning of this chapter. This again has to be compared with the uncertainty in local flow-distribution, swelling rate formulas, limits on local burn up etc.

1.3. Breeding ratio

For the early fast breeder reactors, especially the prototype reactor, there is only a weak influence of the breeding ratio itself on fuel cycle costs. A similar view was pointed out by GREEBLER /1.3./. Operation experience in these reactors is now thought to give the most accurate answer for the long term fuel economy. Therefore a larger uncertainty can be allowed for the breeding gain at the moment. An uncertainty of 5 - 10 % is tolerable for the prototype predictions.

Indeed there is still a rather large uncertainty (about $\pm 10\%$) in the predicted breeding ratio. Most of the uncertainty is caused by cross section ratio uncertainties. The main contributors are $\delta_e(^{238}\text{U})$, $\delta_f(^{239}\text{Pu})$, $^{239}\text{Pu}-\alpha$, structural material absorption cross sections over fissile material absorption cross sections in core and blanket and cross section ratios of the higher Plutonium isotopes. Additional uncertainties are introduced by spatial cross section ratio distributions and by core and blanket leakage.

1.4. Control rod worth

The error in predicting the reactivity worth of absorber elements should be compared with the uncertainty margins in the shut down reactivity requirements.

If an overprediction of the critical mass can be compensated by using dummy elements (see section 1.1.) and this has not to be compensated by the absorber system primarily, the total requirement of nominally about 5 % k (not including the secondary shut down system) has an estimated uncertainty of ± 1 % k (90 % confidence level).

This is a relative uncertainty of ± 20 % for the absorber shut down requirement. The necessary overdesign of the absorber rods is determined both by the uncertainty of the shut down requirement and by the uncertainty of the predictions of the absorber rod reactivity worth for a specified shut down capability. It is not reasonable to require a relative uncertainty for the absorber rod worth prediction that is much smaller than 18 %. On the other hand, there is a particular interest in a low combined relative uncertainty because a sufficient shut down margin is a question of reactor safety with the consequence that the design must be done for a confidence level higher than 90 %. A target accuracy of about 10 % for the SNR 300 is consistent with these considerations.

1.5 Reactivity effects

Various reactivity effects have to be calculated in the safety analysis of a reactor. Some of them are related to geometrical changes of the core and blanket and subject to rather large uncertainties due to poor knowledge about the changes in geometrical conditions. This holds, for instance, for subassembly bowing effects on reactivity. Neutron physics uncertainties are not important in such cases.

Also in dynamic codes the models used to calculate fuel temperature changes contain simplifications which lead to uncertainties comparable to the present uncertainties in theoretical Doppler coefficients of about 10 - 20 %. On the other hand there is no serious difficulty in working with corresponding safety margins.

The situation is somewhat different for the maximum sodium void reactivity, which is included in the shut down requirement for the absorber system. The problem is physically quite well defined. For the SNR-300 an accuracy between 15 - 20 % relative is desirable.

1.6. Theoretical methods, necessary for a reliable prediction of physics quantities of fast prototype reactors.

Besides the aspects, already mentioned in the preceding sections, here some consideration is given to the necessary theoretical tools for a reliable prediction of the stationary and transient behaviour of fast prototype reactors.

1.6.1. Methods for the description of stationary reactor behaviour.

It is obvious that design calculations have to be performed in two space dimensions within a multigroup diffusion theory scheme of about 20 groups. The multigroup constants have to be prepared with a weighting spectrum which is appropriate for the special design under consideration. It seems to be sufficient to take an average core neutron spectrum as a weighting function, preferably taken from a fundamental mode fine group calculation. For special aspects, three dimensional diffusion codes have to be applied. This is true for the calculation of off center control rod worths and for the determination of the influence of control rods on the power distribution as well as the calculation of reactivity effects of subassembly bowing. These effects may be studied with the help of a carefully used three dimensional synthesis technique, but rigorous three dimensional codes should be available at least for check up calculations. As the sub-assemblies of fast reactors are designed in hexagonal geometry, the codes should be capable to deal with this geometry. Because of the fact that the neutron mean free path is mostly larger than the pin to pin distances, heterogeneity effects are not very important, but if thicker pin diameters than the presently 6 mm ones should be introduced into the core for economic reasons, tools must be available to consider the neutron transport in this heterogeneous array. Furtheron investigations on sodium void reactivity for cases, where the sodium is ejected out of the various channels, neutron streaming may become important and at least a one dimensional theoretical model should be available to deal with this problem. Transport effects near

control rods, especially for the follower regions, are necessary to be calculated, again at least in one dimensional geometry, preferably in two dimensions. In addition a proper investigation of power profile at core/blanket interfaces requires a transport theoretical check up.

1.6.2. Methods for the description of time dependent reactor behaviour.

The description of the burnup behaviour of prototype reactors requires two space dimensions, together with a flexible scheme for subassembly management. In addition it is desirable to have available a three dimensional burnup code to investigate special effects during the reactor life (e.g. replacement of fuel elements by other elements with different fuel for irradiation tests) and the theoretical description of the overall behaviour of fuel elements during operation as a learning phase for later application of automatic control. These investigations in a first stage could be done with synthesis techniques.

The analysis of the prototype transient behaviour plays a predominant role during licencing procedure of the plant, especially the treatment of severe (hypothetical) accidents. As far as the neutron kinetics part is concerned, the use of sophisticated point reactor models seem to be sufficient, but a check up with space dependent models in two dimensions is desirable. At least equally important as the neutronic part is an adequate theoretical description of the various feedbacks during the course of an accident. This includes a multichannel thermohydraulic model, codes for the treatment of pin and clad behaviour, sodium boiling and ejection, sodium fuel interaction and fuel slumping. The disassembly phase in a hypothetical accident requires a scheme within two space dimensions, which is improved over the usual Bethe-Tait codes in order to treat more properly an accident situation, where sodium is present, at least in parts, of the core. Finally, tools have to be available to calculate the dynamic loading of the containment after a heavy core excursion.

Not only as a matter of convenience, but due to many correlated physical aspects in the description of stationary and transient reactor behaviour, which are correspondingly dealt with in various codes, it is desirable to operate the theoretical tools in a flexible, modularly organized code system.

1.7. Summary of target accuracies for physics quantities

of a fast prototype reactor

The discussion in the preceding section showed that a complete and thorough cost - benefit analysis is very difficult to perform. The evaluation presently cannot be free from intellectual guesses. As already mentioned, a different picture evolves if larger fast reactors in an entire reactor generation are analysed with respect to target accuracies. This is excluded from this report.

Table 1.1. summarizes the main conclusions of sections 1.1. - 1.5.

Table 1.1. Target accuracies for physics quantities of a fast prototype reactor (90 % confidence level).

k_{eff} (End of life)	Peak to average power	Breeding ratio	Control rod worth	Doppler coefficient	Sodium void co- efficient
1.5 %	3-5 %	5-10 %	10 %	10-20 %	15-20 %

References for Chapter 1

- /1.1/ Billaux et al., ANS Winter Meeting, 1970
- /1.2/ Helm, F., KFK 1271/2, September 1971 (pp.121-28)
- /1.3/ Greebler, P. et al., Proceedings of the 2nd Intern. Conference on Nuclear Data for Reactors, Helsinki, 1970, p.CN-26/102.

2. STATUS OF EXPERIMENTAL AND CALCULATIONAL TECHNIQUES

IN FAST REACTOR PHYSICS IN 1969

In order to have a fairly well defined startingpoint for the demonstration of new developments and the achieved improvements, the quality in predicting physics parameters, as listed in chapter 1, is presented as it appeared at the BNES - Conference on Fast Reactor Physics, London 1969. Because of the fact that this status becomes evident in the following chapters also, we restrict ourselves in this chapter to a very brief description of the physics capabilities existing 1969 in the Federal Republic of Germany, together with an estimate of the uncertainties in predicting the main physical design features of a fast system. A comprehensive review of the status 1969/1970 in analysing fast critical assemblies can be found in a contribution to the IAEA-Conference on Nuclear Data for Reactors, Helsinki 1970 /2.1./.

2.1. Experimental fast reactor Physics in 1969

In 1969 there existed about a 2 1/2 years experience with the fast zero power facility SNEAK at Karlsruhe. Part of the experimental techniques had been developed at the fast/thermal reactor STARK, which is a modified ARGONAUT reactor in which the central graphite zone is replaced by a fast zone.

The status of the experimental techniques in 1969 may be described simply by noting what was not yet available at that time.

For reaction rate measurements there existed no generally applicable methods for the experimental determination of the fine structure in the heterogeneous array of platelets. First attempts to cover this topic had been made in the uranium cores of the SNEAK assemblies. Plutonium foils to measure reaction rates by activation methods also were not yet available. Fission rate measurements mainly were performed with fission chambers, the method using solid state track recorders was at an early stage of development. Though the precision of measurements of the fission rates in ^{235}U and ^{239}Pu and the capture rate in ^{238}U already was quoted to be quite high, there was some doubt about systematic errors. Therefore most laboratories were developing several independent techniques to obtain cross checks for the measurements of these rates. But an intercalibration of the experimental equipment at Karlsruhe was not yet performed at that time. Finally, no measurements of γ -heating to obtain the power distribution could be performed in 1969.

Although an accuracy of about 10 % was claimed for the spectrum measurement techniques (time-of-flight, proton recoil) mainly used, this figure was based in 1969 on only a few intercomparison measurements. The reasons for this were that the overlapping regions between the different techniques were small and that for some energy regions (for example above 1 MeV) only one technique was available at that time.

2.2. Theoretical fast reactor physics in 1969

The situation in the field of microscopic cross section measurements was very unsatisfactory. In various energy regions of interest for fast reactors the main cross sections for fission (^{235}U , ^{239}Pu) and capture (^{238}U) were partly discrepant between different authors by about 10 % and even more. In consequence, the evaluation of "best-data" sets, recommended for use in fast reactor calculations, also yielded different results in different laboratories. The Karlsruhe Nuclear Data File KEDAK was updated currently. The status achieved in 1969, best is described in /2.2./. Because of this situation in parallel to the KEDAK-activities a reevaluation of our group constant sets was performed with special consideration of differential neutron data together with integral neutron data obtained in zero power facilities. This led in 1969 to the 26-group constant set MOXTOT /2.3./.

Most of the calculations were performed in 1969 in the 26-coarse group representation, using one and two-dimensional diffusion theory. A fine group scheme was under development. The slowing down of neutrons within the broad resonances of medium weight nuclei was calculated from about 1000 energy points within the frame of narrow resonance approximation, thus correcting the microscopic elastic transfer matrices. This REMO correction is described in /2.4./ The results usually were corrected by taking into account the transport effect, using the Karlsruhe version DTK of the SN-code DTF-4. Heterogeneity effects were treated with the code ZERA /2.5./, which treats the energy - and space- dependent resonance-selfshielding by a collision probability theory. Special improved versions for the interpretation of Doppler experiments were nearly completed.

To calculate the Doppler-effect in fast systems, a special code had been developed /2.6./ based on perturbation theory. This code was able to deal only with statistical resonances, interference effects between potential and resonance scattering could not be included.

In calculating the long term behaviour of fast reactors, mainly one dimensional calculations were performed, sometimes supported by two-dimensional calculations in a few group scheme.

As far as the description of the dynamic behaviour of a fast reactor is concerned, in 1969 most calculations were based on the point reactor model. A

first version of a space dependent two-dimensional dynamics code just had been completed. This code uses two-dimensional space trial functions, the time coordinate being synthesized /2.7./. The feed-back part of this code had already some sophistication in the treatment of thermohydraulic features, but was lacking of an integrated sodium boiling module which had been established as a stand alone code /2.8./. The disassembly of a core in a hypothetical accident situation was done with a quasi-two-dimensional Bethe-Tait code, FAUN /2.9./, treating the disassembly in a one group perturbation scheme with a simple hydrodynamic model.

2.3. Prediction of fast reactor physics quantities in 1969

Based on the methods, briefly described in the preceding sections, an estimate of the 1969 uncertainties, related to the prediction of the main physical design features, is given in Table 2.1.

Table 2.1. Estimate of the uncertainties in the prediction of physics quantities for fast reactors, status 1969 (numbers to be interpreted as standard deviation)

k_{eff} (fresh core)	Peak to average power	Breeding ratio	Material worth	Doppler coefficient	Sodium void coefficient
$\pm 2 \%$	5 %	10 %	30 %	$\leq 15 \%$	50 %

As already mentioned in chapter 1, one must be careful in extrapolating the experience, obtained by the comparison of theoretical and experimental results obtained in zero power reactors, to larger prototype systems. For instance heterogeneity effects in prototype reactors are negligible, transport corrections are smaller than in the experiments. The theoretical treatment of these aspects in 1969 was not yet too sophisticated and thus implied some source of uncertainty (together with the unsatisfactory nuclear data situation). Therefore it seems not to be unprobable that the prediction of physics parameters in power reactors might have been in a better shape than it appeared from the comparison with integral experiments in fast zero power reactors.

References for Chapter 2

- /2.1/ Böhme,R.A. et al., KFK 1303, IAEA/CN-26/117, (1970)
- /2.2/ Hinkelmann,B. et al., KFK 1340, EANDC(E) 136"U",(1971)
- /2.3/ Kiefhaber,E., Schmidt,J.J. et al., KFK 969, EANDC(E)-118"U", (1970)
- /2.4/ Huschke,H., KFK 770, (1968)
- /2.5/ Wintzer,D., KFK 743, (1969)
- /2.6/ Froehlich,R., KFK 367, (1965)
- /2.7/ Kessler,G., KFK 781/I, (1968) und KFK 781/II, (1968)
- /2.8/ Schlechtendahl,E.G., KFK 1020 (1969)
- /2.9/ Kluge,F.G., Thurnay,K., KFK 1057, (1969)

3. IMPROVEMENTS IN THEORETICAL FAST REACTOR PHYSICS

In this chapter we discuss the progress in reactor theory since 1969. The activities are reviewed under five aspects:

- a) Progress in evaluation and processing of nuclear cross sections.
- b) The mathematical and numerical effort spent to the diffusion - and transport code development as well as investigations on synthesis techniques.
- c) Development of codes for analyzing special physical problems in fast reactors like the investigation of heterogeneity, interface effects and streaming.
- d) The progress in modeling physical problems in time dependent fast reactor calculations.
- e) The evaluation of new schemes for modular code systems.

The check of these improved methods by comparison with experimental results, obtained in fast zero power reactors, will be presented in chapter 5.

3.1. Evaluation and processing of nuclear cross sections

In this section the situation of the microscopic neutron nuclear data and the related group constants is summarized. From the point of view of reactor physics the accuracy of the important nuclear data is not yet sufficient for the reliable design of fast power reactors. In particular the dominating influence of the heavy nuclei on the neutronics behaviour of fast reactors has provoked high accuracy requests for the nuclear data of these materials so that the experimental methods for neutron cross section measurements had to be more refined. With the modern experimental facilities the number of data produced has considerably increased and so the task of the evaluator to derive complete sets of so-called "best" data by taking into account all available experimental information and by judging its reliability has become more laborious and complicated. For an evaluation of all the data types for one specific isotope much time is needed. Mainly for this reason we have adopted at Karlsruhe two different procedures for improving the nuclear data:

1. Careful evaluations of the different experimental measurements by taking into account also detailed structure in the data types and afterwards generation of the corresponding group constants as input in the reactor calculations.
2. Direct changes of the group constants for selected data types of the materials important in reactor calculations and for selected energy groups. This is not done arbitrarily, but on the basis of most recent important measurements for the cross section type and the energy range considered, and also in close collaboration with the evaluators. This way of improving the nuclear data was stimulated by urgent requirements of reactor designers for more reliable predictions of the neutronics behaviour of fast power reactors presently built or designed.

The greatest advantage of the second procedure is that the influence of recent experimental measurements on integral quantities can be investigated immediately after availability of the data. Using the information from integral experiments in fast test reactors, the second method allows sometimes to come to a final decision in the case of discrepant data sets from the point of view of an evaluator. The disadvantages of this method are that it is only practicable for a fairly small number of energy groups, and that it is less appropriate in energy regions where one has fluctuations, or other structural phenomena in the data

types. In these two cases the first way is preferable. It is, in particular for the case of many group and Monte Carlo calculations that we consider the second procedure of improving nuclear data only as a first and provisional step prior to a careful re-evaluation of the data.

3.1.1. The nuclear data file KEDAK

In Karlsruhe we have established the German Nuclear Data File KEDAK (Kerndatenband Karlsruhe). We are also working with the American Data File ENDF/B (Evaluated Nuclear Data File). Our own evaluations are only performed for the KEDAK-library which was established in 1966 /3.1./. The evaluations done for the KEDAK-materials till 1968 are described in the references /3.1., 3.2./.

Since that time a partwise re-evaluation was done for ^{239}Pu /3.3./ in order to include the ν -measurements of Gwin et al., the $\bar{\nu}$ -measurements of Condé et al. and the $\bar{\nu}$ -measurements of Soleilhac et al. which were available at that time (for references see /3.3./). Concerning the fission cross section for ^{239}Pu a number of precision measurements was considered: those of White et al., of Käppeler, Pflöschinger, of Nesterov, Smirenkin and in the higher MeV-range also the corrected Smith, Henkel, Nobles, σ_f -values (references in /3.3./). A new evaluation for ^{239}Pu is now again on the way and $\bar{\nu}$ and σ_T were already revised. Concerning $\bar{\nu}$, recent measurements of Soleilhac in the lower energy range, of Mather et al. and of Savin et al. (references in /3.3./) were taken into account. $\bar{\nu}$ was fitted by a set of straight line functions of different slopes. For σ_T the major changes are due to experimental results of Cabé et al. /3.4./ in the higher keV- and MeV-range. The fission cross section and α for ^{239}Pu will also be revised in the near future.

For ^{235}U a re-evaluation of all data types above the resolved resonance region been accomplished /3.5./. Primarily the fission cross section, the total cross section, α and $\bar{\nu}$ were evaluated. For $\bar{\nu}_{25}(E)$ the deviations from the so long assumed linear energy dependence of $\bar{\nu}$ in the low energy range revealed by recent $\bar{\nu}$ -measurements for ^{235}U were taken into account. Concerning the fission cross section we have incorporated in the low energy range the results of the high-resolution measurements of Blons et al. /3.5./, i.e. that up to 30 keV we have taken into account the structure in this cross section type. In the

higher energy range the evaluation for σ_f is mainly based on the experimental results of White and of Szabo et al. and in the higher MeV-range on the revised Smith, Henkel, Nobles (for references see /3.5./) σ_f -values. Also for the total cross section and α we have included high-resolution measurements in the low energy range and thus established on the file the structure in these data types. In the higher energy range the major changes in σ_T may be attributed to the experimental results of Cabé et al. /3.4./ and lead here to about 5 % higher values than previously /3.2./. Concerning α the major changes in the upper energy region are encountered in the keV-range where the presently recommended α -values are by about 5 - 7 % higher than the previously recommended ones, due to the experimental results of de Saussure et al. from 1966 which have not been available at the time of J.J. Schmidt's evaluation /3.1./.

In Fig. 3.1., Fig. 3.2., and Fig. 3.3. we have compared our recent evaluations for σ_f (^{239}Pu), σ_f (^{235}U) and σ_c (^{240}Pu) with the corresponding ENDF/B 3- and UKNDL- curves. Re-evaluations for the nuclear data of ^{238}U and of the higher Pu-isotopes are planned to be available in the first half of 1973.

Concerning the other KEDAK materials, for Fe, Cr, Ni, ^{23}Na , Mo, ^{12}C the data for the threshold reactions were revised /3.6./. For ^{12}C in addition the cross sections for the inelastic scattering process were re-evaluated. A new evaluation was performed for H. In particular, for the total cross section we have taken over the very accurate experimental results of Cierjacks et al. /3.7./ and for the capture cross section the evaluation of Horsley /3.8./. In the framework of an extension of the upper energy limit on KEDAK from 10 MeV up to 15 MeV all data types for Fe, Cr, Ni and for ^{23}Na , Mo, ^{12}C , H were evaluated in the range 10 - 15 MeV.

Besides the above mentioned activities for updating the materials available on the KEDAK-file there is another activity to increase the number of available KEDAK-materials. Up to now we have on KEDAK only a limited number of materials namely the most important ones for reactor calculations ^{235}U , ^{238}U , ^{239}Pu , ^{240}Pu , ^{241}Pu , ^{242}Pu , Fe, Ni, Cr, Mo, H, D, O, ^{23}Na , ^{27}Al , ^{12}C , Cd. To improve this situation we are going to take over nuclear data from the American ENDF/B file for materials which are not on the KEDAK file and for which we have special requests but not the manpower to perform an own evaluation within a reasonable time scale.

To reach this target a code for the conversion from the ENDF/B-format into the KEDAK-format was written at Mol /3.9./ in collaboration with the evaluation group in Karlsruhe.

The aim of the whole evaluation program outlined in the preceding sections is a considerably improved version 3 of the KEDAK-library which will presumably be released in the second half of 1973.

3.1.2. Procedures for the calculation of group constants

Besides the 26-group approach with group cross section sets of the ABN-type, originally proposed by Bondarenko et al. at Obninsk /3.10-3.13./, which are since several years widely used for fast reactor calculations, a new multi-group approach with 208 energy groups has been developed since 1969 /3.14./, /3.15./. This approach uses 196 energy groups in the energy range from 1 keV to 10.5 MeV with lethargy widths between 0.034 and 0.055, and 12 energy groups below 1 keV with a lethargy width of 0.77. The energy groups below 1 keV are the same as ABN-groups, the groups above 1 keV were obtained by subdividing the ABN-groups into 14 fine groups per ABN-group. This choice of group structure allows condensation to the ABN-structure. The main arguments for this new group structure are the following ones:

- to get a more accurate description of neutron slowing down by elastic scattering
- to get calculated neutron spectra with an energy resolution comparable to measured spectra (about 5 %)
- to avoid difficulties that arise from the weighting of the broad scattering resonances of light and medium weight isotopes.

As it was intended from the very beginning, to have one-dimensional diffusion-, consistent P_1 - and S_N - calculations in many groups, it was necessary, not to take a too large number of groups. Therefore, only above 1 keV a fine group structure was used. The chosen 208 group structure turns out to be a good compromise between accuracy and numerical expense. The group structure is fine enough to allow a good representation of the elastic scattering transfer at least for the zero'th and first order for all light and medium weight materials that are important for fast reactors. It is also fine enough to justify the assumption that the neutron flux within one group may be approximated by $\text{const.}/\Sigma_t(E)$,

and the neutron current by $\text{const.}/\Sigma_t^2(E)$. This approximation seems to be appropriate because the broad scattering resonances, for which the NR-approximation does no longer hold, are resolved by this group structure. For resonances smaller than the group structure, a NR-approximation should give a fairly good approximation. The group structure allows an energy resolution better than 6 %, which is sufficient to describe measured neutron spectra.

For the calculation of the macroscopic 208-group constants, the 26-group processing procedures can no longer be applied. The concept of resonance selfshielding factors does not allow to take into account interference of resonances of different isotopes. Therefore, for the 208-group approach the following procedure is used. Each fine group is subdivided into five intervals per group, i.e. 980 energy intervals in the energy range from 1 keV to 10.5 MeV. This number of intervals should be sufficient to represent adequately the cross sections of the light and medium weight materials. For each group and material the five unweighted averages of the cross sections over the intervals are stored on a library named GRUBA. For the transfer elements for elastic and inelastic scattering from one group to another also five values per outscattering group are stored. The $\Sigma_t(E)$ of the mixture is taken into account exactly in the 980 energy interval representation. Only for heavy isotopes resonance self-shielding factors are used, because 980 intervals are not sufficient to resolve these resonances.

3.1.3. Group constant libraries and codes

For the 208-group calculations the library GRUBA has been established. This library contains all informations necessary for the calculation of a 208-group constant value. At the moment information is available for the following materials: H, C, O, Na, Al, Cr, Fe, Ni, Mo, ^{235}U , ^{238}U , ^{239}Pu . These materials are taken from the KEDAK-library /3.3./, further materials will be taken over from ENDF/B in the near future. Besides these materials a larger number of further materials is available which has been adopted from the Russian 26-group cross section set /3.10./.

For the preparation of a GRUBA library from the KEDAK-library there exist several codes, which shall be combined to one code system named FIDAS in the near future.

The central code for the calculation of the macroscopic group constants is GRUCAL. It starts from the GRUBA-library and calculates all types of group constants necessary for diffusion-, consistent P_1 - and S_N - calculations.

Further work has also be done in the field of the 26-group cross section sets. For the preparation of 26-group cross section libraries of the ABN-type from the KEDAK-library an improved and extended version of the code MIGROS /3.11./, called MIGROS-2 /3.16./ has been established. Compared to MIGROS, the main refinements and extensions are the calculation of current weighted self-shielding factors from resolved and unresolved resonance parameters, the calculation of inelastic matrix elements from excitation cross sections and from an evaporation model, and the calculation of zero'th and higher order (up to P_5) elastic scattering matrices from angular distributions.

3.1.4. The MOXTOT- and KFK INR-Set

As explained before, it was necessary to improve our set of group constants prior to a complete re-evaluation of our KEDAK-file. In this revision of group constants which was performed essentially without using KEDAK, the results of cross section measurements and evaluations as well as the results of integral experiments in fast test reactors could be taken into account due to the close cooperation of nuclear data evaluators and reactor physicists. The preparation of the MOXTOT set in 1969 /3.17., 3.12./, was a first step in this direction. It resulted in encouraging improvements for the prediction of neutron physics parameters of fast reactors. Using this data-set, it was possible to predict the criticality of all zero power reactor assemblies, studied as test cases at that time, within an uncertainty limit of $\pm 2\%$. Furthermore, we observed an almost clear separation between the criticality values of uranium- and plutonium- fuelled assemblies: the first ones generally predicted supercritical and the latter ones predicted subcritical.

Compared to the SNEAK-set /3.18., 3.11./, which was prepared in 1967 on the basis of the KEDAK-file, the following important changes of group constants were included in the MOXTOT-set:

- (1) For ^{238}U we used in the energy range 5 eV - 100 keV the low capture cross section of MOXON /3.19./. Between 100 - 500 keV the capture cross section obtained by Pönitz et al. /3.20./ and by Menlove and Pönitz /3.21./ replaced the original SNEAK set values.
- (2) For ^{239}Pu the old KAPL σ -values were superseded by improved values derived essentially from the experimental results of GWIN et al. /3.22./ available at that time.
- (3) The inelastic scattering probabilities of the Russian ABN-set which were not changed in preparing the SNEAK-set have been modified by data calculated on the basis of the KEDAK-file. The KEDAK-materials involved were C, O, Na, Al, Cr, Fe, Ni, ^{235}U , ^{238}U , ^{239}Pu , ^{240}Pu , ^{241}Pu , ^{242}Pu .
- (4) For ^{235}U , ^{238}U and ^{239}Pu the fission cross section in the high energy range (3 - 10 MeV) has been reduced in accordance with the corresponding efficiency correction for the long counter measurements. For $\bar{\nu}$ of ^{239}Pu the results of the measurements of Fréhaut et al. /3.23./ and Condé et al. /3.24./ have been taken into account. For the higher stable plutonium isotopes ^{240}Pu , ^{241}Pu and ^{242}Pu the Russian ABN group constants were replaced by data based on an evaluation by Yiftah et al. /3.25./.

Although we achieved a considerable improvement using the MOXTOT set for the calculation of integral parameters in fast test reactors, a further revision of the group constants turned out to be necessary in order to reduce the uncertainty range for criticality prediction and to decrease the deviations between calculated and experimental results of important quantities other than the criticality, e.g., reaction rates, which are important for the long term assessment of the breeding capabilities of fast power reactors. Using MOXTOT-set as starting point we made the following changes, concerning mainly the heavy isotopes:

- (1) Taking into account the recent evaluation of Hinkelmann /3.3./ for ^{239}Pu , together with slight modifications due to recent experimental results.
- (2) Reducing the cross section for inelastic scattering on ^{238}U and hardening the spectra of the inelastically scattered neutrons.
- (3) Modifying the group constants for σ_c (^{238}U) in such a way that they are compatible with recent differential measurements and evaluations of the cross section ratio σ_c (^{238}U)/ σ_f (^{235}U).
- (4) Taking into account new measurements for σ_{tot} of ^{235}U , ^{238}U and ^{239}Pu .
- (5) Reducing remarkably the old KEDAK-values for α (^{235}U) below 1 keV.
- (6) For the determination of the group constants for elastic down-scattering we used as a weighting spectrum the collision density of a typical sodium cooled fast reactor, namely that of the German prototype SNR 300.
- (7) It has been shown that the precise form of the energy dependence of the fission neutron spectrum of different isotopes must be taken into account.

As a result of this second step in group constant improvement, a set of group constants, termed KFK INR set, was established /3.13./ which was able to predict the criticality of a large variety of critical assemblies within an acceptable deviation of $\pm 1\%$ from the corresponding experimental results (see chapter 5).

It seems worthwhile to mention that we have primarily considered criticality values as important integral parameters on which the improvement of the group constants is based. Reaction rate ratios have been of minor importance in this respect: we only used the general experience that the ratios σ_{f8}/σ_{f5} and σ_{f9}/σ_{f5} have been underestimated with the preceding set of group constants. Reactivity coefficients have not been regarded as basic integral parameters for the improvement of group constants. Therefore, it must be considered to be a remarkable success of the present improvement of group constants.

That very satisfactory agreement was found between calculated and measured results, not only for the criticality values but also for the reaction rate ratios and for reactivity coefficients, particularly for those assemblies which were evaluated recently when the preparation of the improved set of group constants had already been completed. This gives further confidence that the present set can be considered as a firm and reliable basis for nuclear reactor design calculations. However, the present accuracy and uncertainty limits may still not be completely sufficient. In addition, some materials, such as higher plutonium isotopes, fission products, less usual structural and absorber materials may undergo a change of their present importance, so that further improvements in the set of group constants may become necessary in the future.

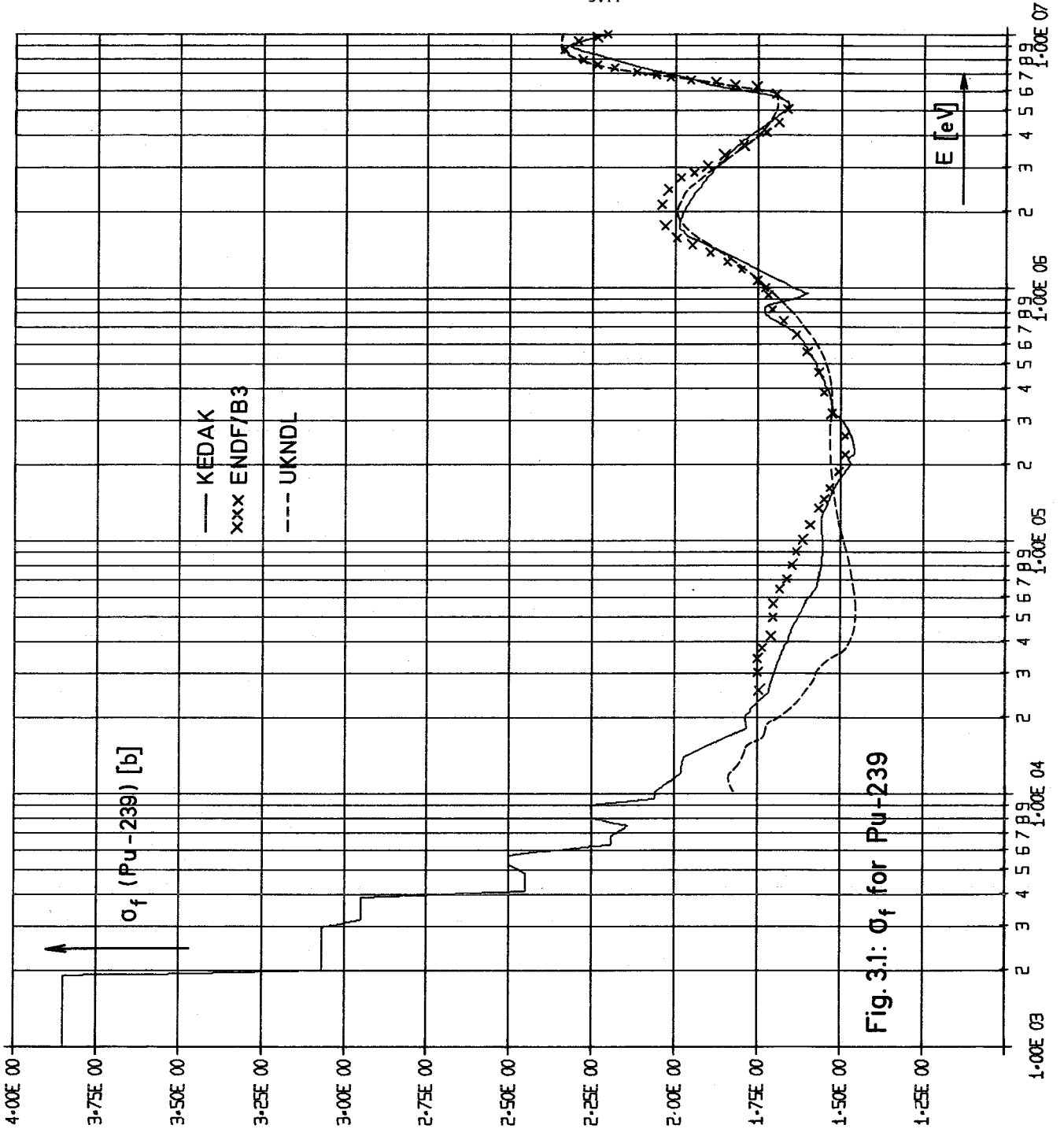


Fig. 3.1: σ_f for Pu-239

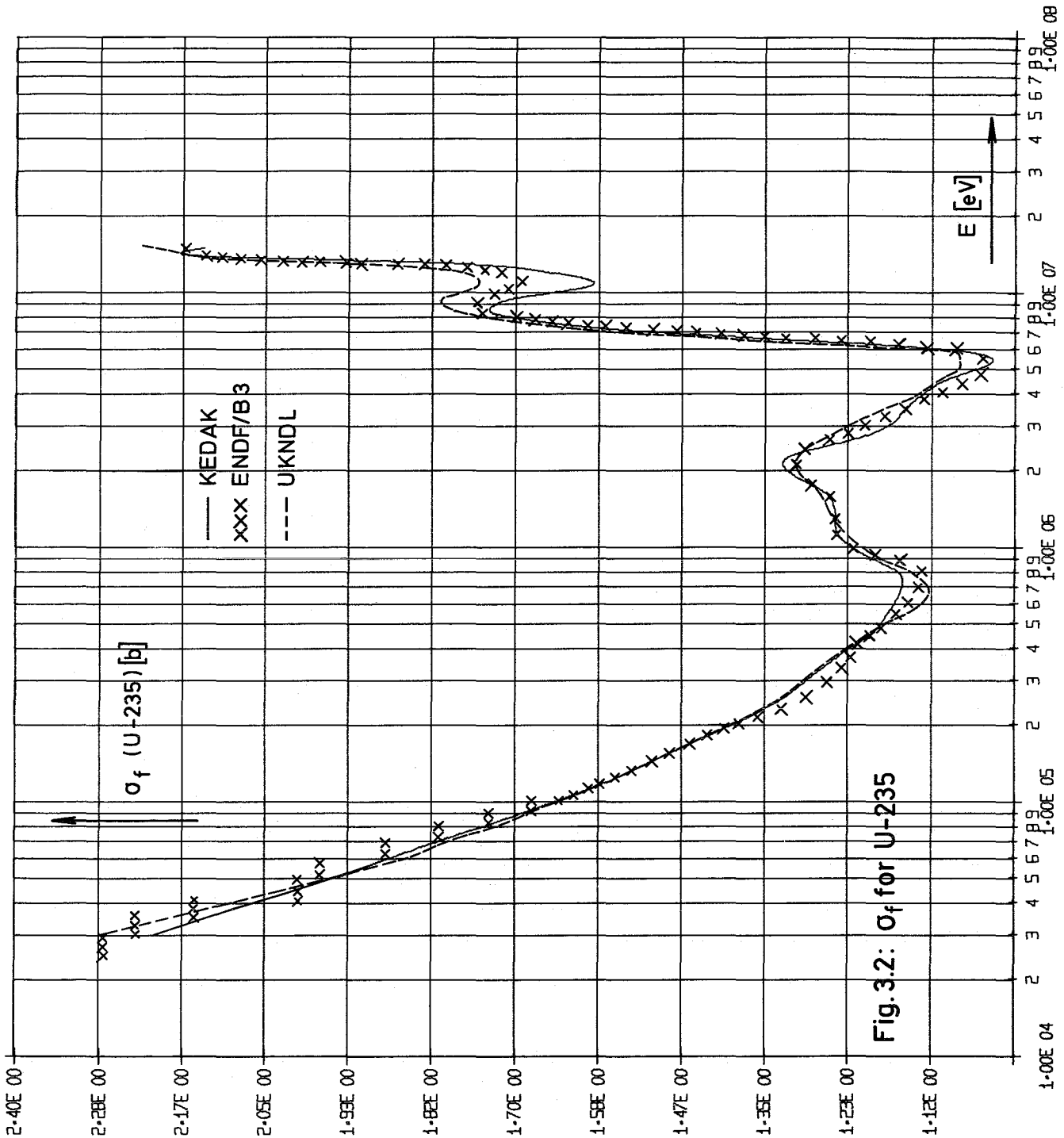
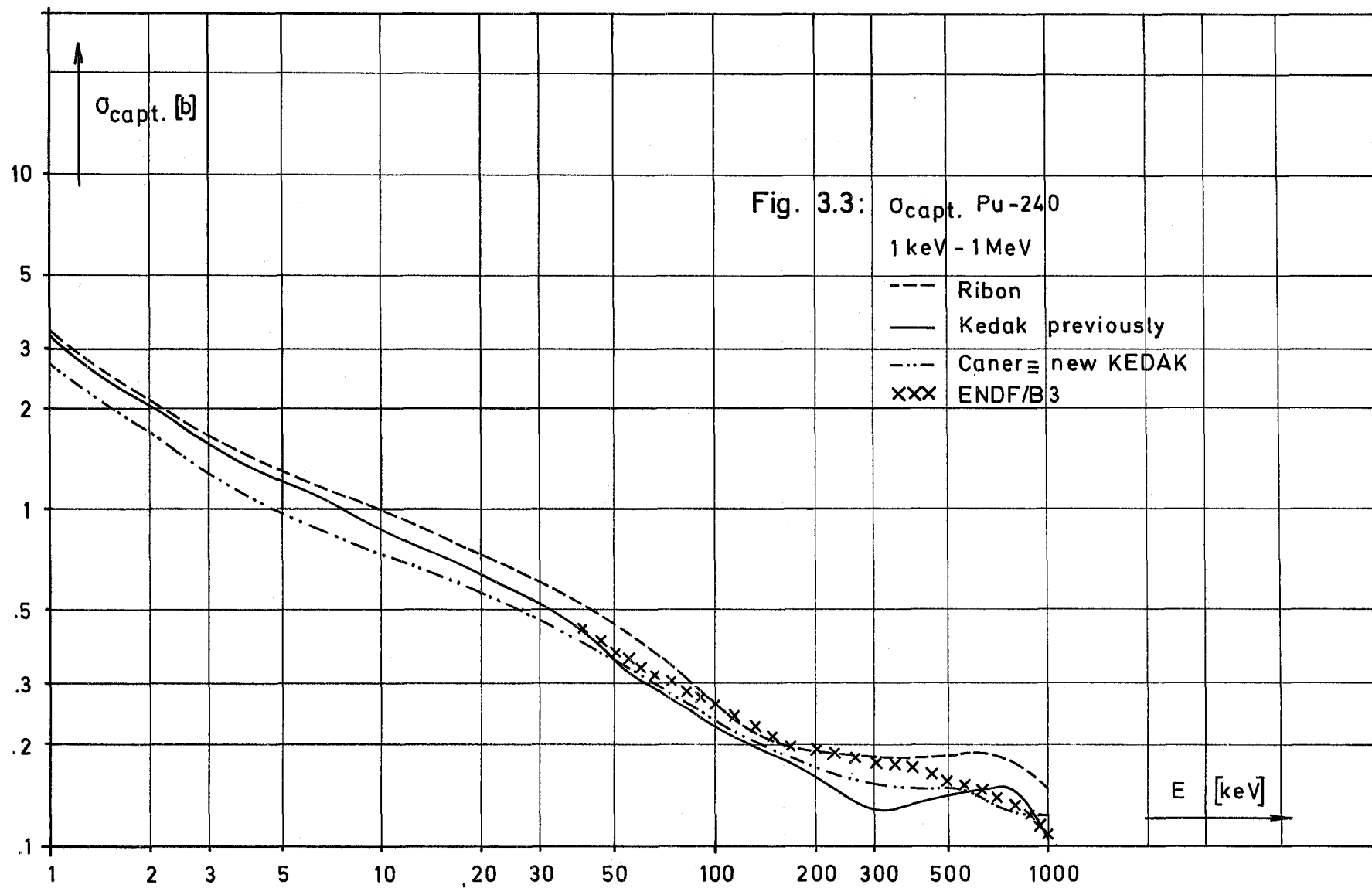


Fig.3.2: σ_f for U-235



3.2. Development of diffusion and transport theory methods

The development of codes for solving the static diffusion or Boltzmann equation, was concentrated on multigroup schemes in two and three space dimensions. A brief description of the main characteristics of the relevant codes is given in this section.

3.2.1. Diffusion codes.

The two dimensional diffusion code DIXY

The original NUSYS system (see section 3.7.1.) contained already the first version of the Karlsruhe two dimensional multigroup diffusion program DIXY for refined fast reactor physics and design studies. This program has been enlarged widely for an effective use on third generation computers. Its essential characteristics, proven to be effective in numerous applications, can be listed shortly as follows:

- a) The homogeneous steady state diffusion equations for normal or adjoint neutron fluxes can be solved in xy-, rz- or r θ -geometries, subjected to different boundary conditions; non diffusion regions are allowed.
- b) Geometrical criticality search and time-eigenvalue calculations are possible.
- c) The inhomogeneous problem (fixed source) can be solved.
- d) Included are programs for reaction rate density calculations and for first order perturbation theory.
- e) To solve numerical neutron flux problems the power iteration method is applied in connection with a special inner iteration technique: a four line cyclically reduced block overrelaxation scheme, similar to the PDQ5 method /3.81/.
- f) Moreover computing time is reduced by interpolating a given coarse mesh neutron source distribution to get an improved fine mesh source guess, thus in normal cases half of the time is saved.

g) Fast procedures for calculating the matrix elements of the finite difference equations (by box integration) have been built into DIXY, thus allowing frequent recalculations to adapt a special problem to the available fast memory without use of many external storage devices (normally less than two).

With the use of modern programming techniques, as variable dimensioning, the use of a rather pure FORTRAN near to ANSI standards, etc., a very effective program is available now for a wide range of computers, e.g. for the IBM/360 models 50, 85, 91, IBM/370-165, and for CDC computer models 6400 and 6600.

The three dimensional diffusion code D3D

D3D is a computer program for the solution of the homogeneous multigroup diffusion equation (without upscattering) for three dimensional slab (X, Y, Z) and cylinder (θ , r, z) geometries. The coupled system of partial differential equations is reduced to a system of linear algebraic equations using a box integration technique. The outer iteration is performed by the classic fission source power method. The inner iterations are performed by two successive block overrelaxations. Within one group the planes are used as the blocks for a normal successive overrelaxation procedure. Within each plane the cyclically reduced four line block overrelaxation is used as implemented in the two dimensional diffusion program DIXY.

To accelerate the convergence of the iterations, a hierarchy of coarse meshes is constructed from the original fine mesh. The coarse mesh equations are solved and this solution is used after applying an interpolation procedure as an estimate for the next refinement in the hierarchy. In this way one proceeds until the solution for the original fine mesh is obtained.

To avoid useless iterations, the accuracy of the solution may be increased from interpolation step to interpolation step as well as within an interpolation step.

The optimum relaxation parameters are precalculated from the greatest eigenvalues of the Gauss-Seidel matrices. These greatest eigenvalues are obtained by the power method applying the interpolation procedure to the eigenvectors.

The data are handled as follows: The scattering and fission matrices are recalculated during the outer iterations. The matrices of the inner iterations are stored. If more core storage than the minimum (which only depends upon the number of the points in a plane) is allocated, it is used to substitute partly or totally the external storages to restrict data transfer. Due to variable dimensioning there is no restriction about number of groups, meshpoints, regions and so on.

D3D solves the adjoint problem, problems with space dependent fission spectrum and non diffusion regions.

D3D was developed for fast breeder applications. Reactor calculations with 26 groups and 20000 space-mesh points have been performed.

The input description is available.

The three dimensional diffusion code KADI in rectangular cartesian coordinates.

The three dimensional, multi-group simultaneous diffusion equations for downscatter problems are transformed by a conventional box integration technique into a system of simultaneous linear seven-point difference equations. The solution proceeds with inner iteration on the flux for each group, within outer iterations on the fission source. The outer iteration is performed by the power method. The inner iterations are performed by an alternating direction implicit method. The code is primarily intended for investigating the applicability of a three-step alternating direction implicit method for calculating fast breeder problems. The code is written in IBM FORTRAN IV and Assembler language for computers like IBM/370-165, and has no restrictions for the number of energy groups and the number of mesh points. KADI permits an optimal use of the available main storage region in the sense that the working area is automatically extended to the full size of the allocated main storage region in order to reduce the number of input/output operations on external datasets.

Solving within each group the linear system

$$(U+V+W)\phi = q$$

the following three-step alternating direction implicit iteration scheme is used:

$$(c^{(p+1)} + U)\phi^{(p+1/3)} = ((c^{(p+1)} + U) - r(U+V+W))\phi^{(p)} + rq$$

$$(c^{(p+1)} + V)\phi^{(p+2/3)} = c^{(p+1)}\phi^{(p+1/3)} + v\phi^{(p)}$$

$$(c^{(p+1)} + W)\phi^{(p+1)} = c^{(p+1)}\phi^{(p+2/3)} + w\phi^{(p)}$$

with iteration index $p=0, 1, \dots, p_0$ and arbitrary flux $\phi^{(0)}$

The block-tridiagonal matrices U, V, and W result from the discrete representation of the diffusion term in x, y, and z-direction respectively and the removal term. Although U, V, and W in general do not commute, certain model iteration parameters $r, c^{(p+1)}$, and p_0 are used. The parameter computation is based on methods suggested by Hadjidimos / 3.82 /, Guittet / 3.83 /, and Douglas jr. / 3.84 / for model problems.

The blocks are solved for each step by the standard Gauss forward elimination / backward substitution technique. The inner iteration proceeds with repeated application of the sequence $(c^{(p+1)})$ of length p_0 with fixed r . The parameter calculation requires rigorous upper and lower eigenvalue bounds of U, V, and W. The latter are determined by an inverse power method suggested by Varga / 3.85 /.

At present the code is tested, and the produced numerical results recommend carrying on the code development.

The three dimensional neutron-flux-evaluation computer program AUDI 3

Contrary to the two dimensional diffusion computer program DIXY, which contains an own evaluation part, a different strategy is pursued for three dimensional neutron-flux-evaluation.

At the moment the already mentioned three dimensional computer codes KASY, D3D and KADI store the results on external data files. Only one computer code will do the evaluation for all three dimensional programs.

Only few conventions for the arrangement of the three dimensional flux-distribution on the external file have to be observed, depending on the actual geometry and the sequence of the energy group.

This evaluation code is AUDI3. Global evaluation is possible with AUDI3 as well as local evaluation. The following first set of possibilities for the evaluation of three dimensional neutron flux distributions is given

- a) Output of neutron-flux results in given regions and along given traverses parallel to the coordinate directions. The latter also in flux-maps on the plotter.
- b) Flux integrals for reactor-zones of constant material-compositions
- c) Neutron lifetimes
- d) Fractions of delayed neutrons
- e) Reaction rates and densities and also sums and combinations of reaction rates.

It is intended to incorporate also a three dimensional perturbation part in AUDI3.

3.2.2. SN - codes

The one dimensional transport code DTK / 3.86 / has been developed from the well known DTF-IV-Code. DTK differs from the DTF-IV-Code in the following essential features:

- a) DTK has "interfaces" with the program system NUSYS (see section 3.7.1.)
- b) An improved initial source guess has been built in.
- c) A variety of buckling options has been incorporated.
- d) In plane geometry, the user may prescribe the incoming energy - and space-dependent angular flux at the right boundary.
- e) Chebyshev extrapolation for the outer iterations has been built in.
- f) It is possible to pass fluxes from one case to another. If SN-Order and the number of intervals do not agree, DTK is able to interpolate.

The two dimensional transport code SNOW /3.87 / has been developed at Karlsruhe. It is able to work with all standard geometries and to perform nearly all calculations for physical and design calculations. By this it differs only little from other two dimensional codes. We draw the attention only to some aspects concerning the methods incorporated in SNOW.

- a) Chebyshev extrapolation is used for the inner and the outer iterations and this option is working very well in contradiction to other codes, where this acceleration method is reported to fail.
- b) A package of interpolating routines, incorporated in SNOW, permits that scalar fluxes and angular fluxes at the non-vacuum-boundaries may be passed from cases with lower SN-order and a small number of intervals to cases with higher SN-order and more intervals. The careful use of this interpolating method has given an immense saving of computing time, often about 50 %, independent of other acceleration methods /3.88 /.

We yet found other aspects which enforced the use of this method. It turned out that a rigorous use of the interpolating method provides a sequence of approximate solutions (Keff, etc.) of the problem; its behaviour may provide information on how accurate the solution of the nondiscretized problem is approximated.

Secondly, an assumed sequence of interpolating steps with increasing SN-order and increasing numbers of points is used and it proves that the final step has been chosen too large, that means that a smaller number of points would have been sufficient to produce a special result. If the interpolating method is used, the large step is consuming only a small amount of computing time.

We tested many procedures proposed to avoid negative fluxes and the ray-effect in two dimensions. We are convinced that there are until today no satisfactory remedies to prevent the user from these troubles. Beyond all we found that some special negative-flux-fixup-procedures caused incorrect solutions for symmetrical problems (symmetry with respect to the line $x = y$ in plane geometry).

At present, a stationary one dimensional transport code is developed for multigroup problems (>200 groups) with energy-dependent meshsize, so that for distinct groups different numbers of intervals can be specified. This will enable the user to choose a conventional meshsize for the most groups and to use e.g. 1000 points for some groups. We believe that further efforts must be made to achieve the same accuracy in source problems with small or absent multiplication as in problems with multiplication.

3.2.3. Monte Carlo techniques

Work on fast reactor Monte Carlo (MC) codes in Germany has to some extent consisted in the adaptation of foreign codes, e.g. the MORSE code. Independently MC-codes have been developed at INTERATOM and Karlsruhe. These codes differ in many aspects.

The Karlsruhe Monte Carlo Code KAMCCO uses a continuous energy model and fully includes time dependence. This code development had a threefold target:

- 1.) Provide a means for analysing fast neutron experiments, especially time-dependent pulsed neutron problems,
- 2.) Checking nuclear data available in KEDAK format,
- 3.) Checking other computation techniques.

In consequence of 2.) and 3.) many commonly accepted approximations have been intentionally avoided. Thus, the angular dependence in elastic scattering and the cross sections in the unresolved resonance region are kept in an essentially unapproximated form. In KAMCCO neutrons carry energy, time and a weight as continuous variables. Russian roulette and non-analogue techniques for treating capture are used to an extent specified input. KAMCCO has 2 options. In option 1 a generation cycle (or source iteration) scheme is used, similar to the TIMOC scheme /3.26/. A pool of fission neutrons is established and constantly updated with new coordinates of fractionally generated neutrons. The pool is made stationary by cyclic addition and anti-cyclic extraction of fission neutron coordinates.

KAMCCO option 2 follows a census time scheme, i.e., neutrons with pre-determined source coordinates are started at time $t = c$. These neutrons, and also all daughters from fission, are pursued up to a given time limit. Additional features, included only in this option, are splitting and the MELP-leakage estimator /3.27./. These features become effective to a degree determined by input.

Preferred applications are the calculation of criticals and checking of nuclear data for option 1 and calculations connected with experiments, especially of the pulsed neutron type, for option 2. The geometry package can deal with all assemblies that are subdivided into regions bounded by first and second order surfaces. Void volumes can be included, standard boundary conditions are total absorption (vacuum) or reflection on planes.

Nuclear data sets for KAMCCO runs are prepared from data in KEDAK format (see 3.1.1.) by the code DASU and associated codes. During the random walk cross sections are computed on a per isotope basis from data in core storage. For each isotope and each cross section type a specific energy grid is used which allows linear interpolation in the non-resonance energy regions. In the region of widely spaced resonances cross sections are computed from a limited number of contributing resonances using a Breit-Wigner single level formalism (Doppler-broadening is optional). In the region of narrowly-spaced resonances cross sections are randomly chosen from probability tables. Such tabulations, which allow also energy and temperature interpolation, have been set up for the Pu- and U-isotopes with an auxiliary MC program DISTRESS.

Inelastic scattering is performed on discrete levels or, at high energy, through the evaporation model. Elastic scattering retains first order anisotropy in the center-of-mass system and involves transformation to the lab system.

At each collision the reaction type is chosen with a suitably modified probability, so that the resulting neutron weight after the collision becomes independent of the isotope and reaction type involved. This feature efficiently

reduces the variance otherwise connected with $(n, 2n)$ - and fission collisions.

During the random walk all relevant coordinates and data are placed in a buffer field, which is asynchronously analyzed by a package of estimation routines. The types of estimators and the quantities estimated are specified in detail by a separate input package. The user may choose the collision, the track length (=flux) estimator or an optimum linear combination of both.

Estimates may be obtained for integral parameters (k_{eff} , gain, loss, leakage, time to birth, time to death etc.) and for "differential" quantities. For this second group of quantities the random walk data can be analyzed with respect to spatial regions, energy and time intervals, isotopes and reaction types, singly and in combination. An advanced version of this estimation package also estimates quantities which are ratios of integrated rates as well as the associated statistical error.

The code is run on an IBM/370-165 and needs about 240 - 300 k bytes for routine jobs. No special work-files besides input and output are used. KAMCCO is written almost exclusively in IBM-FORTRAN IV. To a moderate extent use has been made of ASSEMBLER-routines, e.g. for dynamic storage allocation and data transfer as well as for random number generators and table look-up.

Table 3.1. shows some results. The remaining discrepancies against experiments and results obtained with the KFK INR-set are most probably due to uncertainties in nuclear data and/or differences in the data basis used. It should be mentioned also, that no heterogeneity corrections have been applied to these MC results.

Table 3.1. Results of Monte Carlo calculations with KAMCCO

Assembly	Computing time in min. (370-165)	k_{eff}	Statistical error δk (%)
GODIVA	8	0.994	0.20
TOPSY	8	0.993	0.57
JEZEBEL	8	0.981	0.17
POPSY	8	0.974	0.62
SUAK U1B	8	0.830	0.49
SUAK UH1B	8	0.893	0.56
SNEAK 3A1	8	0.999	1.10
ZPR III-48	17	0.989	0.81

The Monte Carlo computer programs developed at INTERATOM have in common a reactor model which consists of a number of different volumetric elements, i.e. rectangular or hexagonal cells. Such cells may contain standard internal structures. The energy is treated in the multigroup model; the angular dependence of scattered neutrons is correct with respect to the zero- and first- order Legendre polynomials in laboratory system. Standard multigroup cross sections are part of the input.

The program MOCA solves the static Boltzmann equation in order to estimate the eigenvalue k_{eff} as well as reaction rates in selected reactor zones (which should not be too small). This is done by following in parallel a fixed, sufficiently large, number of neutrons, called team or population, over many generations through the reactor. In these programs special emphasis has been placed on the possibilities to run problems without using an excessive amount of core storage and to decrease the remaining small systematic error, connected with this technique, by a post-iteration method involving only a moderate increase in the computing time /3.28./.

This team method /3.29/ is also used in MOCA to solve the neutron transport equation for subcritical assemblies with a fixed source distribution. The entire range $0 < k_{\text{eff}} < 1$ is covered and as $k_{\text{eff}} \rightarrow 1$, the method changes automatically to that of the homogeneous problem.

The program PUNKT-MOCA, an adjoint MC code, has been developed to calculate specifically the average flux in a single region of a reactor which is critical or made critical by adjustment of ν . This region may also be a point. Arbitrary flux-weighting with respect to the energy is included. Of course, to get meaningful results for the flux distribution several point values have to be estimated. PUNKT-MOCA also uses the team-method however, the neutrons undergo a reverse transport process (adjoint game) and are weighted with a roughly estimated energy-independent flux distribution. In small reactors (diameter < 100 mean free paths) this estimate is of no importance and may be constant. The required computing time for a statistical error (standard deviation) of 5 % is less than 5 minutes (CDC 6400) for one value of the pointwise flux distribution or of a region average. The MOCA code has been in use as a standard tool for SNR or KNK design calculations (KNK is the compact sodium cooled reactor at Karlsruhe).

3.3. Theoretical foundation, code development,
and application of flux synthesis methods

In the last few years synthesis methods have been developed for approximately solving the three-dimensional diffusion equation and the one-dimensional Boltzmann equation. These synthesis methods are based on the expansion of the unknown solution in known expansion functions or modes and unknown coefficient functions, and result in some reduced systems of equations from which the coefficient functions can be determined. The solutions of these reduced systems of equations can be obtained with considerably smaller computational effort than those of the original equation. A short survey of most of the methods proposed in the last time is given by M.L. Steele in "Reactor Technology" /3.30/.

A systematic discussion of the theoretical foundation for various flux synthesis methods has been performed for the solution of the one-dimensional steady state neutron transport equation for slabs as well as for the solution of the steady state multi-dimensional diffusion equation. Different physics situations have been considered with emphasis on fast breeder reactors. Several serious anomalies have been found and are mentioned.

In order to get experience for synthesis calculations several test-codes to solve the Boltzmann equation have been developed, and also a three-dimensional diffusion equation synthesis code development effort for various geometries and boundary-conditions has been accomplished and is described in this chapter.

Flux synthesis results are compared on the one hand with S_N calculations and with fine mesh diffusion theory difference equations methods on the other hand.

3.3.1. Problem definition and introduction of general flux

synthesis methods for the diffusion theory model.

The static neutron flux distribution for large fast breeder reactors can be obtained with reasonable accuracy as solution of the multigroup diffusion equations. Numerical calculations will always require a discretization of the problem, therefore the attention will be restricted to the discrete form of the multigroup diffusion equations only. In matrix form these equations can be written as follows:

$$A \phi = \frac{1}{k} B \phi \quad (1)$$

The order I of the square matrices A and B is equal to the number of energy-space meshpoints. A includes diffusion, removal, and scattering processes, whereas B represents the fission processes. ϕ is a column vector representing the neutron flux at the I energy-space meshpoints. k is the eigenvalue (k -effective) of the problem.

It has been shown /3.31/ under very weak assumptions (including arbitrary scattering matrices, general fission transfer matrices, interior nondiffusion regions, non-transitive but weakly connected problems, etc.) that Eq. 1 has the following existence, unity, and positivity properties:

Properties (P)

1. There exists a unique eigenvector $\phi_1 \geq 0$, $||\phi_1|| = 1$.
2. $\phi_1 > 0$.
3. The corresponding eigenvalue k_1 is simple and $k_1 > |k_i|$ for $i \neq 1$.

These properties are very important from a theoretical and a practical point of view. From a theoretical point of view a rigorous mathematical understanding of the criticality phenomena for the discrete diffusion theory model is achieved; from a practical point of view the convergence of several iterative solution methods is guaranteed.

For three dimensional problems the number of energy-space meshpoints I can be very large (10^5 to 10^6) and it would be time consuming to solve Eq. 1 by an iterative procedure. Flux synthesis methods can be a very efficient alternative for the solution of Eq. 1 and will be introduced here in a general form:

Two rectangular $I \times R$ ($R < I$) matrices T and W of rank R are considered. The column vectors of T (W) may represent the R basic trial (weight) functions which are assumed to be known. Then the flux vector ϕ can be expanded as follows:

$$\phi = T \underline{d} \quad , \quad (2)$$

where \underline{d} is an unknown column vector of order R (driving coefficients). If one multiplies Eq. 1 from left by W^* (the transposed matrix W) and inserts ϕ from Eq. 2 into the resulting equation, one obtains the general form of the discrete flux synthesis equation:

$$(W^*AT) \underline{d} = \frac{1}{\lambda} (W^*BT) \underline{d}. \quad (3)$$

This is an eigenvalue problem for the unknown column vector \underline{d} of order R . The eigenvalue λ has been distinguished from k because in general the eigenvalues λ are different from the eigenvalues k . For most synthesis methods R will be chosen much smaller than I and one would expect that it is easier to solve Eq. 3 than to solve the original problem.

This formulation of flux synthesis methods is rather general and includes all the wellknown synthesis techniques (coarse mesh rebalancing, coarse mesh Galerkin, Bettis type blending, multichannel blending with discontinuous trial functions, etc.) as special cases /3.32/.

3.3.2. State of the art for various flux synthesis methods and different physics situations.

For a long time it had become something of a folk theorem that the linear independence of the basic trial functions and also of the basic

weight functions would guarantee the success of flux synthesis methods, and that adjoint weighting would be generally preferable to Galerkin methods. These widespread opinions are simply not true, as has been shown by proper counter examples /3.33-34/.

From a theoretical and practical point of view it appears to be necessary that the synthesis equation 3 has the properties (P), which were presented in the previous section for Eq. 1. With non-negative basic trial functions this would guarantee that the synthesized flux $\phi = T \underline{d}$ is non-negative, and it would also imply the convergence of the power iteration procedure or of an appropriate Wielandt iteration procedure for Eq. 3 to the fundamental eigenvector \underline{d}_1 (>0) and the eigenvalue λ_1 (>0).

The state of the art for various flux synthesis methods and different physics situations has been summarized in Tables 3.2 and 3.3. The information is presented in a somewhat condensed form and needs further explanation:

THEORY means the status of theoretical foundation. If the entry says COMPLETE, then it has been proven that the corresponding synthesis equation 3 has the properties (P). The entry "A $\phi_a \geq 0$, $\nexists 0$ COMPLETE" is a short notation for the fact that the synthesis equation possesses the properties (P) if the additional assumptions A $\phi_a \geq 0$, A $\phi_a \nexists 0$ are fulfilled for the approximative flux vector ϕ_a . The entry NEGATIVE EIGENVALUE (FLUX) POSSIBLE indicates that a counter example or anomaly has been found with a negative eigenvalue λ which is largest in modulus (with a partly negative and partly positive flux corresponding to the largest eigenvalue).

EXPERIENCE is an abbreviation for numerical experience and the corresponding entry should indicate whether or not anomalies have occurred for realistic numerical calculations and how much numerical experience has been gained.

One observes that the coarse mesh rebalancing method (Table 3.2) has a complete theoretical foundation and the numerical experience is good for all physics situations. Coarse mesh rebalancing methods have been used most successfully for convergence acceleration of iterative

TABLE 3.2 THEORETICAL FOUNDATION AND NUMERICAL EXPERIENCE FOR COARSE MESH METHODS

PROBLEM TYPE		COARSE MESH REBALANCING	COARSE MESH GALERKIN
ONE GROUP	THEORY	COMPLETE	COMPLETE
	EXPERIENCE	GOOD	GOOD
DOWN SCATTERING NO GROUP COLLAPSING	THEORY	COMPLETE	COMPLETE
	EXPERIENCE	GOOD	GOOD
DOWN SCATTERING WITH GROUP COLLAPSING	THEORY	COMPLETE	NEGATIVE EIGENVALUE POSSIBLE. $A\phi_a \geq 0, \neq 0$, COMPLETE.
	EXPERIENCE	GOOD	PARTLY BAD
UP AND DOWN SCATTERING NO GROUP COLLAPSING	THEORY	COMPLETE	NEGATIVE EIGENVALUE POSSIBLE. $A\phi_a \geq 0, \neq 0$ COMPLETE.
	EXPERIENCE	GOOD	LIMITED
UP AND DOWN SCATTERING WITH GROUP COLLAPSING	THEORY	COMPLETE	NEGATIVE EIGENVALUE POSSIBLE. $A\phi_a \geq 0, \neq 0$ COMPLETE
	EXPERIENCE	GOOD	LIMITED

TABLE 3.3 THEORETICAL FOUNDATION AND NUMERICAL EXPERIENCE FOR BLENDING METHODS.

PROBLEM TYPE		GALERKIN	ADJOINT
ONE GROUP	THEORY	LARGEST POSITIVE EIGENVALUE. NEGATIVE FLUX POSSIBLE.	LARGEST POSITIVE EIGENVALUE. NEGATIVE FLUX POSSIBLE.
	EXPERIENCE	GOOD	GOOD
DOWN SCATTERING NO GROUP COLLAPSING	THEORY	LARGEST POSITIVE EIGENVALUE ? NEGATIVE FLUX POSSIBLE.	NEGATIVE EIGENVALUE POSSIBLE. NEGATIVE FLUX POSSIBLE.
	EXPERIENCE	GOOD	GOOD
DOWN SCATTERING WITH GROUP COLLAPSING	THEORY	NEGATIVE EIGENVALUE POSSIBLE. NEGATIVE FLUX POSSIBLE.	NEGATIVE EIGENVALUE POSSIBLE. NEGATIVE FLUX POSSIBLE.
	EXPERIENCE	PARTLY BAD	PARTLY BAD
UP AND DOWN SCATTERING NO GROUP COLLAPSING	THEORY	NEGATIVE EIGENVALUE POSSIBLE. NEGATIVE FLUX POSSIBLE.	NEGATIVE EIGENVALUE POSSIBLE. NEGATIVE FLUX POSSIBLE.
	EXPERIENCE	LIMITED	LIMITED
UP AND DOWN SCATTERING WITH GROUP COLLAPSING	THEORY	NEGATIVE EIGENVALUE POSSIBLE. NEGATIVE FLUX POSSIBLE.	NEGATIVE EIGENVALUE POSSIBLE. NEGATIVE FLUX POSSIBLE.
	EXPERIENCE	LIMITED	LIMITED

finite difference solution techniques. Coarse mesh Galerkin methods (Table 1) have a complete theoretical foundation for downscattering problems without group collapsing and the numerical experience is good for these physics situations. For all the other physics situations an additional assumption is needed to guarantee the property (P), but the numerical experience is partly bad or limited.

The theoretical foundation of blending methods (Table 3.3) is in an unsatisfactory state. Anomalies have been found for many situations /3.32-36/. Sufficient conditions for properties (P), or at least for the existence of a largest positive eigenvalue, are desperately needed but almost unknown.

For fast breeder reactors downscattering problems with and without group collapsing are of interest. One observes that anomalies have been found for problems with group collapsing for blending methods with Galerkin or adjoint weighting.

For downscattering problems without group collapsing an anomaly has been discovered for the case of adjoint weighting but fortunately the numerical experience for realistic problems has been good. For downscattering problems without group collapsing and Galerkin weighting it has not been proved that a largest positive eigenvalue will always exist, but on the other hand no counterexample has been discovered so far as we know. For this case most of the computer program development has been done and the numerical experience is extensive and good /3.37/.

Flux synthesis blending methods with group collapsing have also been successfully applied to fast reactor problems by skilled researchers /3.37-39/ but recently very serious anomalies have been discovered /3.33/. Practically useful sufficient criteria for avoiding anomalies in this case are needed.

3.3.3. Development of the computer program KASY.

The computer program KASY (Karlsruhe Synthesis Program) has been developed mainly for fast reactor applications. KASY uses a flux synthesis blending method without group collapsing for downscattering problems.

It has been shown in the previous section (see also Table 3.3) that for the case of Galerkin weighting there is no proof available guaranteeing the existence of a largest positive eigenvalue and on the other hand no counter example has been discovered. This fact is another motivation for the development of KASY, because it is desirable to have a tool available for gaining numerical experience. The mathematical background of the computer program KASY, including the discrete formulation, is described by KAPLAN in /3.40/. The three-dimensional flux-distribution $\phi(X,Y,Z)$ is expressed (also for a discrete net) in the following manner:

$$\phi^g(X,Y,Z) = \sum_k H_k^g(X,Y) \cdot Z_k^g(Z)$$

In this representation, the $H_k^g(X,Y)$ are k precalculated energy-group dependent, linearly independent two dimensional basic trial-functions, g is the index of the energy-group. The $Z_k^g(Z)$ are the mixing- or driving-functions, which have to be determined, and which correspond to the column vector \underline{d} in Equation 2.

In principle any mathematical function of X and Y which fulfills the boundary conditions of the problem may serve as basic trial-function. In connection with KASY, however, such a trial-function is usually a flux-distribution, obtained as solution of the energy-group dependent diffusion equations in two dimensions by use of a two-dimensional diffusion computer program.

The advantage of using such basic trial-functions instead of a complete system of orthonormal mathematical functions, is, that the physics properties of the considered assembly are contained in the trial-functions. There is good reason to hope, that the number of such trial-functions needed to guarantee good results is much smaller than the number of pure mathematical functions required.

To "improve" the condition of linear independence of the basic trial-functions the computer program KASY contains an option to orthonormalize these trial-functions with a so called modified GRAM-SCHMIDT method, described by I.R. RICE in /3.41/. It has been shown /3.42/ that this orthonormalisation accelerates the convergence of the power method used

in KASY, to solve the discrete synthesis equations in order to determine the mixing-functions $Z_k^g(Z)$.

To get the opportunity to compare results of various synthesis techniques, in addition to Galerkin weighting also adjoint weighting and weighting with special mathematical functions is possible in KASY. Synthesis calculations are possible for four different geometries:

- 1.) $(X,Y/Z)$, basic trial-functions in (X,Y) -coordinates, synthesis-direction Z .
- 2.) $(R,\theta/Z)$, basic trial-functions in (R, θ) -coordinates, for sectors with $\theta_{\max} \leq 2\pi$, synthesis direction Z .
- 3.) $(R,Z/\theta)$, basic trial-function in (R, Z) -coordinates, synthesis direction θ .
(This unusual geometry has been included to allow for example the convenient treatment of assymmetricly arranged control rods.)
- 4.) (Δ/Z) , basic trial-functions in regular triangular coordinates, synthesis-direction Z .

The symbols in front of the slash describe the coordinate dependence of the basic trial-functions and the letter behind the slash gives the synthesis direction.

Four outer boundary conditions are provided in KASY: zero flux, zero current or group-dependent extrapolation distance at the upper and lower boundaries in $(X,Y/Z)$ -, $(R,\theta/Z)$ - and (Δ/Z) -geometry, and also joining conditions, i.e. continuity of flux and current at $\theta=0$ and $\theta=2\pi$, in $(R,Z/\theta)$ geometry. (The boundary conditions at the other boundaries must be fulfilled by the basic trial-functions).

There are no limitations for the number of energy-groups and down-scattering of neutrons is allowed from any energy-group to any other. (e.g. 26 energy-groups could be used).

In KASY there are also no explicit restrictions with regard to the maximum number of mesh-points, zones of constant material distributions, material-mixtures and trial-functions. Implicit restrictions are only given with regard to the running-time and the working space in the core-storage of the computer. KASY turns automatically to external storage devices,

if there is not enough free space; but it should be mentioned that naturally a certain, problem-dependent minimum amount of core storage is always necessary. (With regard to the IBM Job-Control-Language these external storage devices must be defined in such cases).

Experience has shown, that the typical running time for one synthesis calculation is in the same range as the running-time needed for the calculation of one two-dimensional basic trial-function. This statement is approximately independent of the numbers of mesh-points, energy-groups, and trial-functions.

For synthesis calculations the preparation of the basic trial-functions consumes the major part of the total running-time. Concerning running-time it is a great advantage that KASY is able either to use the basic trial- and/or weighting functions of a previous run for another following run or to replace only some basic trial-functions by others. In comparison to this, completely new three-dimensional calculations (eventually with a better initial flux guess) have to be performed by computer programs which solve the fine mesh difference equations iteratively.

3.3.4 Comparison of the results of the flux synthesis method with those obtained by iterative solution methods of fine mesh difference equations.

To get an idea of the accuracy of the results (effective multiplication factor, normalized flux, capture and fission rates) obtained by the flux synthesis computer program KASY, comparisons with the results of fine mesh difference equations methods and also with measurements have been carried out, /3.43-47/. Only the results of KASY with those obtained by the computer program TRITON/3.48/ in its version used at Fa. BELGONUCLEAIRE, BRUXELLES, will be compared here. Unfortunately this three-dimensional fine mesh difference equations program has severe limitations: the number of mesh points is bounded by 8000, the number of energy-groups by 5. Therefore, one had to look for a rather simple assembly and it was decided to use a modified model of the ZPR-III-48 with a 370 liter UC- PuC core and the insertion of only one B_4C control-rod with sodium-steel follower at the center of the core. It has not been the intention to calculate the ZPR-III-48 assembly exactly, but to have the same discrete model for the various calculation

methods. The calculations have been performed in (X,Y,Z)-geometry by the code TRITON and in (X,Y/Z) and (Δ /Z) geometry by the code KASY.

The proper selection of the number and nature of the basic trial functions is very important. All basic trial-functions used are two-dimensional flux-distributions for 5 energy-groups, calculated by the two-dimensional diffusion program DIXY/3.49/ in (X,Y)-geometry and by the two dimensional diffusion program TREPAN/3.50/ in (Δ)-geometry.

These basic trial-functions may be grouped into two categories: Core functions and blanket-functions with absorber- or follower material respectively at the central position of the rod.

Fig.3.4 shows the modified model of the ZPR-III-48 assembly in (X,Y,Z)-geometry and also the planes for which the trial-functions have been calculated. The following numbers have been used for the different basic trial-functions.

- 1) core with follower, axial buckling $B^2 = 0.00088 \text{ cm}^{-2}$
- 2) core with absorber-rod, axial buckling $B^2 = 0.00088 \text{ cm}^{-2}$
- 3) blanket with follower, axial buckling $B^2 = 0$
- 4) blanket with absorber-rod, axial buckling $B^2 = 0$

As the geometrical model of the ZPR-III-48 used for these comparison is mainly an axial-symmetric one, two-dimensional results obtained by DIXY-RZ calculations have been taken into consideration.

Table 3.4 shows that the k_{eff} and Δk values agree very well for TRITON, KASY-(X,Y/Z) and KASY- (Δ /Z). For DIXY -(RZ) the model is slightly different what may explain the difference in k_{eff} , but the Δk values are still in very good agreement.

Table 3.5 shows the maximum deviations of fission and capture rates between KASY-(X,Y/Z) and TRITON results. It is worth mentioning that larger deviations do appear only in the corners of the core (7 percent) and of the blankets (66 percent).

TABLE 3.4 k_{eff} and Δk comparison of KASY, TRITON, and DIXY-RZ results for a modified model of ZPR-III-48

	k_{eff}			$\Delta k \cdot 10^4$		Total Computer time (minutes)	Computer used
	Rod out	Rod half in	Rod in	Rod out Rod half in	Rod out Rod in		
TRITON	0.9889	0.9782	0.9683	107.0	206.0	79.0	IBM 360/65
KASY-XY/Z trial-functions 1,2	0.9883 1	0.9776 1,2	0.9677 2	107.0	206.0	5.5	IBM 360/65
KASY-XY/Z trial-functions 1,2,3,4	0.9886 1,3	0.9779 1,2,3	0.9680 2,4	107.0	206.0	7.7	IBM 360/65
KASY-Δ/Z trial-functions 1,2	0.9909 1	0.9801 1,2	0.9699 2	108.4	210.1	2.8	IBM 360/85
KASY-Δ/Z trial-functions 1,2,3,4	0.9914 1,3	0.9805 1,2,3	0.9704 2,4	108.7	209.9	4.3	IBM 360/85
DIXY-RZ	0.9751	0.9642	0.9542	108.3	208.9	0.5	IBM 370/165

TABLE 3.5 Maximum-deviations in the fission and capture rate:

$$\frac{F_{KASY-X,Y/Z} - F_{TRITON}}{F_{TRITON}} \text{ in } \% /14/ \text{ for a modified model of}$$

ZPR-III-48, rod half in.

Zones or boundaries	Largest deviations in %
	<u>fission rates</u>
1. Core, inner part	0.9
2. Core, inner and outer radial boundaries	2.4
3. Core, upper and lower planes	1.6
4. Core, "Corner points"	7.0
5. Radial blanket, surrounding the core	6.0
6. Axial blanket, surrounding the core	10.0
7. Blanket corners	66.0
	<u>capture rate</u>
8. Control rod in the core	1.0
9. Control rod in the blanket	6.0

Some additional remarks:

The convergence criterions used in all the calculations has been $< 10^{-4}$ for two successive values in k_{eff} . All calculations have been performed in a 5 energy-group representation:

group 1 :	10.5	MeV	-	0.8	MeV
group 2 :	800	keV	-	100	keV
group 3 :	100	keV	-	10	keV
group 4 :	10	keV	-	1	keV
group 5 :	1	keV	-	0	

Calculations for (X,Y,Z) geometry have been done with $20 \times 20 \times 20$ mesh points for the half inserted rod and $20 \times 20 \times 10$ mesh points and symmetry-conditions for the fully - and for the not-inserted absorber-rod.

For (Δ /Z) geometry $24 \times 24 \times 20$ or $24 \times 24 \times 10$ mesh points respectively have been taken and for the DIXY-(RZ) calculations 20×24 or 20×12 mesh points respectively have been used.

3.3.5 Half-Range expansion for approximately solving the neutron transport equation for slabs

Whereas the general procedure of synthesis methods for the solution of the Boltzmann equation is well known the methods have been applied only to rather simple examples (monoenergetic Milne and slab problems). To get a better insight into the nature and the difficulties of these methods which seems necessary before treating two-dimensional problems, we have established four different half-range expansions for approximately solving more realistic multigroup slab problems with inhomogeneous boundary conditions. The expansions are of a special form. The expansion functions - to be chosen by the user well suited to the problem to be solved - are either space-dependent or angle-dependent and optionally in both cases in addition energy-dependent functions, which can take into account all the user's knowledge or "physical feeling" of the special problem.

The resultant reduced systems of equations, from which the unknown coefficient functions must be determined, are then systems of Fredholm integral equations. The size of these systems depends on whether the expansion functions are energy-dependent or not. If the energy-dependence is taken into account by the expansion functions, the coefficient functions do not depend on the energy variable and the resultant reduced systems are of small size and can be regarded as reduced "one-group-problems". In the other case, when the energy-dependence is treated more exactly by energy-dependent coefficient functions, the resultant reduced equations are of larger size and can be regarded as reduced "multigroup problems".

Due to the half-range expansion technique it is always possible to satisfy exactly homogeneous or any inhomogeneous boundary conditions.

By applying these methods to some representative problems we obtained the following general conclusion:

If the expansion functions - space-dependent, angle-dependent, space- and energy-dependent or angle- and energy-dependent - are chosen carefully, that is well suited to the problem to be solved, the results obtained are nearly as accurate as those of S_N -calculations of high order, whereas the required computing time is much less than that required by the S_N -calculations of high order.

These general conclusions are illustrated by the following example, precisely described in /3.51/. The angle- and space-dependent neutron-distribution was calculated for a 50 cm thick natural-uranium slab in a 26 energy-group presentation. The neutrons fall into this slab from one side with an isotropic angular-distribution. The energy-distribution is the same as the fission spectrum.

Figure 3.5 shows the angular-distribution of the neutron-flux in the natural-uranium slab in a distance of 5 cm from the surface for the first and the tenth energy-group; Fig. 3.6 shows the same picture in a distance

of 20 cm from the surface.

In these figures the results of various synthesis methods and various degrees of approximation are compared with a S_{16} calculation as reference solution.

The meaning of the particular notations in the figures is the following:

G means multigroup calculation.

E and Z distinguish the development of the neutron flux according to angle- or space-dependent trial-functions in the following manner:

Development according to angular-dependent trial-functions (E):

$$\Phi^g(x, \mu) = \sum_{i=1}^N \varphi_i^g(x) \psi_i^g(\mu)$$

with

$$\psi(\mu) = \frac{\mu a b^2 + b(1 + \mu^2(a^2 + b^2 - 1) - a^2)^{1/2}}{1 + \mu^2(b^2 - 1)} \quad \mu \in [p, q]$$

$$\psi(\mu) = 0 \quad \mu \in [-q, p]$$

with $p=0, q=1$ or $p=0, q=-1$

GEN as solution means the dependence on the following parameters:

$$(a_1^+, b_1^+, a_1^-, b_1^- \dots a_N^+, b_N^+, a_N^-, b_N^-)$$

where N is the degree of approximation.

Development according to space dependent trial-functions (Z):

$$\bar{\Phi}^g(x, \mu) = \sum_{i=1}^N (\varphi_i^{g+}(x) \psi_i^{g+}(\mu) + \varphi_i^{g-}(x) \psi_i^{g-}(\mu))$$

with $\varphi(x) = e^{\alpha x} - e^{\beta d} \quad (0 \leq x \leq d)$

GZN as solution means the dependence on the following parameters:

$$(\alpha_1^+, \alpha_1^-, \dots, \alpha_N^+, \alpha_N^-).$$

N is again the degree of approximation.

β is another parameter to accomplish the boundary-conditions

with $\beta=\alpha$ or $\beta=0$.

The results of figures 3.5 and 3.6 are nearly as accurate as those of S_{16} calculations, whereas the computing time is comparable with those of S_4 calculations.

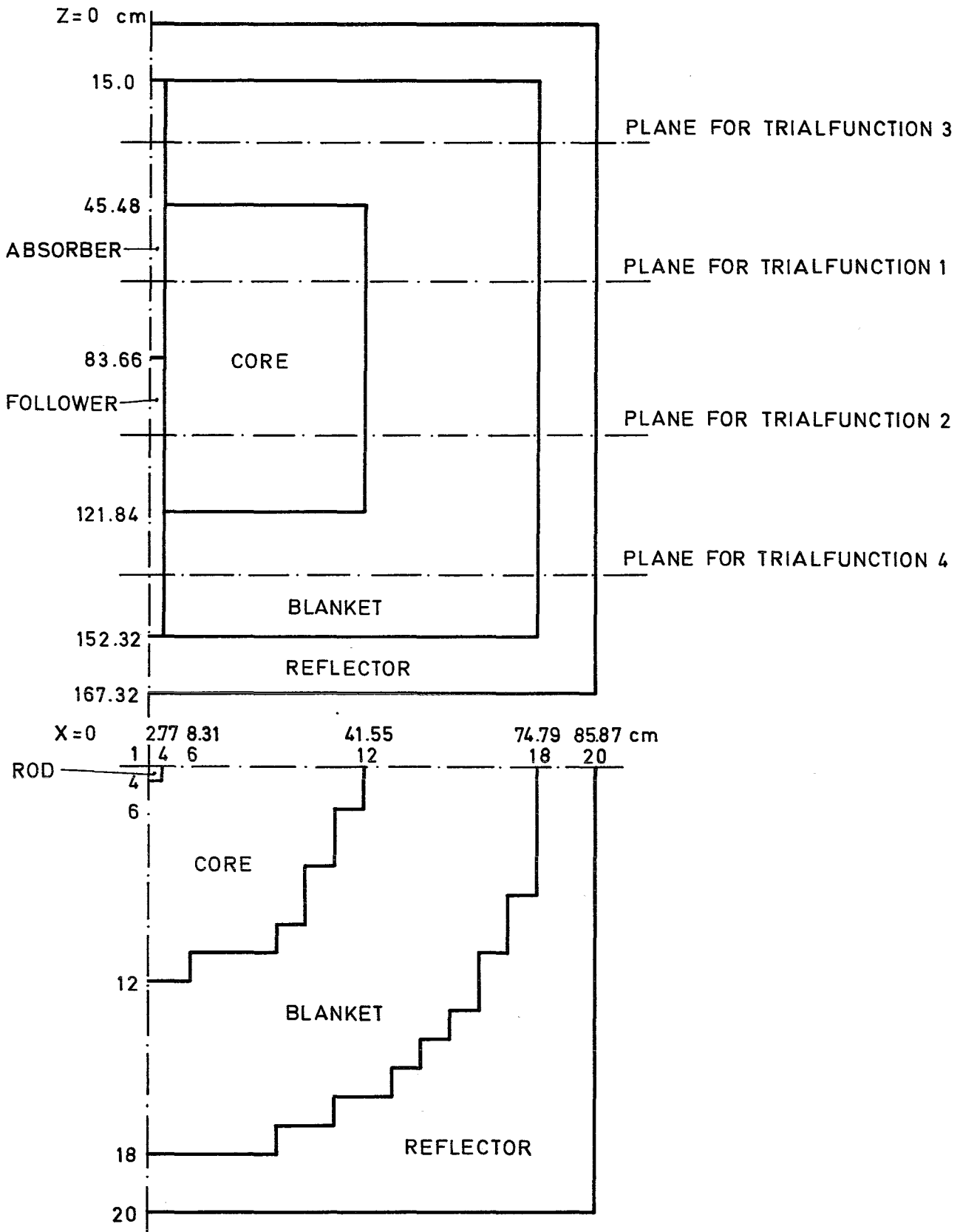


Fig. 3.4 Geometrical model ZPR - III-48 used for the comparison KASY-TRITON

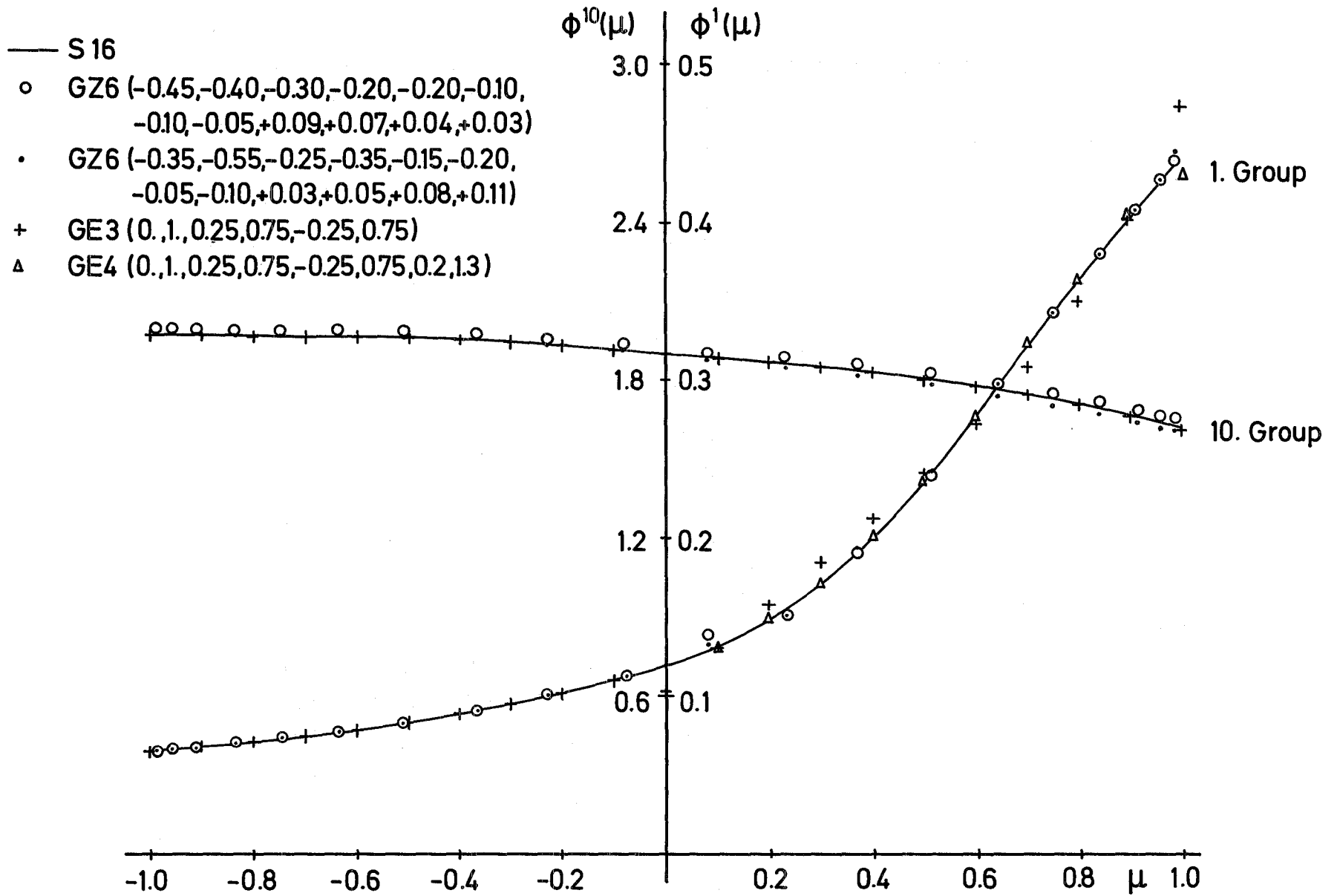


Fig. 3.5 Angular Distribution in a 50cm Uranium Slab (5cm inside)

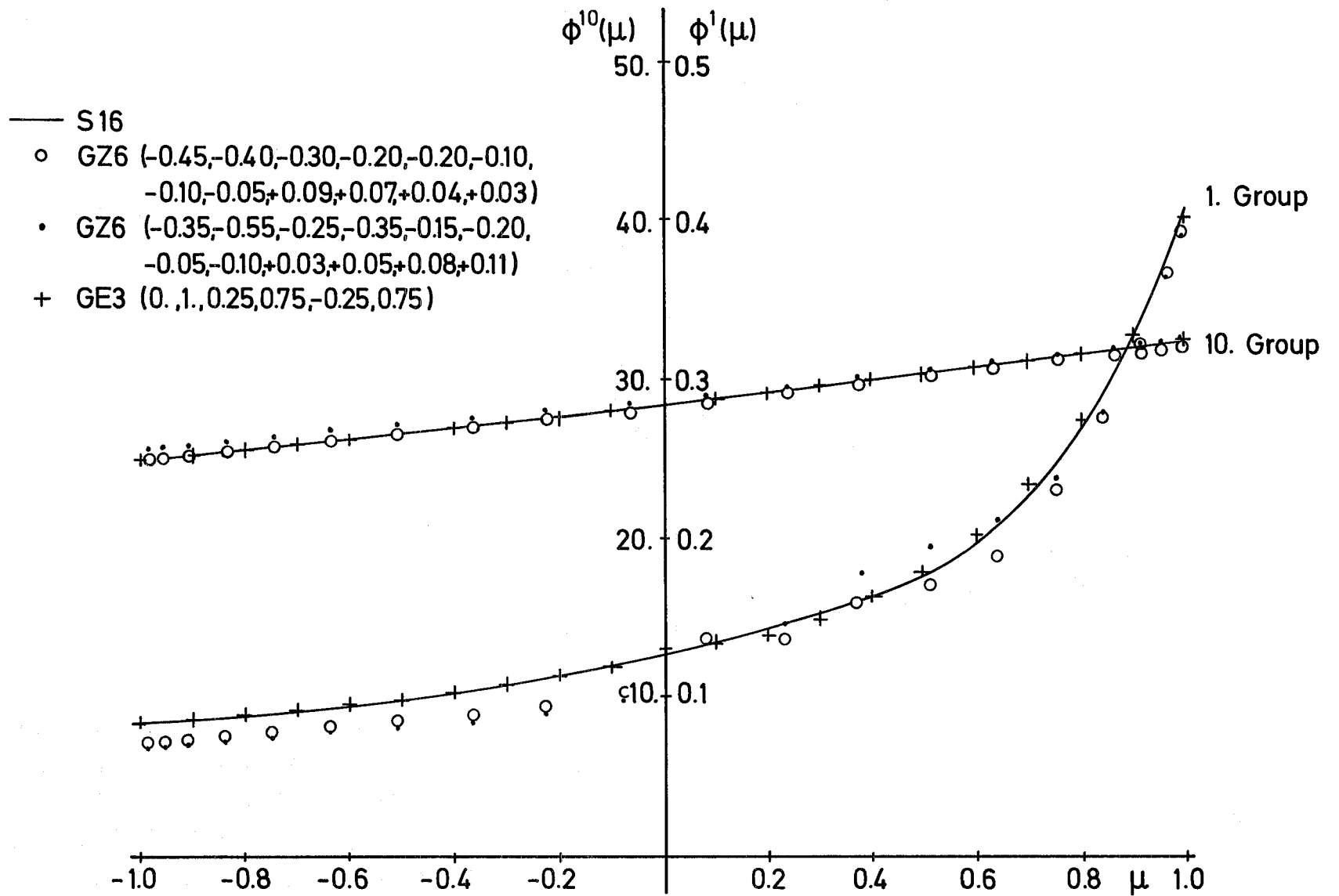


Fig. 3.6 Angular Distribution in a 50 cm Uranium Slab (20 cm inside)

3.4. Development of methods for the treatment
of special physical problems.

In this section those theoretical methods are described, which are required for an adequate analysis of fast zero power facilities and power reactors.

3.4.1. Kaper - A computer program for the analysis of experiments
performed in heterogeneous critical facilities

The KAPER program /3.52/ is a multigroup lattice code developed to analyze experiments performed in plate-type heterogeneous critical facilities. These experiments include those in which the flux fine structure in the lattice must be taken into account, as for example reaction rate and small sample reactivity worth measurements.

The program is a dynamically dimensioned code in an overlay structure. The three main segments consist of a procedure for the calculation of resonance self-shielded cross sections in the multiregion cell, a procedure for the calculation of the cell fluxes (real and adjoint) including reaction rates, and a procedure for the calculation of small-sample reactivity worths.

The fundamental basis of the program is integral transport theory in the collision probability formulation. The multigroup resonance self-shielded cross sections for the multiregion cell are defined by a procedure utilizing the concept of the composition-dependent self-shielding factor ("f-factor") for a homogeneous medium (see section 3.1). A consistent formulation for the heterogeneous medium was developed through the integration of the energy and space dependent integral transport equation. The method in KAPER represents an improvement in the method originally developed by Wintzer for his ZERA code /3.53/. Despite the fact that the f-factor concept represents an approximation in that it contains no information on the distribution of the resonances

of one particular isotope within an energy group, the experience has been that the accuracy and utility of the method for routine calculations is more than satisfactory.

The essential difference between the KAPER and ZERA codes lies in the fact that in KAPER the Boltzmann equation is solved in terms of the neutron flux, rather than the neutron source densities as done in ZERA. It must be emphasized that formally both concepts are equivalent within the narrow resonance approximation. However, it could be shown that the "flux equations" and the use of effective cross sections in KAPER (with the source density as a weighting function) yields more accurate results than the "source-density equations" and the use of reaction coefficients in ZERA. The reason is a relatively strong dependence of the reaction coefficients on the background cross section used in the f-factor concept. This is not the case in the consistent KAPER approach, where in addition the effective cross sections are only weakly dependent on the source density weighting function.

The program KAPER has a particular feature which allows one to calculate the flux distributions (real and adjoint) and reaction rates in a cell differing from the normal cells of the core. This feature has great utility for analyzing experiments that disturb the properties of the cell in the measurement procedure. For example, a cell or a portion of a cell, may be removed for the insertion of a channel in which reaction rates are to be measured with chambers, or in a reactivity worth measurement a low density plate of inert material may be inserted between two plates of the cell in the position in which a sample is to be placed. In both of these cases the periodicity of the cell is disturbed. To solve for the flux it is assumed that at some point removed from the disturbance the equilibrium spectrum of the normal core cell is reestablished. The equilibrium spectrum acts as an external source for the region of disturbance. Therefore the integral transport equation is solved in this region as a fixed source equation. This procedure was checked through a series of reaction rate measurements with thin foils between varying thicknesses of aluminum and stainless steel. The experimental results were well reproduced by the KAPER program.

Included in the KAPER program is a procedure to account for anisotropic diffusion of neutrons. In some experiments, such as sodium void measurements, this may be an important effect which results from the orientation of the plates in the facility. The components of the neutron diffusion, parallel and perpendicular to the plates, are calculated in the heterogeneous cell by utilizing the mean square distance between the collisions of the neutron in an energy group. The procedure is equivalent to the work of Benoist /3.54/ if one neglects the angular correlation terms. The procedure proved quite adequate for the analysis of an axial sodium void traverse experiment performed in the SNEAK fast critical assembly in which the plate orientation was rotated 90° between two experiments.

Reactivity worths are calculated with an exact perturbation formulation of the integral transport equation. By exact is meant that the perturbed flux and unperturbed adjoint are used in the formulation. The perturbed flux in the sample and sample environment is found by the same procedure utilized for the calculation of the flux in a cell different than the normal core cell as explained above.

The experience has been that the consistency of the calculated reactivity worth results improves by several percent, depending on the sample size and the core spectrum, over the results of the normally used first order homogeneous perturbation theory.

Contrary to almost all operating computer codes the KAPER program utilizes for each fissionable isotope its own fission neutron spectrum. This feature is found to be quite important in the calculation of reactivity worths; for example the calculations of the worth of a ^{235}U sample in a mixed oxide core where the major fission neutron contribution is from Pu. In this case the ^{235}U worth can vary by several percent depending on whether an average core fission spectrum, from Pu, is used or the fission spectrum for each individual fissionable isotope.

To demonstrate the improvement in KAPER over ZERA, k_{∞} was calculated for a cell similar to SNEAK-5C /3.55/. This was a null-reactivity assembly with a soft spectrum and strong heterogeneity effects, which contained mainly mixed oxide and graphite.

Table 3.6 shows the k_{∞} values obtained for cells of different thickness. The following comments can be made:

- a) As expected from the theory, all results for the quasihomogeneous case agree well. This indicates that no programming errors are involved.
- b) The two codes, ZERA and KAPER, using the same approximation for the collision probabilities, give k values which differ by 0.6 % for the full cell, and less than that for the smaller cells. Thus, the standard ZERA code may be used unless large heterogeneities are involved.
- c) The k_{∞} values before iteration on the source densities are given in brackets. The figures indicate that the changes due to the iteration are by one order of magnitude smaller than the difference in values given by the two codes. Therefore the iteration is necessary only in cases of large heterogeneity.

Table 3.6

k_{∞} for the SNEAK-5C Simplified Cell

Relative Thickness of the cell	ZERA		KAPER	
	k_{∞}	δk	k_{∞}	δk
10^{-3} (quasi homogeneous)	0.9342	--	0.9343	--
1/4	0.9640	0.0298	0.9627 (0.9628) ⁺	0.0284
1/2	0.9849	0.0507	0.9828 (0.9825)	0.0485
Full	1.0156	0.0814	1.0101 (1.0094)	0.0758

⁺) k_{∞} values in parantheses are values before iteration on the source densities

3.4.2. The use of a probability table method in calculating reaction rates.

The self-shielding factor concept, used in the ZERA and KAPER codes (see 3.4.1.), is an extremely useful tool for fast reactor calculations. Some modifications, superior to the Bell approximation, were made, necessary by the large heterogeneity effects for reaction rates in zero power fast reactors.

As already discussed in 3.4.1. our cell calculations are based on collision probability methods of integral transport theory. For such procedure the use of tabulated probabilities seems to be a rational approach. This also holds for Monte Carlo computations. Thus, probability table methods have been developed independently by Oosterkamp /3.56/, Levitt /3.57/ and Borgwaldt /3.58/, (see also 3.2.3.). Here we outline the proposal of Oosterkamp.

The collision rate of neutrons with the nuclei of a certain isotope is given by the integral over energy of the total cross section times the flux. It is assumed in the self-shielding factor concept that the flux in a group is inversely proportional to the total macroscopic cross section. The contribution of an energy interval to the reaction rate is thus not explicitly a function of energy. We can take, then, those energy steps with the same cross section value for a particular isotope together if we approximate the resonance cross section by a histogram.

We obtain then the probability that a random energy in the interval the value of the total cross section of the isotope lies in a chosen interval.

In a similar manner effective cross sections can be derived for capture and fission.

The Karlsruhe cross section sets used for the evaluation of fast reactor experiments are based on the f-factor concept. We decided,

therefore, to make a transformation from f-factors to probabilities and effective cross sections. Khairallah /3.59/ has shown that good agreement could be obtained by as few as 2 to 4 steps. We were mainly interested in very heterogeneous cells. Thus we required that not only good agreement be obtained for different background cross sections but also that the steps be not too large in order to follow accurately spatial transients. First we made a two step fit from which we determined maximum and minimum cross sections, assuming that we have a single level Breit Wigner resonance. The steps are then logarithmically spaced between these values and the probabilities are fitted. We required that no negative effective cross sections and probabilities exist and that the sum of the capture and fission cross section is not greater than the total cross section. It became obvious that the system was ill determined. By using a slowly converging process we obtain however "reasonable" results. The agreement with the tabulated f-factor for the reaction rates was better than 1 % (far better than the accuracy of the f-factors themselves). A maximum of seven steps was used with a factor of two to three between the steps.

An advantage of the probability table method is that there is no need to define a background cross section. The probability to have a certain cross section combination in a mixture is the product of the probabilities for the selected cross sections of each isotope, since the resonances of different isotopes in a mixture are not correlated.

The computer code REAC II uses this concept. Thus far modules to calculate k_{eff} , flux, adjoint and reaction rate for one dimensional plate geometry have been completed. The code uses collision probabilities and constructs then reaction matrices. The source densities are then iteratively solved. In a second phase the reaction rates are calculated. Typical running times for a 20 zone cell are 5 minutes on a IBM 370-165.

3.4.3. Many group perturbation calculations for the determination of reactivity coefficients.

It is well known that the reactivity worths of predominantly scattering nuclei are not well calculated in the usual coarse group scheme. Strictly, for the determination of reactivity coefficients the cross sections Σ or their differences $\delta\Sigma$ are weighted by the normal and adjoint flux, i.e. neglecting the space dependence, expressions of the form

$$\int dE \phi^+(E) \cdot \delta \Sigma(E) \phi(E) ; \int dE \int dE' \phi^+(E) \delta \Sigma(E'-E) \phi(E')$$

$$\int dE \int dE' \{ \phi^+(E) - \phi^+(E') \} \cdot \delta \Sigma(E'-E) \phi(E')$$

must be evaluated. The last expression makes evident that the slope of the adjoint flux, i.e. $d\phi^+(E)/dE$, is of extraordinary importance for the calculation of the corresponding quantity, called degradation term of the reactivity coefficient. This was the reason to study the influence of the energy resolution in the multigroup formalism on calculated central reactivity coefficients.

Here we studied the application of bilinear weighting for the first time for group collapsing using fine group representations of the normal and adjoint fluxes as weighting functions. The fine group lethargy width above 1 KeV approximately corresponds to $\Delta U = 0,05$. This work continues earlier studies of the same kind /3.60-3.61/ which were performed when only a 26 group energy scheme was available. In Table 3.7 the results of bilinear $(\phi^+ \phi)$ weighting are compared with those obtained using the usually applied normal flux (ϕ) weighting. This was done primarily for the determination of central reactivity coefficients in collapsed group structures.

From the results of Table 3.7 and further similar results it can be concluded, that as long as the central reactivity coefficients of predominantly fissile or absorbing materials are considered, flux

weighting is appropriate or at least sufficiently accurate for group collapsing. However, if the reactivity coefficients of predominantly scattering materials are to be determined precisely, flux weighting may become insufficient for group collapsing to, e.g., 26 coarse groups even in such cases where the fine group fluxes are accurately known, as in our example. Bilinear weighting is highly preferable in that case. In principle, the results of bilinear weighting for group collapsing to 26 groups in our case should be in exact agreement with the corresponding original fine group results. The minor deviations found in the last line of Table 3.7 are due to purely numerical effects.

As one might expect, the relatively bad agreement observed for the reactivity coefficients of predominantly scattering materials is caused by discrepancies in the coarse group adjoint flux.

When the coarse group adjoint flux is determined with flux weighted coarse group constants, the result does not agree with the average of the corresponding fine group representation. This is clearly demonstrated in Fig. 3.7 which shows that bilinear weighting leads to the correct average coarse group adjoint flux.

For reasons of completeness it should be mentioned that the results of Table 3.7 and Fig. 3.7 were obtained by fundamental mode diffusion calculations in multigroup formalism for the homogeneous composition accounting for the neutron leakage by using a group - independent buckling.

Table 3.7

Central Reactivity Coefficients for ZPR III-48

	Number of energy groups	Material									
		Al	B10	B11	C	Cr	Fe	Na	Ni		
CRC per atom normalized to B10	208	5.66	1000.	2.07	1.27	8.35	11.17	2.81	14.67		
Contribution of the degradation term to the total CRC	208	0.7116	0.0028	0.7134	0.4116	0.5285	0.3541	0.3873	0.0511		
Weighting function for group collapsing		Few-group CRCs normalized to the corresponding 208-group results								$\frac{k_{eff}}{k_{eff\ 208}}$	$\frac{1}{l_{208}}$
ϕ_{208}	110	1.0087	0.9997	1.0222	1.0361	0.9967	0.9966	1.0042	0.9930	1.00001	0.9997
ϕ_{208}	61	0.9845	0.9980	1.0658	1.1363	1.0027	0.9835	0.9983	1.0324	1.00002	0.9980
ϕ_{208}	40	1.0180	0.9960	1.1348	1.3055	1.0217	0.9823	0.9242	1.0258	1.00002	0.9959
ϕ_{208}	26	1.0311	0.9872	1.1251	1.4262	0.9755	0.9958	0.9604	1.0660	1.00001	0.9895
ϕ_{208}^+, ϕ_{208}	26	1.0055	1.0000	1.0126	1.0223	1.0017	1.0017	1.0032	1.0016	1.0000	1.0000

Group Structure

Energy range	Whole energy range	E < 1keV	1.0-2.15 keV	2.15-4.65 keV	4.65-10.0 keV	10.0-21.5 keV	21.5-46.5 keV	46.5-100.0 keV	100.0-200.0 keV	200.0-400.0 keV	400.0-800.0 keV	0.8-1.4 MeV	1.4-2.5 MeV	2.5-4.0 MeV	4.0-6.5 MeV	6.5-10.5 MeV
Number of groups	208	12	14	14	14	14	14	14	14	14	14	14	14	14	14	14
	110	12	7	7	7	7	7	7	7	7	7	7	7	7	7	7
	61	12	7	7	7	7	7	7	7	7	7	7	7	7	7	7
	40	12	2	2	2	2	2	2	2	2	2	2	2	2	2	2
	26	12	1	1	1	1	1	1	1	1	1	1	1	1	1	1

3.4.4. Resonance phenomena near interfaces and boundaries

In the already cited f-factor formalism boundary effects of resonance self shielding are not taken into account. The space dependence of the resonance self shielding is caused by the resonance structure of the neutron flux. Within a homogeneous mixture, far from boundaries, this resonance structure is fairly independent of position. Across interfaces the resonance structure of the neutron flux is influenced by the cross sections of the media on both sides of the interface and is rapidly varying with space. For the case of two adjacent half spaces, assuming NR-approximation, a solution for the neutron flux from the integral Boltzmann-equation for isotropic scattering can be given within a resonance. This solution is used as weighting function for the effective space dependent group cross sections. These in principle can be calculated directly from the resonance cross sections. But this direct calculation must be done for every combination of isotopes on both sides of an interface and would be very time consuming.

With the help of a rational approximation of the exponential integral

$$1 - E_2(x) = \frac{1,260578 \cdot x}{0,363948 + x} - \frac{0,260578 x}{2,60162 + x}$$

an approximate calculation of the space dependent effective group cross section from f-factor tables is possible /3.62/. The f-factors are tabulated as a function of a background cross section σ_0 . The rational approximation allows a transformation of the space dependence to a σ_0 - dependence. Two terms for the rational approximation turned out to be sufficient. The formalism has also been extended to thin zones.

Following remarks can be made:

The space dependent resonance self shielding is only important within two mean free paths on both sides of interfaces.

For small reflected systems, space dependent resonance self shielding leads to higher elastic scattering rates in the reflector. The consequence of this is normally a higher criticality. In Fig. 3.8 the ratio of the total scattering rate with and without consideration of space dependent resonance self shielding, in the nickel reflector of a 15 cm uranium sphere is plotted. S_8 calculations have been done.

The notations are:

CR: only correction at the core reflector-interface is considered.

$$\Delta K = + 0,0017.$$

RV: only correction at the reflector-vacuum interface is considered.

$$\Delta K = + 0,0013.$$

CRV: correction at both reflector interfaces and the small thickness of the reflector is considered.

$$\Delta K = + 0,0031.$$

At the core-blanket interface of fast reactors effects of space dependent resonance self shielding must be expected because of the higher ^{238}U concentration in the blanket than in the core. In the blanket the absorption rate will be higher by several percents than predicted with space independent group cross sections. This means that the Pu production is changed. For power reactors this can cause local changes of the power distribution at the interface of several percent, because more ^{239}Pu is produced. In Fig. 3.9 an example for the change of the absorption rates in ^{238}U for the fast critical assembly SNEAK-3A2 /3.63/ is given.

3.4.5. Calculation of neutron streaming effects in gas cooled fast reactors

In order to investigate streaming and heterogeneity effects in gas cooled fast reactors, a theory was developed /3.65/ which describes these effects as usual in terms of a homogenized direction dependent diffusion coefficient.

The theory was based on the work of P.R. Barrett /3.64/ for thermal reactors. Starting from Boltzmann's integral equation, one can deduce a balance equation for the lattice cell of a reactor zone. The assumptions made for deriving the balance equation are:

1. The extension of the regular, hexagonal lattice is large and neutrons born in the boundary region will not contribute directly, i.e. without further collisions, to the flux in a cell far away from the boundary.
2. Only the zero'th and first moment of an angular expansion of the elastic scattering cross section will be taken into account (anisotropic elastic scattering). All other cross sections are assumed to be isotropic.
3. It will be assumed that the scalar flux and the neutron current are not dependent on the lattice structure of the medium (no flux fine structure). Transport calculations for the cell have shown that this is a good approximation for fast reactors.
4. The scalar flux at a point r' in the lattice may be expressed by a Taylor series expansion around a point r in a reference cell of the lattice. Only the first three terms of such an expansion are retained. This implies that diffusion theory is valid in the homogenized lattice. Consequently, in an analogous Taylor series expansion of the current only the first two terms are retained.

These assumptions are sufficient to derive the mentioned balance equation for a cell in the lattice. If now the leakage L out of the cell is described by an expression analogous to that in diffusion theory for homogeneous media i.e.

$$L^g = \sum_x D_x^g \frac{\partial^2 \phi^g}{\partial x^2}$$

(x defines the axis of the coordinate system and g is the index for the lethargy group) and if one assumes a relation between scalar flux and current of the form:

$$J_x^g = -D_x^g \frac{\partial \phi^g}{\partial x}$$

then an expression can be derived from the balance equation for D_X^g

$$D_X^g = \frac{\frac{1}{6} \sum_i \Sigma_{t,i}^g \omega_i \sum_k R_{i \rightarrow k, g}^{2, g}}{1 - \sum_{h \neq g} \frac{\partial J_X^h / \partial \chi}{\partial J_X^g / \partial \chi} \sum_i \sum_{d, i}^{h \rightarrow g} \omega_i \sum_k R_{i \rightarrow k, \chi}^g}$$

In this formula

g denotes the index for the lethargy group

i denotes the index for zone i in the reference cell

k denotes the index for any zone k of any cell in the lattice, from where a neutron, born in zone k , may contribute directly to the flux in zone i in the reference cell

J_X^h is the current component in direction χ in lethargy group h in the reference cell

ω_i is the volume fraction of zone i in the reference cell

$\Sigma_{t,i}^g$ is the total macroscopic cross section in zone i and lethargy group g

$\Sigma_{el, i}^{h \rightarrow g}$ is the first moment of the elastic transfer cross section from group h to group g in zone i .

The terms $R_{i \rightarrow k, \chi}^{2, g}$ and $R_{i \rightarrow k, \chi}^g$ are defined as follows:

$$R_{i \rightarrow k, \chi}^{2, g} = \frac{\Sigma_{t, k}^g}{V_i} \int_{V_k} d\vec{r}' \int_{V_i} d\vec{r} [3 \Omega_x^2] R^2 \frac{e^{-\widetilde{\Sigma}_t^g R}}{4\pi R^2}$$

$$R_{i \rightarrow k, \chi}^g = \frac{\Sigma_{t, k}^g}{V_i} \int_{V_k} d\vec{r}' \int_{V_i} d\vec{r} [3 \Omega_x^2] R \frac{e^{-\widetilde{\Sigma}_t^g R}}{4\pi R^2}$$

where V_i, V_k are the volumes of cell-zones i, k

$R = |r - r'|$ is the distance between any point r' and a point r in zone i in the reference cell,

Ω_x is the χ -component of a unit vector in direction r, r' and $\widetilde{\Sigma}_t^g R$ denotes the optical path length from r to r' .

In the case of a homogeneous medium the above quantities reduce to

$$\sum_K R_{i \rightarrow K, \chi}^g = \frac{1}{\Sigma_{t, hom}^g} ; \quad \sum_K R_{i \rightarrow K, \chi}^{2, g} = \frac{2}{(\Sigma_{t, hom}^g)^2}$$

and therefore one can denote these quantities in the heterogeneous case as directed mean free paths from i to k and directed mean square free paths from i to k . It may further be mentioned that in the homogeneous case in the above expression for the diffusion coefficient the direction dependency vanishes. The expression reduces then exactly to the one, derived for D in homogeneous media in the P1 approximation. Therefore, in the limit of homogeneous media the derived equation for D_{χ}^g yields the appropriate expression.

Up to now, only preliminary calculations exist, which demonstrate the influence of neutron streaming in gas cooled fast reactors on the nuclear data of such reactors. They are reported here briefly. One-dimensional diffusion calculations with the axial component of the direction dependent diffusion coefficient showed that due to streaming effects the axial leakage of neutrons out of the core is increased by approximately 6 %, leading to a reduction of the effective multiplication factor of about 0,9 %. The used reactor concept was supposed to be typical for gas cooled fast reactors of 1000 MWe power with a coolant volume fraction of about 55 %.

Streaming effects in connection with coolant density changes have also been investigated. They indicate that in special cases, for instance when steam ingress in the primary circuit occurs, an increase in the reactivity due to reduced streaming may occur.

The investigations on this subject are continuing and will be reported elsewhere.

3.4.6. Improvements in the theoretical treatment of the Doppler effect

As already indicated in chapter 2, a computer code, DOPRO, was written for the interpretation of the well-developed small-sample Doppler measurements in the SNEAK facility. The code was practically completed at the London BNES conference in 1969. The theory is based on a perturbation solution of the integral transport equation for the heated sample, and the environment of the sample /3.66/. Analytical studies with this method lead to a full understanding of the resonance absorption of a heated sample in a cold environment.

The standard Karlsruhe code for the calculation of the Doppler coefficient on fast power reactors, based on homogeneous perturbation theory /3.67/, was improved by including the possibility to deal with resolved resonances /3.68/. For the numerical determination of the temperature derivatives of the effective cross sections a very convenient and accurate method, using spline-functions, was introduced. The interaction between potential and resonance scattering was included also.

In addition the temperature dependence of the Doppler coefficient was investigated theoretically. The result is that in reactor zones the temperature dependence is well described by $A/(T+BT^{3/2})$, A and B being constants.

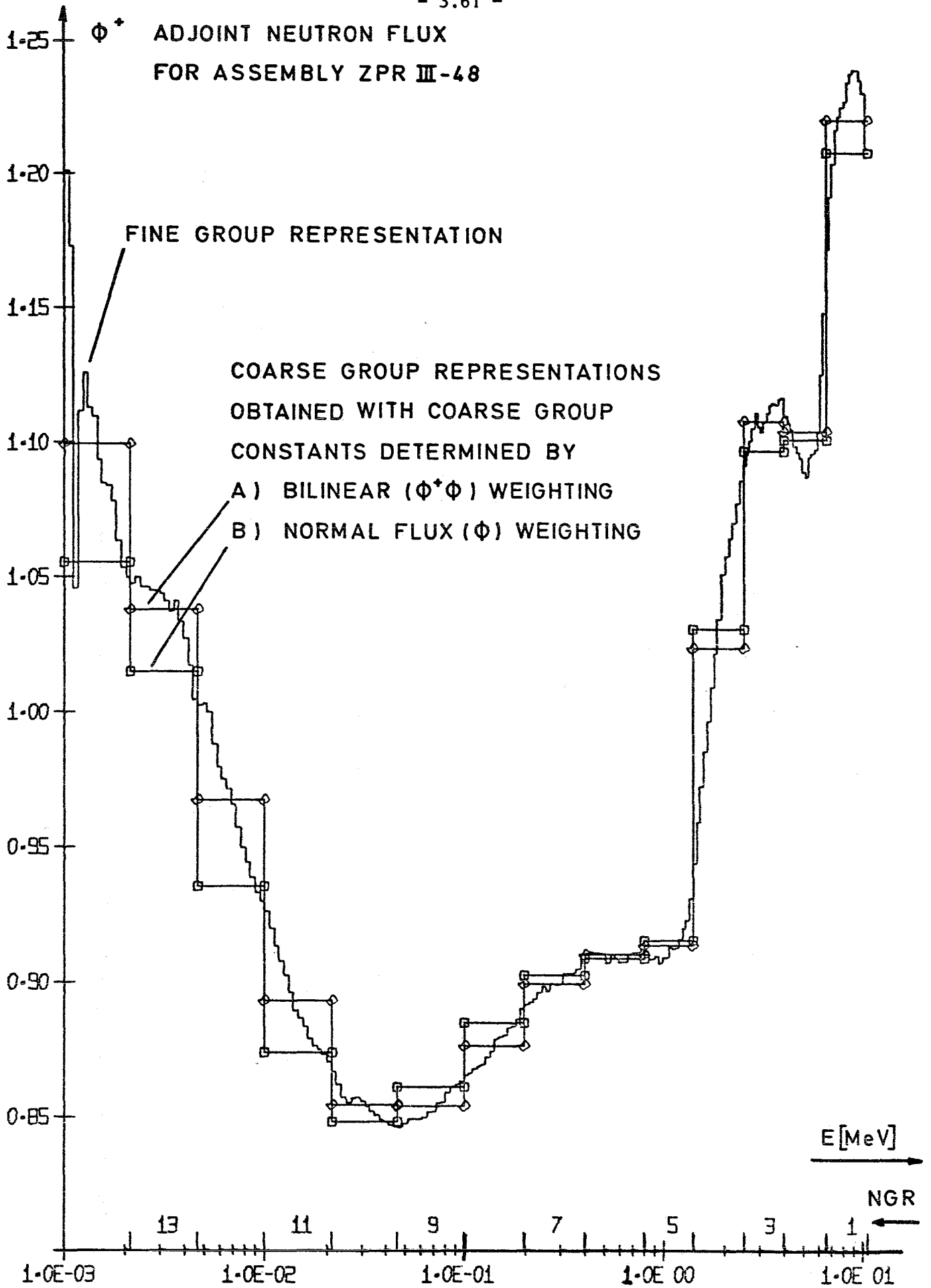


Fig. 3.7 Energy dependence of adjoint neutron fluxes

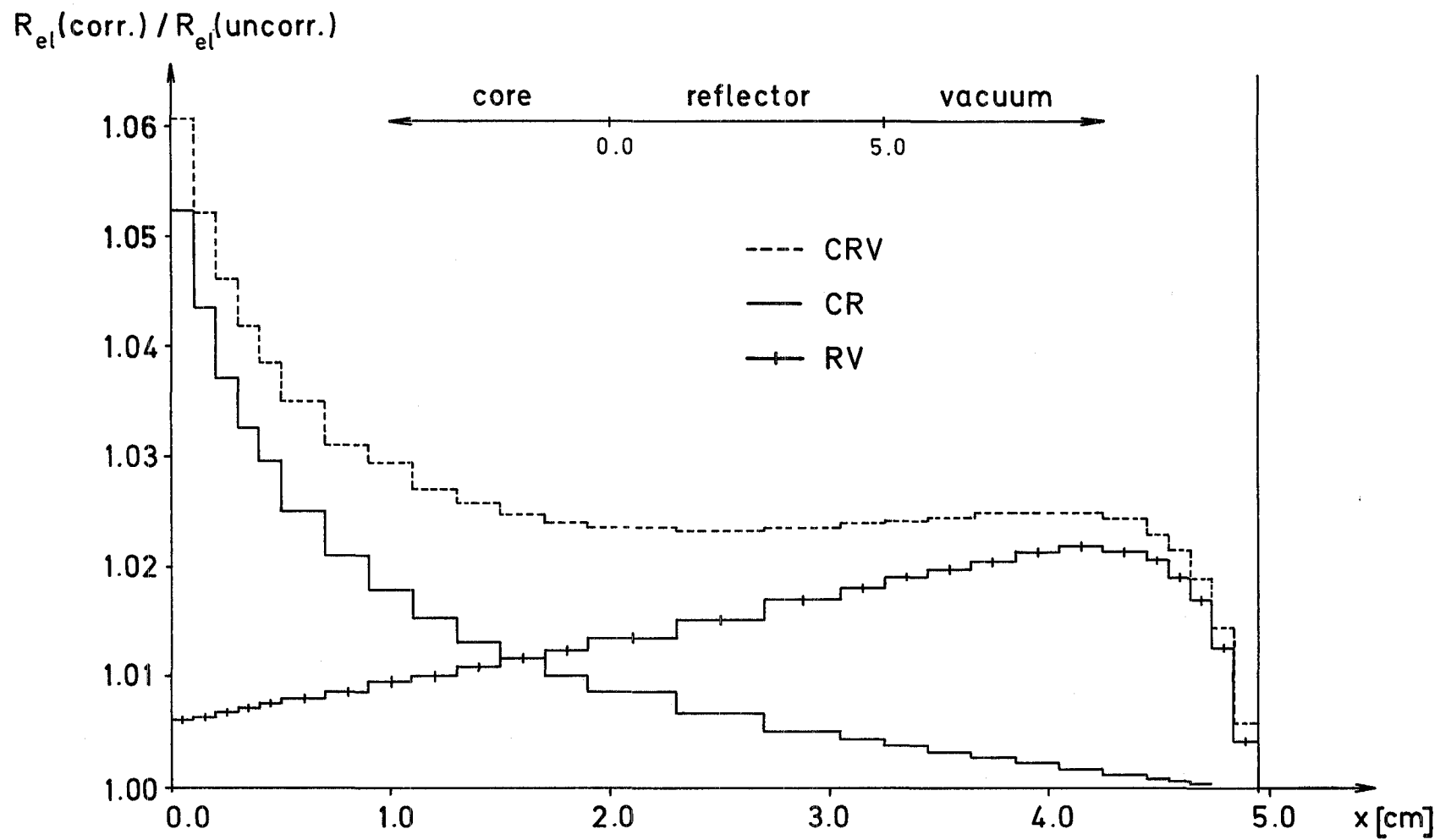
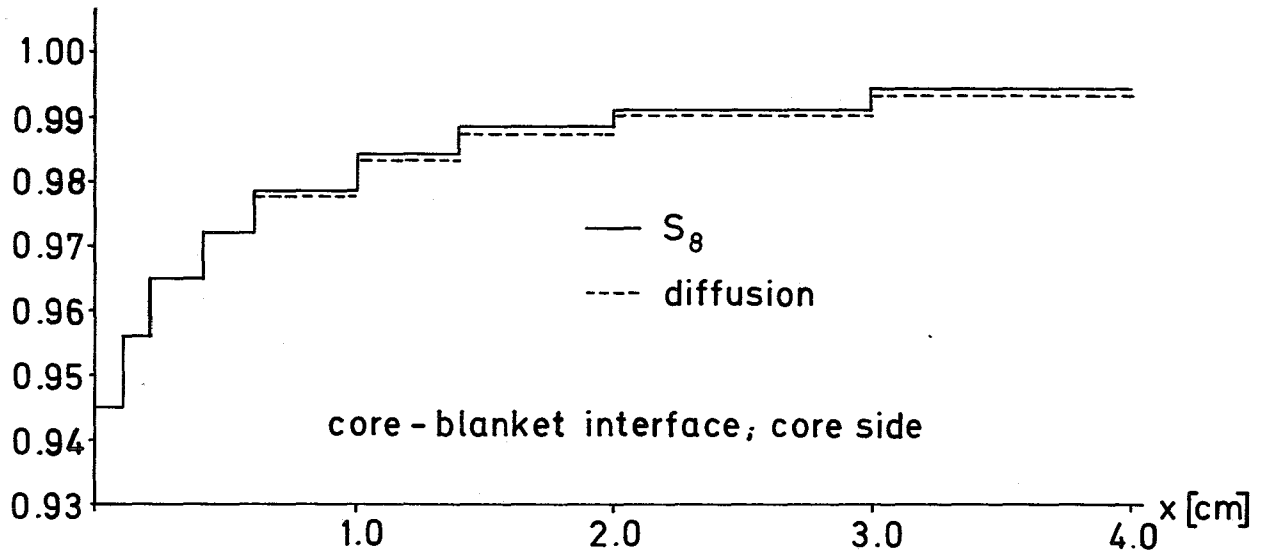
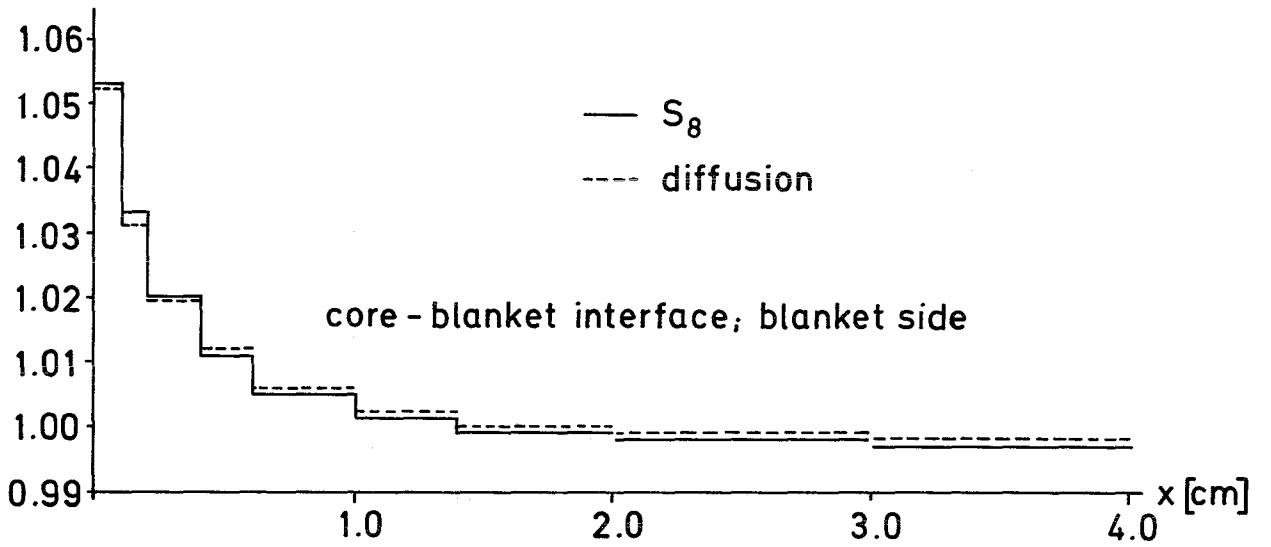


Fig. 3.8 Reaction rate ratios for elastic scattering in nickel

$R(\text{corr.})/R(\text{uncorr.})$



$R(\text{corr.})/R(\text{uncorr.})$



$R(\text{corr.})/R(\text{uncorr.})$

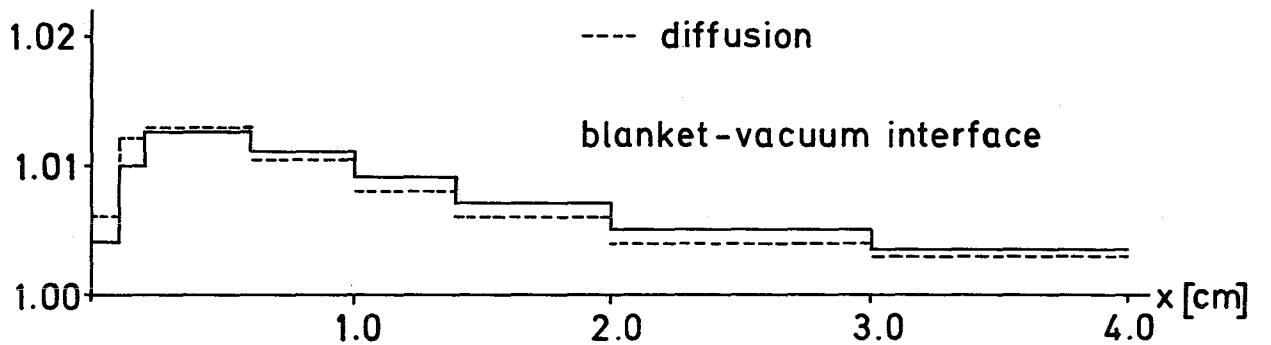


Fig.3.9 Reaction rate ratios for capture in U-238

3.5 Burnup-code developments for fast reactors

The development of burnup codes for fast reactors in Germany has taken two directions since 1969. At that time, at INTERATOM-Bensberg a two-dimensional code with four neutron energy groups, and at GfK-Karlsruhe only a one-dimensional burnup and management code for a fixed isotope scheme comprising ^{235}U , ^{238}U and $^{239}\text{Pu} - ^{242}\text{Pu}$ were available. From the reactor designer point of view, a multidimensional burnup and management code was necessary. On the other hand, a code with flexible isotope schemes had to be prepared for, e.g., the evaluation of irradiation experiments. These tasks were fulfilled separately and so far have not been combined.

GfK did not develop its own two-dimensional burnup code, but rather adopted the code ASB of INTERATOM /3.69/, coupling it to its own cross section evaluation routines contained in the NUSYS-system. Gradually, ASB was enlarged at GfK and improved to become ASB 71. It can handle:

- a) Only r-z-geometry; up to 99 compositions; the maximum number of zones and mesh points depends on the total size of the problem only.
- b) Up to 26 energy groups with downscattering over any number of groups; up-scattering is not allowed.
- c) Management operations including reloading and fuel shuffling with time steps determined by a reactivity, burnup or direct time step length criterium. Controlrod movements may be taken into account but are not automatized.
- d) The time dependence of the concentrations of ^{238}U , $^{239}\text{Pu} - ^{242}\text{Pu}$ and optionally, ^{235}U , one or several fission products and, optionally as well, the burnup of absorbers.

In its present version, ASB 71 is very convenient and useful, offering a lot of practical help to the user. Some of the features helping with the practical application are:

- a) The use of dynamic storage assignment, which makes the dimensions of a case a function of the maximum main storage region available only. On the other hand, the user may tailor the main storage region to the size of his problem.

- b) A restart option allowing a time consuming case to be separated into several smaller runs.
- c) The program description is stored in the computer and permanently updated. Subroutines are included which give the optimum dimensioning of the external data sets.

ASB 71 was first used to study the time dependent behaviour of a prototype gas-cooled reactor. Lately, studies were made concerning the number of energy groups necessary for a good description of the reactor time behaviour, and the influence of absorber burnup was calculated.

The zero-dimensional burnup program PYRE developed by Little and Hardie /3.70/ was the basis of the program PYGMY /3.71/ treating flexible isotope schemes. This zero-dimensional program takes into account:

- a) The time dependence of reactivity, neutron spectrum, isotope concentrations, and power or flux level for a constant total flux or power. A special irradiation option is available, which skips the reactivity and spectrum determination and works with constant spectra and flux levels in time intervals supplied by the user.
- b) Management operations such as shut-down-times, different power or flux levels and charging and discharging of fuel-batches can be taken into account.
- c) The radioactivity of the individual batches can be calculated.
- d) The following processes leading from one isotope to another can be handled: capture, decay, (n,2n) and fission, including the branching of chains in one process, e.g. competing β^- and β^+ decay.
- e) Automatic time step length adjustment is used.
- f) Since a numerical procedure for integrating the isotopic equations is used, even the most complicated isotope schemes can be handled. As the numerical integration procedure used in PYRE tends to diverge for too big time steps, another implicit method is incorporated in PYGMY.

The performance of this program has been very satisfactory, and if one of the space dependent programs would have to be equipped with a flexible isotope scheme, a suitably altered version of PYGMY would be inserted.

Besides this effort it should be mentioned that within the frame of the fast breeder project a two-dimensional code TRIBU was developed for hexagonal geometry by CEN-Mol and Belgonucléaire. This code is based on the twodimensional diffusion code TREPAN.

3.6 Development of kinetics and safety analysis codes

Though not strictly belonging to the subject of this review report, a brief discussion of the safety analysis methods will be included for completeness. It should be mentioned that this development was strongly influenced by the work performed mainly at Argonne National Laboratory, USA.

In the consideration of safety problems of fast reactors, presently, at least in Germany, the investigation of hypothetical accidents plays an important role. Mainly two kinds of accidents have to be considered: the pump flow coast down with trip failure of both safety systems, and the insertion of reactivity ramp rates. With respect to these two kinds of severe whole core accidents the development of theoretical models for the description of the thermodynamic and hydraulic behaviour of the fuel, clad, coolant and structure is as much important as the development of numerical procedures for the solution of the space-time dependent multigroup diffusion equations. Therefore theoretical models have been developed for the description of the elastic-plastic deformation of the pin /3.72/, the sodium expulsion and reentry phenomena /3.73/, the slumping of subassemblies after clad melting /3.74/ and the fuel coolant interaction /3.75/. Further development seems to be necessary for a better description of slumping effects and the behaviour of fuel particles in the expanding interaction zone, if disassembly of fuel pins occurs with liquid sodium inside the coolant channel. Those detailed models are necessary on the one hand because of the now better understood physical processes involved, and on the other hand, because it is necessary to describe whole core accidents much more detailed if nuclear plants of 1000-2000 MWe have to be considered. For the large nuclear plants the better knowledge of the physical processes with regard to safety aspects hopefully reduces the conservatism involved in the considerations of hypothetical accidents today.

As far as the neutronic part is concerned, the theoretical activities at GfK-Karlsruhe deal mainly with the development of point reactor kinetic codes and codes using approximate methods for the solution

of time- and space-dependent problems.

With respect to point reactor kinetics we developed the REX Code /3.76/, which allows to calculate the effect of reactivity ramps and variations of the inlet enthalpy of the coolant. The point reactor kinetics approximation of the time dependent neutron diffusion equation is coupled with a multichannel thermodynamic and feedback part. Feedback effects are determined by precalculated reactivity coefficients for the different materials like fuel, coolant and structure. REX deals only with problems where the core geometry remains intact and boiling of a liquid coolant does not occur. The code was widely used for studies of the dynamic behaviour of fast reactors with sodium or steam as coolant.

In the field of time- and space-dependent problems the development follows two different approximations for the solution of the two-dimensional multigroup diffusion equation. The first one uses a variational principle with time-discontinuous trial functions (RADYVAR 2) and the second one the quasistatic approximation (KINTIC 1). Both codes will have the same multichannel thermodynamic and feedback part, so that comparison studies between different methods of the solution of the neutron diffusion equation can be made. Both codes in their present stage describe the predisassembly phase of a whole core accident.

3.6.1 The improved synthesis code RADYVAR 2 and its feedback parts

The main parts of RADYVAR 2 /3.77/ can shortly be described as follows:

- a) Consistency iteration between the static neutron flux and the thermohydraulics of the core.
- b) Solution of the time-dependent multigroup diffusion equations, using a variational principle with time discontinuous trial functions. This approximation admits different methods of the solution:
 - 1) point kinetics, 2) adiabatic kinetics, 3) normal synthesis with iteration of the trial functions, 4) improved synthesis with quasistatic and improved quasistatic trial functions.

For 1) and 2), the multigroup diffusion equation is solved for a so called macrotime step, using recalculated trial functions at discrete times inside the time step. These trial functions take into account the cross section variations due to feedback-effects, determined from the preceding integration of that step.

- c) Simulation of different time-dependent perturbations of the core, e.g. rod ejection, flow coast down, blockage of subassembly groups, pressure loss in the covergas plenum as well as combinations of such disturbances.
- d) Description of the time-dependent thermodynamic and hydraulic behaviour of single coolant channels representing different radial zones of the core, especially the mechanisms of expulsion and reentry phenomena, if sodium boiling takes place /3.73/.
- e) Feedback-mechanisms due to the temperature dependent broadening of resonance lines of the microscopic cross sections of the fuel and the volumetric expansion of subassemblies taking into account the variety of possible interactions between materials as fuel, cladding, coolant and structure.
- f) Feedback mechanisms due to axial and radial displacement of material zones relative to the fixed geometrical representation of the core. This part takes into account bowing effects and axial expansion of the different materials as fuel, clad and structure.
- g) Description of the thermoelastic deformation of the fuel, the elastic-plastic deformation of the cladding, the change in the fuel-clad gap and the phase-change in the fuel /3.72/.
- h) Simulation of the effects of fuel-coolant interaction and slumping in single subassemblies.

A special version of RADYVAR 2, called CAPRI, uses only the adiabatic approximation for the solution of the neutron diffusion equation. RADYVAR 2 will be coupled in the near future with an improved disassembly code, being under development now. At INTERATOM-Bensberg a twodimensional code ARES /3.80/ has been developed to describe the loadings of the reactor tank after a severe accident.

3.6.2 The quasi-static approach KINTIC

Since synthesis is an approximative method, it was deemed necessary to have at least one other method for comparative studies. Because fully numerical codes in more than one dimension are still very time consuming on present day computers, the quasistatic approach to neutron kinetics has been chosen /3.78/.

The result of this second code development is the program KINTIC-1 /3.79/ whose present characteristics may be summarized as follows:

- a) Iteration of the steady state reactor: Criticality may be achieved by changing the geometrical configuration or the material concentrations in some zones of the reactor. Furthermore an iteration is done to achieve consistency between cross sections and the temperature field.
- b) Neutron kinetics: Quasistatic method and, since the insertion of these methods presented no additional difficulties, adiabatic and point kinetics method. The improved quasistatic method just is being implemented.
- c) Thermodynamics and feedback: Up to now, the code contains the 1968 version of the RADYVAR thermodynamics part, which is able to follow an excursion up to the onset of coolant boiling, fuel slumping or fuel element rupture. In the future it is planned to link the code to the newer thermodynamics module and the modules treating fuel slumping, sodium void, fuel element failure etc. The feedback presently comprises Doppler effect, density changes and core expansion.
- d) External perturbation: All sorts of material movements initiating an excursion may be simulated. With the newer version of the thermodynamics module, changes in coolant velocity or entry temperature may be treated in addition.

e) Characteristics of the program: Dynamic storage assignment has been used. The program has a modular structure permitting an easy deletion or insertion of modules. For the cross section evaluation, which is done beforehand, the program is coupled to the NUSYS (see section 3.7) cross section routines. An evaluation, which is currently being developed, may be used to produce plots and lists of time or space dependent variables.

Apart from extensive test calculations, KINTIC-1 has been used to examine the significance of space dependent effects in the SEFOR prompt critical transient.

3.6.3 Investigation on group collapsing schemes and energy synthesis

From the preceding discussion it is evident that space time dependent codes will consume much computing time, if calculations are performed with more than about 6-10 prompt neutron energy groups. Therefore studies have been performed to investigate the validity of various group collapsing schemes and the energy synthesis method for the analysis of fast reactor transients. A partial voiding of the central zone and the complete voiding of the central zone coupled with fuel slumping, were two transients considered for a simple, large, representative 1-dimensional breeder reactor model. The transient calculations were performed using the exact, finite-difference one-dimensional space-time program RAUMZEIT, which was modified to handle energy synthesis and up to 26 energy groups.

The results indicate that the energy synthesis method, with a limited number of trial functions, gives excellent agreement with the exact 26 group transient results. Total powers were always within 7% and local powers within about 10% of the exact values. The spectra trial functions were taken as the static perturbed and unperturbed averaged fluxes. The weighting functions were the corresponding adjoints.

Straight flux weighted group collapsing even with up to 12 energy groups was not sufficient to give good transient results. This was primarily because the reactivity effects were not calculated accurately enough for transients with reactivities in the neighbourhood of \$1. Bilinear weighting, with 8 groups on the other hand, gave good results for both total power and power distributions, particularly, when a combination of perturbed and unperturbed adjoints was used. However, it appears that problems with discontinuities at interfaces may arise when different averaged fluxes and adjoints are used for the weighting in different regions. When these effects are considered and the usual interface conditions are modified accordingly, the results shown in Table 3.8 are obtained.

Table 3.8 TRANSIENT RESULTS FOR TOTAL POWER WITH VARIOUS SCHEMES

PARTIAL VOIDING				FUEL SLUMPING				
Time	26 group	SYNTHESIS	8 GROUP BILINEAR	Time	26 group	SYNTHESIS	8 GROUP BILINEAR	
sec			INITIAL FLUX INITIAL ADJOINT	sec			INITIAL FLUX INIT. ADJOINT	INITIAL FLUX FINAL ADJOINT
0	1.0	1.0	1.0	0	1.0	1.0	1.0	1.0
.05	1.331	1.331	1.331	.001	1.282	1.276	1.281	1.281
.10	2.037	2.035	2.033	.002	1.845	1.839	1.842	1.839
.15	2.079	2.079	2.073	.004	1.718	1.718	1.714	1.719
.20	2.136	2.136	2.126	.006	1.624	1.628	1.617	1.626
.30	2.346	2.346	2.326	.010	1.831	1.836	1.813	1.833
.40	2.732	2.736	2.694	.014	2.877	2.812	2.812	2.868
50	3.460	3.477	3.382	.018	11.755	11.508	10.745	11.460
.60	3.721	3.741	3.628	.020	134.37	124.56	103.51	122.34
Comp. Time [min]	38	0.25	1.6	40	0.3	1.7	1.7	

3.7. The development of modern modular code systems

In this section the developments at GfK-Karlsruhe and INTERATOM - Bensberg are described.

3.7.1. The Karlsruhe program system KAPROS

In the Karlsruhe nuclear research center (GfK for short) the development of own large computer programs for more sophisticated fast reactor models began with the availability of a second generation computer, an IBM 7070/74, during the years 1962 - 1964.

As a consequence the necessity of systematic linkage of such big programs raised during this period leading to the linkage conventions of the Karlsruhe Nuclear program SYSTEM NUSYS, a modular program system with a simple one-level overlay structure and an intermodular data transfer via magnetic tape.

This original NUSYS was in use until computers of the third generation were available at GfK. During the year 1968 the system had been converted into an IBM/360 - form (for models 65, 85, 91) on a preliminary manner because the usual NUSYS calculation had to be continued without any interrupt and, on the other side, input data like group constants etc. had to be prepared by NUSYS modules for the improved flux prediction modules DIXY, KASY, DTK etc. (see sections 3.2. and 3.3.), then in progress. Moreover there was only little experience with the new computers to conceive a final modular system at this time.

The essential restrictions in the IBM/360 -version of NUSYS lie in the intermodular data transfer only within fast memory, thus leading to high turnaround times even for small cases, and in the rigid old overlay structure that hadn't been changed.

Thus the NUSYS-follower system KAPROS (=Karlsruhe Program System) is intended to improve the situation. Modern techniques in flexible program linkage, e.g. dynamical structures⁺, will be realized as well as a data transmission on external storage devices in direct access.

⁺ IBM System 1360 Operating System, Supervisor and Data Management Services
Form C28 - 6646

KAPROS is now in a state, where planning is nearly finished and implementation of the system's kernel has already started to work. The first fully operating version with all NUSYS modules built in is expected for the first quarter of the year 1973.

The essential KAPROS characteristics are summarized in the following survey:

- a) KAPROS is an open modular system. There are no restrictions concerning number or size of included modules. Expected number of modules: 100 - 1000 (NUSYS contains about 50 modules)
Representative module size: 1000 - 5000 FORTRAN statements.
- b) Module chaining (paths or procedures) is done by means of dynamical structures, i.e. each module is available in executable form (so called "load module") as member of a library and it can be invoked subroutinelike by any other module.

Thus self-developing paths, even with recurrent module calls, are possible in a modest range of module changes (order of magnitude: 100) per KAPROS job at all.

- c) It is provided to unload all calling modules, so that in the path each new module can occupy the same storage locations as its calling predecessor. The remaining storage, not used by the actual module, is taken for in core data transfer. In this way an optimal storage economy is reached.
- d) IBM-FORTRAN has been introduced as problem oriented control language in KAPROS to describe new procedures. Most of the futural KAPROS users have some experiences with this language, which offers many helps like branching instructions, powerful arithmetic facilities, etc. for building up less or more complex procedures, that can be themselves inserted as new modules within the system. In KAPROS this will be the way to develop new and more complex methods or to simplify data handling.
- e) There is a data pool called "lifeline", containing all "data blocks", i.e. all interfaces of the modules running in a KAPROS job.

The lifeline is subdivided in three parts:

- e1, The in-core lifeline IL for a fast data block transfer from module to module within the same job. The IL consists of all free storage locations not used for instructions or buffers at a moment. The size of the IL varies with each change of a module (see Fig. 3.10).
- e2, The scratch lifeline SL is an external direct access storage (disk) for

large data blocks transmitted between modules of the same job.

It is expected that most of the KAPROS modules will be able to switch from IL to SL transmission and can thus easily be adapted to varying storage sizes.

- e3. The restart lifeline RL (see Fig. 3.10) comprises all data blocks that are to be transferred between modules of separate KAPROS jobs during a short period (one week).

The KAPROS data management provides direct access storage to hold such blocks, thus offering possibilities for the restart of a job with improved input perhaps after a preceding error interrupt (restart).

On the other side the RL plays the role of a buffer between KAPROS and private user libraries (see KSA 1 in Fig. 3.10) or the KAPROS archive KSA 2, where data blocks normally will have longer lifetimes.

- g) Provisions are made in KAPROS for detecting program errors or other abnormal situations such as shortness of time etc.
- h) A statistics library should also help to detect construction failings within the KAPROS frame work.
- i) Incorporation of non-KAPROS modules can be reached in a stepwise process with increasing system benefits for this module.
- k) In a later version the inclusion of interactive graphical input-output modules should increase comfort and effectivity of KAPROS.

Fig. 3.10 shows a KAPROS job with its possible resources running in a multiprogramming environment.

One of these resources - the module library - is of highest interest for KAPROS users, because it contains as members all the modules that can be used in a KAPROS job. The module library of the first system version is to consist of the following modules whose functions are briefly enlisted (former NUSYS modules are specified by (N)):

- | | |
|-----------------|---|
| GRUCAL | - a general group constant preparation program on the basis of the Karlsruhe cross section library GRUBA (section 3.1.) |
| SIGMA | - transforms the group constant block from GRUCAL into a special NUSYS form. |
| oo352 (N) | - a group collapsing program in connection with SIGMA output. A zero dimensional spectrum calculation option is built in. |
| oo447 (N) | - calculates any zero dimensional reaction rate densities or relations of densities. |
| oo448 (N) | - a zero dimensional DOPPLER coefficient program. |
| o6731 (N) | - a one dimensional multigroup diffusion program. |
| oo445 (N) | - calculates space dependent one dimensional reaction rate densities or relations of densities. |
| 1442o (N) | } - special one dimensional evaluation routines (densities, rates, combinations) |
| o2761 (N) | |
| o678o (N) | |
| o6771 (N) | - calculates one dimensional neutron balances. |
| o22oo (N) | - a one dimensional perturbation program with options for effective delayed neutron data, for neutron lifetime etc. |
| o221o (N) | - zero and one dimensional criticality searches |
| 14444 (N) | - power and criticality iteration |
| o1732 (N) | - compares and plots calculated and measured reaction rates. |
| o17o6 (N) | - calculates the DOPPLER coefficient on the base of perturbation theory. |
| 1o76o (N) | - ZERA, calculates influences of heterogeneous cell structures on resonance self shielding. |
| o1o56 (N) | - a special Karlsruhe one dimensional burnup module |
| o1793/94 (N) | } - a procedure to correct elastic scattering cross section (REMO method) |
| 415o1/o2/o3 (N) | |

- 31901 (N) - calculation of bucklings and savings.
- 31902 (N) - a DOPPLER coefficient program assuming a $1/T$ dependence of k_{eff} from temperature T .
- 41504 (N) - plots curves on a printer
- 41505 (N) - reorganizes special NUSYS data blocks
- 31903 (N) - an editing module for NUSYS data blocks.
- 00451 (N) - a utility program for data block handling.
- DIXY - a two dimensional multigroup diffusion program with special parts for perturbation calculations and evaluations.
- KASY - a synthesis program on KAPLAN's method, calculating three dimensional multigroup neutron fluxes with help of two dimensional "trial function" (section 3.3.).
- D3D - a three dimensional multigroup diffusion program for high numbers of space energy mesh points, e.g. 500 000 and more (section 3.2.1).
- DTK - the Karlsruhe one dimensional multigroup (up to 208) SN-program (section 3.2.2.).
- SNOW - the Karlsruhe two dimensional multigroup SN-program.
- KINTIC - a two dimensional fast reactor kinetics program calculating space-time dependent multi-group neutron fluxes on the base of a quasistatic approximation (section 3.5.).

3.7.2. The INTERATOM modular code system IANUS

The INTERATOM nuclear code system IANUS has been planned and developed to provide efficient and practical means for the performance of a variety of nuclear design calculations on a CD 6400 computer. Although only neutronic problems can be handled presently, practically no restrictions for extending IANUS to other fields of reactor calculations exist.

IANUS is constructed in modular form; the moduls are automatically linked and managed by special routines incorporated in the system. Data exchange among modules is managed by means of the IA-developed data transfer system, UEBERGABE, that has successfully been applied outside of IANUS for several years /3.89/.

General description of program management

In principle the system is organized in an overlay structure. It is composed

of a small main overlay, the system overhead, four primary overlays, which are responsible for the mastering of the main system tasks, and additionally an open number of additional primary overlays, which represent the modular collection of calculational algorithms and service programs. Each primary overlay may include one additional level with a practically unlimited number of secondary overlays.

The minimized system overhead contains the overlay loader of the operating system with a length of about 100 central memory words. The statement `CALL OVERLAY (IANUS, I, 0)` will cause the overlay (=module) number I in the IANUS library to be loaded into the central memory.

The first and the second of the primary overlays read and process all information in the user's input stream, which determines the sequence of modules to be executed. They also perform the formatted input for the module data from the standard input medium and check it for format errors and omissions. All data are maintained on a particular sequential file and can be stored for long term storage on the general external data tape by the catalogue module in overlay 4 after execution has been achieved.

The third overlay carries out the main control functions of the system, especially those of the overlay loader control. It determines the number, I, of the next overlay to be loaded and transfers it to the main overlay. In the first instance, the order of program execution is indicated by the input control specification. Beyond this, however, a calculational path can be influenced by decisions made during the progress of computation and any module in a specified series can change the initial loading number. This sharing of program control logic, utilized for the performance of iterating, repeating and branching schedules in IANUS, allows a nearly unrestricted implementation of new modules, each of which may be supplied with a number of problem dependent control decisions. This arrangement guarantees flexibility also in a very extended system because it does not require any change in the main control overlay and it avoids any growth in its size, when new modules are implemented.

The main control overlay also provides the capabilities for the restart in cases of abnormal termination. Restart is possible at characteristic, pre-determined points in a sequence. In performing a restart the original formatted input may be updated easily.

Overlay Four directs the transfer of results from the temporary data storage (on disk) to the general external data tape for long period of storage and also catalogues the input data sets as described.

The principle of data management

Independently of the formatted data on the card input file created in Overlay 2 the computational modules communicate together through the use of a common data bank maintained on a temporary random access disk-file in binary mode. This communication is managed efficiently and at high transfer rates by the UEBERGABE-system, by means of data blocks. A data block, supplied with a system of appropriate identifiers and names, is always built up in three dimensions and has a problem dependent size. It is completely self-describing, in particular, the arrangement, the size and the types of the physical quantities are contained in detail. Quantities (fluxes, cross sections, volumes, material distributions, reactivities etc.) may be single values as well as arrays in a maximum of three dimensions. By addressing the "tables of content" and the block identifiers the UEBERGABE input procedure retrieves any collection of data in any block of the actual bank, when the types, dimensions and block identifiers (of the desired array) are specified. The specifications of "control" data may either be supplied by the user's input or be generated internally according to the requirements of special problems using standard directives for a control data generating procedure in UEBERGABE. These most essential features of UEBERGABE effects a wide range of data management possibilities reaching from a very flexible level under user's control up to an almost fully automated one. Efficient data transfer is also supported by the use of standard type names.

Special characteristics;

The IANUS system has been implemented on a CD 6400 series computer for the SCOPE 3.3. operating system. Except for a few minor utility routines, FORTRAN EXTENDED has been used for programming. The limited size of the computer system (a 49 K words memory, 4 magnetic tape units and 3 disk units) required special efforts and also restrictions to maximize the utilization of the central processor for calculational purposes as well as to allow multi-programming operation in normal use. Under these conditions it is really unfeasible to keep a large volume data base or even considerable parts of it in the central memory and to perform direct data exchange among modules via core storage.

Therefore, the data base always resides on a disk storage during execution. The transfer time is minimized by the use of the efficient input/output routines in the SIS (SCOPE INDEXED SEQUENTIAL)-software package of CDC, which can operate randomly and sequentially on the same file. Owing to the small number of disk units available, the long term storage of results on permanent files is also not practical and the sequential mode operation of SIS is applied for cataloguing final results on binary tapes and for restoring them into a temporary data base.

Several measures supporting an efficient core management, are performed by special subroutines with the following functions:

1. Buffer allocation under program control. User libraries on permanent or tape files are connected and disconnected by the calling module directly. For the rest of the time these tape units and permanent files are available for other users.
2. Data array compacting and automatic overflow to random access storages with retrieval within a module.
3. Problem dependent dynamic storage allocation for each executed overlay. In addition dynamic addressing is used for module programming. Modules are normally subdivided into different overlays for the distinct calculational and service tasks to be handled.

The system described above has been completed and is presently operable with a limited number of modules. Additional modules are going to be implemented in the near future, especially those ones, which are needed for extensive burn-up calculations.

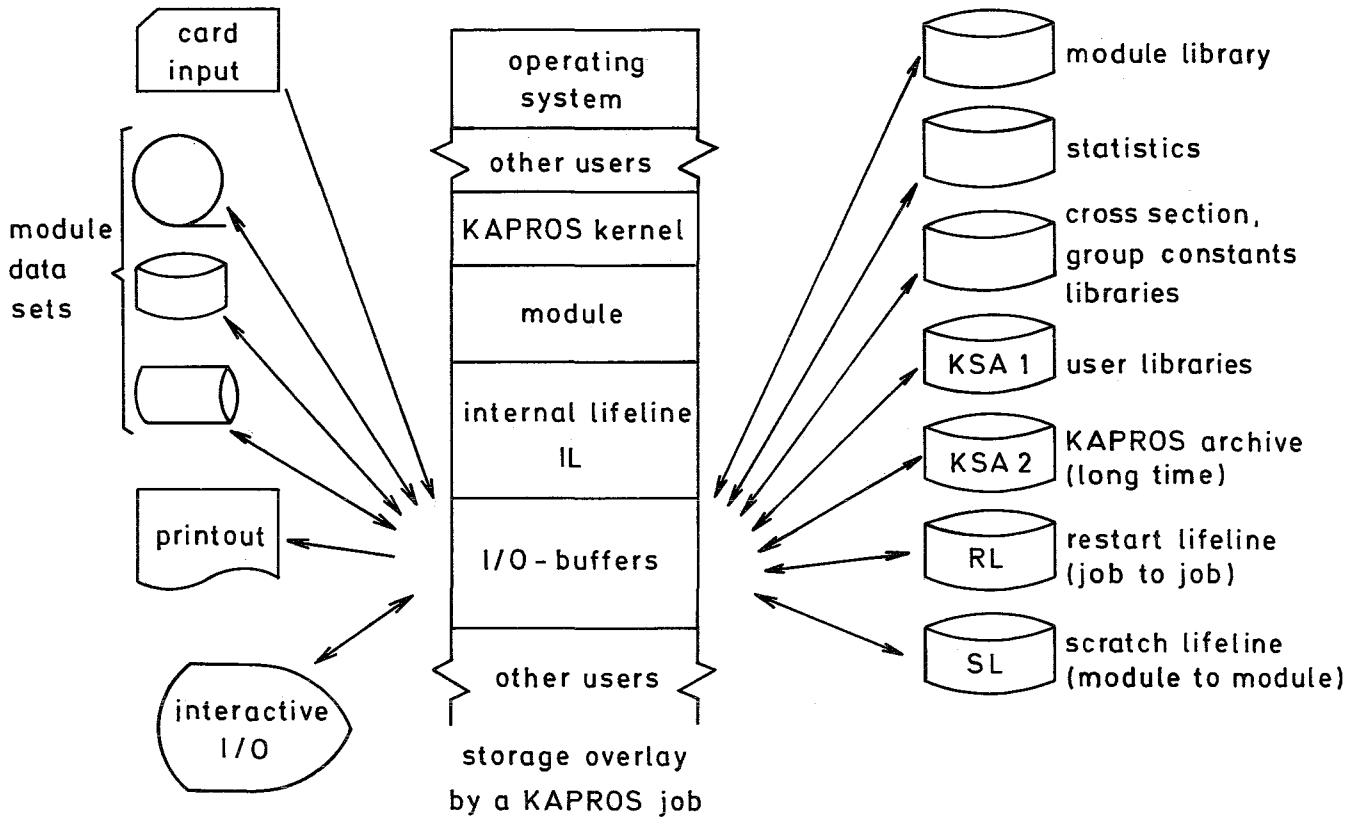


Fig. 3.10 KAPROS resources

References for chapter 3

- /3.1./ J.J. Schmidt KFK 120 (=EANDC-E-35U), 1966
- /3.2./ I. Langner, J.J. Schmidt, D. Woll, KFK 750,
(EANDC (E)-88 "U"), 1968
- /3.3./ B. Hinkelmann, B. Krieg, I. Langner, J. J. Schmidt, D. Woll
KFK 1340 (=EANDC (E) 136 "U"), 1971
- /3.4./ J. Cabé, M. Cance, A. Adam, Proc. 2nd Int. Conf. on Nucl. Data
for Reactors, Helsinki 1970, Vol. II, pp 31
- /3.5./ B. Schatz, KFK-1629 (=EANDC (E) 151 "U"), 1972
- /3.6./ R. Meyer, private communications 1970 and 1971
- /3.7./ S. Cierjacks et al. KFK-1027, 1969
- /3.8./ A. Horsley, Nucl. Data A 2, 243, 1966
- /3.9./ J. Schepers, to be published
- /3.10./ L.P. Abagjan, N.V. Bazazjanc, I.I. Bondarenko, M. N. Nikolaev, Gruppen
konstanten schneller und intermediärer Neutronen für die Berechnung von Kern-
reaktoren, KFK-tr-144
- /3.11./ H. Huschke, KFK 770, EUR 3953d, (1968)
- /3.12./ E. Kiefhaber and J.J. Schmidt, KFK 969, EANDC(E)-118 "U" (1970)
- /3.13./ E. Kiefhaber, KFK 1572 (1972)
- /3.14./ J. Braun, B. Hinkelmann, H. Huschke, I. Langner, D. Sanitz, I. Siep,
D. Woll, Proceedings of the "Reaktortagung" of the "Deutsche Atomforum"
1971 p. 110
- /3.15./ H. Huschke, D. Sanitz, D. Woll, J. Braun, KFK 1270/2, EUR 416401,
(1970), p. 122-12
- /3.16./ H. Huschke, B. Krieg, I. Langner, B. Schatz, I. Siep, P. Vertes, H. Wiese,
to be published as KFK-report; see also: Proceedings of the EANDC Working
Group Meeting at CNEN, Bologna (1972)
- /3.17./ E. Kiefhaber et al., Proceedings of the International Conf. on the
Physics of Fast Reactor Operation and Design, p. 94, BNES, London
June 24-26, (1969)
- /3.18./ H. Küsters et al., Proceedings of the IAEA Conf. on Fast Reactor Physics,
Karlsruhe 1967, Vol. I, p. 167; see also KFK 628, 1967
- /3.19./ M.C. Moxon, E.R. Rae, private communication to J.J. Schmidt (1969)
- /3.20./ W.P. Pönitz et al., KFK 635, EUR 3679e (1967)
K.H. Beckhurts et al., Proceedings of the IAEA-Conf. on Fast Reactor
Physics, Karlsruhe 1967, Vol. I, p. 67
- /3.21./ H.O. Menlove, W.P. Pönitz, Nucl. Sci. Engng. 33, p. 24, (1968)

- /3.22./ R. Gwin et al. (1968); G. de Saussure, private communication to J.J. Schmidt (1968)
- /3.23./ J. Fréhaut et al., EANDC (E)-89 "U", pp. 221, 224 (1968)
- /3.24./ H. Condé et al., Journ. Nucl. En. 22, p. 53 (1968)
- /3.25./ S. Yiftah et al., Proceedings of the IAEA Conf. on Fast Reactor Physics, Karlsruhe 1967, Vol. I, p. 123
- /3.26./ H. Rief, H. Kschwendt, Nucl. Sci. and Eng. 30, 395 (1967)
- /3.27./ H. Borgwaldt, KFK-1391 (1971)
- /3.28./ J. Lieberoth, Nucleonics 11, vol. 5 (1968)
- /3.29./ J. Lieberoth, Habilitationsschrift, Technische Hochschule Aachen (1972)
- /3.30./ M. L. Steele, Reactor Technology 13 (1970)
- /3.31./ R. Fröhlich, Nucl. Sci. Eng. , 34, 57 (1968) and J. Merkwitz, Tagungsbericht der Reaktortagung des Deutschen Atomforums, Bonn, 30.3.-2.4. 1971,
- /3.32./ R. Fröhlich, to be published in the proceedings of the conference on Numerical Reactor Calculations, IAEA, Vienna, Austria, January 17 to 21, 1972
- /3.33./ R. Fröhlich, Tagungsbericht der Reaktortagung in Hamburg, 11.-14. April 1972
- /3.34./ J.B. Yasinsky, and S. Kaplan, Nucl. Sci. Eng., 31, 354, (1968)
- /3.35./ C.H. Adams and W. M. Stacey, Jr., Transactions of the American Nuclear Society, 12, Number 1, (1969)
- /3.36./ V. Luco, Transactions of the American Nuclear Society, 14, Number 1, (1971)
- /3.37./ W.M. Stacey, JR., Proceedings of a Seminar on Numerical Reactor Calculations, Vienna, 17-21, January 1972
- /3.38./ K.O. Ott, Trans, Am. Nucl. Soc., 14 (1971)
- /3.39./ W.M. Stacey, Trans. Am. Nucl. Soc., 14 (1971)
- /3.40./ S. Kaplan, Nucl. Sci. Eng., 13, 1962
- /3.41./ J.R. Rice, Mathematics of Computation, Vol. 20, 1966
- /3.42./ G. Buckel, KFK 1349, Juni 1971
- /3.43./ S. Pilate et al., KFK 1345, August 1971
- /3.44./ G. Buckel et al., to be published in the proceedings of the conference on Numerical Reactor Calculations, IAEA, Vienna, Austria, January 17 to 21, 1972

- /3.45./ F. Heim et al., KFK 1399, June 1971
- /3.46./ G. Jourdan et al., Tagungsberichte der Reaktortagung
in Berlin, 20.-22. April 1970, Seiten 141-144
- /3.47./ A. Daneri et al., Fiat Report FN-E-97 (Research
Contract Euratom-Fiat-Ass. No. 089-66-2 TEEI), May 1968
- /3.48./ Triton, Euratom, Ispra
- /3.49./ W. Höbel, et al., KFK-report in preparation
- /3.50./ J. Quenon et al., Belgonucléaire Internal Report
BN 6903-01, Nr. 309.11/131/ni/138, March 1969
- /3.51./ W. Schwetje, Thesis, University Karlsruhe 1970
(published in NSE)
- /3.52./ P.E. Mc Greath and E.A. Fischer, KFK-1557 (März 1972)
- /3.53./ D. Wintzer, Proceedings of an IAEA Symposium Fast
Reactor Physics Karlsruhe, November 1967
- /3.54./ P. Benoist, Nucl. Sci. and Eng. 34, 285-307 (1968)
- /3.55./ F. Helm et al., KFK-1399 (1971)
- /3.56./ W.I. Oosterkamp, KFK-1036, Karlsruhe 1969
- /3.57./ L.B. Levitt, Trans. Am. Nucl. Soc. 648 (1971)
- /3.58./ H. Borgwaldt, KFK-1272/1
- /3.59./ A.K. Khaizallah and I. Recolin, IAEA-SM-154/37,
Vienna 1972
- /3.60./ E. Kiefhaber, Nuc. Sci. Eng. 38, p. 178 (1969)
- /3.61./ E. Kiefhaber, KFK-882, EUR 4161e, (1969)
- /3.62./ H. Huschke, KFK-1353 (1971)
- /3.63./ R. Schröder et al., KFK-847, EUR 3721 e (1968)
- /3.64./ P.R. Barrett, Nuclonic Bd. 12, Heft 5 (1969)
- /3.65./ E. Eisemann, KFK-1577 (1972)
- /3.66./ E.A. Fischer, KFK-844 (1969)
- /3.67./ I. Siep, KFK-983 (1969)
- /3.68./ I. Siep, Thesis, University Karlsruhe (1972)
- /3.69./ L. Mayer, KFK-1079 (1969)
- /3.70./ W.W. Little, R.W. Hardie, BNWL (1965)
- /3.71./ L. Mayer, KFK-1056 (1969)
- /3.72./ B. Kuczera, KFK-1272/2
- /3.73./ P. Wirtz, KFK-1272/2

- /3.74./ G. Angerer, to be published
- /3.75./ L. Calderola, Submitted for Publication to Nucl. Eng. and Design, H. Jacobs, K. Thurnay, Int. Conf. on Eng. of Fast Reactors for Safe and Reliable Operation, Karlsruhe October 1972, paper 38g
- /3.76./ K. Hornyck, KFK-799 (1968)
- /3.77./ G. Kessler, Nucl. Sci. Eng. 41, 115 (1970)
- /3.78./ K. O. Ott, D. A. Meneley, Nucl. Sci. Eng. 36, 402 (1969)
- /3.79./ L. Mayer, H. Bachmann, KFK-1627 (1972)
- /3.80./ K. Doerbecker, see Int. Conf. on Eng. of Fast Reactors for Safe and Reliable Operation, Karlsruhe, October 1972, paper 47
- /3.81/ L.A. Hagemann, WAPD-TM-364, (1963)
- /3.82/ Hadjidimos, Comp. J., 10,324-328(68/69)
- /3.83/ J. Guittet, J. Math. Analysis Appl., 17,199-213(1967)
- /3.84/ J. Douglas, jr. Numerische Math. 4,41-63(1962)
- /3.85/ R.S. Varga, Matrix Iterative Analysis, 1962
- /3.86/ C. Guenther, W. Kinnebrock, KFK 1381
- /3.87/ C. Guenther, W. Kinnebrock, KFK-Report, to be published
- /3.88/ W. Kinnebrock, KFK 1362
- /3.89/ H. Baur, INTERATOM - Internal Report D-A-142 (1969)

4. IMPROVEMENT IN EXPERIMENTAL FAST REACTOR PHYSICS

For measurements of integral reactor data and comparison with calculations three fast facilities were operated at Karlsruhe. The coupled fast-thermal reactor STARK /4.1/ with its uranium fueled central test region was engaged in studies of fast reactor lattices. Of special interest was a repetition of measurements performed on a hydrogen containing core region formerly investigated in the SNEAK-reactor /4.2/.

The subcritical facility SUAK /4.3/ was widely used for neutron spectrum studies. Neutron spectra in large zones composed of only a few elements were studied in the past. The facility was recently prepared for measurements in plutonium fueled lattices. The fast critical facility SNEAK was mainly used for the mock-up of plutonium-fueled power reactors and for assemblies especially suited for physics experiments.

In all three facilities the fast core regions were built up from square platelets and blocks with edge lengths of 50.7 mm and heights varying between 1.6 mm and 6.3 mm. Platelets of different composition were stacked in periodic sequences to yield the desired average composition.

The experimental techniques employed in measurements on these facilities were continuously improved in the last years.

The development of experimental techniques for the investigation of plutonium fueled assemblies required special attention. In the SNEAK-facility the plutonium fuel is in the form of sintered PuO_2/UO_2 encased in stainless steel cans with 0.3 mm wall thickness. The outer dimensions of a fuel platelet are 50.7x50.7x6.3 mm. To facilitate measurements inside the fuel, special platelets were fabricated which are similar to those used in the ZEBRA-reactor (Fig.4.4). These platelets have 3 holes each which allow the insertion of foils or fission track recorders into small cavities inside the fuel. The remaining space of the cavities is filled up by special pieces made from sintered fuel.

For easy handling of these platelets without undue risk of contamination all open surfaces of the fuel in the coupons is plated with a nickel coating of about 10 μm thickness. Thus, reaction rate measurements performed in the fuel can be carried out with a minimum of perturbation to the lattice.

4.1. Reaction rate measurements

Already in the course of experiments in uranium fueled assemblies it became evident that accurate reaction rate measurements require an elaborate technique. It could easily be demonstrated that the fission rate determinations by means of fission chambers introduced in core or blanket regions are often erroneous. This is very pronounced for threshold reactions like ^{238}U fission. There are mainly two sources of error:

1. Fission chambers integrate the neutron flux over a large region of the lattice cell, while in fact the fission rate is non-zero in fuel regions only.
2. Chamber walls, supporting structure, and cables soften the neutron spectrum impinging on the detector to such a degree that the observed spectral index is not necessarily that of the surrounding lattice.

To reduce the volume of integration, very small ^{239}Pu and ^{235}U fission chambers were developed. These chambers have an outer diameter of 1.5 mm and an active length of 4 mm. They can be inserted into small gaps between fuel pieces in such a way that integration is performed essentially over the thickness of a fuel platelet. Strong perturbations of the regular cell structure were prevented by fitting the chambers to minute preamplifiers built into a single platelet of structural material. The chambers were used for ^{239}Pu fission rate measurements in the SNEAK-5 assembly /4.4./. Recently activation detectors of uranium and plutonium oxide were manufactured for SNEAK by UKAEA Plutonium Fuels Laboratory, Winfrith, and reaction rate measurements by activation methods are preferred to fission chambers, because it is difficult to account for the remaining perturbation in neutron spectrum, and the fluence required for a measurement of sufficient statistical accuracy is high. However, the development of miniature chambers is continuing for applications with fissile layers of ^{240}Pu and ^{241}Pu .

Reaction rate measurements with activation foils have none of the formerly mentioned disadvantages. Besides uranium metal foils of different shape and enrichment plutonium-uranium oxide foils of 12 mm diameter and 0.25 mm thickness with varying isotopic ratios are available. These foils are covered by a 10 μ -nickel coating like the special platelets. In irradiation experiments different detectors are combined in such a way so as to have on the average the same composition as the fuel surrounding the foils and to allow a separation of the contributions of the different isotopes. The techniques applied in the evaluation of irradiation experiments are described in the next section.

For mapping of fission rate distributions as often desired in more technically oriented experiments, activation as well as fission chamber measurements are carried out. For reaction rate fine structure measurements, the recording of fission fragment tracks in plastics appears very promising. The present state of these techniques is also discussed below.

4.1.1. Measurement of fission and capture rates by activation techniques

This section deals with activation measurements using foils. The techniques discussed are those used in SNEAK, the fast zero power facility at Karlsruhe. Methods used in the other fast research facilities (SUAK, STARK) are very similar to these.

Activation measurements cover a broad range in each critical or subcritical assembly. Quantities to be measured are: global traverses through core and blanket zones, fine structures of reaction rates in the lattice cells and spectral indices (reaction rate ratios per atom) especially of the fissile and fertile materials which mainly determine the neutron economy of a fast reactor. Compared with measurements performed with fission chambers, the activation method has certain advantages. Only small amounts of material normally not present in the cell have to be inserted, and large holes or channels are avoided.

To fully use these advantages, special techniques have been developed. Metal and oxide foils of uranium and plutonium in different enrichments are now available. Singly or as sandwiches to match as well as possible the original fuel composition, they can be placed in special fuel platelets equipped with holes and filling pieces as described before.

The most widely used method for fission rate measurements is the integral counting of γ -rays emitted from activated foils above a certain energy threshold (e.g. 500 keV). NaI (Tl) crystals in connection with photomultiplier tubes are used as detectors. If depleted uranium foils are used, the ^{238}U capture rates are determined by counting γ -X-coincidences produced by ^{239}Np in the 100 keV-region /4.5/. All foils in a batch are normalized to reference foils that were irradiated between calibrated parallel plate fission chambers to get the absolute fission rates and the spectral indices.

The activities of the foils in a batch can vary widely as they are irradiated in reactor positions with different fluxes, or for enrichment reasons. Since the gain of photomultiplier tubes depends on the counting rates, peak stabilizers are used in the electronic chains. One stabilization method makes use of the γ -"peak" near 100 keV, which is composed of γ - and X-rays from the ^{239}Np decay as well as X-rays from ^{238}U and ^{235}U caused by external excitation (fission product and background gammas). These latter contributions may cause a time dependency of the shape of the peak. Therefore the stabilization was restricted to γ - and X-rays from ^{239}Np by additional gates (Fig. 4.1) and with this equipment time-independent results were obtained. A second stabilization method takes the 412 keV γ -line of activated gold foils attached to the detectors as reference peak. The gamma rays emitted by ^{198}Au are well below the chosen energy threshold settings and contribute negligibly to the coincidences in the 100 keV region. Only few fission product gammas are in the neighbourhood of the Au line. Therefore the stabilization is not influenced by changes of their gamma spectrum and remains fixed to high degree of accuracy during the measuring period, normally a few days after irradiation. Using plutonium foils, the detectors are shielded with 2 mm of lead and 1 mm of cadmium to depress the low energy residual activity of the foils. The ^{198}Au stabilizing method is used successfully also in this case.

Fission product gamma counting rates C_γ are not only proportional to fission rates R but also to the yields Y_i of the fission products

$$C_\gamma \approx \sum_i Y_i(E) \cdot R$$

Here the sum is taken over all fission products contributing above the γ -energy threshold and $Y_i(E)$ indicates, that the yields are dependent on the neutron energy causing the fission process. For different measuring

positions the changes in neutron energy spectrum can be considerable, due to heterogeneity effects in the cell or due to zones of different fuel enrichment. As a consequence the simple proportionality between fission product γ -activity and fission rate is invalidated. To investigate this problem in detail, depleted and enriched uranium foils were irradiated between calibrated fission chambers in the core center and in the blanket of a fast assembly. The spectral index σ_{f8}/σ_{f5} changed from 0.033 to 0.021. The γ -activity of the irradiated foils was measured several times from 10 to 500 hours after irradiation using a Ge (Li) detector and a 4 k ADC. Due to the high resolution of the detector, 15 fission products out of 12 mass chains, which contribute most to the fission product activity, could be isolated. From the gamma rate ratios and the chamber rate ratios, yield ratios for the two positions were calculated. Fig. 4.2.a and 2b show the results for fission products of ^{238}U and ^{235}U . Fig. 4.2.c shows the yield ratios for ^{235}U irradiations in a thermal and a fast flux. There are indications, that the general trend depicted in Fig. 4.2.c is reproduced in Fig. 4.2.b in a much smaller scale. For integral measurements with NaI detectors above 500 keV, however, the error introduced in relative fission rate measurements due to changes in neutron spectrum is calculated to be less than 0.5 % for a global traverse through a fast reactor into the blanket. For intracell measurements with spectral changes much smaller the errors are even smaller. On the other hand, the errors are large for large spectral changes as demonstrated in Fig. 4.2.c. Therefore, if such measurements are required, i.e. for calibration purposes, they are always connected to fission chamber measurements in the corresponding spectra. Applying the above mentioned techniques properly, the overall accuracy for fission rate measurements by the integral method in one reactor zone is mainly limited by counting statistics. For typical irradiation data in SNEAK - 1 h duration at 2 to $5 \cdot 10^9$ neutrons/cm²sec - the statistical error is about 0.5 % for depleted uranium foils and 0.1 - 0.2 % for enriched uranium and plutonium foils. If the neutron spectrum is changing, i.e. in zones of different enrichments, the error contribution due to possible yield changes has been shown to be less than 0.5 % in fast assemblies.

The error of spectral index measurements is composed of the error of foil measurements, carried out at the position of interest and between fission chambers needed for normalization, and of the error of the

chamber measurements. The second one is the limiting factor for the overall accuracy of about 1.5 %, as the relative effective masses of the chambers are only known to about 1 % for $^{238}\text{U}/^{235}\text{U}$ and 1.5 % for $^{239}\text{Pu}/^{235}\text{U}$.

As mentioned above, ^{238}U capture rates are determined by measuring the gamma-X-rays coincidences in the 100 keV region due to ^{239}Np decay. To get the more interesting value $\overline{\sigma}_{c8}/\overline{\sigma}_{f5}$ (or $\overline{\sigma}_{c8}/\overline{\sigma}_{f9}$) either a calibration in a thermal neutron flux is made or capture and fission rates are determined absolutely /4.6/. In the second case, correction factors in the order of 50 % have to be introduced due to the selfabsorption of the 100 keV gammas in the 0.1 mm thick activation foils and in the backing of the ^{243}Am source used for detector efficiency calibration. Therefore, only relative capture rate measurements are of a good accuracy and reliance and the thermal calibration is preferable if the coincidence method is applied. In this case, however, one has to make sure that the spectrum is well thermalized, since small contributions from epithermal neutrons lead to large errors in the effective ^{238}U capture cross sections.

Absolute measurements of ^{238}U capture rates with an accuracy of about 1 % can be made using semiconductor detectors. With a Ge (Li) detector it is possible to resolve the higher energy gammas of ^{239}Np in the region from 210 to 330 keV. Of these peaks the 277 keV peak is not influenced by fission product gamma rays and can even be determined with high precision using uranium foils enriched up to 35 % in ^{235}U . The detector efficiency is determined by means of an ^{243}Am source calibrated by low geometry α -counting. The correction for gamma selfabsorption is about 5 % for the 277 keV line using 0.1 mm thick uranium foils. Measurements using sintered UO_2/PuO_2 foils containing 26.6 % plutoniumoxide have been done. In this case, however, the accuracy of the peak area determination is about a factor of 5 less than with depleted foils due to the high residual activity of ^{239}Pu . A difference between the results obtained with such detectors and those measured by depleted uranium detectors could not yet be clarified.

To get the spectral index $\overline{\sigma}_{c8}/\overline{\sigma}_{f5}$ (or $\overline{\sigma}_{c8}/\overline{\sigma}_{f9}$) the absolute capture rates are compared to absolute fission rate measurements made with chambers. The elaborate procedure limits at the moment the accuracy of the spectral index measurements, as no chambers with an effective mass known to better than 2 - 3 % are available. Therefore, work is in progress to improve absolute fission chamber measurements.

To illustrate the capability of the activation method, recent results are shown. In SNEAK-9B, an axial mock up of the fast breeder prototype SNR 300, the fine structure of reaction rate distributions were measured in core and blanket cells. Fig. 4.3. shows the results for ^{238}U fission and capture, corrected for the overall flux gradient in the measuring positions. KAPER-calculations, using the KFK INR-set were made for the equilibrium spectra of the two zones (see chapter 3). They are compared with the experimental results obtained in cells, which are several mean free paths from the core-blanket boundary.

4.1.2. Calibration of fission rate measurements

As described in previous sections the γ -spectrum emitted from activated fuel shows - besides its proportionality to the fission rate - a complicated dependence on the fissionable isotope, the neutron spectrum causing fission, on duration of the irradiation, and time elapsed from the end of irradiation. Therefore it is advantageous to calibrate each activation experiment by simultaneous irradiation and evaluation of an additional set of activation foils placed between the fissionable layers of a pair of ionisation chambers. The chambers are of the parallel plate type. The effective diameter of their fissile layer is about 12 mm, it contains between 40 and 300 μg of fissile isotopes. The chamber walls are made of aluminium of 0.5 mm thickness.

Usually during an irradiation the pair of chambers with the set of reference foils is placed in the reactor zone to be mapped. The chambers are located so removed from the activation foils that no perturbation of the neutron flux in the vicinity of the detectors occurs.

A comparison of the γ -activity emitted by the reference foils and by the batch of detector foils yields the relative fission rate at each position. From the number of events recorded by the calibrated fission chambers during reactor operation absolute fission rates and fission ratios at each detector position are obtained.

The error of the relative activation measurement can be made $< 1\%$. It is mainly determined by instability of the γ -detecting electronic circuit and by statistics.

The statistical error of the fission chamber count rate is negligible against the systematic error introduced by the calibration of their effective fissile layer.

The deposits of U (natural), ^{238}U and ^{235}U -chambers were manufactured by D. Kuhn and H. Meister. They were assessed by accurate weighing procedures within an error limit of about 2% . ^{233}U layers deposited by identical methods were checked by low geometry α -counting. Agreement was found within 1% . Cross checks in thermal and fast neutron fluxes confirmed the mass ratios and provided also the ratio of the effective mass of the reference ^{238}U -chamber to that of the ^{235}U -chamber with a standard error of 1% .

Finally the effective mass of the ^{239}Pu reference chamber was assessed in the thermal column of the STARK-reactor with respect to the ^{235}U chamber. An error of 1% was assumed for this calibration due to the uncertainty of the thermal fission cross sections.

Absolute effective masses were estimated from the weighing of the ^{235}U foil. They are needed for obtaining the capture to fission ratio as described above, but also for the evaluation of experiments involving the determination of the reactivity scale by a spontaneous fission source.

The error limits which at present can be reached under optimal conditions in reaction rate measurements are listed in Table 4.1.

Table 4.1: Minimum error in reaction rate measurements

	^{235}U fission	^{238}U fission	^{239}Pu fission	^{238}U capture
reaction rate	2 %	2 %	3 %	1 %
$\frac{\sigma_x}{\sigma_{f5}}$	-	1.0 %	1.5 %	3 %

The reference fission chambers used at Karlsruhe were compared with a set of chambers calibrated by Campan (CEA Cadarache) by low geometry α -counting of the ^{239}Pu deposit. The fission ratios were found in agreement within the error limits, but the absolute masses quoted by Campan for the Karlsruhe reference chambers are 3 to 4 % lower. This discrepancy will be solved by additional calibrations. Several comparisons were made for σ_{c8}/σ_{f5} measurements. J.P. Brunet of Cadarache calibrated his measurements in the thermal column of the HARMONIE reactor and obtained within the error limit agreement with data obtained by the methods described before.

Further comparisons of independent methods for fission rate measurements, e.g. with fission track recordings, will clarify the remaining discrepancies, but probably reduce the errors quoted in Table 4.1 only slightly.

4.1.3. Fission track recording

Solid state track recorders (SSTR) are used to measure the fine structure of the fission rate over a platelet of the SNEAK assembly. This method recommends itself by the small and very often negligible perturbation caused in the reactor lattice. Lexan SSTR-foils of 60 μ thickness are used in close contact with thin source foils (Fig. 4.4).

The source foils contain a few micrograms of fissionable elements plated onto a 50 μ -aluminium foil. During an exposure of the detector system to a neutron flux, fission products are emitted from the source foils.

Fission products impinging on a SSSTR leave visible tracks. The number of tracks in a SSSTR, therefore, can be taken as a measure of the fluence.

After the irradiation of a stack of source foils and recorders the lexan foils are removed, cleaned and etched for 40 minutes in a 6N KOH bath at $50^{\circ}\text{C} \pm 0.5^{\circ}\text{C}$. The etching process enlarges the tracks produced by the fission products in the Lexan foils to a length of about $10\ \mu\text{m}$ and a diameter of about $1\ \mu\text{m}$. The etching is stopped by immersing the lexan foils in a 1% solution of acetic acid, then they are washed in an ultrasonic bath with distilled water. They are then dried and clamped between two microscope slides.

The counting of tracks per surface area of the SSSTR is performed by two different methods:

- 1) An optical microscope (Leitz-Orthoplan) with a total magnification of 100 is used in conjunction with a Leitz-Classimat. At this magnification the field of view as seen by the TV camera of the Classimat is about $0.04\ \text{mm}^2$. The instrument has a provision to shift the field of view automatically for scanning larger areas. To ensure that the detector remains in the focus throughout the scanning an automatic focussing device has been constructed /4.7./ and is initiated after every lateral displacement of the microscope table. The counting logic of the Classimat can resolve overlapping tracks only to a limited extent /4.8./.

- 2) In the second method of track counting, henceforth called computer counting, almost all the overlappings are resolved. The image information, in the form of a binary matrix of 576×576 bits, as delivered by the Schmitt-trigger of the Classimat, is written on a magnetic tape with the help of the direct memory access channel of the computer DDP-124. The processing of this image information is carried out with a Fortran program. This program enables counting of all the tracks whose area exceed a prefixed limit and do not cross the upper or the left hand boundary of an electronic mask. The counting losses experienced (see below) are due to:
 - 1) Overlappings like . Here, though the overlappings are resolved the scanning of the first track may reduce the size of the second track to such an extent that, a small fraction of those tracks is excluded from counting.

2. Since the scanning is not continued beyond the boundaries of the mask some of the boundary tracks also experience reduction of size and are not counted.

Both of these effects cause a smearing of the peak in the area distribution curve (Fig. 4.5) towards smaller areas. The counting losses are determined by exact calibration as described below.

To calibrate both these methods of counting, SSTR foils of different track densities are prepared by bombarding them with the fission products of a ^{252}Cf source. The scanning area of the SSTR is chosen to yield a minimum track count of $3 \cdot 10^4$ with a statistical error of 0.6 %. The results are given in Fig. 4.6. The measured track densities (N) can, in both cases, be fitted with the formula:

$$N = N_0 e^{-bN_0}$$

where N_0 is the true track density and b is a fit parameter.

In case of Classimat counting ($b=1.5 \cdot 10^{-4}$ mm²/track) the curve is for track densities greater than about 2000 track/mm² too flat to be of use for precision measurements. The calibration curve for computer counting however, can be used up to 10^4 tracks/mm² due to smaller counting losses. The value of b determined here is $2.01 \cdot 10^{-5}$ mm²/track with a standard error of 3 %. This uncertainty in b would cause an error of 0.6 % at track densities of 10^4 track/mm². Counting losses at this density are about 20 %.

In addition to the above mentioned effects the imperfection of the image and insufficient contrasts are also responsible for the counting losses. The staining of tracks as practised by Richmond and Ruegger /4.9./ did not bring marked reduction in counting losses. Repeating the calibration process from the beginning reveals that the new value of b is close to the previously determined value but is not within the error limits. Therefore, if absolute measurements of the reaction rates are required a few SSTR foils of known track densities should be etched and evaluated together with the detectors for simultaneous calibration.

Uranium and plutonium fission rate measurements with track recorders in the SNEAK9B lattice showed poor reproducibility. It is not attributed to counting errors but to difficulties encountered in mounting the source foil - detector arrangement. The evaluation of about 100 pictures taken from one SSTR took about 75 hours computing time of the DDP 124. This is no serious drawback for the computer evaluation since the counting is performed automatically while this computer is not used otherwise. Therefore, some more effort will be required to improve the procedures for track recorder preparation.

4.1.4. Fission rate mapping by the whole platelet method

A method for determining the relative fission rate distribution in SNEAK by measuring the γ -activity on the irradiated fuel platelets is being developed.

A single photomultiplier and 2" x 2" NaI (Tl) crystal encased in a 20 cm thick lead shield is used to detect the gamma activity; and a simple automatic sample changer has been constructed. A conical lead aperture is inserted between the detector and the platelet, and it has also been found necessary to use a lead filter to reduce the intensity of the low energy gamma-rays. The integral counting rates above several different discriminator thresholds are recorded.

In principle the method is very simple and has the advantage of not introducing extraneous material into the core, thus eliminating the possibility of the measurement itself introducing perturbations. It is also attractive for reactor operation, because the γ -scan of the platelets can be carried out after any other experiment which requires about 3 to 5 kWh reactor power. Consequently this method could prove superior to fission chamber measurements especially if large gradients in power distribution are expected.

However there are a number of difficulties inherent in this approach, the main problem being in obtaining the fission rate distribution from the counting data. Since the platelets usually consist of a mixture of isotopes, a knowledge of the relative fission yields is necessary to obtain the total fission rate distribution. For uranium metal platelets we can write

$$Z = R_5 \gamma_5 + R_8 \gamma_8$$

where Z is the measured counting rate at some particular time; R_5 and R_8 are the fission rates of ^{235}U and ^{238}U in the platelet being counted, γ_5 and γ_8 are lumped parameters which are functions of the respective yields, of detector efficiency, of duration of the irradiation, of the time elapsed from the end of the irradiation, of the neutron spectrum during the irradiation, etc. Writing the total fission rate $R_T = R_5 + R_8$, it follows that:

$$Z = R_T \gamma_5 \left(1 + \left(\frac{\gamma_8}{\gamma_5} - 1 \right) \frac{R_8}{R_T} \right)$$

Then, assuming that γ_5 is independent of the neutron spectrum change over the measuring region, the relative counting rates of a series of platelets from an irradiation are proportional to the total fission rates within the platelets apart from the correction factors

$$\gamma_8 \left(\frac{\gamma_8}{\gamma_5} - 1 \right) \frac{R_8}{R_T} .$$

The ratio $\left(\frac{\gamma_8}{\gamma_5} \right)$ should be mainly a function of the relative yields, and estimates of this ratio have been obtained from various measurements. Although the statistics were poor and the evidence for the time behaviour of the ratio was conflicting, it was found, that $\frac{\gamma_8}{\gamma_5} = 1.00 \pm 0.005$ should account for variations in this ratio arising from the time behaviour (up to a few days after irradiation), from the different discriminator settings (approximately 430 keV to 900 keV), and from the differences in spectrum over the measuring region.

In a fast core $\frac{R_8}{R_T}$ is typically of the order of 0.2. If this ratio decreases by a factor of two in going to the core boundary, the 5 % uncertainty in the $\left(\frac{\gamma_8}{\gamma_5} \right)$ ratio would result in only a 0.5 % uncertainty in the estimated total fission rate at the boundary relative to the estimate at the core center.

The situation with the PuO_2UO_2 platelets used in SNEAK is considerably more complicated, but in principle can be evaluated in a similar way,

and it is expected that the contributions from the higher plutonium isotopes and the uranium will lead to a total correction factor, analogous to that above, of a few percent. Here it will be necessary to estimate the changes in relative fission rates $\frac{R_8}{R_{III}}$, etc. over the measuring region; however, since the total correction factor is small, these can be obtained to sufficient accuracy by a simple diffusion calculation.

A statistical error of $\pm 1\%$ has to be added to the results of the γ -analysis to account for the uncertainty of the fuel mass contained in each platelet. This source of error can be eliminated by careful weighing procedures during fuel fabrication.

The principle of the method had been tested to a limited extent in several SNEAK-assemblies. Although the whole platelet method involves a number of assumptions and contains several sources of potential uncertainty, in practice it has been found to give consistent results, and it is believed that an accuracy of better than $\pm 1.5\%$ in the total fission rate distribution can be obtained.

The method can be extended to measuring the variation of activity over the surface of the platelets by using a suitable slit aperture between detector and platelet. This enables, for example, the power distribution in the vicinity of a control rod to be determined. A few such measurements using a 2 mm wide slit were performed in SNEAK-2C using PuO_2UO_2 platelets (without corrections for isotopic yields).

As an example the fission rate distribution along the central axis of assembly SNEAK-8 is shown in Fig. 4.7. This assembly was uranium fueled. It consisted of a central test region with $k_{inf} \approx 1.0$, surrounded by a highly reactive driver region and a depleted uranium blanket. The fission rate distribution was obtained from the γ -emission of the uranium platelets with enrichments of 35%, 20%, 0.7% and 0.4% used for constructing the driver and the test zone.

The ratio $\frac{R_8}{R_T}$ varies extremely: from 0.27 at the center to 0.36 at the boundary of the test zone, and from 0.05 to 0.07 in the driver. If $\frac{\gamma_8}{\gamma_5} = 1$ is chosen, agreement between fission chamber measurements and γ -activity scan is found within 2 %, which is in accordance with the estimate given above. Since fission chamber measurements along steep gradients of the fast neutron flux generally show a smoothing tendency the results of the γ -scan appear even more representative for the fission rate distribution. A diffusion calculation (KFK INR set, 2D-program DIXY) performed for a flux distribution symmetrical to the midplane of the core shows good agreement in the large test zone. However, it underestimates the total fission rate in the driver region by about 3 to 4 % on the average.

To summarize, the whole platelet technique appears to be a promising complementary measuring technique, and is a step towards the methods that will be employed to determine the power distribution in the SNR from the irradiated fuel pins.

4.1.5. Measurement of the γ -heating with RPL-glasses

The power profile of a reactor is not only determined by the fission rate distribution but also by the energy deposited by γ -absorption. γ -heating may contribute up to 20 % to the total absorbed energy. The spatial distribution of γ -absorption can appreciably deviate from the total fission rate distribution. Therefore, new experimental techniques for measuring the profile and absolute values of the γ -heating have been developed.

Ionizing radiation generates luminescence centres in silver-activated metaphosphat glasses (RPL-glasses). The density of the luminescence centres is a measure of the absorbed energy (per mass unit). This density is measured by means of the luminescence radiation which is emitted when the glasses are irradiated by ultraviolet-light. Details of the method are given elsewhere /4.10/.

The γ -heating $[W/g]$ in some material is determined by

$$H\gamma = C_1 \cdot v_{\text{mac}} \cdot I\gamma/t$$

C_1 was obtained from comparison measurements in monoenergetic γ -fields with glass detectors and calibrated ionization chambers, v_{mac} is the average (over the corresponding γ -spectrum) of the ratio of the mass-energy-absorption-coefficients for the material to be investigated and the glasses (it is within a few % equal to one for most materials), $I\gamma$ is the γ -contribution to the total effect in the glasses and t the measuring time. In the mixed neutron- γ -field of a fast reactor the total effect in the glasses

$$I_{\text{tot}} = I\gamma + I_n$$

is composed of the γ -and the (relatively small) neutron-contribution. The neutron effect is mainly due to the recoil nuclei generated by the fast neutrons. For the determination of the γ -heating the neutron effect is corrected by

$$I_n = C_2 \cdot q \cdot \phi \cdot t$$

C_2 is determined in a field with known γ -and neutron-characteristics. q is the real recoil energy generated per unit mass and unit fluence. The fluence $\phi \cdot t$ is calculated from measured absolute ^{235}U fission rates.

Fig. 4.8 shows as example the central axial traverse in SNEAK-9B. The neutron effect (I_n/I_{tot}) amounts to about 18 % in the inner part of the blanket, in the other region it is slightly greater than 10 %. In the core center the γ -heating is 22.1 $\mu\text{W/g}$ (at 1 kW reactor power) and decreases to about 1 $\mu\text{W/g}$ in the outer part of the blanket.

4.1.6. Activities to improve the reliability and accuracy of reaction rate measurements

Reaction rate measurements in critical facilities are needed for the accurate prediction of the breeding ratio and the power distribution in fast breeder reactors. They are also a valuable tool for checking group cross section sets. Therefore, efforts to improve the accuracy of the measurements are justified.

For γ -heating measurements the sensitivity of the glasses for fast neutrons should be determined more accurately, since it is the main contribution to a possible systematic error of about 5 %.

Fission rates and fission ratios can be measured with 1 to 3 % precision. This is usually accurate enough for a power profile mapping. It is felt that the further development of the techniques requires less attention than the improvement of the calibration procedures, which can help to make predictions of related reactor parameters, e.g. the breeding ratio, more reliable (see chapter 6).

So, e.g. the measurement of the fission rate by counting of fission product gammas for the calibration of σ_{c8}/σ_{f5} -ratios in a thermal neutron flux should be scrutinized. Although the effective mass ratio estimate of fission chambers appear to be satisfactory, the discrepancies found in absolute determinations should be solved. The future activities will concentrate on the following steps.

- Establishing an absolute basis for fission track recording
- Comparison of truly independent calibration methods
- Comparison of results obtained by different groups using their methods for measurements in identical lattices under identical conditions.

Intercalibrations of the last type were already practiced. Measurements in assembly SNEAK-8, which was almost identical with the Winfrith assembly ZERA 8, provided a first check on σ_{f8}/σ_{f5} and σ_{c8}/σ_{c5} .

In several SNEAK assemblies detectors of the Karlsruhe and the Cadarache group were irradiated simultaneously, but evaluated separately. The majority of the results was in good agreement. Finally, first experiments of the Karlsruhe group were carried out in the Mol $\Sigma\Sigma$ -facility. They will provide a comparison with the standards used in Belgium and the USA.

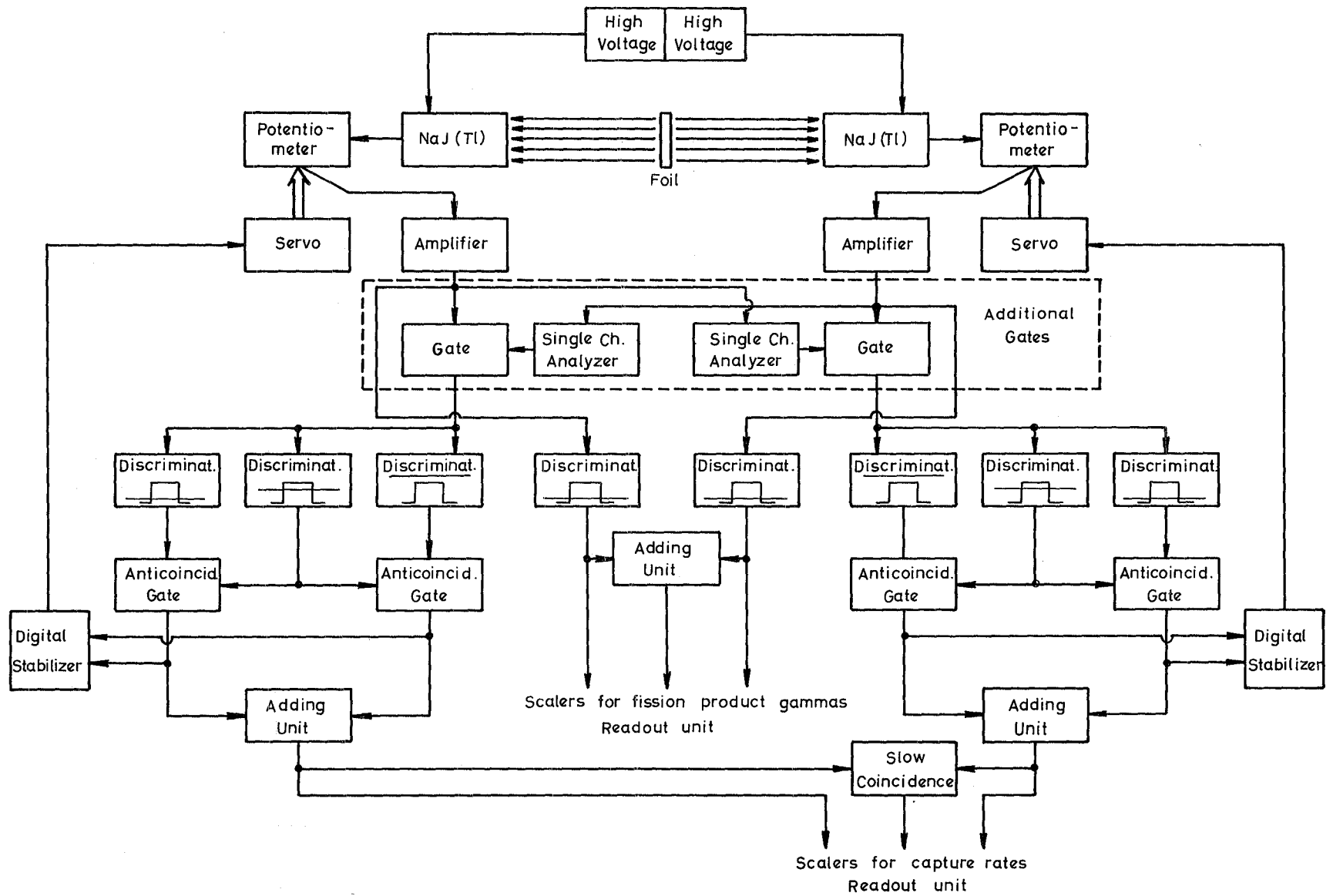


Fig.4.1 Electronic equipment for γ -x-coincidence (capture) and fission (product) γ measurement

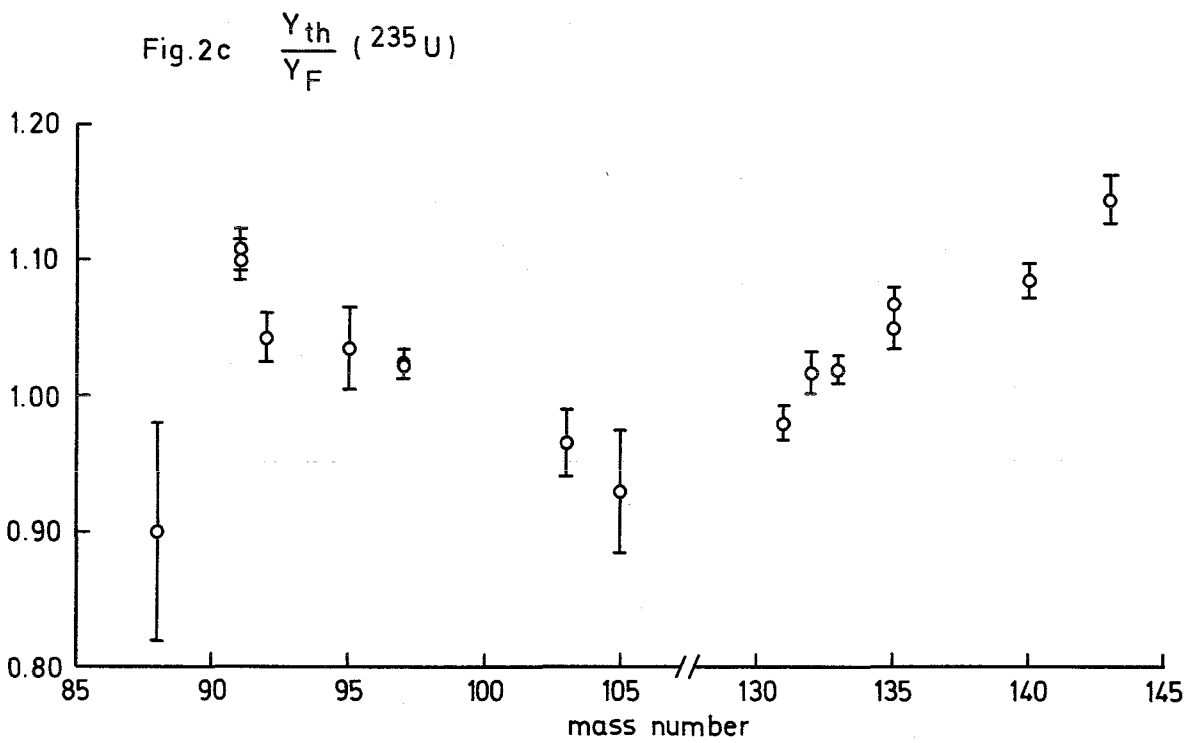
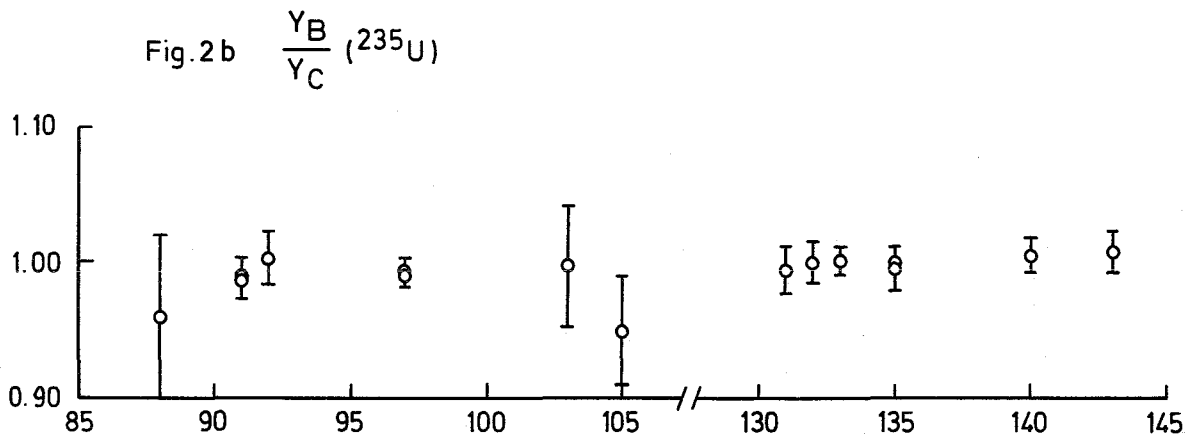
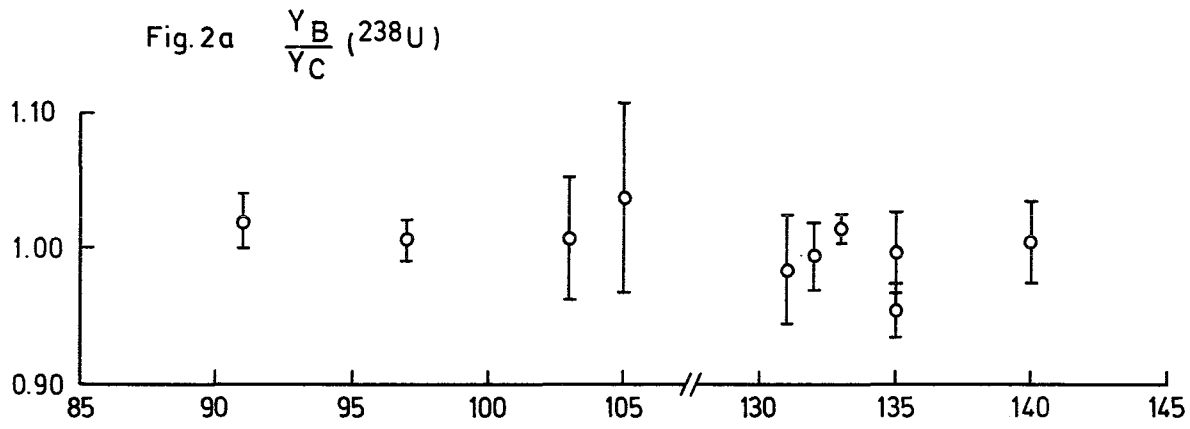


Fig. 4.2 Ratios of fission product yields

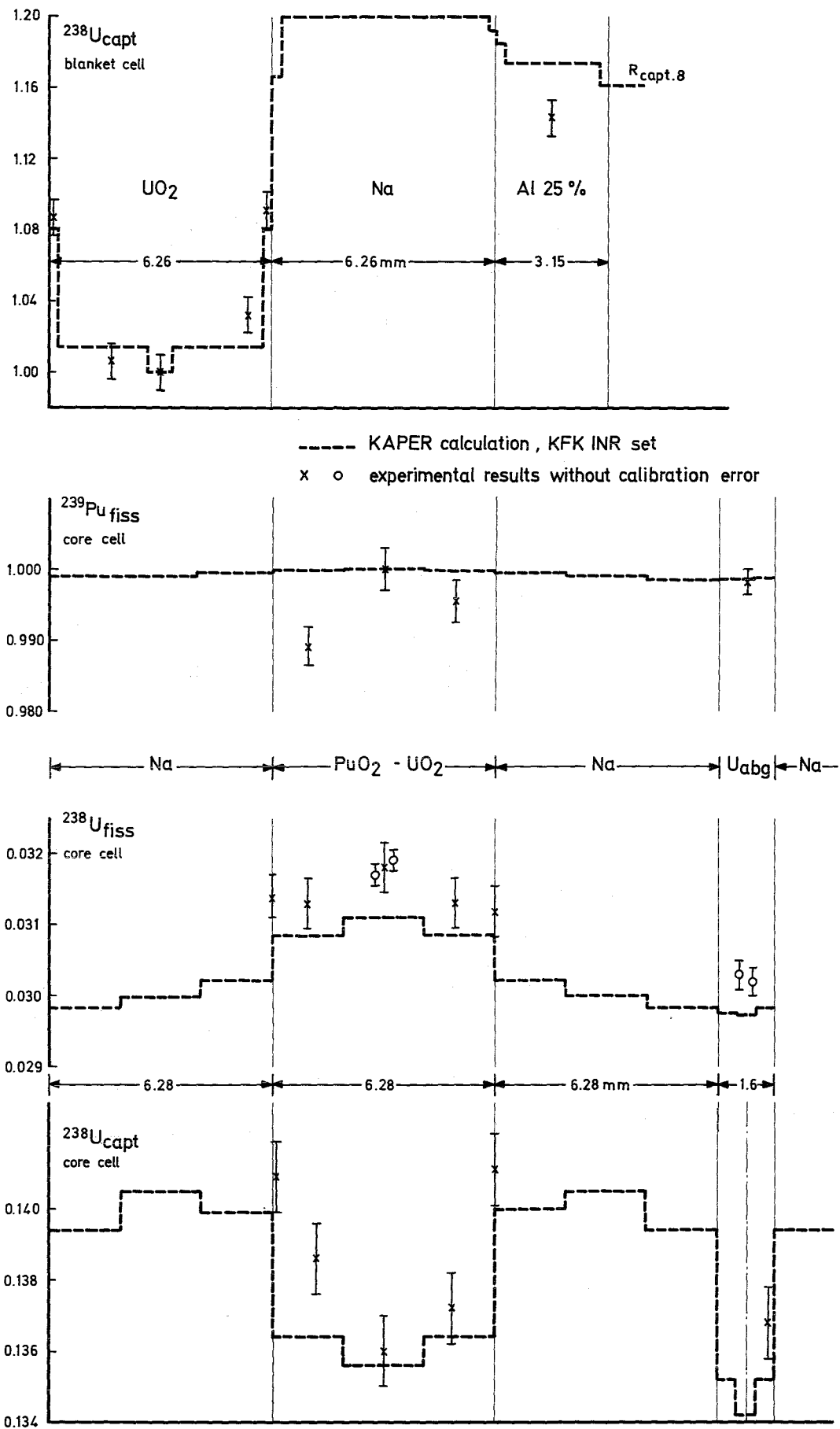
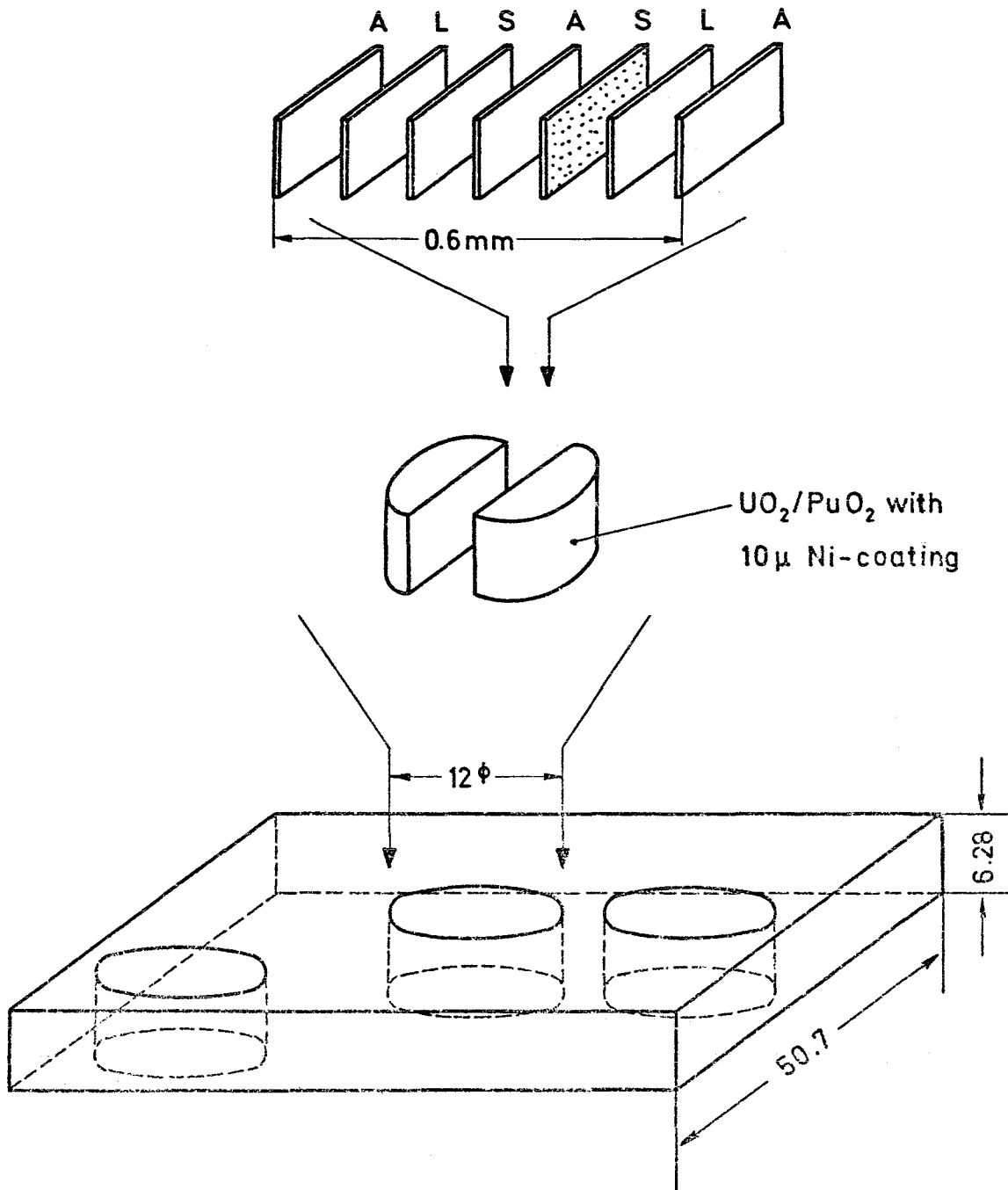


Fig.4.3 Reaction rate distribution in lattice cells of SNEAK-9B



- A Aluminium
- L Lexan
- S Source

Fig. 4.4: Special UO_2/PuO_2 platelet with access holes, filling pieces, and SSTR

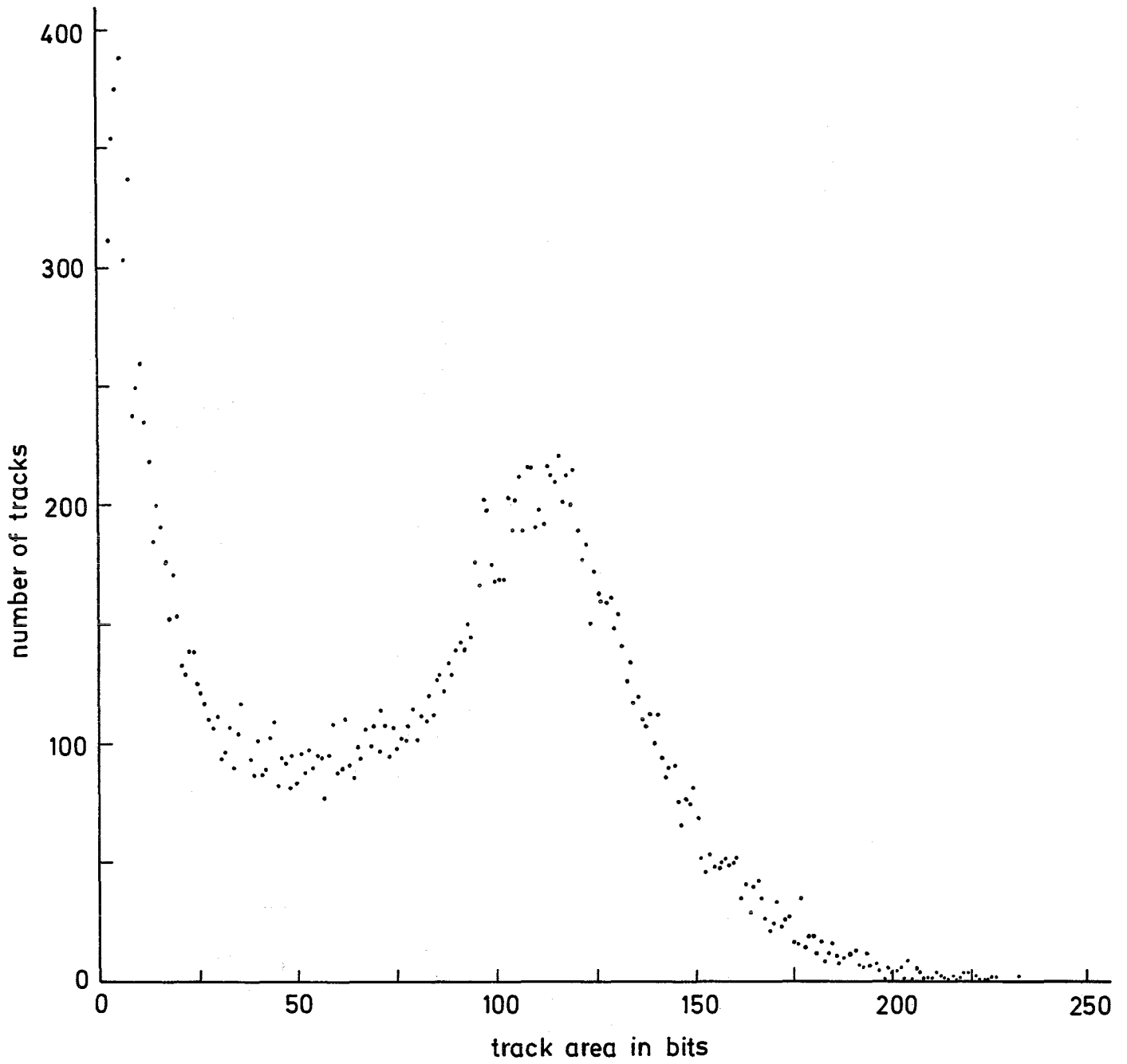


Fig.4.5 Track area distribution

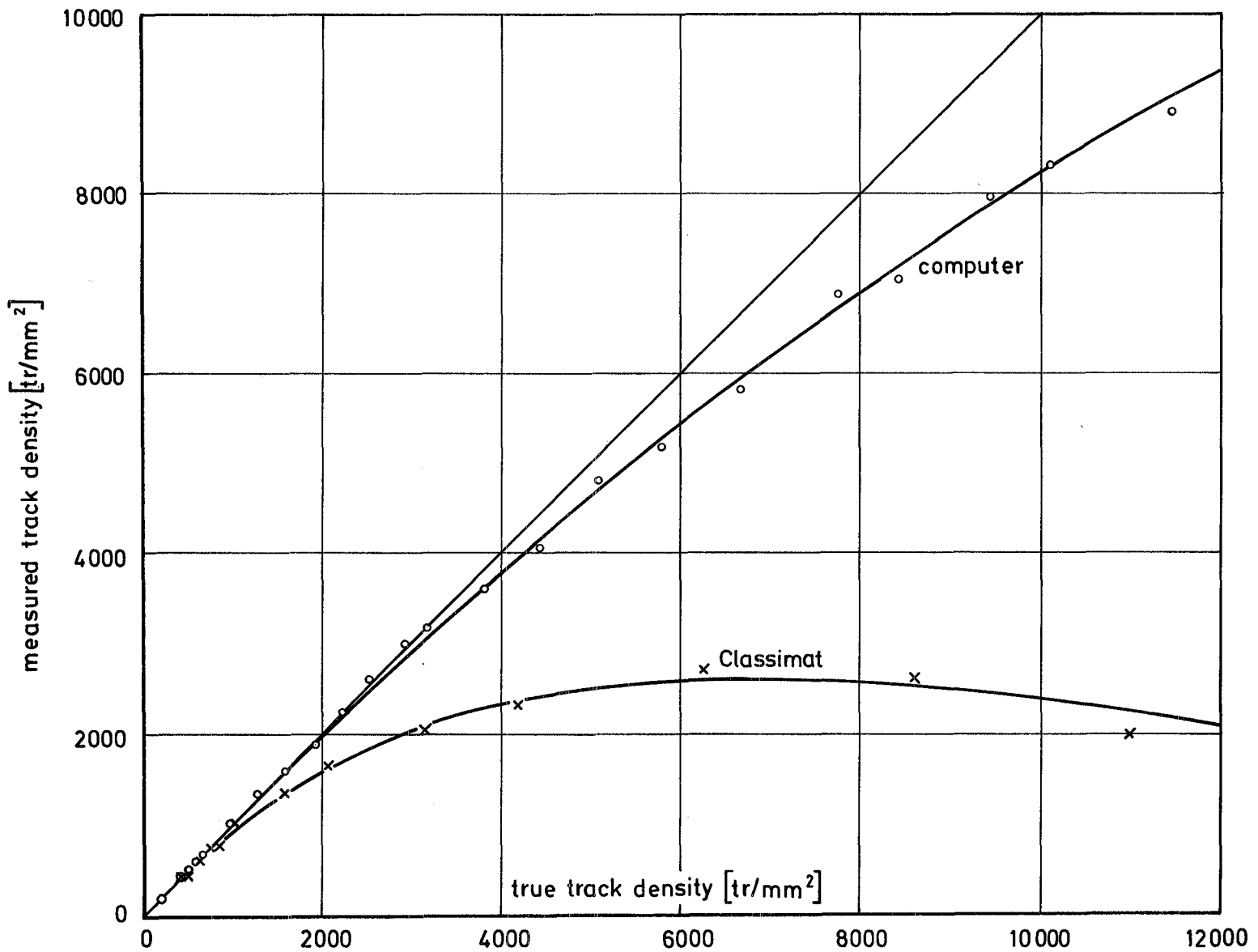


Fig. 4.6 Calibration curves for FISSION TRACK RECORDING

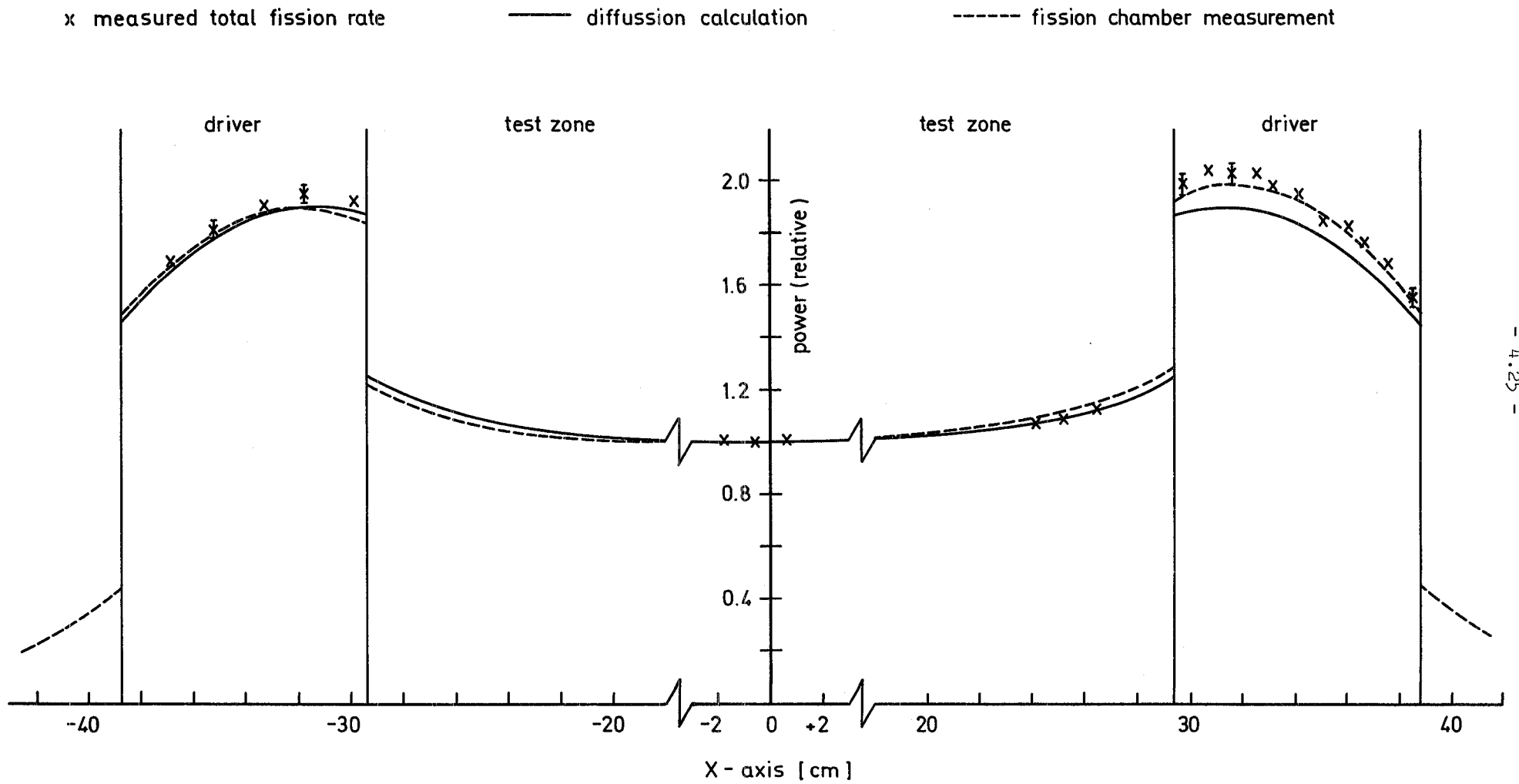


Fig. 4.7

SNEAK-8 Axial power traverse measured by γ -counting of the fuel platelet activity

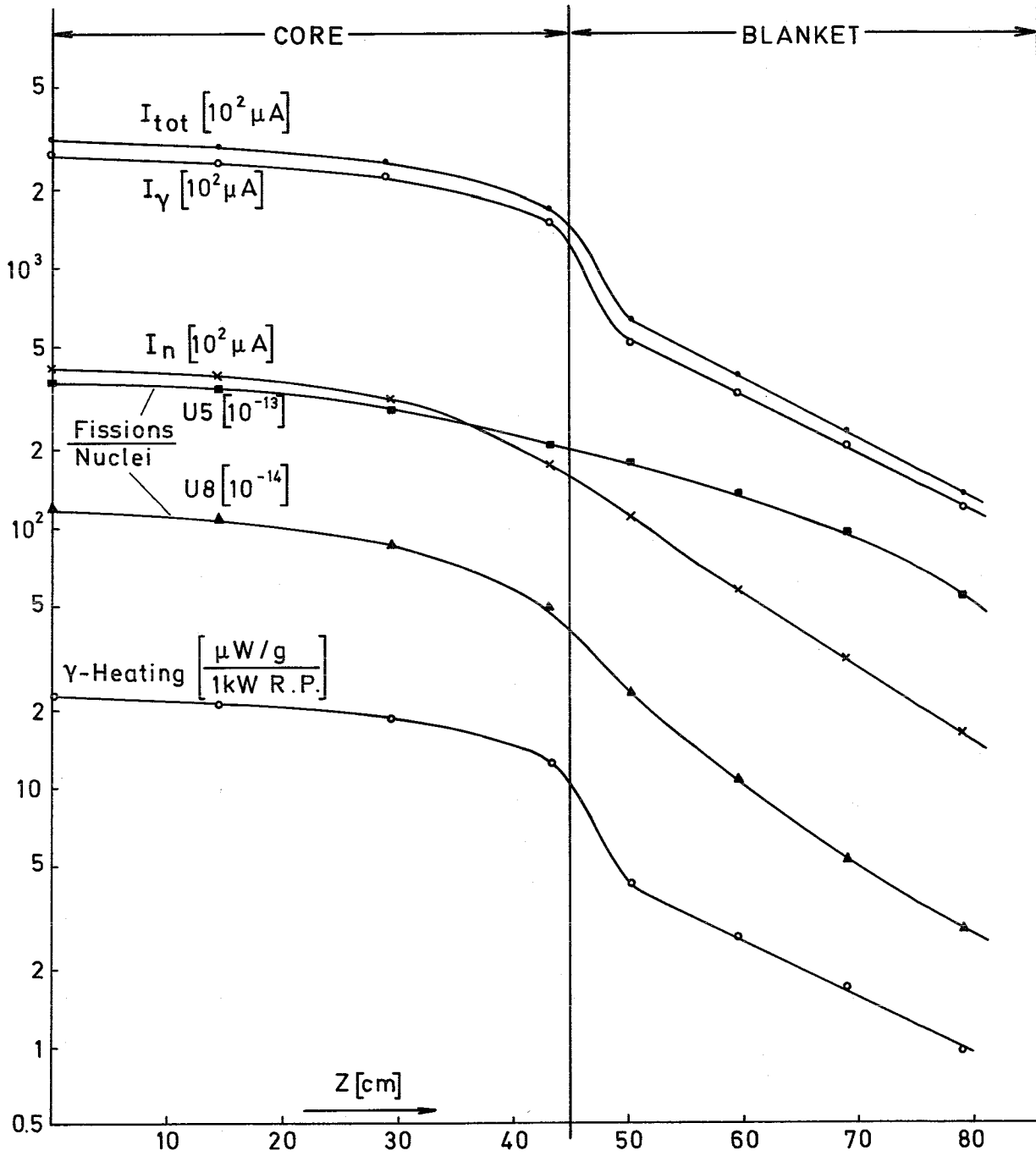


Fig.4.8 Central axial traverse of RPL-measured γ -heating in SNEAK-9B

4.2. Spectrum measurements

Considerable effort has been devoted to improve the methods of neutron spectrum measurements in fast reactors. The aim was to get reliable information about the neutron distribution in addition to the information obtained from reaction rate measurements. Only the complete picture of neutron behaviour in fast systems can provide means for resolving deficiencies in the theoretical treatment.

In the following sections the spectroscopic devices and the results of intercomparison measurements are described.

4.2.1. Proton recoil proportional counters

Spherical, BENJAMIN-type /4.11/ ($\phi = 3.94$ cm) and cylindrical (diameter up to 10 cm, length up to 100 cm) counters are used. The counters are filled with hydrogen, methane, krypton (for wall-effect reduction) and mixtures of these to a total pressure of up to 4 atm. Energy calibration is carried out by adding some (≈ 0.1 Torr) ^3He to the filling and observing the 764 keV peak. The position of the peak was checked with monoenergetic neutrons from the ^7Li (p,n) ^7Be -reaction and with a lead-pile slowing-down time spectrometer /4.12/. According to these measurements the energy E is related to the measured pulse height by

$$E = \frac{E_c - E_o}{I_c} \cdot I + E_o$$

where E_c is the energy of the calibration peak, I_c the corresponding pulse height and E_o equals 0.4 keV and 30 keV for hydrogen and methane respectively (Evaluation is assumed to be confined to energies above 20 keV and above about 200 keV for hydrogen and methane respectively).

The evaluation is done with a code similar to that described by BENJAMIN /4.13/. For the spherical counters the (wall-effect distorted) response functions are calculated by the analytical method of SNIDOW /4.14/,

for the cylindrical counters by a Monte Carlo code /4.15/. Calculated response functions have been compared with measured distributions of monoenergetic neutrons.

Generally, the measured distributions show larger deformations (from the ideal rectangular shape) than the calculated ones, especially if the wall-effects are small /4.16/. These discrepancies are assumed to be partly due to low-energetic neutron background and, especially for the cylindrical counters, due to the decreasing gas amplification at the end of the counter which is not taken into account until now in the Monte Carlo Code.

The energy range covered by the proton recoil counters is from about 10 keV (inconstancy of energy loss per ion pair for hydrogen below 10 keV /4.12/) to about 1.5 MeV for the spherical and to 10 MeV for cylindrical counters (neutron entrance parallel to the wire) /4.16/.

4.2.2. ^3He -Semiconductor-Sandwich-Spectrometer

A new type of ^3He -semiconductor-sandwich-spectrometer has recently been developed and tested /4.17/. This spectrometer differs from the ^3He -sandwich-spectrometer used by other authors

- 1) by a discrimination possibility against γ -background and
- 2) by the possibility to correct for energy losses of the protons and tritons in the ^3He -gas. Therefore, it is possible to extend its useful energy-range down to 100 keV.

The space between the two circular Si-surface barrier detectors is used as proportional counter. A 40 μ thick counting wire fixed in the midplane between the two semiconductor diodes forms the anode. The spectrometers are normally filled with 2.5 atm ^3He and 10 Torr CH_4 . The proportional counter is operated at rather low voltages (around 500 volts) leading to moderate gas multiplication factors. The distance between the two Si diodes is 0.6 cm. Si diodes with a sensitive area of some hundred mm^2 and a depletion depth of some hundred μ are used.

The spectrometer system only accepts such events which have produced pulses both in the semiconductor detectors and in the proportional counter, the amplitudes of which exceed certain levels introduced by the electronic system. The possibility of discrimination against γ -background is based on the fact that the specific ionization of Compton electrons (mainly produced in the Si-diodes) is much smaller than that of protons or tritons. Correspondingly the energy losses of the latter in the ^3He -gas are considerably larger than that of electrons with the same energy. The electronic system of the spectrometer is shown in Fig.4.9 Its fast coincidence unit (resolving time 200 nsec) which opens a linear gate considerably reduces the number of summed semiconductor pulses before adding up the proportional counter pulses. Therefore, pile-up between the broad proportional counter pulses (shaping time 2 μsec) and the summed semiconductor pulses stretched to 3 μsec is strongly reduced. The three-fold sum is multiplied by the proportional counter pulse in a logarithmic computer. The product is generally considerably larger for proton-triton pairs than for electrons. Therefore, proton-triton pulses can be separated from electron pulses by a single channel analyzer.

The energy resolution of the whole system amounted to about 60 keV fwhm. This good resolution is mainly achieved by the addition of the proportional counter pulses, which improves it from about 200 keV to 60 keV. The calibration of the semiconductor diodes was carried out with a ^{233}U - α -source deposited on a thin VYNS foil and placed in an evacuated spectrometer of similar design. By means of this energy calibration the position (channel number) of the thermal peak of the ^3He (n,p)t-reaction was determined and then the amplification of the proportional counter was changed until the experimental position agreed with the calculated one in order to get the right correction for the energy losses in the gas.

From each measured pulse height spectrum such events resulting from (n,p) and (n, α)-reactions in the Si diodes had to be subtracted. This was achieved by another measurement with a similar spectrometer where the ^3He -gas had been replaced by ^4He . Due to the high efficiency this background was less than 15 % over the whole energy range.

For calculating the neutron spectrum from the measured pulse height distribution it is necessary to know both the $^3\text{He}(n,p)t$ -cross section and the geometrical efficiency of the spectrometer. The geometrical efficiency has been calculated by a Monte Carlo program /4.17/ and the results of this program were checked for different neutron beam entrance directions and different energies between 100 keV and 2 MeV. The agreement between measurement and calculation was satisfactory. The $^3\text{He}(n,p)t$ cross section used for the evaluation is that recommended by ALS-NIELSEN /4.18/.

4.2.3. Time-of-Flight-Spectroscopy

Fast neutron spectrum measurements have been performed for many years at the fast subcritical facility SUAK.

This facility is designed to build and to investigate fast subcritical cores of $k_{\text{eff}} \leq 0.90$ or even non-multiplying systems, and is provided with pulsed ^{14}MeV neutron sources and a flight tube of 100 m. Spectrum measurements by time-of-flight techniques and by other methods are described and compared in previous reports /4.19-21/. At the time these reports were published the largest inaccuracy of the time-of-flight spectroscopic technique was due to inaccuracies in neutron detection efficiency of time-of-flight detectors and systematic errors in background determination. Thus, our latest work has concentrated on reducing both sources of errors and at the same time on extending the measurable energy range.

Fast neutron time-of-flight detectors have a more or less strongly energy dependent neutron detection efficiency and none of them is suited to measure the entire spectrum from 10 eV to 10 MeV. Three detectors are used, a ^6Li -glass NE 905 scintillator of 111 mm diameter and 25,4 mm thickness, a Boron 10-vaseline slab plus 4 NaI-crystals and a 50,8 by 50,8 mm cylindrical NE 213 liquid scintillator. Their energy dependent neutron detection efficiency was calculated. The codes and cross section data were analyzed in detail, and checked by calculating already published efficiencies of other detectors relying on the same principle. These calculated efficiencies

and the spectroscopic techniques were furthermore checked; in particular in the energy range of their overlapping energies, by measuring with each detector the spectra of the pulsed sources "UNAT" and "UPOL" /4.22/. These sources are designed to achieve time-of-flight measurements with good energy resolution and good statistical accuracy within short runs. Many repetitive measurements and transmission measurements of black resonances were performed to understand and reduce systematic errors. The "UNAT" source is a parallelepiped of 15x15x20 cm made of natural uranium only, with a pulsed 14 MeV neutron source of 2 ns burst width /4.23/ at the center. The "UPOL" source is built by covering one side of the "UNAT" source with 2 cm of polyethylene. Both sources have nsec decays /4.24/, thus allowing short flight paths, thus high counting rates and convert the 14 MeV source into a source-spectrum extending from 14 MeV down to thermal energies.

The Boron 10-vaseline slab is a practical approach of the desired standard neutron flux detector with energy independent detection efficiency and is suited for that purpose. To calculate its efficiency a special Monte-Carlo code has been written /4.25/. A parametric investigation of the influence of inaccuracies in the cross-section data underlying the detection process demonstrates that the inaccuracies in cross-section data are negligible below 2 MeV /4.26/. The Monte Carlo code was checked by calculating the efficiency of the Harwell Boron 10-vaseline slab /4.27/ and the largest deviation amounts to 9 % at 100 keV. A calculation of the Karlsruhe Boron 10-vaseline slab by the Cadarache Monte-Carlo-Code is actually in process. Disadvantages of the Boron 10-vaseline slab are: the small efficiency, the gamma sensitivity, the poor timing accuracy and its heavy shield. Therefore the Boron 10-vaseline slab is used only as a neutron flux standard within the energy limits from 1 keV to 2 MeV. For routine spectrum measurements it is preferred to use the ^6Li -glass- and NE 213 scintillator which are calibrated to the first in the energy range mentioned above, but outside these energy limits they rely on their own calculated efficiency.

The efficiency of the ^6Li -glass scintillator was calculated with the Karlsruhe Monte-Carlo code KAMCCO /4.28/ and with the $^6\text{Li}(n,\alpha)\text{T}$ cross-section data of the ENDFB III file which rely on the latest data of UTLEY and DIMONT /4.29/. The code and the cross-section data are checked by calculating already published efficiencies of SOWERBY /4.30/, CAMERON /4.31/ and NEILL /4.32/. In the energy range from 100 eV to 10 keV the values of /4.30/, /4.31/ and /4.32/ are reproduced to within respectively $\pm 0,9\%$; $\pm 3,0\%$ and $\pm 8,0\%$. The background determination by transmission measurements of black resonances, particularly below 1keV, are much more easy to perform with the highly efficient and well shielded ^6Li glass scintillator than with the Boron 10 slab detector. Therefore, and according to the confidence gained in the calculated efficiency of the ^6Li -glass scintillator, the latter is used as a neutron flux standard below 1 keV. To measure time-of-flight spectra and time dependent spectra of fast decaying systems a NE 213 liquid scintillator, with pulse shape discrimination and lower threshold at 250 keV, is used. When used as a pulse height spectrometer the neutron spectrum is obtained by the unfolding code FERDOR /4.33/ or by a simplified analysis TRADI /4.34/ relying on a transformation of pulse height spectra into recoil proton energy spectrum with subsequent differentiation. To check the reliability of this detector 96 response functions were determined between 300 keV and 14 MeV, the integral efficiency was calculated by an analytical procedure which fits to the values of VERBINSKY et al. /4.35/, and the spectrum of a bare Cf-source was determined to have a Maxwell-energy of 2.07 MeV.

Each detector is checked by calculational and experimental procedures. A final check is obtained by comparison of the measured spectra, "UNAT" and "UPOL" assemblies, of each detector in the common measured energy ranges. The ^6Li -glass and Boron 10 vaseline detectors agree within $\pm 2.5\%$ within lethargy groups of $\Delta u = 0.15$ in the energy range from 3 keV to 10 keV. The Boron 10 vaseline detector and NE 213 scintillator agree within 2.0 % within lethargy groups of $\Delta u = 0.15$ in the energy range from 400 keV to 2.5 MeV. Finally the agreement between Boron 10 vaseline and proportional counters, see also Fig. 4.10, within lethargy groups of $\Delta u = 0.15$ is better than 5 % in the energy range from 100 keV to 1.3 MeV.

If time resolution corrections are small, the accuracy of measured time-of-flight spectra, integrated into group fluxes with $\Delta u = 0.15$ is 5-10 % between 100 eV and 4 MeV whereas the error bars increase on the wings of the spectra to 10 % or even 20 %.

4.2.4. Intercomparison of Techniques and Accuracy of Spectrum Measurements

The techniques described here have been checked against each other in a series of measurements and against the results of other laboratories in the $\Sigma\Sigma$ -facility at MOL /4.36/. Table 4.2 summarizes some of these comparisons performed in the last time. SUAK UNAT (see chapter 5.8) is a small natural uranium block ($20 \times 15 \times 25 \text{ cm}^3$) with 14 MeV source in the center. Measured is the leakage spectrum. The depleted (0.4 %) Uranium Pile (see chapter 5.8) has the dimension of $81 \times 81 \times 105 \text{ cm}^3$ and is driven by a 15 cm natural uranium converter adjacent to the thermal column of the reactor FR 2. In some distance ($\approx 50 \text{ cm}$) from the converter a very nearly asymptotic spectrum is reached.

The secondary standard $\Sigma\Sigma$ at MOL is a 5 cm natural uranium shell of 25 cm outer diameter and is located in a spherical cavity of 50 cm diameter hollowed out in the horizontal thermal column of BR1 /4.37/. Spectra are measured in the center of the shell.

Fig. 4.10, 4.11, 4.12 show the result of the comparison measurements. The spectra are area normalized in the overlapping region. The TOF and proton recoil spectra for SUAK UNAT (Fig. 4.10) agree practically within the statistical uncertainties, i.e. within a few percent over the common energy region 0.1 - 1.2 MeV. The same is true in the overlapping region (0.1 - 1.4 MeV) for the asymptotic spectrum in the depleted uranium pile measured with spherical proton recoil counters and the ^3He -semiconductor spectrometer.

The spectra measured in the $\Sigma\Sigma$ -facility (Fig. 4.11) are area normalized to a calculated spectrum and the ratios of experimental and theoretical spectra are shown in the lower part. Within about $\pm 6 \%$ this broad group ratios are equal for the experimental techniques investigated. Fig. 5.27 finally shows prompt fission spectra measured with cylindrical proportional counters and the ^3He -semiconductor spectrometer.

Table 4.2

Comparison Measurements

Assembly	Techniques	Overlapping energy region
SUAK UNAT	TOF, proton recoil (cyl.)	0.1 - 1.2 MeV
Depleted Uranium Pile	^3He -semicond., proton recoil (spher.)	0.1 - 1.4 MeV
Prompt fission spectra	^3He -semicond., proton recoil (cyl.)	0.1 - 7 MeV
$\Sigma\Sigma$ -MOL	KARLSRUHE: ^3He -semicond., proton recoil (spher.) PETTEN: ^3He -and ^6Li -semicond., proton recoil (spher.) MOL: ^6Li -semicond., proton recoil (spher.)	According to what techniques are compared (Fig. 4.11)

Here the discrepancies are somewhat larger especially near the energy limits of the techniques. But it should be mentioned that in this case both the spectra and the experimental conditions (hard spectra, large amount of wall-scattered neutrons) are not representative for fast-reactor spectrum measurements.

From the comparison measurements the following conclusions have been drawn:

- For spectra and experimental conditions typical in measurements of fast reactor-type spectra the experimental results (integrated over broader groups) of the well-established techniques (TOF, proton-recoil proportional counter, ^3He - and ^6Li -semiconductor spectrometer) agree generally within some $\pm 6\%$ in the overlapping regions. Because this figure refers to four independent techniques, it is assumed that the experimental accuracy of the techniques mentioned above is within the $\pm 10\%$ limit. In cases with discrepancies remarkable larger than the figure given above, generally, it turned out that they were due to a bad performance of the spectrometer system and/or an error in the evaluation. Therefore it is strongly recommended to use at least two different techniques also for routine measurements.

- Although a steady improvement of the methods is necessary and will be done, a significant reduction in the experimental error seems improbable in the next future. Therefore, if it is the goal of spectrum measurements to improve cross sections, one should confine to systems where discrepancies due to inaccurate cross sections between calculated and measured spectra are expected to be remarkable larger than the accuracy figure given above.

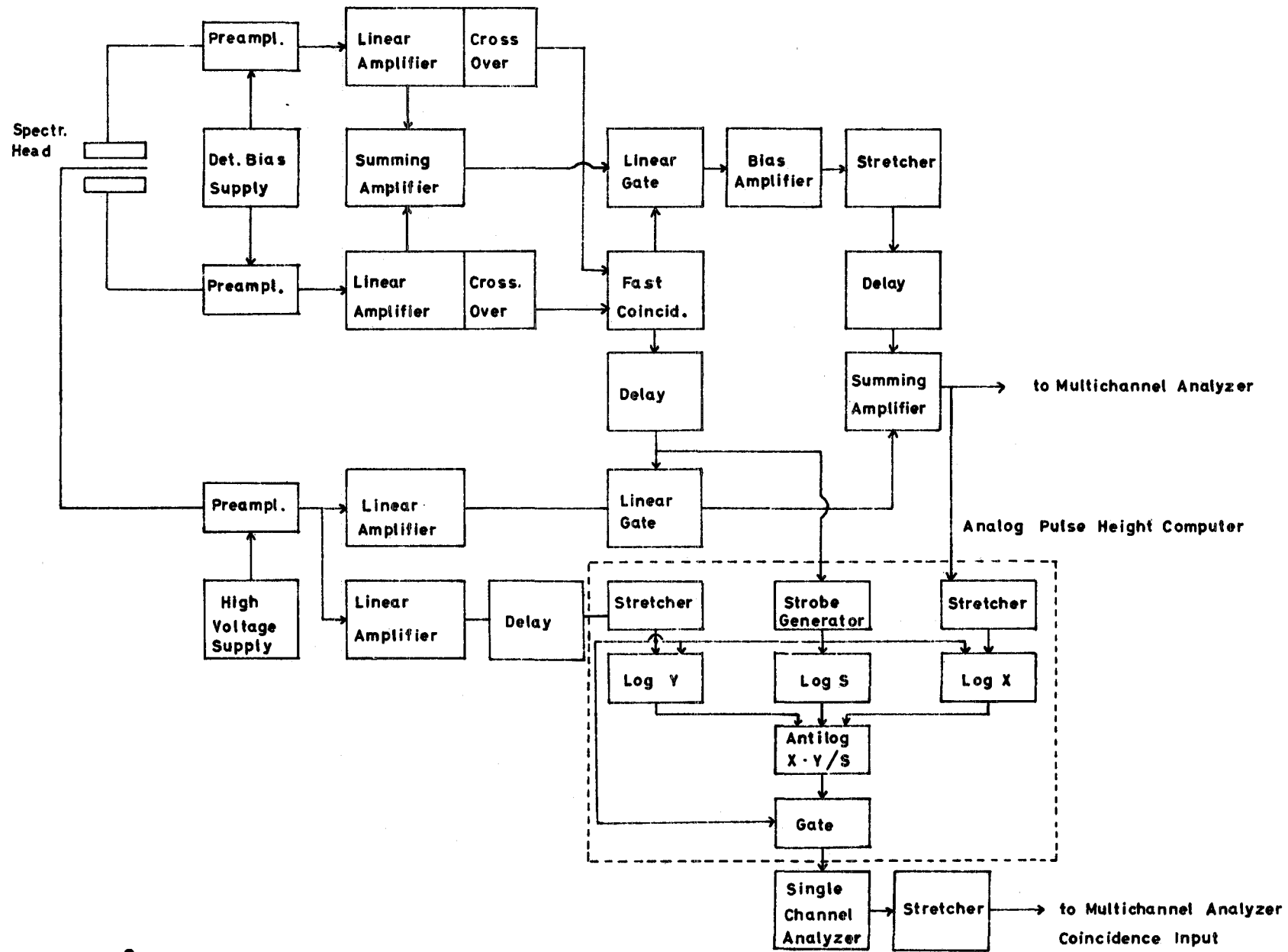


Fig.4.9 ^3He -semiconductor electronics

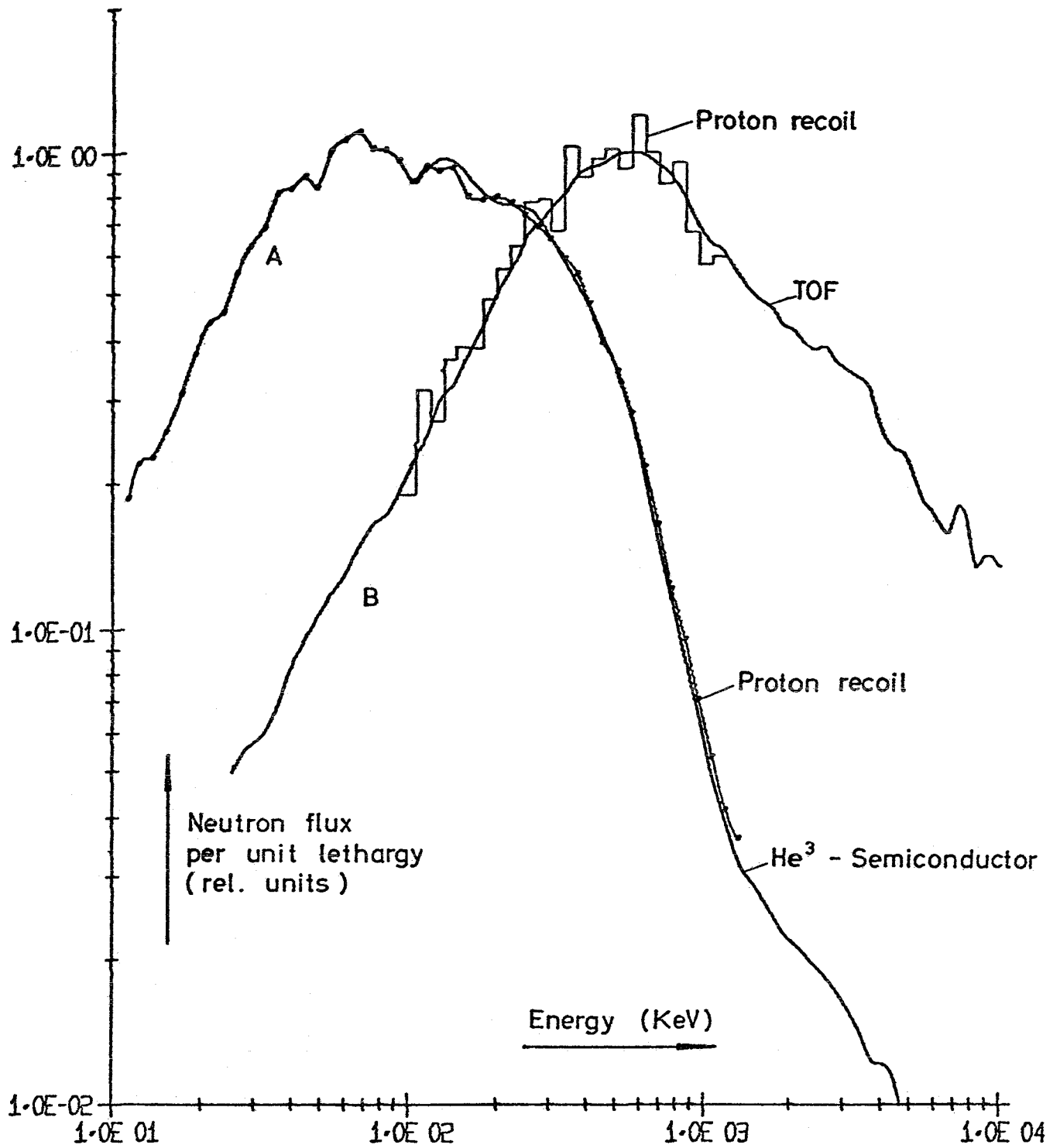


Fig.4.10 Comparison of different types of spectrum measurements

A: Asymptotic spectrum of a depleted uranium exponential pile

B: Leakage spectrum of a small natural uranium block (20 x 15 x 25 cm³, 14 MeV source in center)

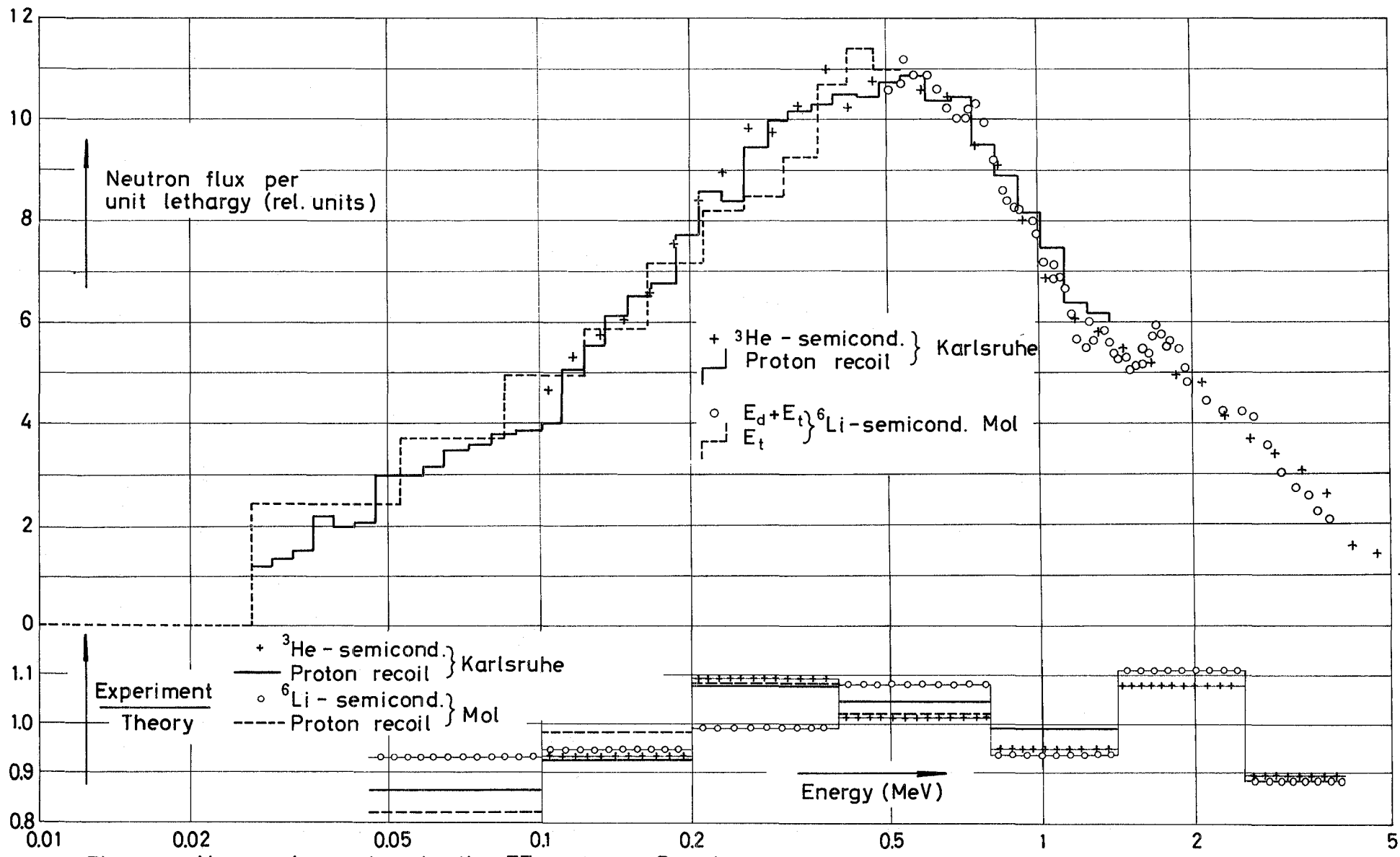


Fig.4.11 Measured spectra in the $\Sigma\Sigma$ at Mol. Broad group ratios of measured to a theoretical spectrum

References for Chapter 4

- /4.1/ Meister, H. et al., KFK 217 (1964)
- /4.2/ Bickel, W., Engelmann, P., Walze, H., Wittek, G., KFK 632, October 1967
- /4.3/ Borgwaldt, H., Kuchle, M., Mitzel, F., Wattecamps, E., IAEA Conf. on Pulsed Neutron Research, Vienna 1965, Vol.2., p.399
- /4.4/ Böhnel, K., Meister, H. (comp), KFK 1176, June 1970
- /4.5/ Tunnicliffe, P.R., Skillings, D.J., Chidley, B.G., Nucl.Sci.Eng. 15, 268 (1963)
- /4.6/ Seufert, H., Stegemann, D., Nucl.Sci.Eng. 28, 277 (1967)
- /4.7/ Goel, B., Eggmann, R., Nucl.Instr.Meth. 104, 255, (1972)
- /4.8/ Günther, G., KFK 1461 (1971 and Leitz Mitteilungen Suppl.Vol. 1 No. 2 (1972) 56
- /4.9/ Richmond, R., Rüegger, B., Neue Technik 10, 433 (1971)
- /4.10/ Doerfel, H., Werle, H., Compacts der Reaktortagung 1972, p. 121
- /4.11/ Benjamin, R.W. et al., AWRE-NR 2/64 (1964)
- /4.12/ Werle, H., Nucl.Instr.Meth. 72 (1969) 111
- /4.13/ Benjamin, P.W. et al., AWRE No. 09/68 (1968)
- /4.14/ Snidow, N.L., BAW-TM-442 (1965)
- /4.15/ Werle, H., Geiger, K.W., to be published
- /4.16/ Werle, H., Nucl.Instr.Meth. 99 (1972) 295

- /4.17/ Bluhm,H., KFK 1270/2, p.121-1 (1970)
- /4.18/ Als-Nielsen,J., CCDN-NW/6 (1967)
- /4.19/ Wattecamps,E. et al., Proc.Int.Conf.Phys. of Fast Reactor Operation and Design, BNES, June 1969, London, p.61 (1969)
- /4.20/ Wattecamps,E., Proc.Specialists Meeting Argonne Nov. 1970, IAEA-138
- /4.21/ Werle,H. et al., Reaktortagung 1971, Bonn, Compacts p.58 (1971)
- /4.22/ Rusch,D., Wattecamps,E., KFK 1271/4 (1971) 121-3
- /4.23/ Rusch,D., KFK 1271/2 (1971)
- /4.24/ Pieroni,N., Rusch,D., Wattecamps,E., KFK 1272/2 (1972)
- /4.25/ Brandl,V., Karlsruhe-KFK-report No. 1185 (1970)
- /4.26/ Kappler,F., Wattecamps,E., Private Communication
- /4.27/ Coates,M.S. et al., AERE-RE-5364 (1968)
- /4.28/ Arnecke,G. et al., PSB-Internal Report
- /4.29/ Utley,C.A. et al., Proc.Symp. EANDC-Argonne-Oct. 1970
- /4.30/ Sowerby,M.G., Patrick,B.H., Utley,C.A., and Diment,K.M., Jour. of Nucl Energy 24 (1970) 323
- /4.31/ Cameron,J., Harrison,L.M., and Parker,J.B., Nucl.Instr. and Meth. 56 (1967) 45
- /4.32/ Neill,J.M. et al., Nucl.Instr. and Meth. 82 (1970) 162
- /4.33/ Burrus,W.R., and Verbinski,V.V., Nucl.Instr. and Methods 67 (1968) 181

- /4.34/ Pieroni,N., to be published
- /4.35/ Verbinski et al., Nucl.Instr. and Meth. 65 (1968) p.8
- /4.36/ Bluhm,H. et al., KFK 1658 (to be published)
- /4.37/ Fabry,A. et al., EACRP Meeting (1971)

5. CHECK OF IMPROVED METHODS IN INTEGRAL EXPERIMENTS

As can be seen from chapter 3 and 4, since 1969 the effort both on the theoretical and experimental side was remarkable. It is clear that the improvements of theoretical and experimental techniques in themselves lead to a much more distinct confidence into the results obtained with these tools. The present chapter now deals with the question, how far the improved methods are able to diminish the differences between calculated and measured integral physics quantities obtained in zero power facilities. If considerable improvement is achieved a correspondingly greater confidence evolves in the prediction of these parameters for fast power reactors. But, because the check is performed in zero power facilities, not all aspects, which are discussed in chapter 1 and 3, can be considered in those experiments. Thus a relatively open situation with respect to time dependent reactor characteristics and large temperature effects remains, as will be discussed in chapter 6. This chapter 5 summarizes the experiences obtained mainly at GfK-Karlsruhe in the past few years with regard to the prediction of the topics, listed in chapter 1, which are relevant to the start up and partly to the operation of fast power reactors.

5.1. Criticality and reaction rate ratios

As already mentioned in section 3.1., the preparation of the KFK INR set of group constants resulted in a greatly improved agreement between calculated and measured results for the criticality parameter of various zero power reactors. This is illustrated in Table 5.1., where the experimental criticality values are compared with the corresponding calculated results obtained by application of three different sets of group constants: the SNEAK set prepared in 1967, the MOXTOT set prepared in 1969, and the KFK INR set prepared recently. We have considered a fairly large variety of assemblies differing significantly in size, composition and energy distribution of the neutron spectrum. For most of the assemblies the criticality deviation with the KFK INR set lies within the acceptable uncertainty range of $\pm 1\%$, with the exception of two assemblies, namely SUAK-UH-1B and SNEAK-5C, for which our present methods of calculation probably are not yet refined enough.

Another remarkable feature of the KFK INR set is the fact that, unlike the MOXTOT set, it yields similar criticality deviations for classes of similar assemblies. Generally, no systematic tendency can be observed in the criticality deviations of similar assemblies differing mainly in the substitution of ^{235}U by ^{239}Pu . This can be concluded by comparing the results for SNEAK-3A2 and SNEAK-3B2, SNEAK-2A-R1 and SNEAK-6A-Z1, and GODIVA and the two JEZEBEL criticals.

In this context one should mention that our studies revealed the great importance of the energy dependence of the fission neutron spectrum. As is shown in more detail in /5.1./, it is essential to take into account in the nuclear calculations the different energy distributions for the fission spectrum of different isotopes. For most assemblies it is sufficient to use the fission spectrum belonging to that isotope in the mixture which undergoes most fissions, i.e. generally ^{235}U or ^{239}Pu . For some assemblies, however, it may even be important to take into account the contribution of the ^{238}U fissions to the combined fission spectrum of all fissile isotopes.

In addition to the criticality values we compared the calculated and measured results also for other quantities e.g. reaction rate ratios and reactivity coefficients. The results of recent experiments analyzed subsequent to the revision of our set of group constants support the adequacy of the KFK INR set with respect to the calculation of reaction rate ratios. This is

Table 5.1. Comparison of Calculated and Measured Criticality Values

ASSEMBLY	EXPERIMENT k_{eff}	SNEAK Set		MOXTOT Set		KFKINR Set	
		k_{eff}	Δk	k_{eff}	Δk	k_{eff}	Δk
SUAK U1B	0.86 ± 0.01	0.855	-0.005	0.856	-0.004	0.852	-0.003
SUAK UH1B	0.945 ± 0.01	0.918	-0.027	0.930	-0.015	0.925	-0.020
ZPR III-10	1.0	0.999	-0.001	1.011	+0.011	1.001	+0.001
ZPR III-25	1.0	0.980	-0.020	0.998	-0.002	1.000	±0.
ZPR III-48	1.0	0.977	-0.023	0.989	-0.0011	1.007	+0.007
ZPR III-48B	1.0	0.975	-0.025	0.987	-0.013	1.006	+0.006
ZEBRA-6A	1.0	0.974	-0.026	0.985	-0.015	0.998	-0.002
SNEAK-3A1	1.0	0.994	-0.006	1.019	+0.019	1.004	+0.004
SNEAK-3A2	1.0	0.989	-0.011	1.012	+0.012	1.001	+0.001
SNEAK-3B2	1.0	0.984	-0.016	0.998	-0.002	1.005	+0.005
ZPR III-55	1.0	0.958	-0.042	0.934	-0.016	1.011	+0.011
SNEAK-5C	1.031 ± 0.005	1.026	-0.005	1.042	+0.011	1.052	+0.021
3A0	0.930	0.938	+0.008	0.937	+0.007	0.932	+0.002
SNEAK-3A1	0.962	0.967	+0.005	0.968	+0.006	0.963	+0.001
Series 3A2	1.000 ¹⁾	1.000	-	1.000	-	1.000	-
3A3	1.048	1.039	-0.009	1.036	-0.012	1.046	-0.002
GODIVA	1.0			1.016	+0.016	1.011	+0.011
JEZEBEL (clean Pu)	1.0			1.000	±0.	1.011	+0.011
JEZEBEL (dirty Pu)	1.0			0.997	-0.003	1.009	+0.009
VERA-11A	1.0			1.000	±0.	1.006	+0.006
ZEBRA-8H	1.027			0.996	-0.031	1.022	-0.005
ZPR IX-25	1.0			0.975	-0.025	0.995	-0.005
SNEAK-8	1.007 ± 0.002			0.934	-0.023	0.999	-0.008
SNEAK-8Z	1.018 ± 0.003			0.997	-0.021	1.012	-0.006
SNEAK-2A-R1	1.0			1.029	+0.029	1.013	+0.013
SNEAK-GA-Z1	1.0			1.000	±0.	1.007	+0.007
SEFOR-1C	1.0			0.997	-0.003	1.011	+0.011

1) Normalization for the SNEAK series

illustrated in the following Table 5.2. where the results obtained with the KFK INR set are compared with the corresponding values for its predecessor, the MOXTOT set. The most important discrepancy remaining concerns the capture rate in ^{238}U , especially for recent SNEAK-experiments. This discrepancy may, eventually, not be completely attributable to the set of group constants but could be caused, at least partially, by the experimental standard or the experimental technique used for the measurement and evaluation of this type of reaction rate.

Table 5.2.

Comparison of Theoretical and Experimental Reaction Rate Ratios
for Recently Analyzed Criticals (Theory/Experiment)

Assembly	Group Set	F^8/F^5	C^8/F^5	F^9/F^5
SNEAK-6D	MOXTOT	0.87	1.01	0.91
	KFKINR	0.99	1.05	0.98
SNEAK-7A	MOXTOT	0.79	0.98	0.92
	KFKINR	0.90	1.03	0.99
SNEAK-7B	MOXTOT	0.82	1.04	0.94
	KFKINR	0.95	1.07	1.02
SNEAK-8	MOXTOT	0.88	1.06	-
	KFKINR	1.01	1.10	-
SNEAK-8Z	MOXTOT	0.88	-	-
	KFKINR	1.02	-	-

The improvement obtained for the calculation of reactivity coefficients by using the KFKINR set instead of, e.g., the preceding MOXTOT set will be illustrated in the subsequent section 5.4. of this report together with the discussion of other improvements in the measurements and calculations of material worths.

5.2. Evaluations of power density measurements in

SNEAK 2 and 6

Space-dependent reactor rate distributions have been measured in the SNEAK-assemblies- 2 and 6 from which the validity of power density distributions calculated for the SNR could be checked.

Such measurements have been performed partly on clean cores made of two enrichment zones fueled either with uranium (SNEAK-2A) or with plutonium (SNEAK-2C)/5.2/ or with plutonium and uranium (SNEAK-6A,B, D) /5.3-4/. The measurements have also been extended into the blanket region. The blanket had in some cases a composition very similar to that of a breeder-blanket (UO_2 -Na-SS).

On the other hand, in SNEAK-2C, -6A and 6D during the course of control rod experiments (see section 5.5) the influence of the presence of control rods, fully or partially inserted, was measured on the core power distributions.

5.2.1. Measurements performed

The distributions of ^{235}U , ^{238}U and ^{239}Pu fission rates were measured, axially, radially and sometimes also azimuthally, using in general fission chambers, and also sometimes activated foils or platelets.

The traverses measured for the individual isotopes were combined to give the total fission rate traverses, using in general measured values of fission ratios at a reference point. The accuracy of such experimental, total fission rate traverses (i.e. relative traverses) is of the order of 0.5 % in the core region.

All details concerning the realization of these measurements are given in section 4.1 of this report. As described there, fission chamber measurements, which are the basic measurements in this section, create a perturbation in the core, and need additional foil measurements for precise calibrations.

5.2.2. Methods of calculation

The standard methods of calculation used in the SNR design in 1969 were characterized by the use of:

- diffusion theory
- cross-section set NAPPMB
- two-dimensional models, RZ or XY.

Concerning the models for a operating power reactor, the attempt was made to combine adequately the results obtained in the two different geometries RZ (problem cylinderized, ring of control rods, partial insertions possible) and XY (with consideration of the SNR exact triangular geometry in the program TREPAN /5.5./). The maximum power peaks of the three-dimensional map were obtained by a very simple synthesis (see for example ref. /5.6/).

In order to automatize this synthesis, computer programs were then written in the SNR Konsortium: TOUTATIS at Belgonucleaire /5.7/ and LEISY at INTERATOM / 5.8/, based on a direct synthetisation of the power density distributions (not the flux).

Here the development of the flux synthesis technique and its application with the program KASY (see section 3.3.) corresponded to a substantial improvement for the calculation of the fission map in the presence of partially inserted control rods.

Use was normally made, as well in the SNEAK evaluation as in the SNR design, of diffusion theory and of the cross section set NAPPMB. In some cases transport theory (S_n method) and/or MOXTOT cross sections were also used additionally. For the evaluation of the measurements discussed in this section the KFK INR cross section set was not applied.

Few-group condensation effects were systematically studied and minimized, in such a way that the two- and three-dimensional calculations could be generally performed using condensed cross-sections. The effect on relative fission distribution due to all calculational approximations together (mesh spacing not refined enough, 4-group condensation and approximate B_z^2 values in XY geometry) were verified to be smaller than 0.5 % in all the cases for the core regions.

5.2.3. Evaluation of fission ratios

The results of evaluation of the central core fission ratios measured in SNEAK-6D, extracted out of /5.4./ are presented as a typical example in Table 5.3. below:

Table 5.3.

Central core fission ratios in SNEAK-6D

Fission ratios	Final corrected experimental values	Calculated values	
		NAPPMB	MOXTOT
σ_{f8}/σ_{f5}	0.0293	0.0280	0.0258
σ_{f9}/σ_{f5}	0.983	0.953	0.902

The experimental values have been measured by foils. The calculations took into account the heterogeneity of the cell (in this case, made of MASURCA rodlets) which affects σ_{f8} by as much as 5%. The heterogeneity correction was calculated using the collision probability programs ZERA and KAPER, see section 3.4.1.

In the present case one observes that MOXTOT does not represent an improvement with respect to NAPPMB; this problem of spectral indices is fully documented in section 5.1.

As far as total fission rate in the core is concerned, it is important to note that:

- one is interested in relative power density distribution, normalized to unity at a reference point or at the core average value;
- in the core fuel zones of interest, ^{239}Pu is the main contributor by about 85 % (^{235}U if uranium zones), ^{238}U contributes for about 10 %, while ^{235}U and the higher Pu isotopes bring the remainder.

Under such conditions an uncertainty on fission ratios plays a minor role on the resulting total fission rate.

In the core zones one can reasonably approximate the power density by the total fission rate distribution. This does not apply however to the blanket regions for which the ^{238}U becomes the main contributor to fission rate (in fresh blankets), and the power profile should be given by a sum of terms, by two main being proportional to the total fission rate and to the gamma heating-rate respectively, as it is discussed in 5.2.6.

5.2.4. Evaluation of power traverses in the clean core

Various results of evaluation are given in references /5.2./, /5.3./, /5.4./. As typical example, Fig. 5.1-3 represent the case of the axial traverses in SNEAK-6A/B, for respectively ^{235}U fission (Fig.5.1) ^{238}U fission (Fig.5.2) and total fission rate (Fig.5.3).

Foils and chambers results were available. They compare well, except in blanket region for ^{238}U . In the core region the agreement calculation/experiment is fairly good (The calculation refers to the MOXTOT set in RZ geometry in this case). With a normalization at core center the maximum deviations at the core-blanket interface are of the order of 3 % for ^{235}U and ^{238}U (and also ^{239}Pu , not shown here). For the total fission rate some compensation take place. The agreement is very good.

It is interesting to point out the influence of the calculated corrections on these relative traverses for the core regions:

- transport correction ($\frac{T-D}{D}$): < 1 % for practically all the points of the traverse in the core, 2.5 % at the core-blanket boundary.
- heterogeneity correction (i.e., effect when using heterogeneity corrected cross-sections instead of homogeneous ones): always < 1 %.

On the other hand, using NAPPMB instead of MOXTOT does not change the relative traverses by more than 0.3 % except at core blanket boundary.

The effect of few-group condensation is also very small within the core region but significant at the core-blanket boundary.

For the evaluation of the central axial traverse simple one-dimensional calculations give practically identical results as two-dimensional (RZ) calculations; the influence of a variation in the input traverse bucklings is small.

As a general conclusion, for a plutonium core without control rods the total fission rate distributions in the radial and axial directions is predicted generally within 2 %. The maximum to average power ratios are 1 % overestimated.

5.2.5. Influence of control rods

The influence of one central rod and of one to three off-center rods on the core power distribution has been investigated in SNEAK-2C, in a sector made of two plutonium zones. The influence of the central rod was again studied in SNEAK-6A and D, in a cylindrical core having a plutonium central zone.

The control rods were fully, partially or not inserted (i.e. followers inserted).

Traverses were measured either radially through rod positions, (or axially in fuel positions close to rod positions.

Results of evaluations are detailed in /5.2 / (SNEAK-2C) and /5.9 / (SNEAK-6A/D).

Typical results of evaluations are shown in Fig. 5.4-7

Presented here are results obtained with a sufficient accuracy by two-dimensional (XY) models. In the cases of partially inserted off-center rods only the three-dimensional (XY/Z) model could be used. The accuracy of the used synthesis method is described in section 3.3.

In the vicinity of control rods, diffusion theory cannot predict well the slope of the curves, particularly for ^{238}U fission (see Fig 5.6 and 5.7). Transport theory (S_n method used with $n = 4$) predicts better the fission rate depression caused by an absorber: for ^{238}U within $B_4\text{C}$ the difference transport/diffusion may reach 7 %.

As a general conclusion, in the presence of one or several control rods, partially or fully inserted, the prediction of the maximum to average ratios is worsened, with respect to the core without rods, by additionally :

- 1 % radially (the calculation-to-experiment ratios become 1.02)
- 2 % axially (the calculation-to-experiment ratios become 1.03)

5.2.6. Power distributions in the blanket

Fig.5.1,2 and 3 show how the calculated fission rate traverses in axial blanket regions compare with experiments in SNEAK-6A for, respectively ^{235}U (Fig.5.1) ^{238}U (Fig.5.2) and total fission rate (Fig.5.3). This axial blanket is of the type of a fresh breeder blanket.

One observes that these calculations, made with MOXTOT, which include transport and heterogeneity corrections give a good agreement with experiment: within 5 % in the first 5 cm of blanket, within 10 % after 20 cm thickness.

The heterogeneity correction was necessary especially in the comparison with foil results. It was shown that the rate ratio: foil position over cell average, was strongly spectrum-dependent. The cell calculations (ZERA, KAPER) were therefore made for each blanket point with the adequate energy-dependent B^2 values extracted out of a preceding RZ calculation.

The transport correction (S_{14}) improves generally the predictions. The correction is negative in the first cm of blanket, and becomes positive further on.

In the blanket regions the use of MOXTOT instead of NAPPMB results in a significant improvement of the fission traverses.

Few-group condensation is normally not adequate for blanket regions, due to the significant changes in neutron spectrum versus blanket thickness. In case one is forced to reduce the computing time with two- or three-dimensional models one has then to subdivide the blanket and define different condensation spectra along the blanket thickness.

Contrary to core regions, the assumption that the profile of the total fission rate represents the power density, is no longer valid in blanket. The gamma heating rate in particular becomes important in the blanket and has another spatial dependency.

Consequently first attempts have been made in SNEAK-6D to measure the spatial variation of the gamma heating rate using thermoluminescent dosimeters. The technique and some of its results are described in section 4.1.5 of this report. Here will be shown only a particular presentation of these results in Fig. 5.8: one observes that in the axial blanket the ratio of gamma heating rate over total fission rate is 4 times larger than in the core.

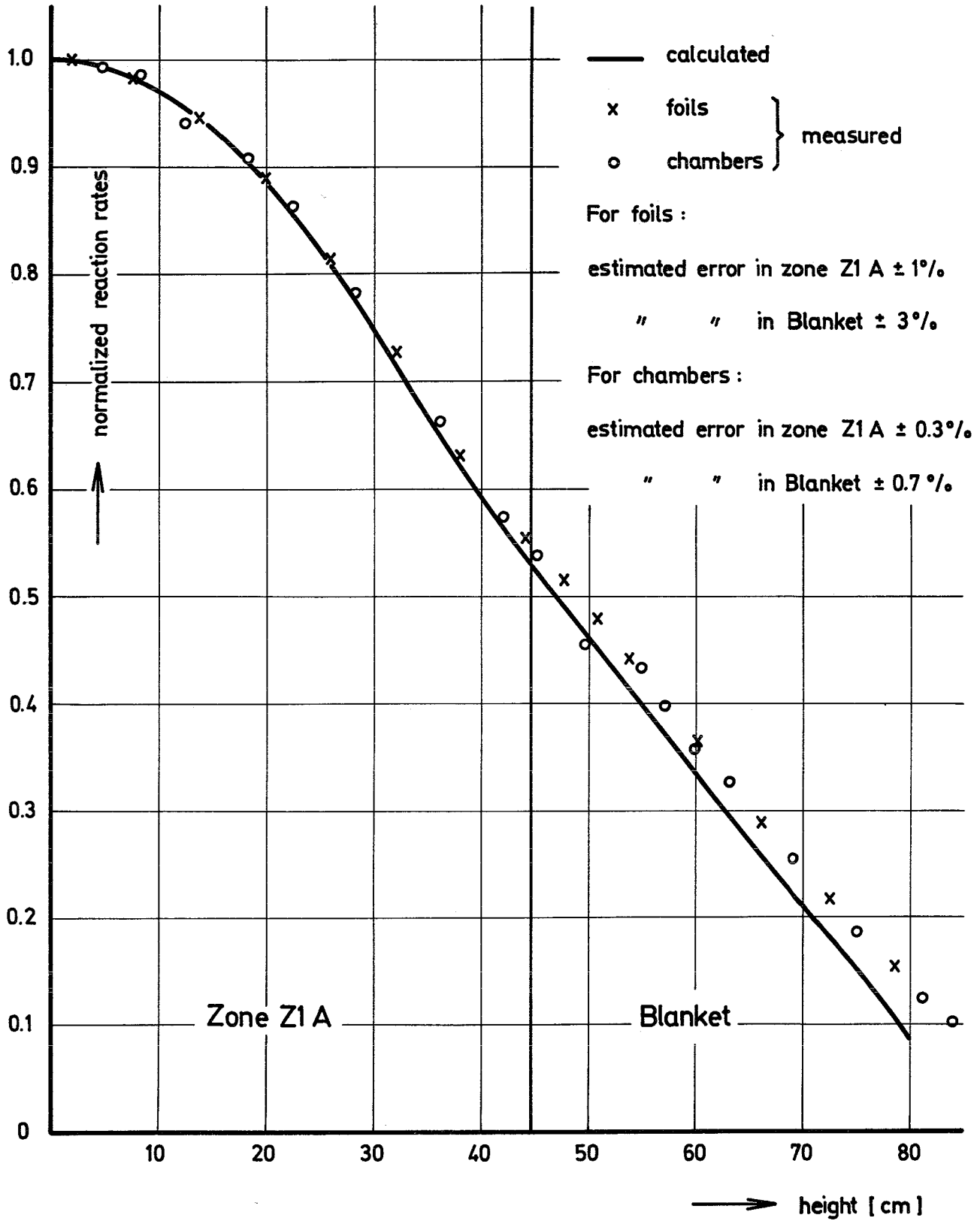


Fig.51 SNEAK - 6A / 6B
Axial Fission Rate Traverse for U235

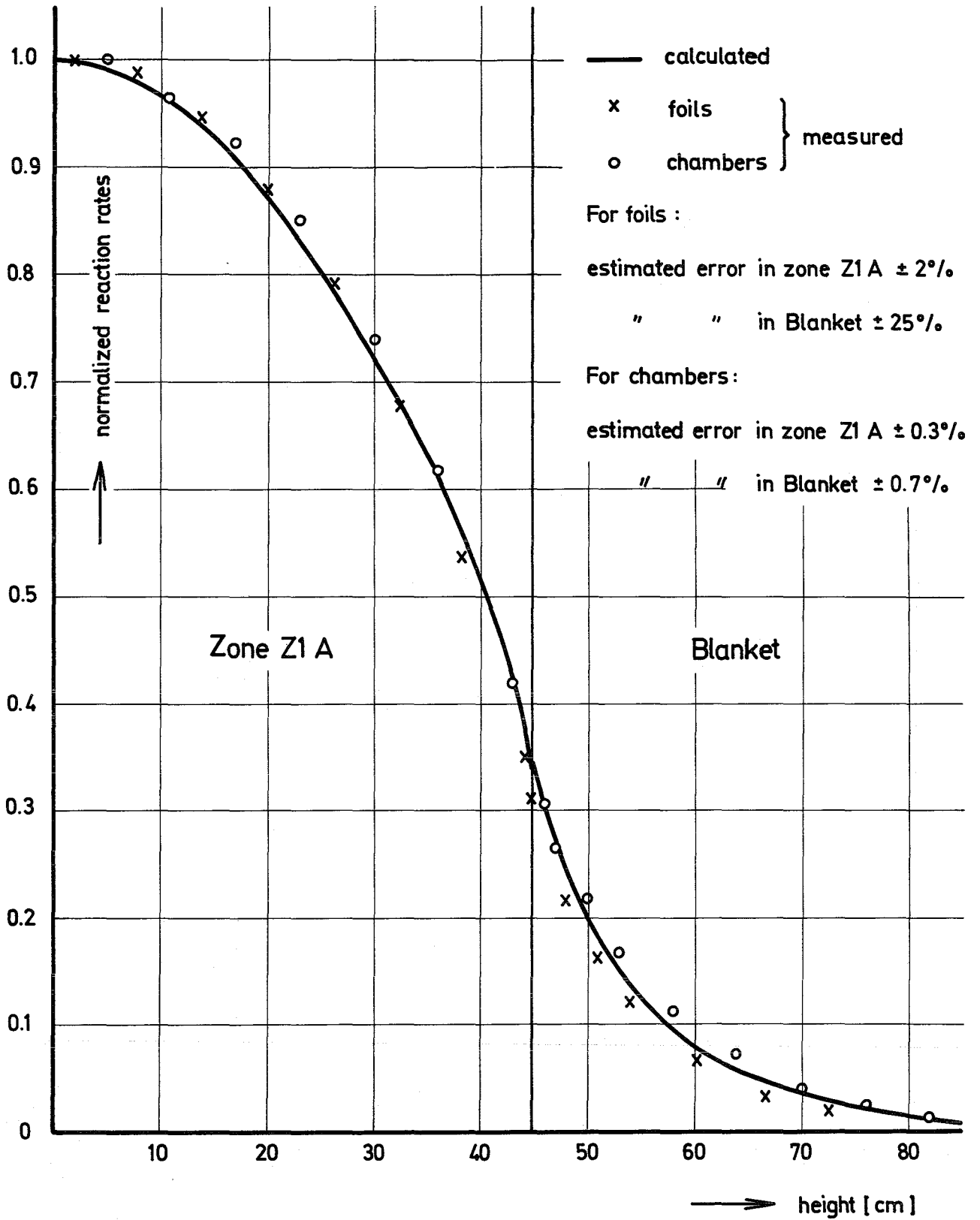


Fig. 5.2

SNEAK - 6A/6B

Axial Fission Rate Traverse for U238

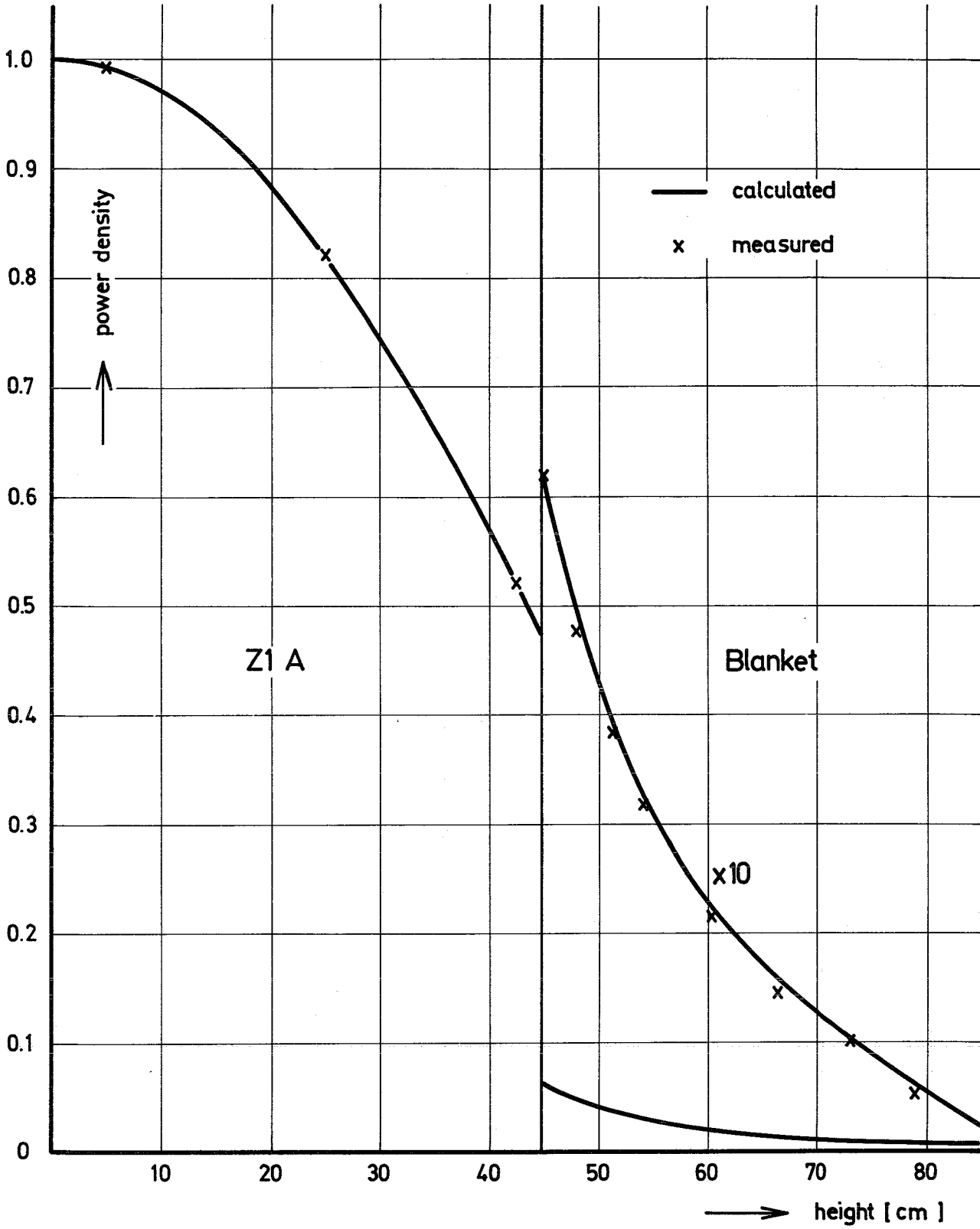


Fig.53

SNEAK - 6A / 6B

Axial Power Distribution

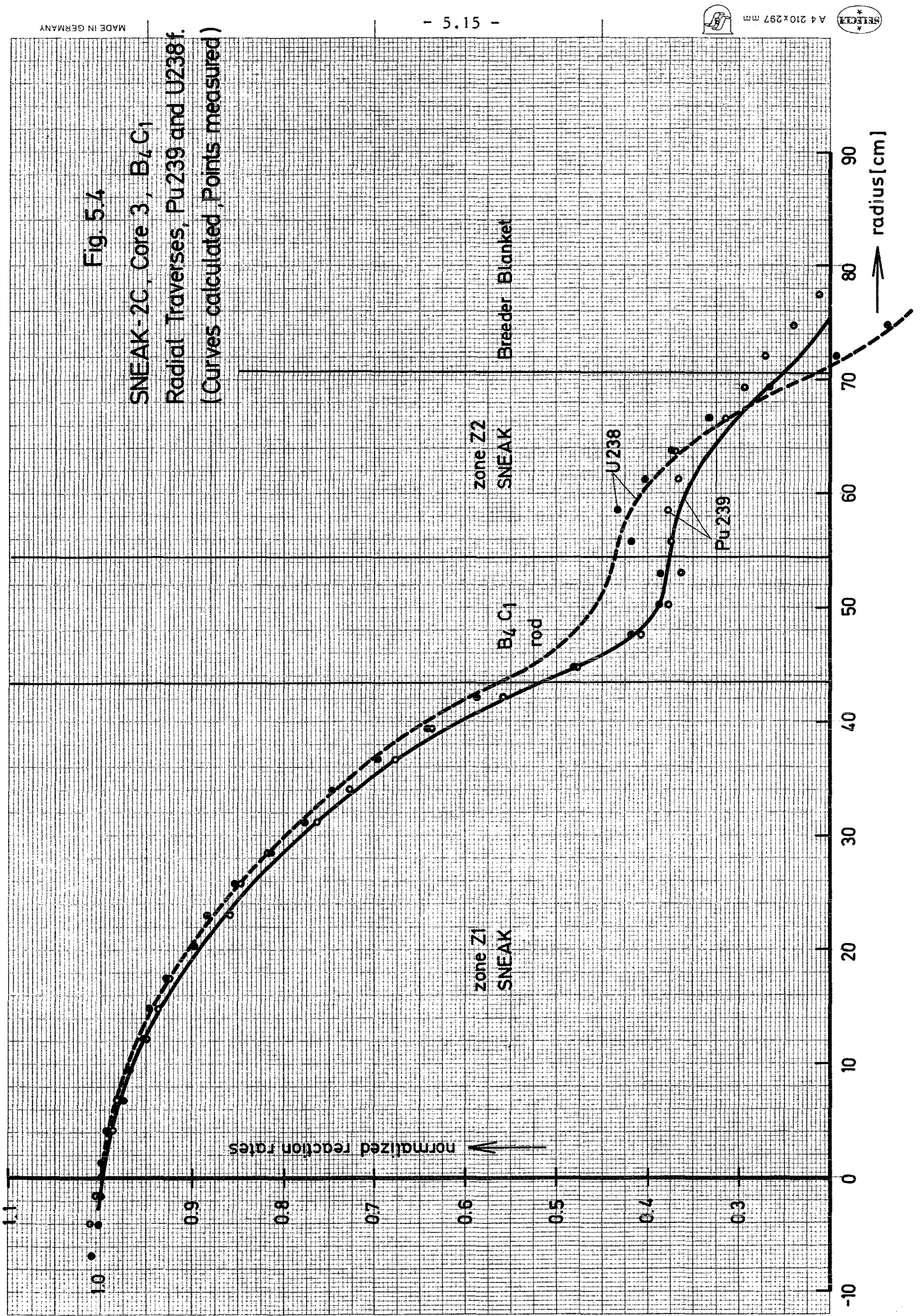


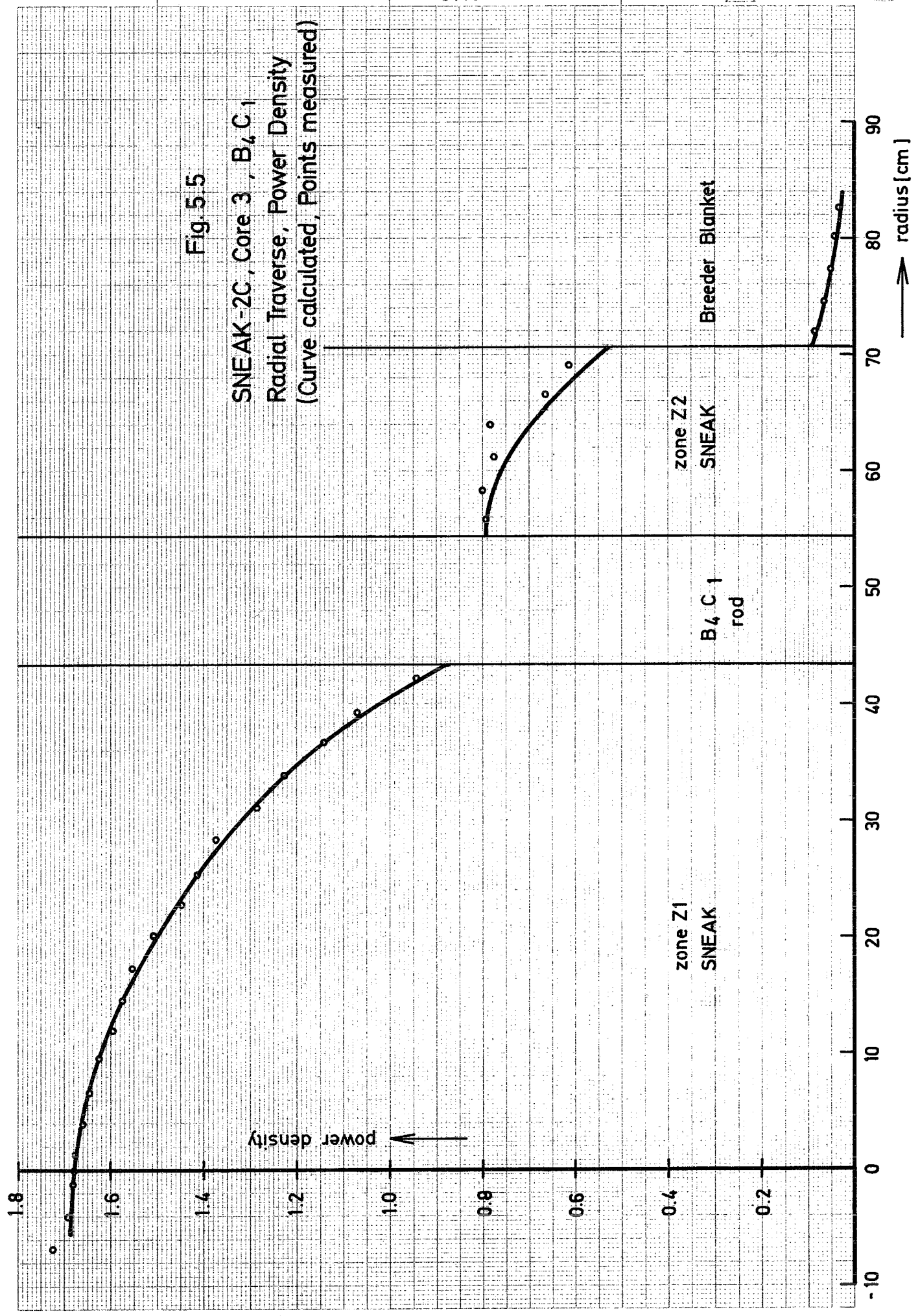
Fig. 5.4

SNEAK-2C, Core 3, B₇C₁
 Radial Traverses, Pu239 and U238f.
 (Curves calculated, Points measured)



Fig. 5.5

SNEAK-2C, Core 3, B₄C₁
Radial Traverse, Power Density
(Curve calculated, Points measured)



radius [cm]

power density

zone Z1
SNEAK

B₄C₁
rod

zone Z2
SNEAK

Breeder Blanket

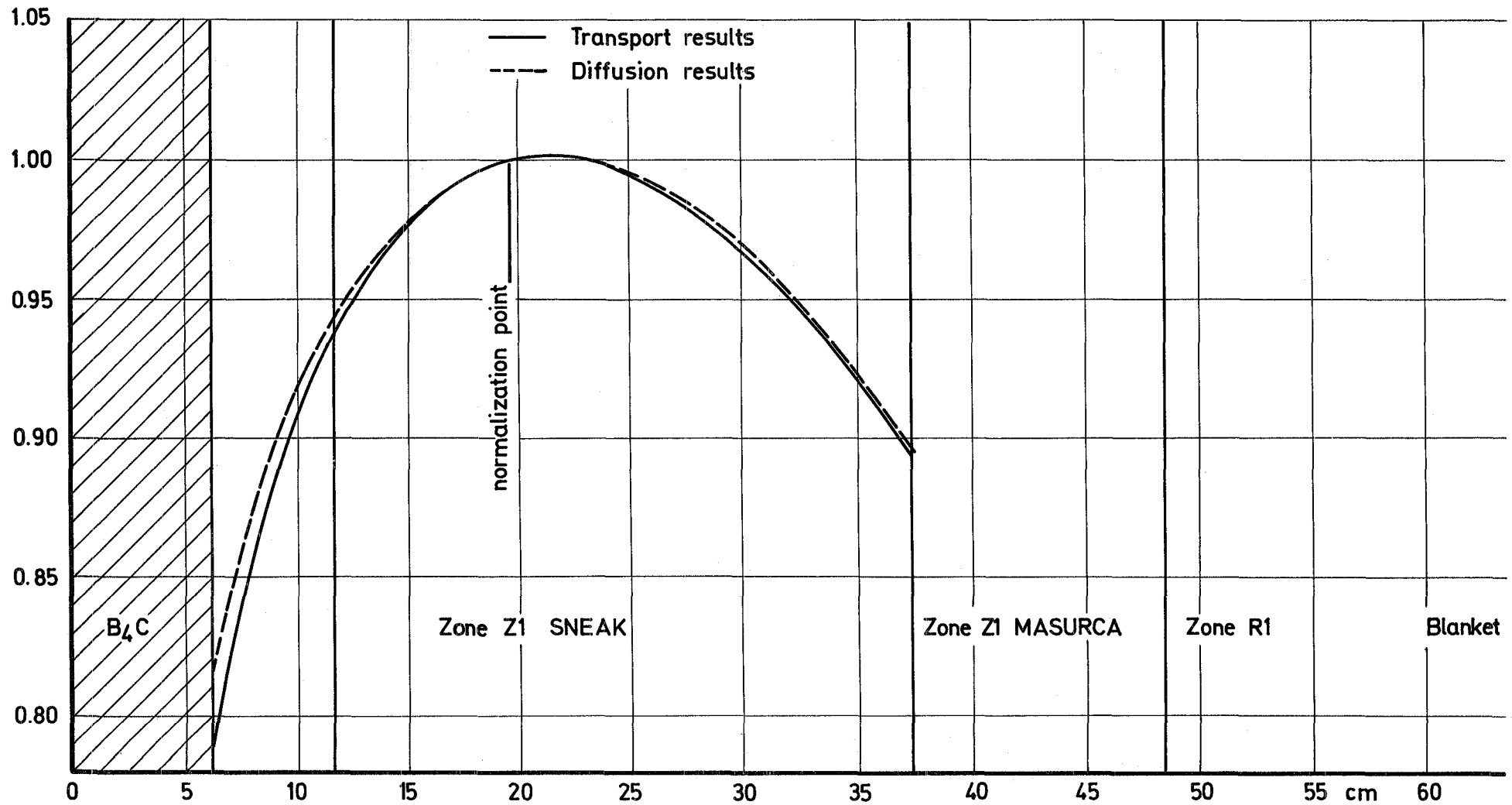


Fig. 5.6

SNEAK-6A Control Rod Experiment
 Traverse : Radial B₄C
 Pu 239 Fission

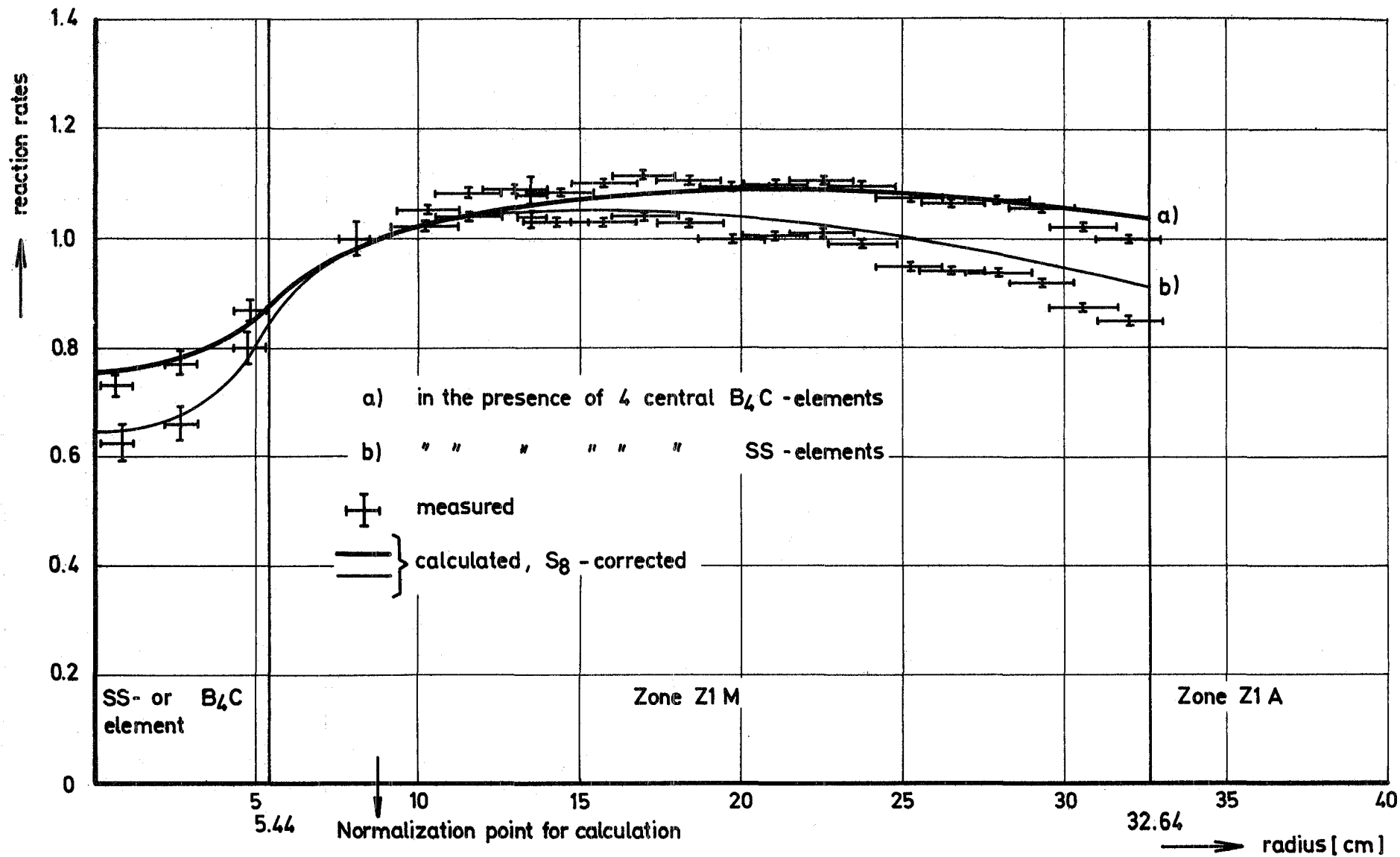


Fig. 5.7

SNEAK-6D Radial Fission Rate Traverse for U238
normalized to one Atom

5.3. Analysis of buckling measurements

The material buckling is a fundamental value in reactor physics. Therefore great efforts were made to measure the buckling of a reactor zone to the highest possible accuracy.

One method for a direct B_m^2 -determination is based on the measurement of reaction rate traverses. Traverses are measured with fission chambers of various fissile materials. In order to get an accurate value for the buckling from the curvature of these traverses the influence of the higher spectral modes induced by the blanket of the reactor must be eliminated. A method to separate the higher modes from the fundamental mode is described in /5.10./. But this procedure yields incorrect results if the inner zone of a reactor is so small, that throughout its volume the neutron spectrum is influenced considerably by the outer zone. Hence a modified method was developed /5.11./ which will be described here briefly.

From orthogonality it follows that a detector should have the cross section proportional $D(E) \cdot \phi_0^+(E)$ to yield a traverse exactly proportional to the fundamental mode ($\phi_0^+(E)$ is the asymptotic adjoint flux). Since such a detector does not exist, one uses the following procedure:

Four traverses are measured with different fission chambers (^{235}U , ^{238}U , ^{237}Np , ^{239}Pu). These same traverses and the traverse of a fictitious detector, with the cross section $D(E) \cdot \phi_0^+(E)$ are calculated. Now a "semiexperimental $D \phi^+$ -traverse" is derived from the 4 measured and the 5 calculated traverses by applying a linear regression method to each point. Before the regression is performed, the measured values are approximated by polynomial fits of the 8th order. Depending on the geometry, the material buckling is finally determined by a cosine or J_0 fit to the resultant semi-experimental $D \phi^+$ -traverse.

The fission chambers used for the experiment are only 6 mm in diameter and have an active length of 25 mm. The experimental channel can be quite small and results in a negligible perturbation. A comparison of traverses measured with chambers and foils did not show any systematic deviation in the region considered for the buckling measurement. Fine structure is largely smoothed by the length of the chambers. It becomes measurable only for the radial ^{238}U -traverses, where its influence must be eliminated by a suitable choice of the measuring positions.

Error calculations show that the error of B_m^2 due to counting statistics is small (about 0.1%). Somewhat larger systematic errors are due to the calculation of the traverses and to the linear regression. The attainable accuracy for B_m^2 is therefore probably in the vicinity of 0.3 %.

In Table 5.4 the measured material bucklings for the SNEAK assemblies 7A, 7B and 9B are given in the first column. Both configurations of SNEAK-7 are pure plutonium cores (SNEAK-7A has a harder spectrum than SNEAK-7B). SNEAK-9B is a core with an inner plutonium zone and an outer uranium driver zone. The second column gives the relative discrepancy $\frac{C-E}{E}(\% B_m^2)$ for the MOXTOT set. The calculation was performed with a zero-dimensional program of the NUSYS-system, iterating to a k_{eff} , which is equal to 1.0 minus the REMO- and heterogeneity - corrections. In the next column these values are multiplied with the fractional contribution of the leakage to the total neutron balance. These numbers should be the same as the directions in the k_{eff} 's obtained from fundamental mode calculations (4th column) that is, from zero-dimensional calculations using the experimental bucklings. The same is repeated in column 6 or 8 for the KFK INR set.

It appears that the k_{eff} 's of the fundamental modes are higher than those calculated for the complete assemblies, which are listed in column 5 and 9. If one observes that the buckling measurements by fission rate traverses determine essentially the reflector savings, this result indicates that the measured reflector savings are usually larger than the calculated ones. (This argument holds only for the one-zone cores 7A and 7B and not for the two-zone core 9B.)

Therefore, it may be preferable to test cross section data against measured bucklings, rather than against critical masses, because then one avoids to interpret errors in the calculated extrapolation length as errors in cross sections of the core material.

Table 5.4.

Measured values for B_m^2 and comparison of measurements and calculations for B_m^2 and k_{eff}

	Experiment $B_m^2 [m^{-2}]$	MOXTOT				KFK INR			
		$\frac{C-E}{C}$ (% B_m^2)	$\frac{D B_m^2}{\nu \Sigma_f} \cdot \frac{C-E}{C}$ (% B_m^2)	$\frac{C-E}{C}$ (% k_{eff})		$\frac{C-E}{E}$ (% B_m^2)	$\frac{D B_m^2}{\nu \Sigma_f} \cdot \frac{C-E}{E}$ (% B_m^2)	$\frac{C-E}{C}$ (% k_{eff})	
				Fund. Mode	Complete Assembly			Fund. Mode	Complete Assembly
SNEAK-7A	59.68	3.9	1.7	1.7	- 0.1	5.1	2.3	2.3	1.5
SNEAK-7B	34.74	0.9	0.3	0.2	- 1.2	6.6	2.1	1.9	1.2
SNEAK-9B	14.68	-0.2	- 0.07	0.0	+ 0.1	4.8	1.7	1.6	0.9

5.4. Analysis of central material worth measurements

Small-sample reactivity worth measurements at the core center can, in principle, give valuable information on the cross sections of the material under study, and also on the flux and adjoint flux spectrum of the assembly. However, as there were several severe difficulties in the interpretation of such measurements, much of the experimental data accumulated in earlier years were never used.

The worth of materials with a large slowing-down cross section depends very much on the details of the adjoint spectrum. The details are probably not adequately described in the 26-energy group structure, to which the work on reactivity worths was mainly confined so far. Therefore, most of the following discussion will be restricted to absorbing and fissile materials. The influence of a many group structure on the material worth is discussed in section 3.4.3. and may be regarded as supplementary information to this section.

One major problem is the uncertainty in the reactivity scale, which is particularly large in Pu-²³⁸U fuelled assemblies, where reactivity worths are overestimated by calculation by as much as 30 %. The second important problem is the dependence of the small-sample worth on the sample size, and on the kind of embedding of the sample in the plate structure of the assembly. In general, the standard interpretation of worth measurements by first order perturbation theory is, therefore, not adequate. In the following, the effort spent at Karlsruhe to understand these two points will be briefly reviewed.

5.4.1. The problem of the reactivity scale

Central reactivity worths are generally overestimated by calculation. However, the overestimation is larger in Pu assemblies than in similar uranium fuelled assemblies. This point can be seen by comparing results from pairs of assemblies like 2A and 6B in SNEAK, which are similar, except that 2A was purely uranium fuelled, whereas 6B contained an inner Pu zone. The worths of ²³⁵U, ²³⁹Pu, and ¹⁰B are 6 % more overestimated in 6B than in 2A. As mentioned above some results reported in the literature are overestimated by as much as 30 %.

In order to investigate this point, a systematic study to determine the effective delayed neutron fraction β_{eff} and the normalization integral was carried

out in the two Pu-fuelled assemblies 7A and 7B in SNEAK. The ratio $^{238}\text{U}/^{239}\text{Pu}$ was 3.0 in 7A, and 8.0 in 7B. In both assemblies, the apparent worth of a ^{252}Cf -source was measured. The worth (in β) is given by the expression

$$\rho_{\text{Cf}} = \frac{S_{\text{Cf}}}{\beta_{\text{eff}} \nu R_f F} \left(\frac{\phi_{\text{Cf}}^+}{\phi_f^+} \right)$$

It is ρ_{Cf} : reactivity of the Cf-source (in β)

S_{Cf} : source strength

R_f : absolute fission rate per cm^3 of core material

$\phi_{\text{Cf}}^+ / \phi_f^+$: importance ratio of Cf-neutrons and reactor fission neutrons (close to one)

and
$$F = \int d^3r R_f(r) \phi_f^+(r) / R_f(o) \phi_f^+(o)$$

is the normalization integral. The worth of ^{252}Cf , combined with the absolute fission rate, gives the quantity $\beta \nu F$, which is a measure for the reactivity scale. In addition, the normalization integral F can be determined from measured axial fission rate traverses, combined with traverses of the Cf-worth. As ν can be calculated from basic data with good accuracy, an experimental value of β_{eff} is obtained. The results of these measurements, and of calculations with the KFK INR set, are given in Table 5.5. The normalization integral is calculated well, but β_{eff} is underestimated in both assemblies. This indicates that the delayed neutron fractions used in the calculations are too low.

In a second experiment in SNEAK, β_{eff} ratios were measured by oscillating uniformly loaded core elements. The oscillation leads to a pseudo reactivity effect due to the transport of delayed neutron precursors, which is proportional to the precursor concentration in a particular loading. From measurements with different loadings, β_{eff} ratios of the isotopes ^{235}U , ^{238}U and ^{239}Pu were obtained. The results show that the ratio β_8/β_5 is about 8 % larger than the value quoted by Keepin /5.12./, whereas β_9/β_5 is 25 % larger. In spite of rather large experimental errors of about 8 %, these results indicate that the β values which were accepted so far as standard are too low. If the β_{eff} of 7A and 7B, as calculated by the KFK INR set, are increased by these factors, one obtain $0.00408 \pm 5\%$ for 7A, and $0.00449 \pm 5\%$ for 7 B, in good agreement with the results of the ^{252}Cf -experiment. The rather large increase of about 25 % for β_9/β_5 is surprising, and it is felt that it might be too large. But there was not found an obvious error

Table 5.5

Results of β_{eff} Measurements with
a ^{252}Cf -Source

	$\beta vF, \text{cm}^3$	F, cm^3	v	β_{eff}
<u>SNEAK-7A</u>				
Experiment	491 \pm 4%	40000 \pm 2%		0.00416 \pm 5%
Calc. KFKINR	424	40000	2.95	0.00359
<u>SNEAK-7B</u>				
Experiment	1195 \pm 4%	92000 \pm 2%		0.00446 \pm 5%
Calc. KFKINR	1048	90000	2.92	0.00400

in this result up to now; further investigations will be done.

5.4.2. Heterogeneity effects in the reactivity worth determination

The normal procedure of calculating reactivity worths of small samples with first order perturbation theory is not adequate for two reasons. The first is that in practice a small sample of the material under study is inserted into the lattice of the reactor core and not into a homogeneous mixture of the lattice. Therefore the worth of the sample may be quite position dependent if the lattice has a flux fine structure. The second reason is that the insertion of the sample into the lattice produces itself a change in the properties of the lattice. That is, the sample may act as a source, or sink, for neutrons in the lattice. In addition, except for very thin samples, there is a flux fine structure through the sample depending on its self-shielding properties.

In order to be able to treat the actual problems involved in the measurement of a small sample reactivity worth, a computer code, KAPER, was developed at GfK-Karlsruhe. The features of this code are outlined in section 3.4.1. and may be looked up there. With the help of this code we feel satisfactorily well equipped to analyse material worth measurements, as is shown below.

5.4.3. Present status of the interpretation of material worth measurements

The present state of the art concerning material worth measurements may be demonstrated by quoting the results obtained in the two Pu-cores of SNEAK-7. This is done in Table 5.6. The values calculated with MOXTOT and KFK INR are also quoted; the calculations were performed with the KAPER program. Both cross section sets overestimate the worths, which is due to low β values. The consistency of the results is rather poor with the MOXTOT set, but good with the KFK INR set. It must be mentioned that the ^{252}Cf worth is on the average 7 % more overpredicted than the material worths. It is unlikely that this rather large difference is entirely due to errors in the cross section data; part of it may be due to an error in the absolute calibration of the fission rate.

Thus, the present status is such that a 7 % difference between material worth measurements on one side, and β_{eff} determination on the other side, remains to be explained. An effort is underway to check all the important results and the calibrations, and to repeat some of the key measurements.

Table 5.6 Measured and Calculated Central Reactivity Coefficients, 10^{-3} $\$/g$

Sample	Sample weight (gm)	Experiment	SNEAK-7A		SNEAK-7B		
			Calc. / Exp.		Experiment	Calc. / Exp.	
			MOXTOT	KFKINR		MOXTOT	KFKINR
^{235}U	3.7	2.25 \pm 3%	1.213	1.082	1.265 \pm 2%	1.185	1.082
^{238}U	124	-0.110 \pm 3%	1.385	1.078	-0.0670 \pm 2%	1.330	1.100
^{239}Pu	2.5 (7A) 4.0 (7B)	3.03 \pm 3%	1.150	1.085	1.695 \pm 2%	1.082	1.062
^{240}Pu	3	0.72 \pm 8%	0.81	0.99	0.30 \pm 10%	0.83	1.06
^{10}B ($10^{-3}\$/\text{cm}^3$)	0.3	-55.2 \pm 2%	1.283	1.045	-20.7 \pm 2%	1.190	1.005
Cf-source (1/ β vF)		2.04 \pm 4%	1.25	1.16	0.84 \pm 4%	1.18	1.14

5.5. Prediction of Control Rod Worth

In 1969 the SNR reference core comprised two rings of control rods at fixed positions: in the inner ring the absorber of the safety rods was supposed to be made of B_4C , in the outer ring the absorber of the compensating rods was supposed to be made of tantalum. Any absorber rod is continued by a follower (80 % Na + 20 % steel).

Preliminary mock-up type experiments were performed in SNEAK-2, core C (Fig.5.9), already mentioned in 5.2. The amount of plutonium, limited to a fraction of the total core fuel, was placed in a sector. One to three B_4C rods and one Ta rod were placed at an off-center position (outer ring of SNR). Central measurements were also made, for further comparison of both absorbers B_4C and Ta, under conditions which were easier to evaluate. (See ref. /5.2./)

In the core A of SNEAK-6 again central measurements were performed in 1970, in a fully cylindrical core with a central plutonium loading and a height directly comparable to that of the SNR (SNEAK-6: 90 cm, SNR: 95 cm). A number of partial insertion depths of rods were considered, see Fig.5.10 Two particular points were also investigated: a stepwise split-up of a rod (self-shielding effects), and the insertion of a B_4C rod in a central zone voided of Na (safety aspect). (See ref. /5.9./ and /5.13/).

For the reactivity measurements almost all the steps of the measurements used the quasi-critical method: in order to compensate for the negative reactivity insertion due to the control rod, core elements are added at the core edge, and the core is always close to criticality (within $\pm 1 \beta$). The configuration changes are realized in steps small enough to allow the use of calibrated SNEAK shim rods to determine the changes in reactivity.

5.5.1. Methods and data used for the interpretation of the experiments

In 1969 the essential features of the standard methods of calculation used in the Consortium for the SNR design were:

- few-group diffusion theory;
- cross section set NAPPMB /5.14/;
- two-dimensional (RZ and XY) geometrical models.

Obviously the geometrical models were not well aimed at representing a number of control rods located at different radial positions in the core with a variety of partial insertion depths.

The development of the three-dimensional flux synthesis program KASY, described in chapter 3, came in time to apply a more appropriate theoretical tool. Since in a separate check the accuracy requirements for KASY were fulfilled for the problems considered, this program was then systematically applied to SNEAK control rod evaluations, having in mind its later use in the SNR design itself.

At the beginning of the SNEAK 2 experiments the available cross section set prepared at Karlsruhe was NAPPMB . When the subsequent set, MOXTOT 5.15/was released some calculations were repeated with it.

At the time of the SNEAK-6 experiments NAPPMB was still used in the SNR design for the sake of consistency with previous calculations. The same lines were therefore followed, basic use of NAPPMB, complementary use of MOXTOT.

The KFK INR set was prepared in 1971/72 and has not been used for the interpretation of the experiments, mentioned in this chapter.

Diffusion theory was basically applied in the SNEAK control rod evaluation as well as in the SNR design. Only a few cases were recalculated using transport theory, in order to clear up possible reasons of discrepancies.

As for the SNR design, the diffusion calculations performed in more than one dimension used few-group constants (generally 4 groups). The condensation effects were systematically studied and it was shown that even with 4 groups the effects due to condensation could be made very small (e.g. < 1 % relative

for the B_4C rod worth) when adequate precautions concerning the condensation spectra are taken.

All checks, the results of which are reported in the following, were performed in a 4-group scheme, except the transport-diffusion comparisons (13-groups).

5.5.2. Interpretation of experiments

The theoretical investigation was basically centered on the use of the three-dimensional (XY/Z) synthesis model. By this way, two-dimensional (XY) diffusion calculations had to be made in order to produce the trial functions for the synthesis.

Table 5.7 below presents the results of evaluation, as C/E ratios, for the case of a quadratic central Na- B_4C rod in the three SNEAK assemblies considered. The (XY/Z) results are presented, and also for the sake of completeness the simple XY results obtained with the same transverse buckling for in- and out-cases.

Table 5.7. Reactivity worth of a central Na- B_4C rod, calculation-over-experiment ratios C/E:

Methods	SNEAK-2C	SNEAK-6A	SNEAK-6D
<u>fuel - Na</u>			
2D (XY)+ buckling	1.39	1.25	-
3D (XY/Z)	1.25	1.11	1.16
<u>fuel - B_4C</u>			
2D (XY)+ buckling	1.01	-	-
3D (XY/Z)	1.01	1.04	1.06

One observes that the simple 2D model is sufficient for fully inserted absorbers, but not for the fully withdrawn absorbers. This is not surprising, because in case of a withdrawn absorber the axial leakage is different, which gives about 11% difference between 2D and 3D calculations results.

On the other hand in SNEAK-6A the reactivity of a central Na-B₄C rod has been calculated in 2D (RZ) and in 3D (XY/Z) geometry. The results indicate only small differences, of 1.8 % (fuel-sodium) and 1.3 % (fuel-B₄C) respectively, which may come partly from the cylinderisation effect.

It is clear that the 2D (RZ) model produces only valid results in the case of a central rod, and that the 2D (XY) model is unable to represent partially inserted rods. For all cases of off-center rods partially inserted a three-dimensional model is necessary.

In general one notices an overestimate of the rod-out case by 10 to 25 %. One may attribute the general overestimate of diffusion calculations for the reactivity difference upon introduction of such a light medium, to an inadequate treatment of the axial neutron leakage. This will be investigated below. The reduction of the overestimate from SNEAK-2C to SNEAK-6A or D can be explained by the increased core height (60 to 90 cm). The difference of the C/E ratios when going from SNEAK-6A to 6D (+ 5 %) is due to the different anisotropy, the Na follower being made of rodlets in -6D and of platelets -6A; in addition the loading of the rod position in the axial blanket region is not exactly the same.

For the reactivity changes fuel B₄C, one observes in the table a good agreement between the C/E values in -6A and -6D which are larger by 3 to 5 % than the -2C values, the differences do not exceed the experimental accuracy of 5 %. It should be noted that all comparisons of calculated and measured reactivity worth make use of calculated β_{eff} values, according to KEEPIN's data.

The relative variations of β_{eff} due to changing core configuration are taken into account.

The following examples demonstrate the usefulness of the 3D-synthesis technique and the accuracy obtained for off center rod locations.

At first we discuss a special experiment in SNEAK-6A, which was devoted to the study of the self-shielding effects within an absorber rod: for both types of rods, B₄C and Ta fully inserted, reactivity changes were measured also when the four SNEAK elements (5.44 x 5.44 cm of cross-section)

constituting the rod were split up radially, by one and two element widths, see Fig. 5.10.

Table 5.8. below gives the comparison of calculated and measured reactivity changes for all the steps. These reactivity steps are well calculated for both absorbers (the large percentage error for some reactivity differences stems from their small absolute size due to compensating effects). The error in the prediction of the total reactivity worth of a B_4C or Ta rod is of the same order in the split or the non-split condition.

Although compensating effects can exist it seems that with the methods used an exact geometrical representation of the square geometry leads to a satisfactory prediction of the considered self shielding effect.

The same table illustrates another special experiment made in SNEAK-6A the Na- B_4C rod was inserted not only in a reference core but also in a core with a large sodium void zone. One sees that the methods of calculation used (which are not specially adapted to Na void) produce practically the same overestimate of the experimental value for a B_4C rod in a sodium voided zone as in a normal core.

Next we consider the reactivity associated with the progressive replacement of the follower by the absorber (Na- B_4C or Al-Ta). The results of the comparison measurement-calculation are given in Fig. 5.11 which represents the characteristic curve $\delta k = f$ (insertion depth) on the basis of some points measured in SNEAK-6A and calculated (a direct measurement of the characteristic curve in SNEAK-2C gave similar results). The reference point of the reactivity scale is fixed at half insertion in the linear portion of the curve. One observes that the slope of the characteristic curve is overpredicted by calculation. This is consistent with the general overestimate by a few percent of the reactivity changes Na- B_4C and Al-Ta found by calculations.

As mentioned above, there is a general overestimation of the reactivity in the rod-out case. Therefore the validity of diffusion theory was checked by comparing to transport calculations for a central Na- B_4C rod in SNEAK-6A.

Table 5.8.

SNEAK-6A control rod experiment

Some comparisons of calculated and measured negative reactivity changes (ρ)

Cases	Experiment	Calculation	Ratio C/E
1) Shadowing effect with B_4C			
fuel- B_4C (normal configuration)	818.1	853.0	1.04
B_4C to split-up 1	105.7	102.1	0.97
split-up 1 to split-up 2	- 13.8	- 10.6	0.77
fuel- B_4C (split-up 2)	910.0	944.5	1.04
2) Shadowing effect with Ta			
fuel-Ta (normal configuration)	530.0	551.8	1.04
Ta to split-up 1	43.1	41.8	0.97
split-up 1 to split-up 2	- 30.7	- 36.9	1.20
fuel-Ta (split-up 2)	542.4	556.7	1.03
3) Insertion of a B_4C absorber in normal core and in a large central void zone			
in normal core	818.1	853.0	1.04
in Na void zone (in a smaller core)	851.5	883.2	1.04

Transport refers here to the S_n -method with $n = 4$, using as transport cross-sections the current weighted type. The results are given in Table 5.9.

From this table it can be seen that for the reactivity of the absorber B_4C , the one- and two-dimensional transport effects compare well. For the Na follower they differ largely: only in two-dimensions the advantage of transport in correctly describing the axial leakage of neutrons becomes effective.

The use of transport instead of diffusion always results in an improvement of the C/E ratios. But one must observe that for the case of sodium follower a geometrical model which contains the axial direction (i.e. 2D in this case and 3D in the general case) allows a definite conclusion on the transport correction.

Table 5.9. Compared transport and diffusion results
Reactivity of a central (Na-B₄C) rod in SNEAK-6A

Relative deviations (T-D)/D in % for the changes:	1D (R)	2D (RZ)
fuel-sodium	- 1.8	- 8.6
fuel-B ₄ C	- 3.5	- 5.0

It should be noted that in these evaluations no heterogeneity corrections have been applied. However, this correction is felt to be small.

At last will be examined the influence of the improved cross section set MOXTOT on the control rod worth. The effect on the reactivity changes when using MOXTOT instead of NAPPMB is illustrated by the following values (deviations in relative %) extracted out of SNEAK-6D results.

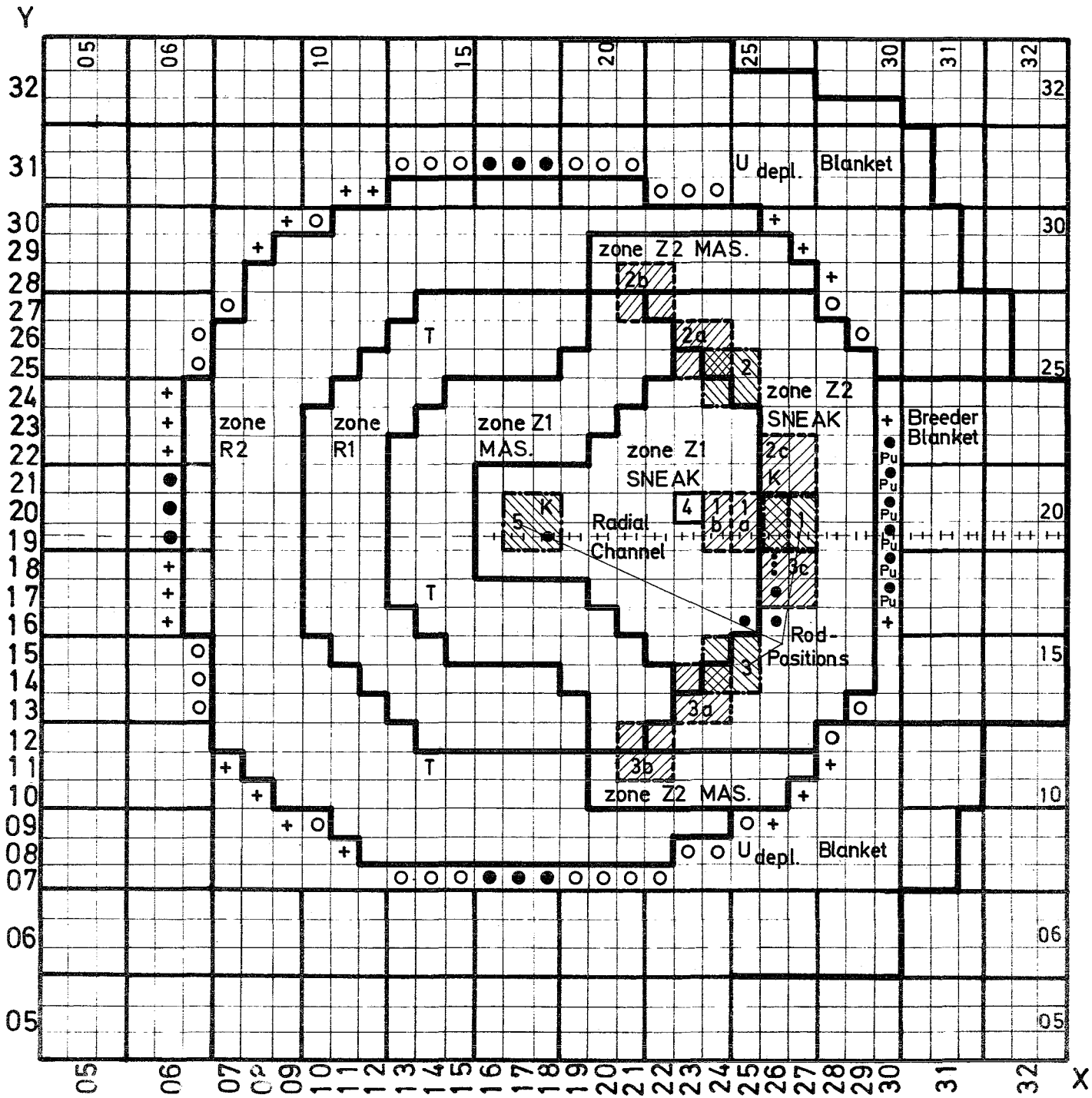
fuel - sodium: - 3.8 %
fuel- B₄C: - 1.5 %

The theoretical results agree by this amount better with experiments, but this improvement is partly fortuitous.

In fact from NAPPMB to MOXTOT the absorber and follower cross sections were not modified, but only the cross sections for the fuel. The calculated control rod reactivity is then influenced by the calculation of the relative weights (importances) of the different fuel zones. In SNEAK-6D the central Pu zone is surrounded by a U driver; MOXTOT gives a lower relative weight for the Pu zone than NAPPMB, which results in a decrease in control rod reactivity.

A comparison with SNEAK-2C confirms this explanation in SNEAK-2C; the sector in which the control rods are placed, is made of two Pu fuelled enrichment zones; the calculated effect MOXTOT-NAPPMB is of opposite sign and of smaller amplitude.

The conclusion here is that the cross section set which shall give good results in the evaluation of control rod worths must predict equally well the k_{eff} (or B_m^2) of the different core zones. With such a set, a not appropriate weight of the different core zones is eliminated.



SNEAK-2C Second Part of the Control Rod Experiments Core Configurations

groups of edge elements

group nr.	number of elements	designation
3	15	●
4	30	○
5	22	+

Fig. 5.9



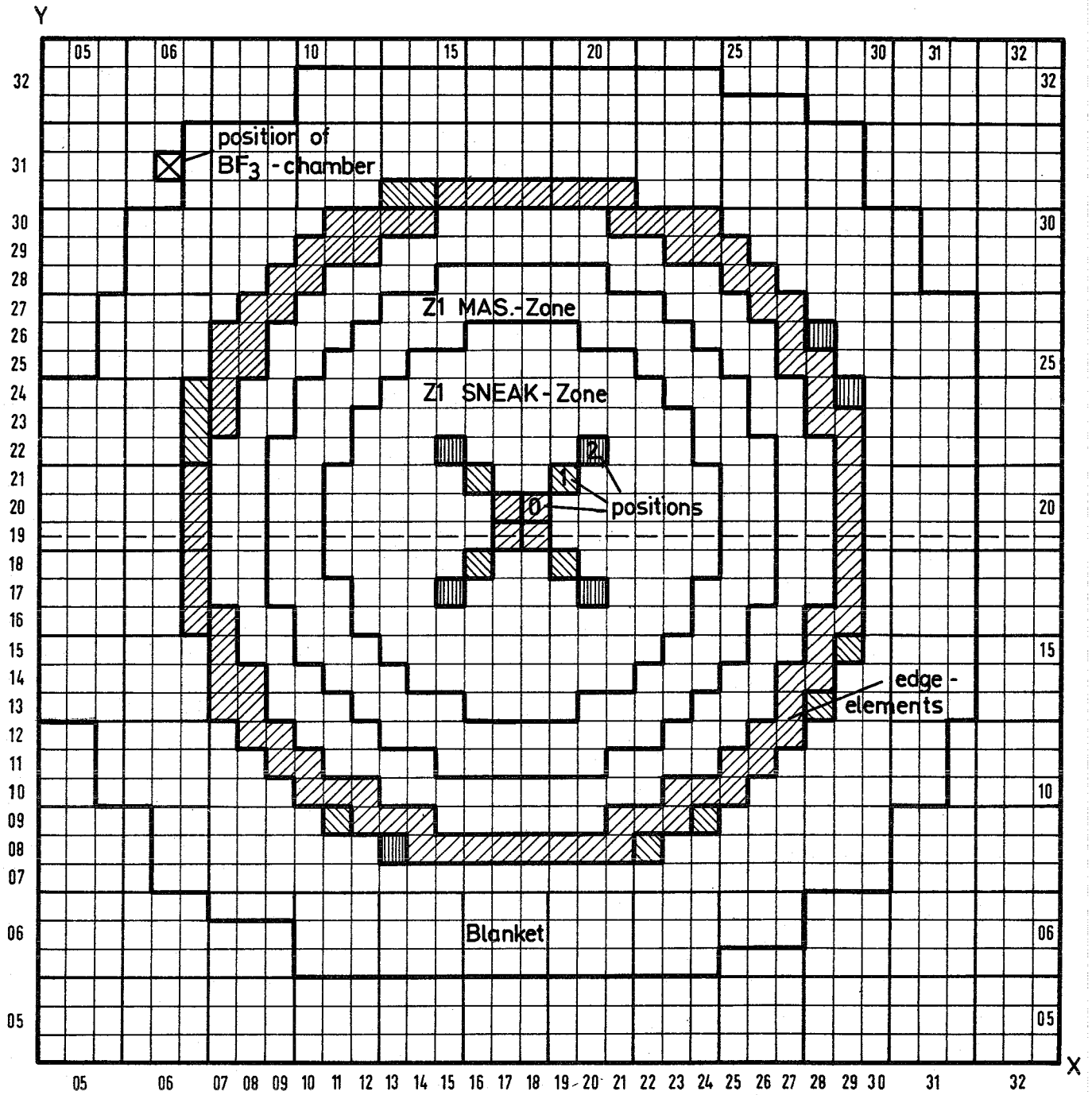
Pos. for azimuthal traverses (foils and platelets)

K = Pos. for axial chamber traverses



Pos. for radial chamber traverses

scale 1:10



SNEAK-6A B_4C -Rod splitted up in two steps

The edge elements correspond to respectively :

-  B_4C , reference position (0)
-  B_4C , first split-up (1)
-  $B C$, second split-up (2)

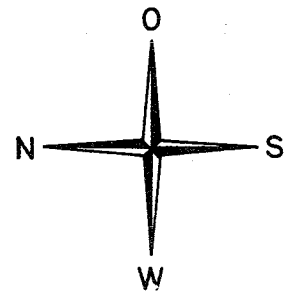


Fig. 5.10

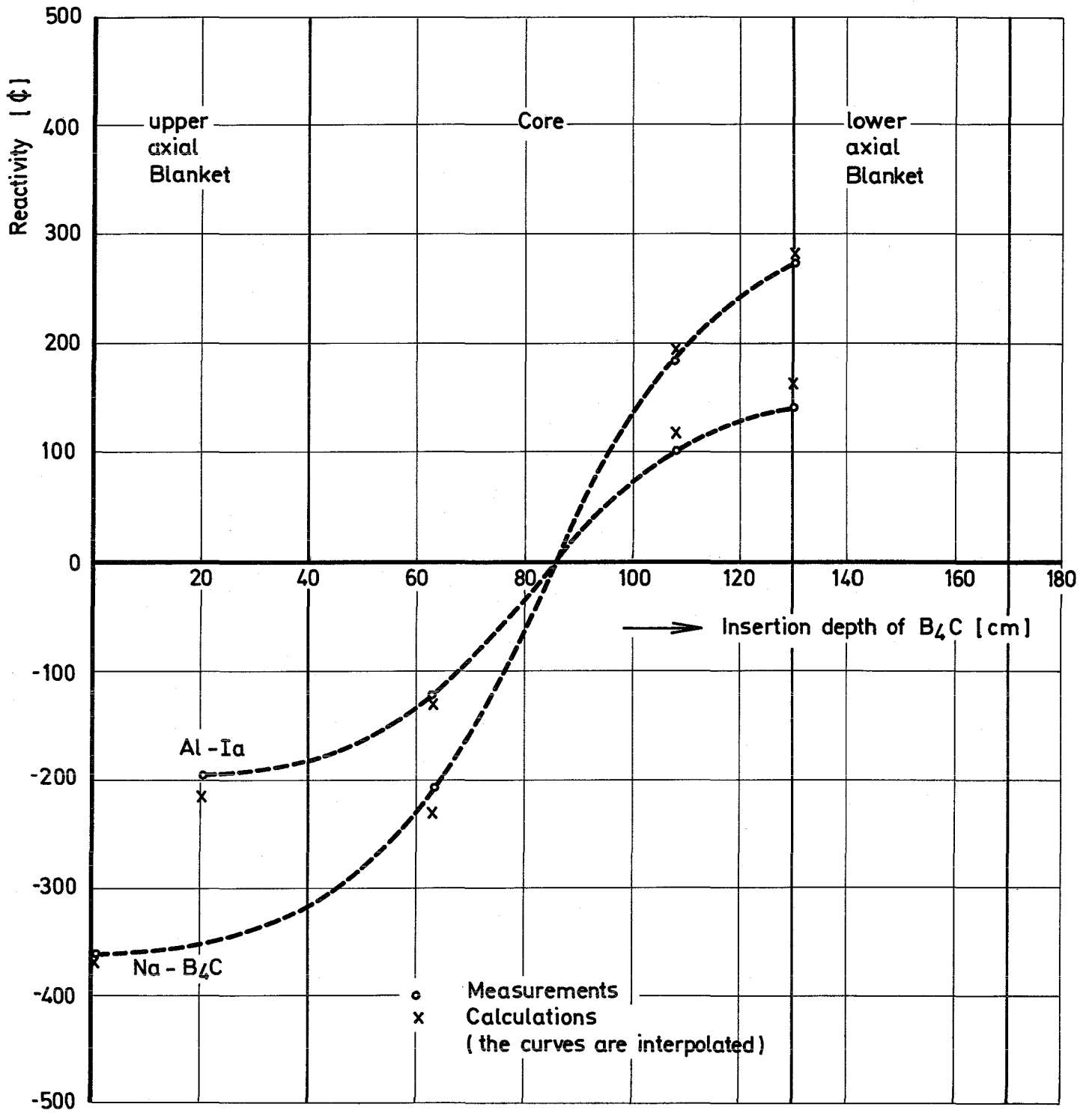


Fig. 5.11 SNEAK - 6A
Characteristic Curves Na - B_4C and Al - Ta
(4 SNEAK Elements)

5.6. Analysis of DOPPLER experiments in SNEAK and SEFOR

Doppler experiments in Core I and Core II of SEFOR /5.18./ and in assembly 9B /5.19./ of SNEAK provided new experimental information for checks with cross sections and methodical procedures in nuclear Doppler calculations. The results of these investigations are being reported and discussed in this section.

5.6.1. SEFOR experiments and check of nuclear calculations

The type of experiments performed in SEFOR and the kind of experimental information is listed in Table 5.10.

Table 5.10.

Type of experiment	Temperature range covered	Type of reactivity feedback information	Estimated uncertainty
Isothermal heating of fuel and sodium	180°C - 400°C 450°K - 680°K	Isothermal temperature coefficient ($\$/^{\circ}\text{k}$)	$\pm 5\%$
Static power experiments at constant sodium temperature	400°C - 1850°C 680°K - 2000°K	Doppler power coefficient ($\$/\text{MW}$)	$\pm 9\%$
Conventional and balanced oscillator experiments	400°C - 1800°C 680°K - 2070°K	Doppler power coefficient fuel time constant ($\$$)	$\pm 12\%$ $\pm 10\%$
Subprompt and superprompt transient experiments	600°C - 1150°C 870°K - 1420°K	Doppler energy coefficient ($\$/\text{MWs}$)	$\pm 9\%$

The Doppler constant $A_D = \beta_{\text{eff}} T \, dk/dt$ could be derived from the measured power and energy coefficients with an uncertainty of $\pm 10\%$. The best average values are - 0.0080 for Core I and - 0.0060 for Core II.

Nuclear calculations based on the KFK INR cross section set lead to results for $-A_D$ which are about 6 % lower than the measured numbers both for core I and for core II. This relation holds if the calculated β_{eff} is based on Keepin's /5.20./

Table 5.11

Second Order Effects in Doppler Calculations

"First order approach" (basis): Perturbation theory
 2 dim. flux and adjoint distribution
 (26 energy groups)
 uniform temperature distribution
 (near room temperature)
 $d\sigma/dT = \sigma_{\infty} df/dT$

Effect	Calculational method	Typical magnitude of correction	
		(SEFOR, Core I)	SNR
global			
Non-uniform temperature distribution in the reactor	Spatial integration of $\frac{A_D}{T} \phi \phi^+$	+ 15%	5-10%
Deviations from $1/T - law$	k_{eff} calculations at different temperature levels	- 8%	- 8%
Heterogeneity corrections			
a) Bell type correction	ZERA correction for cross sections	+ 3%	+ 1%
b) Spectral shift correction		+ 2%	+ 5%
Temperature and flux fine structure distribution within the pellets	RABID calculations	≈ 2%	1-2%
Transport correction	Comparison of axial and radial S_n and Diffusion Doppler calculations	+ 3%	+2%
Deviations from NR approximation	Comparison of DOPRO and RABID calculations	+ 5%	+5%
Crystal binding effects	(neglected)		

Estimated uncertainty of all corrections: ± 8%
 and methodical procedures

delayed neutron parameters.

More recent measurements /5.21./ of the delayed neutron parameters would increase β_{eff} by 5 - 10 % and lead to a larger difference between calculated and measured A_D values.

The agreement permits the conclusion that there are no major uncertainties in resonance parameters, in spectrum calculations and methodical procedures applied for the Doppler calculations. Each of these partial uncertainties is estimated to be 5 - 10 % , so that the total uncertainty amounts to 15 - 25 %.

One experience of the analysis of the SEFOR Doppler experiments is that quite a number of methodical corrections has to be applied to "first order approaches" (Table 5.11.). Several individual corrections are rather small; however most of them lead into the same direction.

Doppler calculations based on two other cross section sets (MOXTOT and NAPPMB) that are currently used in Germany lead to similar results as the KFK INR set (Table 5.12.)

Table 5.12. Relative Doppler Results for SEFOR Core I
Obtained by Different Cross Section Sets

Cross Section Set	$\Delta A_D / A_D$
KFK INR	0 (basis for comparison)
MOXTOT	+ 3 %
NAPPMB	+ 3.5 %
ABN	- 11 %
MOD. ENDF/B-II	+ 12 %

5.6.2. The Doppler experiment in SNEAK-9B

Small-sample Doppler were carried out

a) with a depleted UO_2 sample (up to 700°C). The results are shown in Fig.5.12. The calculations were done with the code DOPRO, which was written for the analysis of heated sample experiments in critical facilities (see section 3.4.6.). Two values for the p-wave strength function, $S_1 = 1.5 \cdot 10^{-4}$ (considered to be realistic, and compatible with present σ_c), and $S_1 = 2.5 \cdot 10^{-4}$ (data on KEDAK) were used. The ratio C/E is 0.85 (low S_1) and 1.04 (high S_1). The diffusion calculation was done with KFKINR. The central worth of ^{239}Pu is overestimated by 10 %.

b) with a PuO_2 sample (diluted with Al_2O_3)

With this sample, the experiment gives practically zero up to 400°C and a small negative effect at higher temperatures. In the calculation, there is a strong cancellation of fission and absorption effects of ^{239}Pu . However, the net effect is still positive, even if the (rather small) effect of radial expansion (40 % of the total calculated effect) is included. Though there is a difference even in sign between experiment and calculation, the absolute difference is of the same order as for the UO_2 sample.

5.6.3. Comparison of the SEFOR and SNEAK results

For comparison with SEFOR, the SNEAK experiment was also analysed using self-shielded cross sections evaluated at different temperatures from calculated f-factors. For the purpose of this comparisons the influence of the "cold core" resonances on the resonance absorption in the "hot sample" was neglected. Then the ratio C/E is 0.90, which is less than in SEFOR.

It must be noted that the spectrum in SNEAK-9B was harder than in SEFOR. Whereas in SEFOR about 70 % of the Doppler effect occurs below 2 keV, in SNEAK 70 % occur below 10 keV (compare Fig. 5.13.). Thus, in the latter case, there is a larger contribution of p-wave resonances, for which the data are still relatively uncertain. This may explain the larger underestimation in the SNEAK experiment.

One can normalize the Doppler effect to the central worth of ^{239}Pu , in order to eliminate uncertainties in the delayed neutron data. The ratio Doppler/

^{239}Pu worth is underestimated by about 14 % in SEFOR, and by 18 % in SNEAK.

5.6.4. SEFOR transient power excursions and comparison with calculations

Experience gained by the analysis of SEFOR experiments included a successive check of codes for the prediction of the reactor response to fast superprompt reactivity excursions. During the transient experiments, a slug containing boron was rapidly (within 130 msec.) ejected from the core. The corresponding reactivity insertion reached values up to 1.3 β . The agreement between experimental power traces and REX /5.22./ calculations was good in all cases investigated. A typical example is shown in Fig. 5.13a.

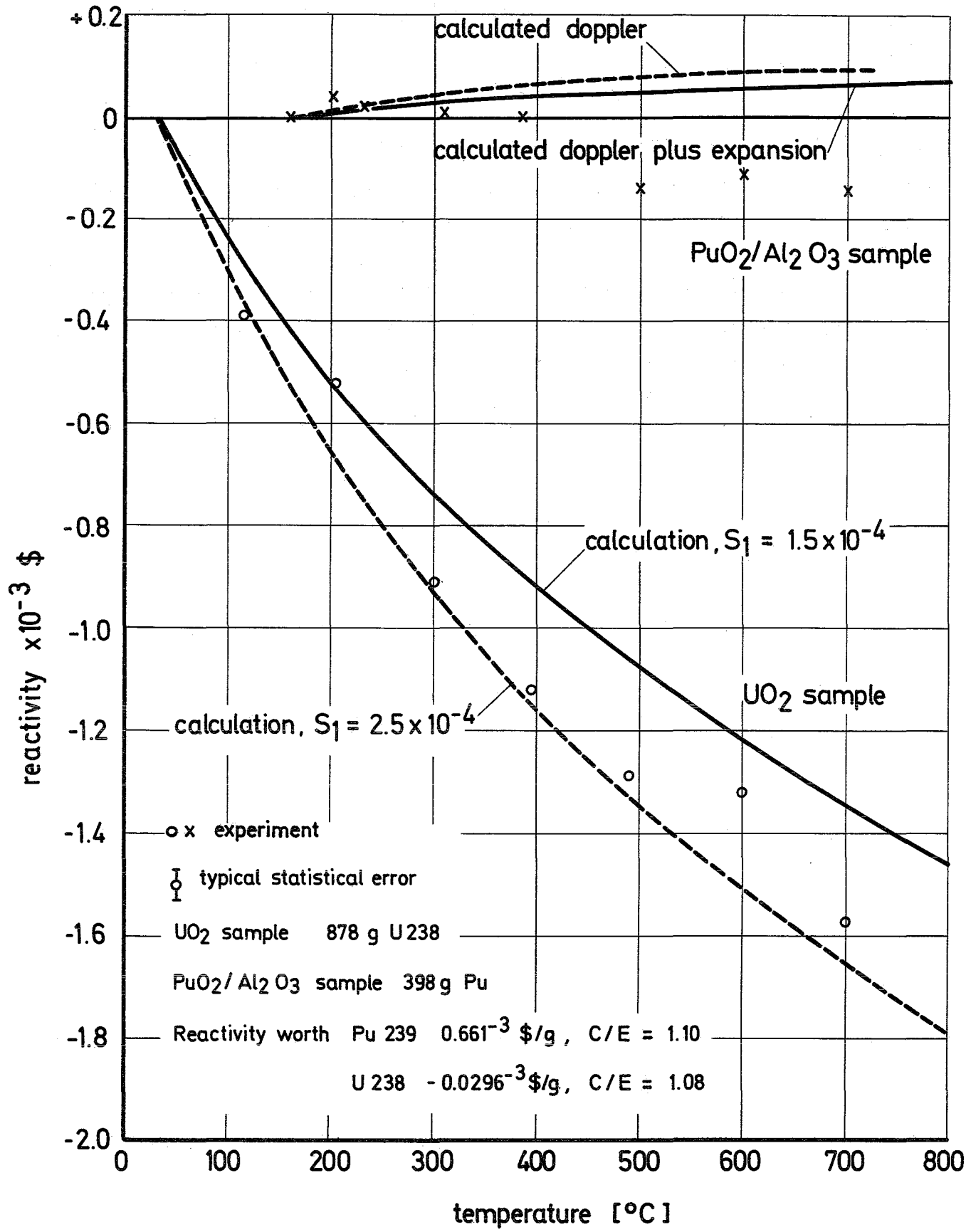
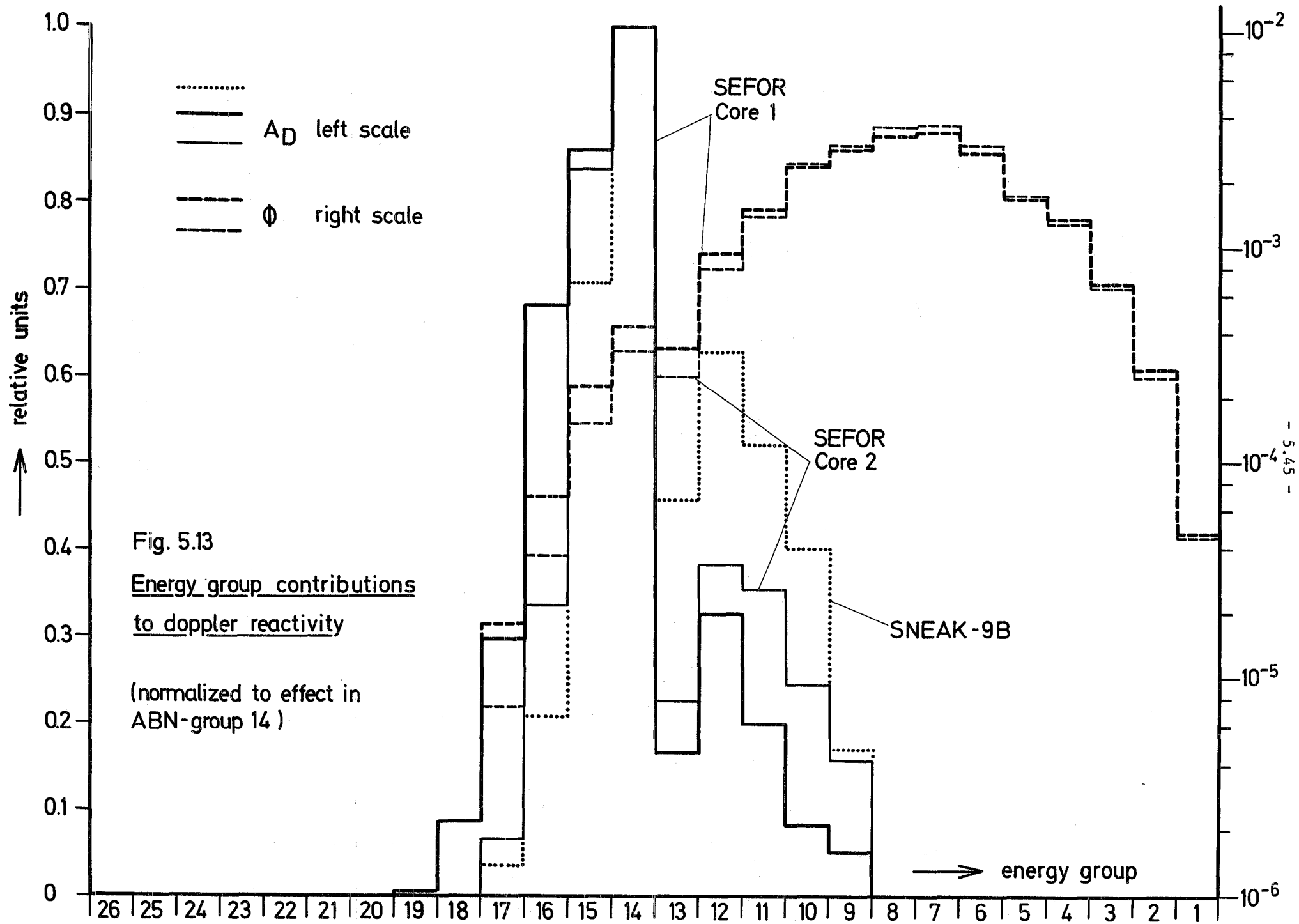


Fig. 5.12 Doppler experiment in SNEAK-9B



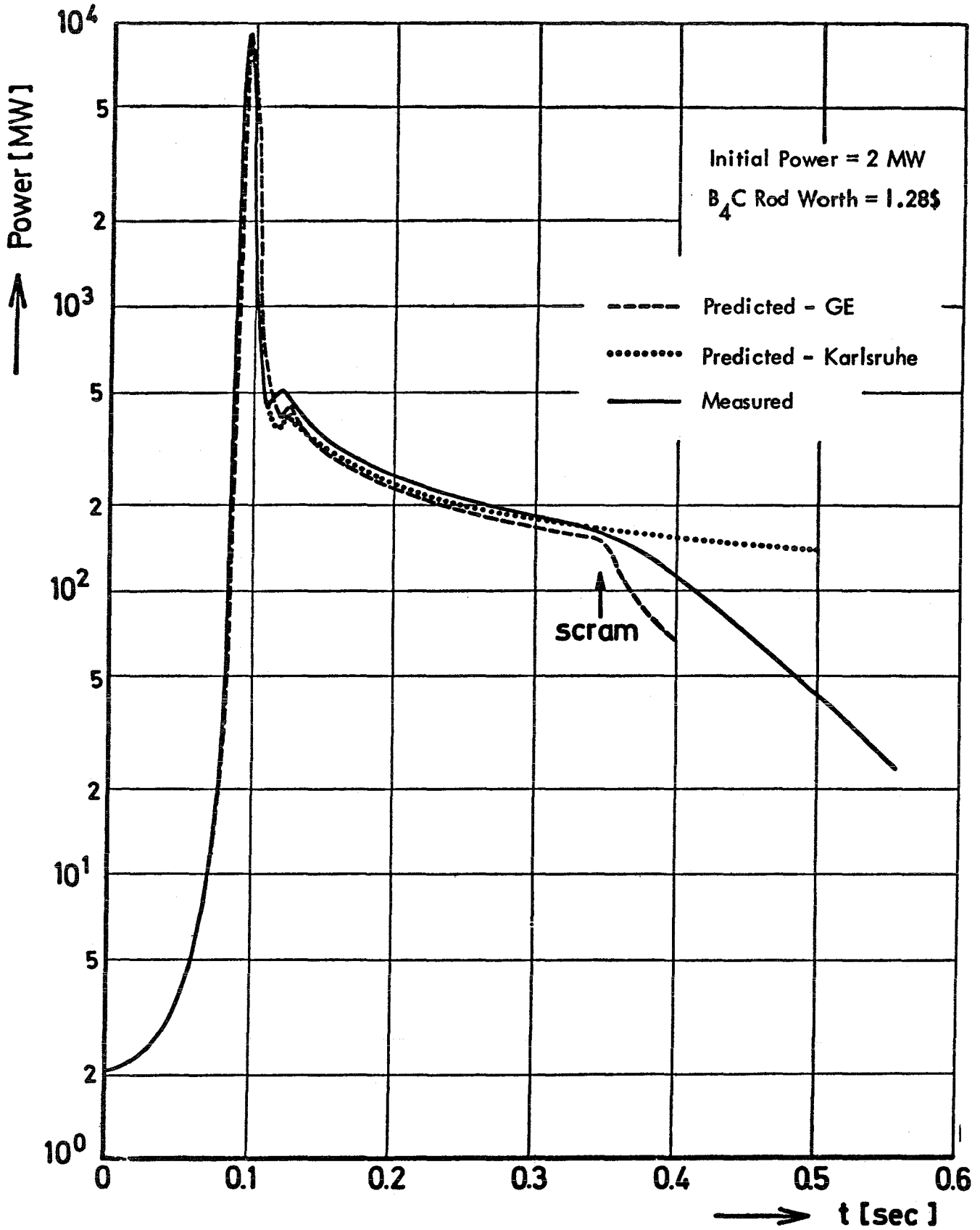


FIG. 13a CORE I SUPER-PROMPT TRANSIENT

5.7. Measurements and Calculations of Sodium

Void Coefficients

As outlined above an approximate knowledge of the Na-void coefficient of a fast power reactor is necessary in order to ensure that certain reactor incidents do not endanger the overall safety of the system. Cases envisioned in the safety considerations include on the one hand local effects where, for example, sodium is voided from one subassembly or part of it as a consequence of local boiling caused by the blockage of a cooling channel. On the other hand one must also consider that a large part of the sodium is voided from the core which could be the consequence of a nuclear excursion.

In the experiments one therefore has to investigate radially limited voids of various axial extensions as well as large voids which should if possible approach the configuration with the maximal positive effect .

For a theoretical understanding of the effect one has to try to separate the degradation and absorption effect which is proportional to $(\phi\phi^+)$, from the leakage contribution which depends on $(\text{grad } \phi \text{ grad } \phi^+)$. For this reason exact measurements of the Na-void coefficient in the center of the assemblies are important. The leakage contribution at this location is zero and by a comparison of the measured effect with the effect for larger or excentrical regions the two contributions may be separated.

Due to the fact, that SNEAK in general is loaded with platelets, anisotropic diffusion must be considered when analyzing the leakage term. Quantitative evidence for this anisotropy was found from analyzing the experimental results. Also, methods have been developed for its calculation so that a comparison of measured and calculated anisotropic leakage was possible. The results of this evaluation must be taken into account when sodium void effects measured in a critical assembly are used to predict the effects in power fast breeders which have a different heterogeneous structure.

Special experiments were performed about influence of an increased concentration of ^{240}Pu and absorbing material (B_4C , simulating the absorption by fission products) on the sodium void effect and also on the effect of cavity formation which occurs when fuel and structural material are removed from the void zone and concentrated on its periphery.

5.7.1. Survey of the measurements

Assemblies containing sodium were first investigated in SNEAK in the year 1969 /5,2/. Since then the Na-void effect was measured in the plutonium-fueled test zone of the following assemblies (all designed in support of the prototype SNR).

SNEAK-2C a sector core with two radial enrichment zones.
SNEAK-6A,6B cylinder symmetrical cores with a central Pu-fueled test zone, with (6A) and without (6B) a MASURCA rodlet buffer zone /5.4. /.

These two assemblies yielded consistent results for void zones near the core axis (the difference by a factor $\frac{F(6A)}{F(6B)} = 0.855$ corresponding to the difference in β_{eff}). Therefore, occasionally the symbol 6A/6B will be used, when data from both assemblies are presented jointly.

SNEAK-6D As above but with the central test zone loaded with MASURCA rodlets and a buffer zone loaded with SNEAK Pu-fuel /5.3. /.

SNEAK-9B Similar as 6B but with a larger central test zone and a simple unit cell /5.17/.

In all of these cores an axial Na-void traverse was measured in the central four elements, starting with a small central void and increasing the height stepwise until it extended axially throughout the core.

In SNEAK-2C also a radial traverse was measured by stepwise displacing a small void zone from the core center outward to the radial blanket

boundary. The measurement was repeated for some points in the presence of simulated control rods.

Two series of large voids where the void radius was increased in a number of steps were investigated in the assemblies 6A and 9B.

A special study on the influence of anisotropic diffusion was conducted in SNEAK-9B by performing axial traverses using a slightly modified unit cell which allowed to orient the platelets both vertically and horizontally. The influence of an increased ^{240}Pu concentration was measured in SNEAK-6A in a test zone containing 5 kg Pu with 22 % ^{240}Pu in the form of PuO_2UO_2 platelets which were used in place of the normal PuO_2UO_2 platelets with 8 % ^{240}Pu . The measurements were repeated when the size of the zone with high ^{240}Pu content was increased using 12 kg Pu with 19 % ^{240}Pu in the form of metal platelets.

Also in SNEAK-6A, the Na-void effect was measured in the center of a zone poisoned with B_4C . This zone was built by replacing one of the 5 Na platelets in each unit cell by a B_4C platelet in 32 elements around the core axis.

A special study was performed on SNEAK-6A on the effect of cavity formation. This experiment considers a situation where in a part of the core a completely voided space is formed by ejection of sodium and compression of fuel and structural material along the edges of the cavity. For the simulation of such an occurrence in a critical assembly, first the sodium is removed in the cavity zone and in the surrounding region as in a normal sodium void experiment. Then fuel and structural material platelets are moved from the cavity into the space surrounding it. The experiment was performed in a central and in an excentrical zone. The calculations turned out to be very difficult, as one is dealing here with transport phenomena in a very complicated geometry. Therefore, for the cavity experiment a significant comparison calculation - experiment can not yet be presented.

5.7.2. Calculational methods and cross section sets

Calculations were performed in general using perturbation theory in two dimensions (RZ) and MOXTOT cross sections /5.15/ corrected for the

heterogeneity of the cell under consideration (MOXTOT-HET). The data for SNEAK-6B and 9B were also calculated using the more recent KFK INR set /557. ./ . Most of the Na-void calculations for SNEAK-2C and 6A were performed by one-dimensional perturbation theory only. This method of calculation is quite adequate to give the shape of a traverse. In order to get realistic absolute values one has to normalize the traverse at least in one point to two dimensional calculations which can be done by comparing directly the results for the void effect or by multiplying the 1D result with the ratio of the 1D and 2D calculated normalization integrals. The shape of traverses calculated in one dimension is also somewhat influenced by the choice of the transverse buckling, in particular when regions near the core boundary are involved. The 1D-results for such points must be considered with caution and cannot be used as normalization points.

For large voids first order perturbation theory is not very accurate since there are significant changes of the fluxes. These cases (large central voids in SNEAK-6A and 9B) are now evaluated by direct diffusion calculation and also by a modified perturbation theory where either the perturbed real flux or the perturbed adjoint flux is used in the calculation (so called exact perturbation theory).

The influence of the cell heterogeneity was studied by calculating some cases also with homogeneous cross sections.

In order to investigate the effect of a more adequate treatment of the elastic scattering resonances the calculations of the axial traverse in SNEAK-6A were also performed using homogeneous cross sections with and without REMO correction (see chapter 2). REMO is a cross section averaging code using the assumption of a smooth energy dependence of the collision density. In its present formulation the REMO correction cannot be calculated with heterogeneity corrected cross sections. So the correction is derived using homogeneous cross sections and can then be applied to Na-void results found with heterogeneity corrected data.

In the case of the KFK INR set the 26 group cross sections were calculated in such a way, that the REMO correction becomes very small for a typical

fast breeder core composition. The correction therefore was only calculated using the MOXTOT set.

In order to take into account the anisotropic diffusion in the plate structure of the critical assembly a formalism to calculate the diffusion coefficient parallel to the platelets and vertical to the platelets was included in the KAPER program (see also section 3.4.1.)

Therefore the KAPER program was used (and not, as usual, the ZERA program/5.20.) to calculate the heterogeneity corrected cross sections for the experiments with different plate orientations, which were performed in SNEAK-9B. As outlined in Section 3.4.1 the KAPER program calculates the cross sections in a perturbed cell taking into account the influence of the spectrum in the unperturbed composition in the surroundings.

The calculations for the experiments in a zone with high ^{240}Pu contents were performed only by perturbation theory in spherical geometry using homogeneous MOXTOT cross sections.

For the cavity experiment in SNEAK-6A problems were posed by the very dilute material in the cavity (high diffusion coefficient), the presence of a number of quite different regional compositions in a relatively small volume and the axially stretched out shape of the cavity which prevented a transformation into spherical geometry.

The total reactivity effect was investigated by two-dimensional transport calculations (TDC /5.21/, S_4 -approximation, 4 energy groups) in R,Z geometry using NAPPMB cross sections /5.14/. The effect of group collapsing (12 to 4 groups) was determined by R,Z diffusion calculations (DIXY). Further extension of the number of groups up to 26 has negligible effect on the reactivities.

In addition 2D-12 group-perturbation calculations (DIXY) were performed for the individual steps in constructing the cavity.

5.7.3. Evaluation of axial traverses

Fig 5.14 shows measured and calculated results for axial Na-void traverses in various SNEAK cores. Table 5.13 gives some numerical values for the ratios calculation/experiment. In each of the assemblies voids of increasing heights (centered at the core midplane) were introduced in the four central elements. For all cases the measured results are given along with data calculated by perturbation theory (2D or 1D normalized to 2D) using heterogeneity corrected cross sections of the MOXTOT-set. In addition for SNEAK-6A/B the results for homogeneous MOXTOT cross sections with and without the REMO correction are shown in Fig. 5.14. Finally calculated results with the presently used KFK INR set (heterogeneity corrected) are given for SNEAK-6A/B and SNEAK-9.

Looking at the results which were found using the MOXTOT and the KFK INR set (both heterogeneity corrected with ZERA) one realizes that for small central voids both sets yield an agreement between measurement and experiment within about 10 %. For larger voids the effect is calculated in general more negative than measured which can be attributed to an overestimate of the diffusion term. With the KFK INR set, the central values are calculated a few percent higher than with MOXTOT and the overestimate of the diffusion term is somewhat increased.

The data with the homogeneous MOXTOT cross sections for SNEAK-6A/B were given mainly to demonstrate the order of magnitude of the REMO correction. Assuming that a correction of this size also applies to the heterogeneous data (for which it cannot be calculated with existing programs) would lead for the MOXTOT set to central C/E values about 15 % lower than those given in Table 5.13 and thus to a larger discrepancy between calculation and measurement. The KFK INR set was adapted to a fast breeder spectrum so that it should yield a considerably smaller REMO correction. A further decrease of the C/E ratios would result if the value of β_{eff} is increased. That such a change may be necessary is indicated by experimental results such as reported in Section 5.4. of this report. For the mixed Pu/U assemblies in which the sodium void experiments were performed it would amount to about 5 to 10 %.

5.7.4. Measurements with different orientation of the platelets

The traverses which were measured in SNEAK-9B with the platelets oriented

Table 5.13

Comparison Calculation - Experiment for the Axial Sodium Void Traverses

Assembly		2C	6A	6D	9B	9B ⊥ ²⁾	9B ²⁾	
CROSS SECTION SET	MOXTOT	C/E, Central Value	0.97	1.00	1.10	0.94		
		C/E, Diffusion Term ¹⁾	1.20	1.31	1.19	1.30		
	KFKLINR	C/E, Central Value		1.10		1.00	1.00	1.02
		C/E, Diffusion Term ¹⁾		1.35		1.34	1.06	1.16
Group Constants prepared by		Z E R A			K A P E R			

1. The diffusion contributions were derived from the deviation of the (measured and calculated) traverses from proportionality to $(\phi\phi^{\dagger})$.

The values given here hold for void heights from about 65 % to 90 % of the total core height. Differing values are found for smaller voids where the diffusion term becomes very small and for larger voids where the influence of the blanket becomes noticeable.

2. These columns refer to a slightly modified unit cell which allowed to orient the platelets vertical (⊥) or parallel (||) to the core axis.

both parallel and vertical to the core axis are shown in Fig. 5.15.

The calculations were performed using KFK INR cross sections processed with the KAPER code with anisotropic diffusion taken into account.

The evaluation yielded the following result

Ratio	<u>Calc.</u>	<u>Meas.</u>
<u>Diffusion term parallel to platelets</u>		
Diffusion term vertical to platelets	1.37	1.27

The C/E ratios for the individual contributions are found in columns 4 and 5 of Table 5.13. One notes that the description of the diffusion term was improved considerably by the use of the new calculational method (note that the diffusion terms are defined as the difference between the central worth extrapolated to the zone under consideration and the actually measured or calculated worth).

5.7.5. Evaluation of radial traverses

In the reference configuration of SNEAK-2C as well as in a configuration with three simulated B_4C control rods on an outer ring the radial dependence of the sodium void effect was measured. This was accomplished by moving a small central void (comprising four SNEAK elements over a height of 17.4 cm) radially outward and measuring the resulting reactivity changes. In the reference core the width of each radial step was 1 SNEAK element, resulting in 14 measured positions; in the case with control rods, measurements were performed for 5 radial points only. (Two additional points were measured, but not calculated, for a configuration where the three simulated control rods were bunched to a single block of 2x6 elements sitting across the direction of the traverse.)

The measured data along with one-dimensional perturbation calculations using various cross section sets (homogeneous or ZERA corrected) are given in Fig. 5.16.

The agreement, in particular for the set MOXTOT-HET is quite satisfactory throughout the traverse. In particular there is no sign of an overestimate of the diffusion term, at least not in the outer core zone where diffusion is most pronounced. This should be due to the fact that diffusion in the radial direction is larger than axially as it occurs parallel to the platelets.

In the presence of control rods the flux is decreased in their vicinity, and consequently gradients become steeper in the inner part of the core and quite flat in the outer zone. This leads to a larger negative effect in the inner zone and to a very low effect in the outer zone of the core. The effect is quite well reproduced by the results of the calculations.

5.7.6. Central voids of increasing radius

Measurement of this type which were performed in SNEAK-6A and 9B have the aim of approaching the maximum possible positive void coefficient for these assemblies. In SNEAK-6A the voids extended through the entire height of the core and their radial extension was increased from 4 elements to 60 elements corresponding to a maximum radius of 23.8 cm. In SNEAK-9B the voids had the height of 60 cm (centered on the midplane, corresponding roughly to the maximum axial effect) and the number of voided elements was increased to 112 corresponding to a radius of 32,5 cm.

Fig 5.17. shows measured and calculated results, and in addition, values found by extrapolating experimental data from the axial traverse.

The extrapolation was performed using the following relations:

$$\rho_n = \rho_0 \cdot \left[\frac{\int_0^{r_n} r J_0^2(B_r r) dr}{\int_0^{R_{ex}} r J_0^2(B_r r) dr} + \frac{\rho_{D0} \cdot B_r^2 \cdot \int_0^{h/2} \cos^2(B_z z) dz \int_0^{r_n} r J_1^2(B_r r) dr}{\rho_0 \cdot B_z^2 \cdot \int_0^{h/2} \sin^2(B_z z) dz \int_0^{r_0} r J_0^2(B_r r) dr} \right]$$

Table 5.14

Results of the Na-void Experiments in ^{240}Pu zones
and in a B_4C poisoned zone in SNEAK-6A

Core Configuration	Void Height (cm)	Equivalent Radius (cm)	Na removed (g)	Effect		C/E
				measured	calculated (ρ)	
Reference	18.36	6.14 (4.E1.)	706	2.32	2.31 ^{a)} 2.61 ^{b)}	1.00 ^{a)} 1.12 ^{b)}
Small ^{240}Pu Zone	18.36	6.14	706	2.50	2.75 ^{b)}	1.10 ^{b)}
Enlarged ^{240}Pu Zone	18.36	6.14	706	2.88	2.84 ^{b)}	0.99 ^{b)}
Boron poisoned Zone	18.36	6.14	566	2.66	2.94 ^{a)}	1.11 ^{a)}
	18.36	10.63 (12 E1.)	1697	6.04	6.66 ^{a)}	1.10 ^{a)}

a) Results are from 1d-cylindrical perturbation calculations with MOXTOT-HET cross sections

b) Results are from 1d-spherical perturbation calculations with MOXTOT-HOM cross sections

Poisoning by B_4C , too, causes an increase in the Na-void effect which is confirmed by the calculations.

5.7.8. The cavity experiment in SNEAK-6A

Fig. 5.18 shows shape and position of the cavities investigated.

The cavities consisted of two zones; an inner zone where essentially all materials were removed and an outer zone where the sodium was removed and fuel and structural materials were condensed.

The experiments were performed in four steps:

- 1) Sodium void in the inner zone
- 2) Partial sodium void in the outer zone
- 3) PuO_2-UO_2 platelets shifted from the inner to the outer zone
- 4) Structural material shifted from the inner to the outer zone

In the inner zone only aluminium spacers remained: they were chosen successively thinner in three steps in order to extrapolate to the complete void.

Table 5.15 shows for the central position the experimental results along with the results of 12 group perturbation calculations for the individual steps and 4 group 2D transport calculations for the total effect. The total effect was also calculated by 2D diffusion theory with 4 and with 12 groups - one may use the difference found here to apply a condensation correction to the transport result. However, considering the crudeness of the method, the relatively good agreement reached is probably fortuitous.

The perturbation calculations which were used to calculate the individual steps give reasonable results for the first two of them (sodium void only) but are not able to describe the effect of shifting the fuel and structural material.

A correct treatment of the excentrical cavity would demand three dimensional transport calculations. Up to this time such calculations were not performed.

The experimental results are given in the last column of the table.

One conclusion of the cavity experiment is that the sodium void effect predominates over the material shifting effect in the geometry chosen. In order to come to more general statements which can be applied to reactor safety considerations more experiments in different geometries and a further refinement of the calculational techniques are necessary.

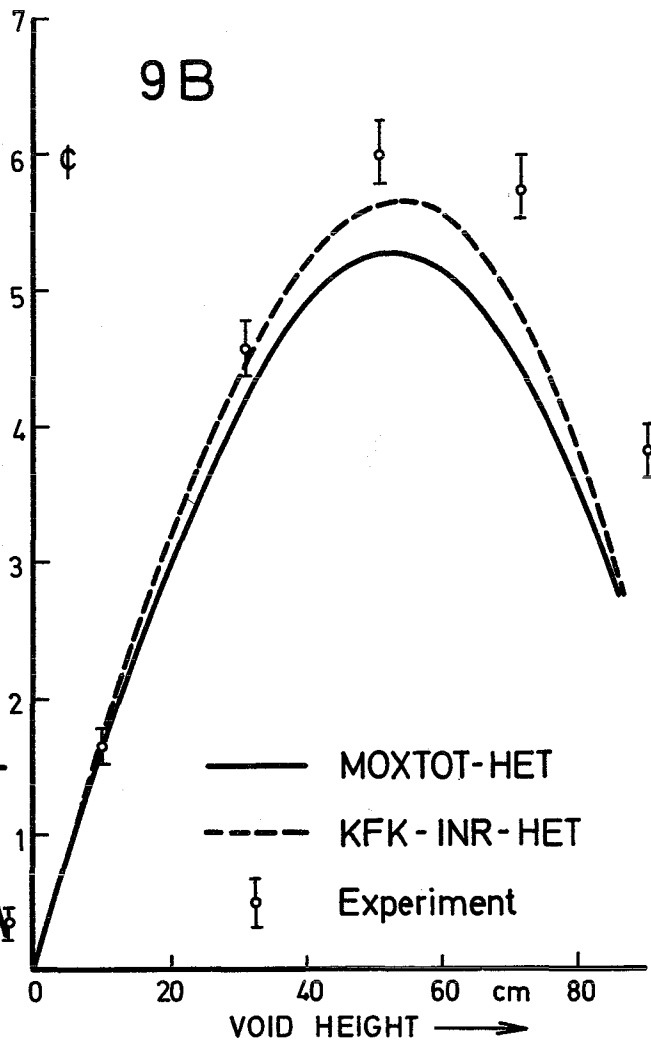
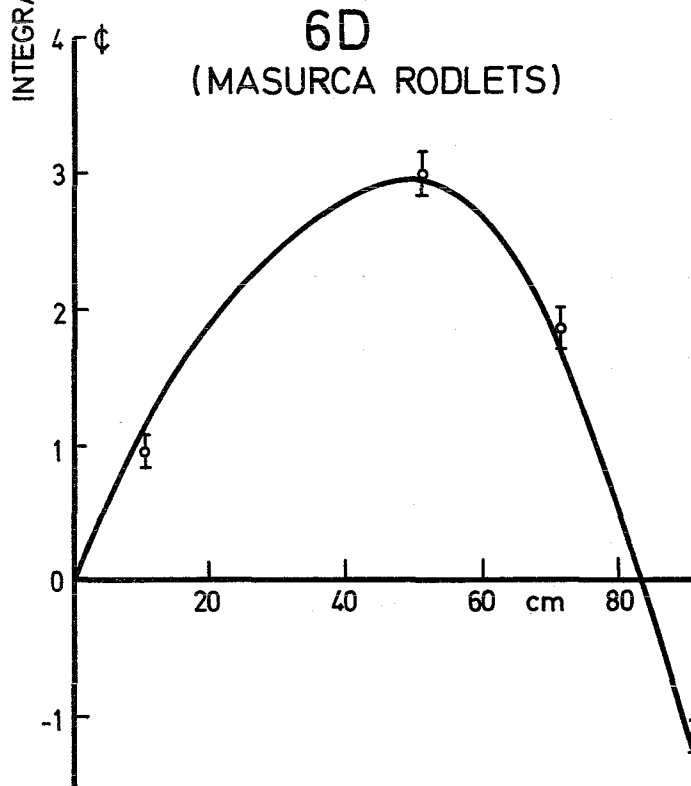
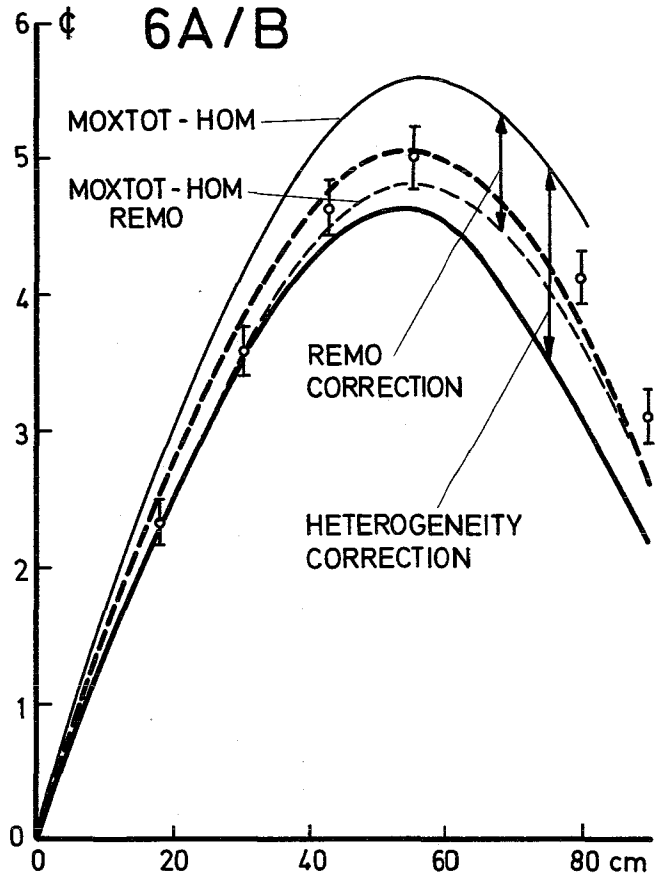
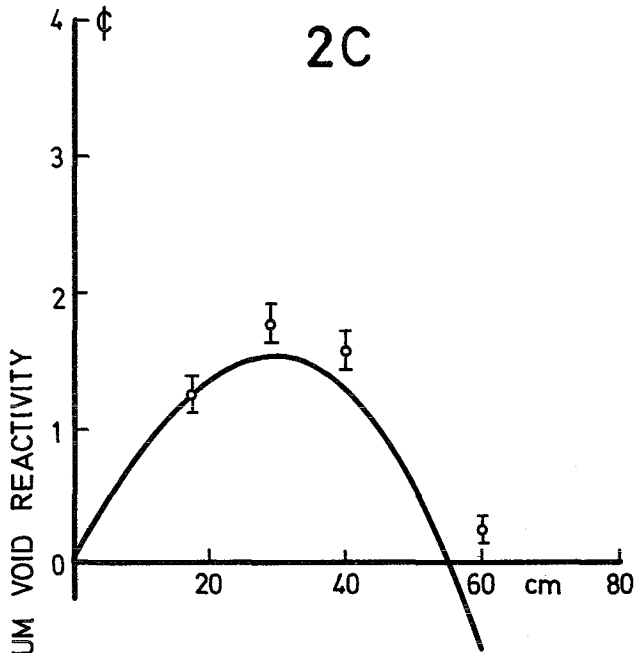
Table 5.15

Reactivity worths for cavities in SNEAK-6A ϵ

Step	Central position					Off center
	Transport 4 Groups	Diffusion		Perturbation 12 Groups	Experiment	Experiment
		4 Groups	12 Groups			
1				5.3	4.6	1.4
2				2.6	2.6	0.7
3				(-12.6)	-0.8	-1.1
4				(-36)	1.7	-1.9
Total	14.9	6.5	-1.2	(-40.7)	8.1	-0.9
Corrected theoretical result					<u>7.2</u>	

Fig. 5.14

Axial Na-void traverses



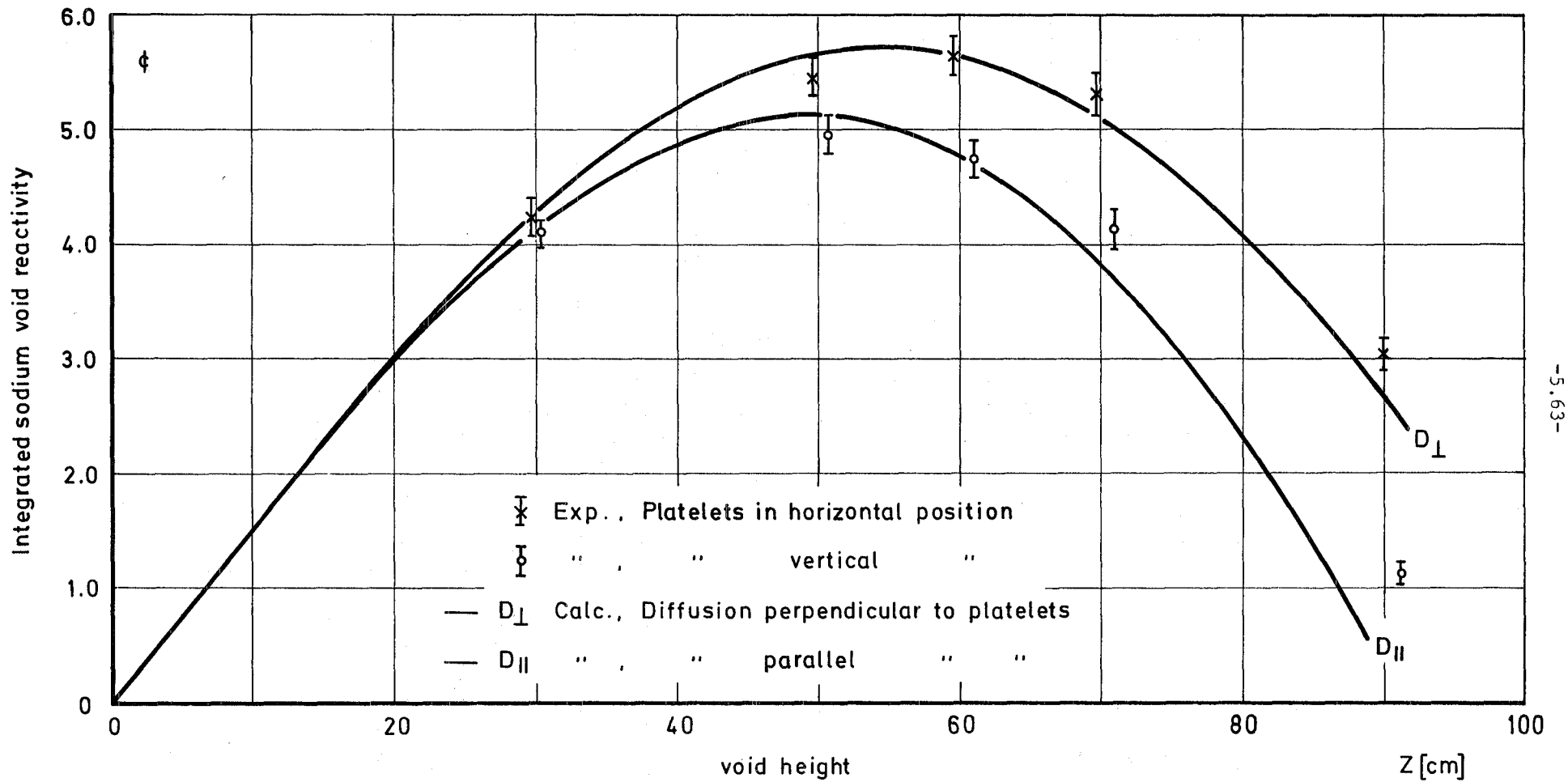


Fig. 5.15 Integrated axial sodium void reactivity effect for different platelet orientations, SNEAK-9B

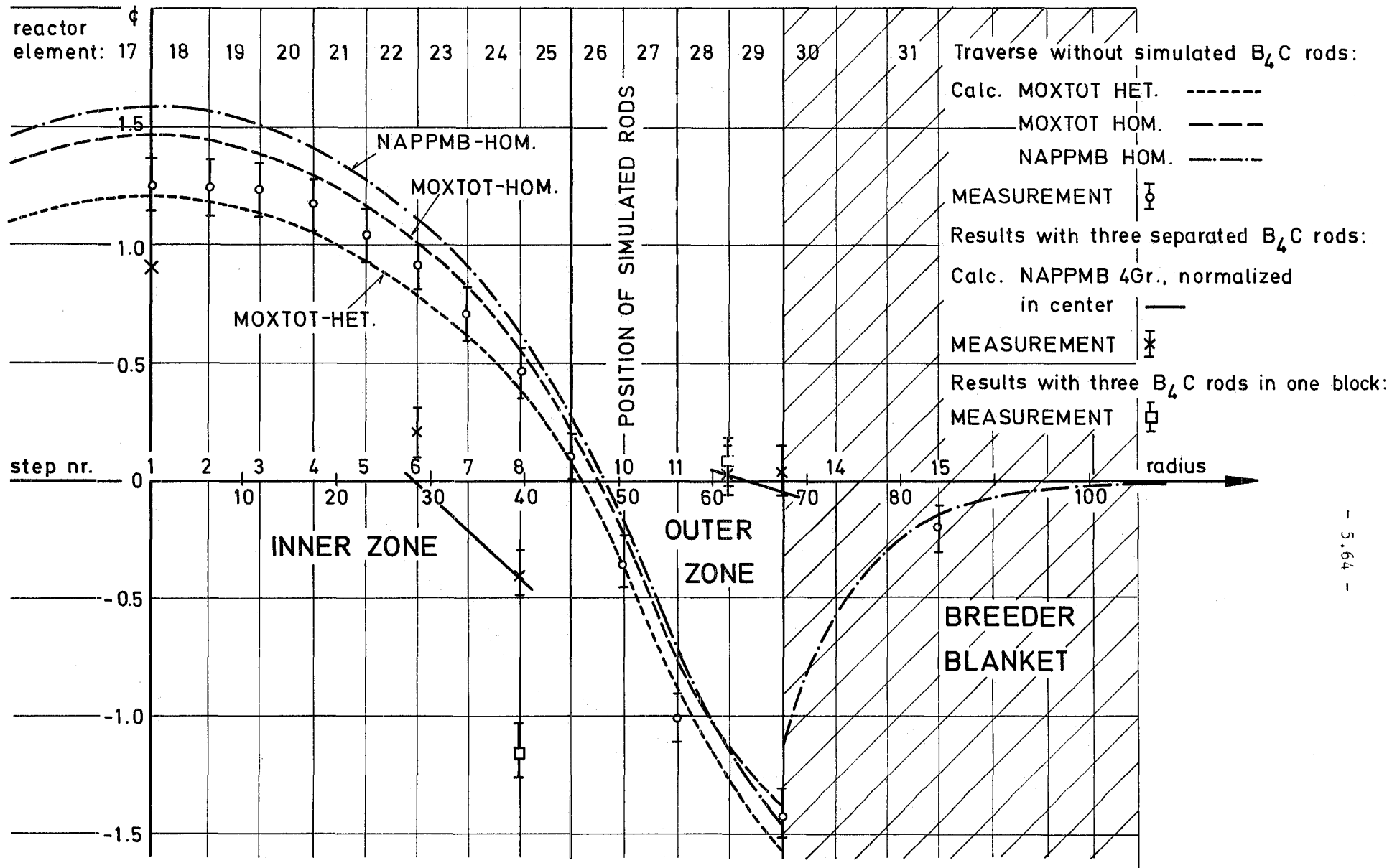
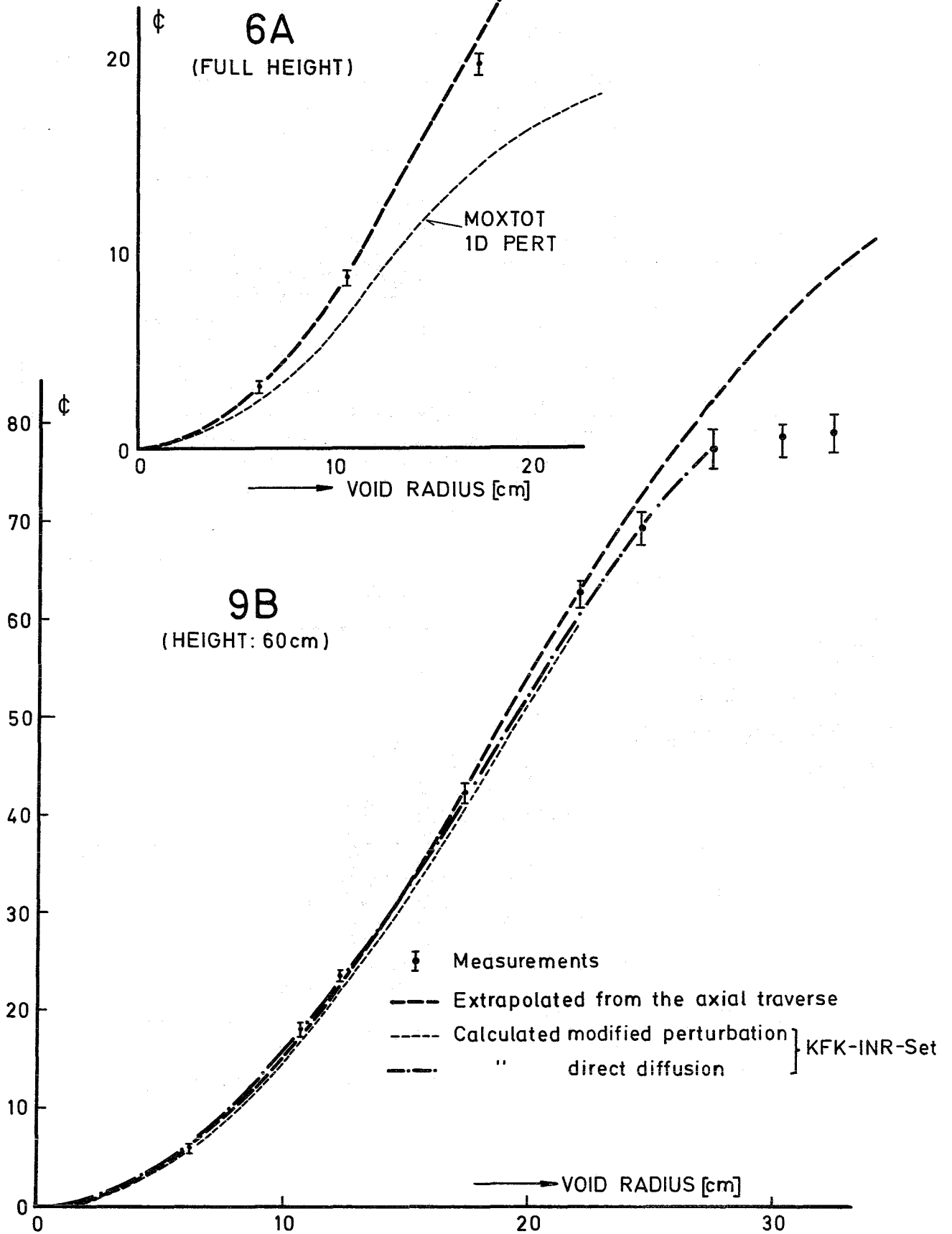


Fig. 5.16 Radial sodium void traverses in SNEAK-2C

Fig. 5.17 Reactivity effect of large voids

- 5.65 -



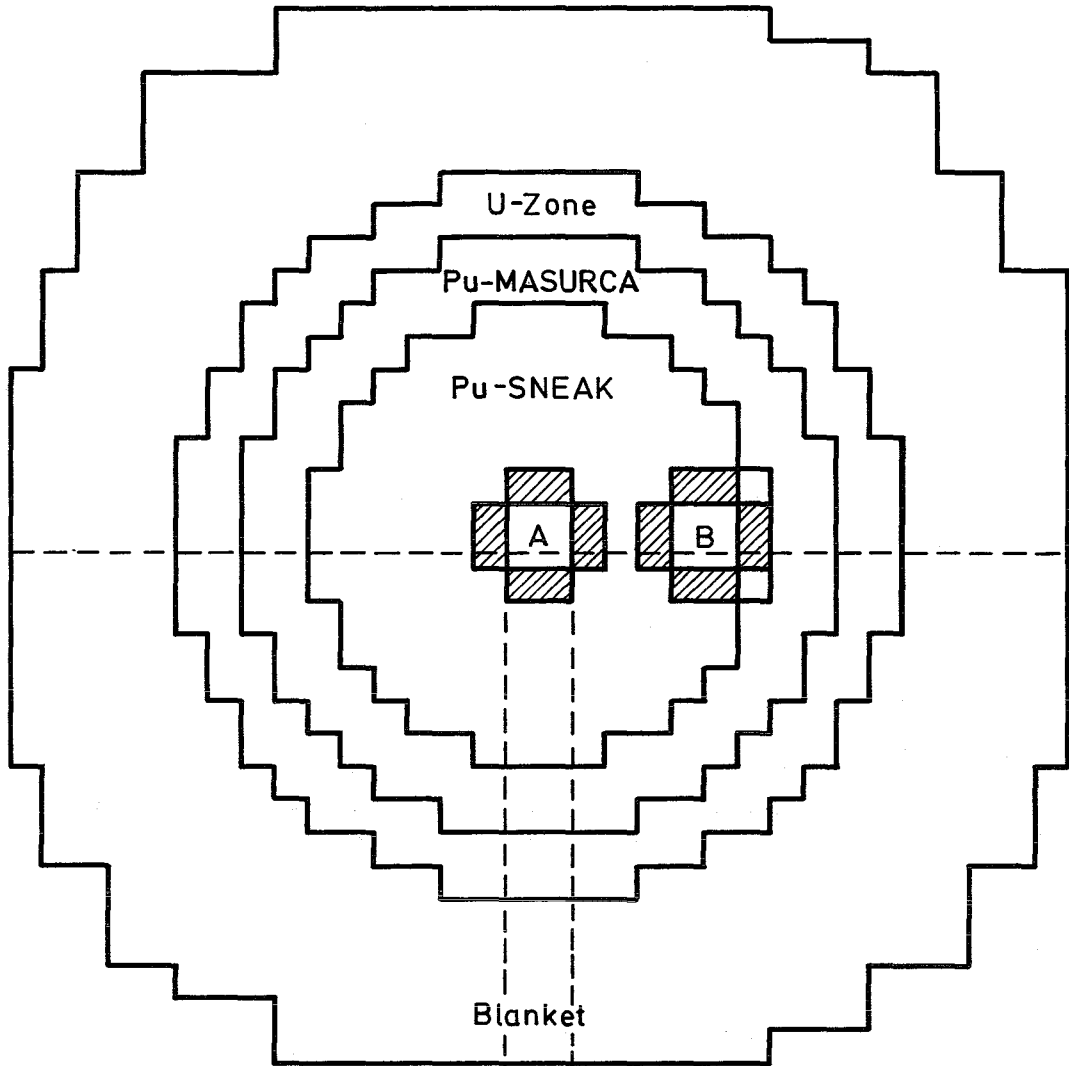


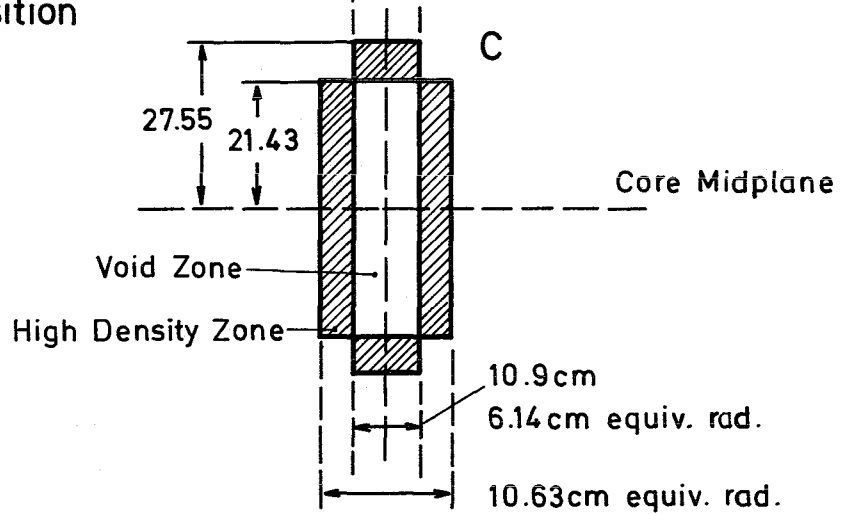
Fig. 5.18

SNEAK 6A cavities

A) Central position

B) Off-center position

C) Side view



5.8. Information from Supporting spectrum measurements

With regard to improve fast reactor design with the help of spectrum measurements, three types of system may be distinguished:

- 1) Mock-up oriented systems
- 2) Critical systems with simple composition
- 3) Flexible, one-material systems with simple geometry

To 1)

A lot of measurements have been done especially in the center of such systems /5.22/. Discrepancies between calculated and experimental spectra are generally small (< 10 %). The spectra are determined by a large number of different type cross sections from different materials and therefore it is practical impossible to assign any discrepancy to a certain cross section. SNEAK-6D /5.23/ is an example of this type. Fig. 5.19 shows the calculated and measured central spectrum.

To 2)

This type has the advantage that the spectrum is nearly space-independent over a quite large central region. On the other hand there is normally a heterogenous structure and one has besides structural materials at least two isotopes, namely ^{235}U and ^{238}U . SNEAK-8 /5.24/ is an example for this type. Calculated and measured central spectra are shown in Fig. 5.20

To 3)

The advantages of this type are: one isotope only, homogeneity and flexible geometry. Thus the size and geometry can be chosen to enhance the influence of the cross sections or methods (e.g. leakage) to be checked. Calculations performed for small spheres with an external source in the center demonstrate that the leakage spectrum and the time dependent spectra depend strongly on inelastic cross section data. On the other hand there arise some difficulties with such systems (for example external source, strongly space- and angular dependent spectra), the importance of which depends on the particular set-up.

Two systems have been investigated which correspond at least in some respects to this type. They are discussed in 5.8.1. and 5.8.2. The results gave rise to some modifications in the cross sections used in calculations. A discussion of this improved cross section set is given in 5.8.3.

5.8.1. Measurements in a depleted uranium system

Neutron spectrum measurements with proton recoil counters and a ^3He semiconductor sandwich spectrometer have been performed at several positions in a massive block of metallic uranium, which has been installed at the thermal column of the FR 2 research reactor. An outline of the experimental set-up and the dimensions of the block are presented in Fig. 5.21. It consists of a 15.2 cm thick natural uranium converter (cross section: 60.9x45.7 cm) and a second part of depleted uranium (0.4 % ^{235}U ; cross section: 81.3x81.3 cm; length 107.6 cm). The block has been directly surrounded by an iron and borated paraffin shield. The maximum attainable thermal flux at the front face of the block amounted to about 10^{10} n/cm² sec. With this it has been possible to measure the neutron spectrum with ^3He counters up to a position of 71 cm and with proton recoil counters up to 91 cm from the source face.

The neutron spectra have been computed using a 208 group cross section set based on the nuclear data file KEDAK and the one-dimensional transport code DTK /5.25/. To be sure that one-dimensional calculations adequately describe the neutron spectra at the axis of the block, we have also performed two-dimensional S_n -calculations with the transport code SNOW /5.26/. It turned out that at large distances from the source face (more than 50 cm) one-dimensional calculations even without buckling corrections give the same results as two-dimensional computations. Using space and energy dependent bucklings generated from the two-dimensional calculations, satisfactory agreement has been reached over the whole interesting region from 10-90 cm. It has also been shown that the energetic fine structure of the 208 group cross section set is sufficient for calculating the strongly space dependent spectra in the front part of the block. But it turned out that the group structure of the ABN set is too coarse. So, if one wants to use this group structure one has to generate several space dependent group cross sections, taking the appropriate weighting spectra from a 208 group calculation.

Starting from KEDAK 208 group constant set, S_n calculations have been carried out to study the sensitivity of spectra against changes of the

cross sections. Changing all relevant nuclear data within reasonable limits it was found that the spectra are extremely sensitive to changes of Σ_{capt} and Σ_{in} whereas all other data only weakly influence the spectra. During all these changes the total cross section has been kept constant. If therefore one cross section is changed, a second one has to be changed too by the same value but in opposite direction. The elastic scattering cross section has always been chosen for this. The anisotropy of the elastic scattering cross section has been normally taken into account by the transport approximation, which should be a good approximation for the extremely marked forward scattering of ^{238}U . However the effect of anisotropy of Σ_e has also been studied by using P_1 approximation. The difference between both calculations was negligible. Unfortunately it was not possible to investigate the influence of the anisotropy of the inelastic scattering cross section. But measurements of Σ_{in} have shown, that the degree of anisotropy of Σ_{in} is small at least for neutron energies below 2 MeV. Therefore we may expect, that the anisotropy of the inelastic scattering cross section cannot explain large differences between calculated and measured spectra. This has been confirmed by spectrum measurements in the central position of the k_{c} core SNEAK 8.

The measured spectra on the central axis at a position of 71 cm from the source are compared to the DTK prediction in Fig. 5.21. The KEDAK data underlying the computation are shown in Fig. 5.22. From our sensitivity studies we must conclude that the large discrepancies around 1.6 MeV and also between 25 and 60 keV (40 % and 70 % respectively) mainly result from the total inelastic scattering cross section, which is much too high between 0.8 and 2 MeV. If we introduce the reduced cross section of Fig. 5.22 for this energy region we get a much better agreement between theory and experiment in both the high and the low energy region. It is hard to explain the discrepancies around 1.6 MeV by an alternative cross section change for example by an enlargement of the low level (44.7 keV, 148 keV, 310 keV) excitation cross sections at the cost of the high level excitation cross sections. It has been shown that

massive changes of this kind only lead to moderate local changes of the spectra. Setting the 1.076 MeV level excitation cross section arbitrarily to zero and adding its values to the 44.7 keV level results in an enlargement of about 10 % in the spectrum between 1 MeV and 2 MeV. For the statistical inelastic scattering a Maxwellian distribution with a temperature $\theta(E) = \sqrt{\frac{E}{A \gamma}}$ is used on KEDAK, with $\gamma = 0.16 \text{ MeV}^{-1}$. Introducing a value of 0.099 MeV^{-1} calculated by Pitterle from a fit of experimental data /5.27/ enlarges the spectrum by at most 10 % around 1.4 MeV neutron energy. Therefore changing the inelastic scattering matrix alone can hardly explain the differences between experiment and theory. Only a reduction of the total inelastic scattering cross section also essentially reduces the spectrum in the low energy region. Accepting therefore the change of the total inelastic scattering cross section between 800 keV and 2 MeV as the most reasonable way to explain the discrepancies between theory and experiment in the high and low energy region we must further reduce Σ_{in} between 70 keV and 300 keV as shown in Fig. 5.22 and/or raise the excitation cross section for the 45 keV level at the cost of the 147 keV level in order to minimize the remaining discrepancies. As there are only measurements for the 147 keV excitation cross section above about 400 keV neutron energy both procedures can be justified. The strong slope of the ratio between theoretical and experimental spectra below 30 keV as shown in Fig. 5.21 below, indicates that the KEDAK capture cross section below this energy value is much too high. This conclusion has been confirmed by all late differential measurements /5.28/5.29/ and we have therefore considerably reduced the ²³⁸U capture cross section.

Finally, to get optimum agreement between experiment and theory, we have raised the capture cross section between 35 and 70 keV and the inelastic scattering cross section below 70 keV (Fig. 5.22). The enlargement of the capture cross section is in good agreement with the late differential measurements of Panitkin /5.28/ and Fricke et al. /5.29/. Alternatively to these changes we could have accepted the KEDAK inelastic scattering cross section and further increased the capture cross section, but then we would have been forced also to reduce the capture cross section

below 30 keV by another 10-15 %. Both manipulations are not in agreement with differential measurements, while the enlargement of the inelastic scattering cross section can well be justified as there are no measurements at all below 100 keV.

The ratio of the theoretical spectra calculated with the adjusted cross section and the measured spectra have also been drawn in Fig. 5.21. In Fig. 5.22 the adjusted cross section is also compared to the 26 group KFK INR set /5.30/ which recently has been deduced from criticality calculations of a number of different fast assemblies. The general trend of reducing the total inelastic scattering cross section has also been confirmed by this group constant set. Larger differences only appear between 800 keV and 2 MeV, but it should be mentioned that in this energy range the KFK INR set uses the old and surely out of date inelastic scattering matrix of the Russian ABN set, which has a similar effect on the spectrum as a reduction of the total inelastic scattering cross section.

The adjusted cross section of Fig. 5.22 also leads to a much better agreement between calculated and measured reaction rate ratios. The ratio $\sigma_f(^{235}\text{U})/\sigma_f(^{238}\text{U})$ which has been measured as 415 ± 20 at the same position as the spectrum in Fig. 5.21 has been calculated with the KEDAK data to 480, while the adjusted cross section gives 404. The experimental value for $\sigma_c(^{238}\text{U})/\sigma_f(^{235}\text{U})$ at this position is 0.145 ± 0.007 while the KEDAK and the recommended cross section values are 0.159 and 0.152 respectively.

5.8.2. Small natural uranium assembly "UNAT"

Calculational investigations demonstrated /5.31/ that the leakage spectrum and time dependent leakage spectra of small homogeneous assemblies with an extraneous 14 MeV-neutron source in the assembly, strongly depend on inelastic cross section data. The accuracy of $\sigma(n,n')$ data and the spectrum of the inelastic scattered neutron of fissile isotopes, structural material and sodium is poor, and these data have an appreciable influence on the accuracy of fast breeder calculations /5.30/.

Recently an experiment was started to measure the leakage spectrum and time dependent leakage spectra of small, homogeneous stacks of one material only. To demonstrate the feasibility and use of such spectrum measurements a parallelepiped of natural uranium "UNAT" was investigated first. The "UNAT" system is briefly described in section 4.2.4. The leakage spectrum of one face of the parallelepiped was measured by time-of-flight, by proportional counters and by NE 213 liquid scintillator. The measured leakage spectra are illustrated in Fig. 5.23, 5.24, 4.10. The measured and calculated spectra are normalized to equal total fluxes in the energy range from 10 keV to 10 MeV.

Erroneous cross sections have an enhanced influence on the spectrum of one-isotope-homogeneous systems, but to take advantage of this, the spectrum calculation must be performed in unusual detail. The leakage spectrum depends on many variables: energy, space, angle, time and from the spectrum of the extraneous source. None of the available codes describes the system in every variable. Therefore two calculations have been performed, describing the system within different approximations. A S_8 -calculation with the DTK-code gives the time-independent vector flux in 208 -energy groups of approximately $\Delta u = 0.15$ from 10 MeV down to thermal energies. The assembly is assumed to be spherical with a mono-energetic neutron source of 10 MeV neutron at the center. The KARCOS- 208 -group cross section set was used /5.32/, which relies on the KEDAK-file. The comparison of measured and Sn-calculated spectra illustrates discrepancies of 30 % at about 2 MeV and 600 keV (see Fig. 5.23). A second calculation was performed with the Karlsruhe Monte-Carlo-code KAMCCO (see 3.2.3.) The 14 MeV neutron source at the center is correctly taken into account. The geometry is described in detail, but the target-hole is neglected. The code uses the NCMONTEA /5.34/ cross section set relying on the KEDAK-library and (n,2n) reactions are included as well. The calculation gives the time-dependent scalar-leakage-spectrum for instance in 13 energy groups of $\Delta u = 0.38$ and time intervals of about 6ns each. A KAMCCO-calculation of a time-independent leakage spectrum, obtained by integration of all time-spectra up to 200 ns, is illustrated in Fig. 5.24. The Sn- and Monte Carlo calculations agree rather well and both disagree with the measured spectrum, thus confirming suspicious cross section data. The size of these discrepancies exceeds the accuracy of measured spectra

(5-10%), and are to be explained by erroneous cross section data.

Preliminary parametric investigations with trial-cross-section data for $\sigma(n,n')$ of ^{238}U indicate that the KEDAK-values at about 2 MeV ought to be reduced by 20 to 30 % to get close agreement between measured and calculated spectra. These conclusions are qualitatively consistent with the recommended cross section corrections deduced from the exponential pile experiment. (Section 5.8.1). To claim quantitative correction factors the calculation and experimental procedure will be improved.

The particular sensitivity of time-dependent leakage spectra to changes in inelastic cross-section data initiated their experimental investigation. Time-dependent leakage spectra were measured by two-dimensional analysis of pulse height and time of a NE213 liquid scintillator located at the center of one face of the "UNAT" assembly. After the injection of a 2 ns burst of 14 MeV neutrons the detector events are analyzed in 8 time channels of approximately 6 ns each and 2-times 512 pulse height channels. Measured and calculated spectra are illustrated in Fig.5.25. A quantitative analysis of the large discrepancies is in progress and this measuring technique indicates promising possibilities to get better insight into $\sigma(n,n')$ data and in particular to check the spectra of inelastically scattered neutrons.

5.8.3. Applications of the adjusted ^{238}U cross section set

The adjusted ^{238}U cross section set has been used to recalculate the reliable natural uranium exponential experiments formerly carried out by Chezem /5.35/ and Campan et al. /5.36/ as well as spectra of some fast assemblies where proton recoil and ^3He spectrum measurements have been done. Tab.5.16 compares the fission rate ratios measured in the natural uranium blocks with the KEDAK and the adjusted cross section predictions. It can be stated that the general agreement is much better with the adjusted than with the KEDAK cross section and

that it is fully satisfactory with the experimental values of Chezem.

In Fig. 5.26 we have compared the measured spectra shown in Fig. 5.19, 5.20 and Fig. 4.11 with the calculated spectra using the KEDAK and recommended ^{238}U cross section. It can be seen from the ratios that we have reached an improved agreement between experiment and theory for all assemblies, but the degree of improvement naturally depends on the sensitivity of the spectra against ^{238}U capture and inelastic scattering cross section changes, being largest for SNEAK 8 and smallest for SNEAK 6D. The ratio between theory and experiment for SNEAK 8, a uranium core with a unit k_{∞} test zone shows qualitatively the same behaviour as the ratio plotted in Fig. 5.21. As anisotropic scattering is of no importance for the conditions at the center of SNEAK 8, our statement that the size of the total inelastic scattering cross section is the most reasonable explanation for the large discrepancies around 1.6 MeV is confirmed. Although the discrepancies between 30 keV and 80 keV have been appreciably reduced there remains a further difference which cannot be explained by experimental errors. Therefore it is supposed, that these discrepancies result from cross sections of other materials like ^{235}U , Ni and Fe also contained in SNEAK 8. This again demonstrates the disadvantage of critical systems with "simple" composition, as has been discussed in section 5.8. Using the adjusted ^{238}U cross section for the calculation of the secondary standard $\Sigma\Sigma$ at Mol also leads to a much better agreement between theoretical and experimental spectra, especially between 900 keV and 2 MeV. As in SNEAK 8 there are involved some structural materials (Al, B₄C) which have a rather large influence on the spectrum particularly at low energies where elastic scattering becomes the dominating moderation process. Finally SNEAK 6D demonstrates the insensibility of mock-up oriented systems against cross section changes of one material. The broad group ratios - dotted curves - in Fig. 5.26 show an agreement between experiment and theory within the experimental errors. It should be remarked that the group ratios

TABLE-5.16 Fission rate ratios in natural uranium blocks

Ratio	Experiment		Theory	
	Chezem	Campan et al.	KEDAK	Adj. Cross Sec.
$\sigma_f(U^{235})$	238 ± 6 foil act. 240 ± 12 radiochem.	230±10 fission chamber	. 293	.251
$\sigma_f(U^{238})$	243 ± 15 fiss.chamb. I 241 ± 13 " II			

TABLE-5.17 Comparision of k_{eff} -values

Assembly	$k_{eff,calc.}$ (KFKINRset) $-k_{eff,exp.}$	$\Delta k = k_{eff,INR} - k_{eff,adj.}$		
		I _a $\sigma_{inel,adj.}$ 0.1 MeV ≤ E ≤ 6.5 MeV	I _b $\sigma_{inel,adj.}$ 0.1 MeV ≤ E ≤ 2.5 MeV	II replacement of ABN by KEDAK-Matrix
SUAK U1B	-0.008	-0.0012	-0.0004	+0.0056
SUAK UH1B	-0.020	-0.0009	-0.0019	+0.0037
ZPR III-10	+0.001	-0.0015	+0.0004	+0.0045
ZPR III-25	±0.	-0.0035	+0.0016	0.0011
ZPR III-55	+0.011	-0.0011	+0.0028	-0.0041
ZEBRA-8H	-0.005	-0.0058	+0.0015	-0.0094
ZPR IX-25	-0.005	-0.0051	+0.0014	-0.0088
SNEAK-6A-Z1	+0.007	-0.0004	+0.0004	-0.0013
SNEAK-7B	+0.012	-0.0013	+0.0007	-0.0024

show large oscillations in the neighbourhood of resonances, especially when the experimental resolution is of the order of magnitude or worse than the resolution of the computation.

The criticality changes relative to the KFK INR set values have been calculated by Kiefhaber / 5.37 / using the recommended total inelastic scattering cross section of Fig.5.22. The results have been summarized in Table 5.17

Although there are some further small differences for the capture and total inelastic scattering cross section below 100 keV between the KFK INR set and the adjusted cross section of Fig.5.22 the Δk values of Table 5.15 can be regarded as representative for the differences between both cross section sets. The Δk values of column II, resulting from the physically reasonable replacement of the ABN-Matrix by the KEDAK-Matrix is only for some systems partly compensated by the lower adjusted inelastic scattering cross section (column Ia). Particularly for the assemblies ZEBRA 8 H and ZPR IX-25 where both changes go into the same direction we get a calculated value for k_{eff} which is about 2 % too low. For the assemblies SUAK U1B, ZPR III-55 and SNEAK-7B however we get a somewhat better agreement than with the KFK INR set.

5.8.4 Spectrum investigations in the fast thermal facility STARK

As has been outlined earlier in this section, spectrum measurements are able to support the check of methods and data, if assemblies are investigated, which differ significantly in the content of one material. In STARK-7A- and 7C /5.38 / two experiments have been performed to check the influence of the calculational procedure on the neutron spectrum near 0.442 MeV oxygen resonance and consequently on fission rate ratios, especially of isotopes with a fission threshold. The main difference in composition in both assemblies is the oxygen content, with STARK-7C containing no oxygen at all. This was obtained by using low density Al-platelets instead of Al_2O_3 platelets.

The emphasis of the investigation was put on the influence of the weighting spectrum to be used for the preparation of broad 26-group constants in the range of the oxygen resonance.

The theoretical treatment was based on a preliminary version of the already described KFK INR-Set, which is named here SET 1. The difference in the underlying basic nuclear data compared to the KFK INR-Set are unimportant for this comparison, however, SET 1 contains a smooth weighting spectrum within the oxygen resonance, while the KFK INR-Set is based on a weighting spectrum, which was obtained by a 208 fine group calculation for the inner zone of the German SNR-prototype reactor. SET 1 should then give from this point of view more consistent results for the STARK-7C assembly without oxygen. In another SET 2 a 208 group calculation was performed for the fast zone of STARK-7A, and the resulting fine group spectrum was used to modify appropriately 26 group condensed elastic removal cross sections of SET 1.

The comparison of the calculations with experiment are shown for the fission rate ratios in Table 5.16 The results, obtained with the final version of the KFK INR-Set, are also listed.

Following conclusions can be drawn from Table 5.16

1. With SET 1 the fission rate ratios for the oxygen free core 7C are much better represented than those for 7A.

2. There is a considerable improvement for 7A, if the appropriate weighting is used in SET 2. Because in this case from the point of view of within broad group weighting the treatment is accurate, the remaining differences are probably due to data uncertainties. Thus every theoretical result should be measured against the data obtained for 7A with SET 2. The KFK INR-Set with the fine structure weighting function due to SNR gives fairly good agreement for STARK-7A, but for 7C the disagreement becomes larger than with SET 1 which has the more appropriate weighting spectrum.

So it can be seen that for a good **interpretation** of the fission rate ratios primarily the appropriate shape of the neutron spectrum is required and particularly the fine structure in the broad resonances of medium weight nuclei has to be taken into account properly.

TABLE 5.18

Comparison of experimental and calculated fission rate ratios for STARK 7A + 7C:

Material	Experiment $\sigma_f/\gamma\sigma_f$		C/E for SET 1		C/E for SET 2		C/E for KFK INR	
	7 A	7 C	7 A	7 C	7A	7 C	7 A	7 C
$^{234}\text{U}/^{235}\text{U}$	0.205 ± 0.004	0.240 ± 0.004	0.941	0.999	1.015	1.030	1.08	1.075
$^{236}\text{U}/^{235}\text{U}$	0.0708 ± 0.0015	0.0818 ± 0.0015	0.958	0.976	1.004	1.004	1.028	1.039
$^{238}\text{U}/^{235}\text{U}$	0.0321 ± 0.0005	0.0362 ± 0.0005	0.988	0.994	1.016	1.013	1.030	1.036
$^{235}\text{Pu}/^{235}\text{U}$	0.986 ± 0.02	-	0.968	-	0.977	-	0.986	-
$^{240}\text{Pu}/^{235}\text{U}$	0.250 ± 0.008	0.287 ± 0.008	0.874	0.911	0.928	0.936	0.968	0.998
$^{241}\text{Pu}/^{235}\text{U}$	1.350 ± 0.025	-	0.979	-	0.977	-	0.981	-
$^{240}\text{Pu}/^{241}\text{Pu}$	0.185 ± 0.006	0.212 ± 0.006	0.895	0.931	0.950	0.957	0.988	1.016
$^{240}\text{Pu}/^{238}\text{U}$	7.79 ± 0.25	7.93 ± 0.25	0.885	0.916	0.912	0.923	0.940	0.963
$^{236}\text{U}/^{238}\text{U}$	2.21 ± 0.05	2.26 ± 0.05	0.970	0.981	0.988	0.990	0.996	1.013

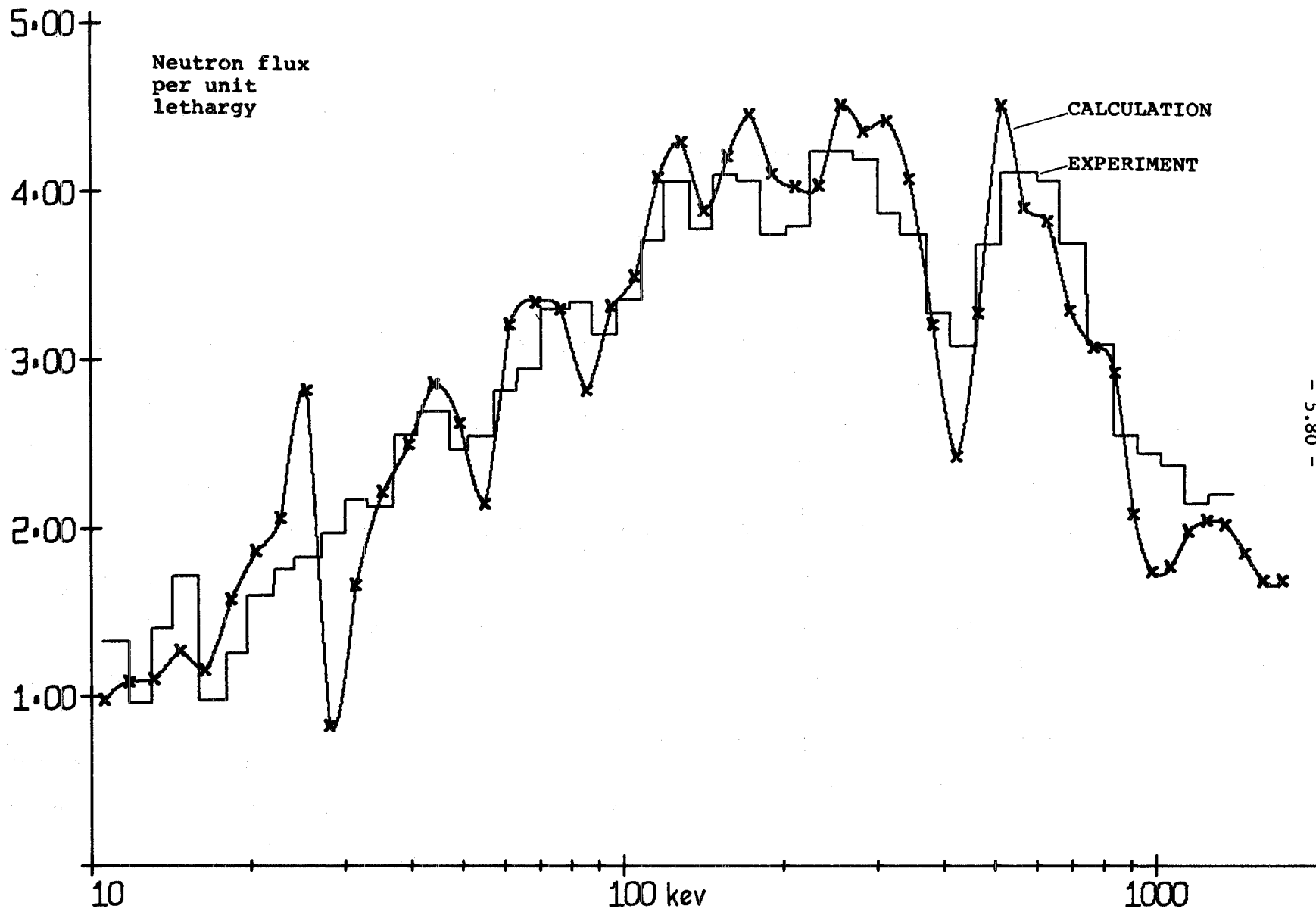


FIG. 5.19 MEASURED AND CALCULATED SPECTRA IN THE CENTER OF SNEAK 60

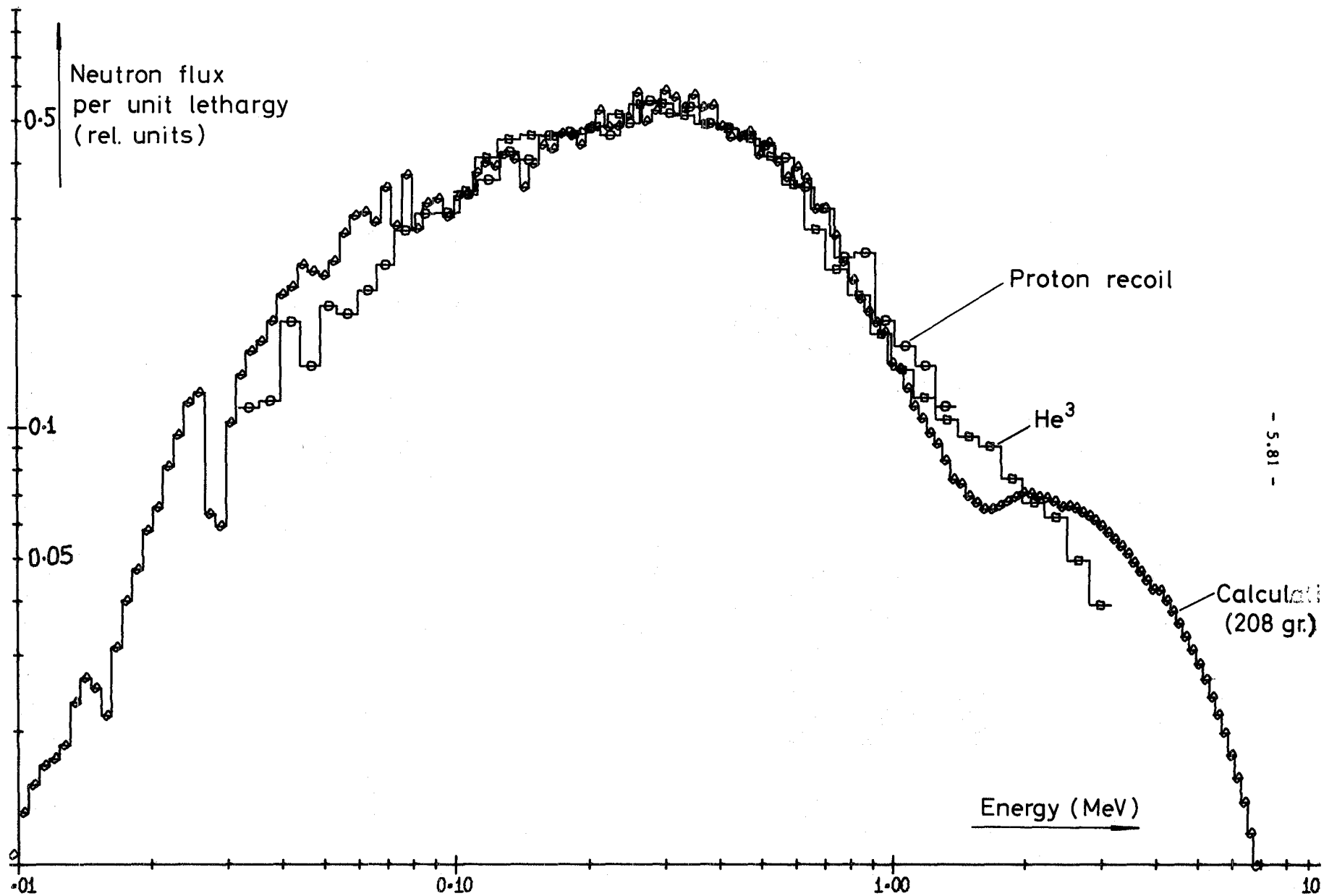


FIG. 5.20 MEASURED AND CALCULATED SPECTRA IN THE CENTER OF SNEAK 8

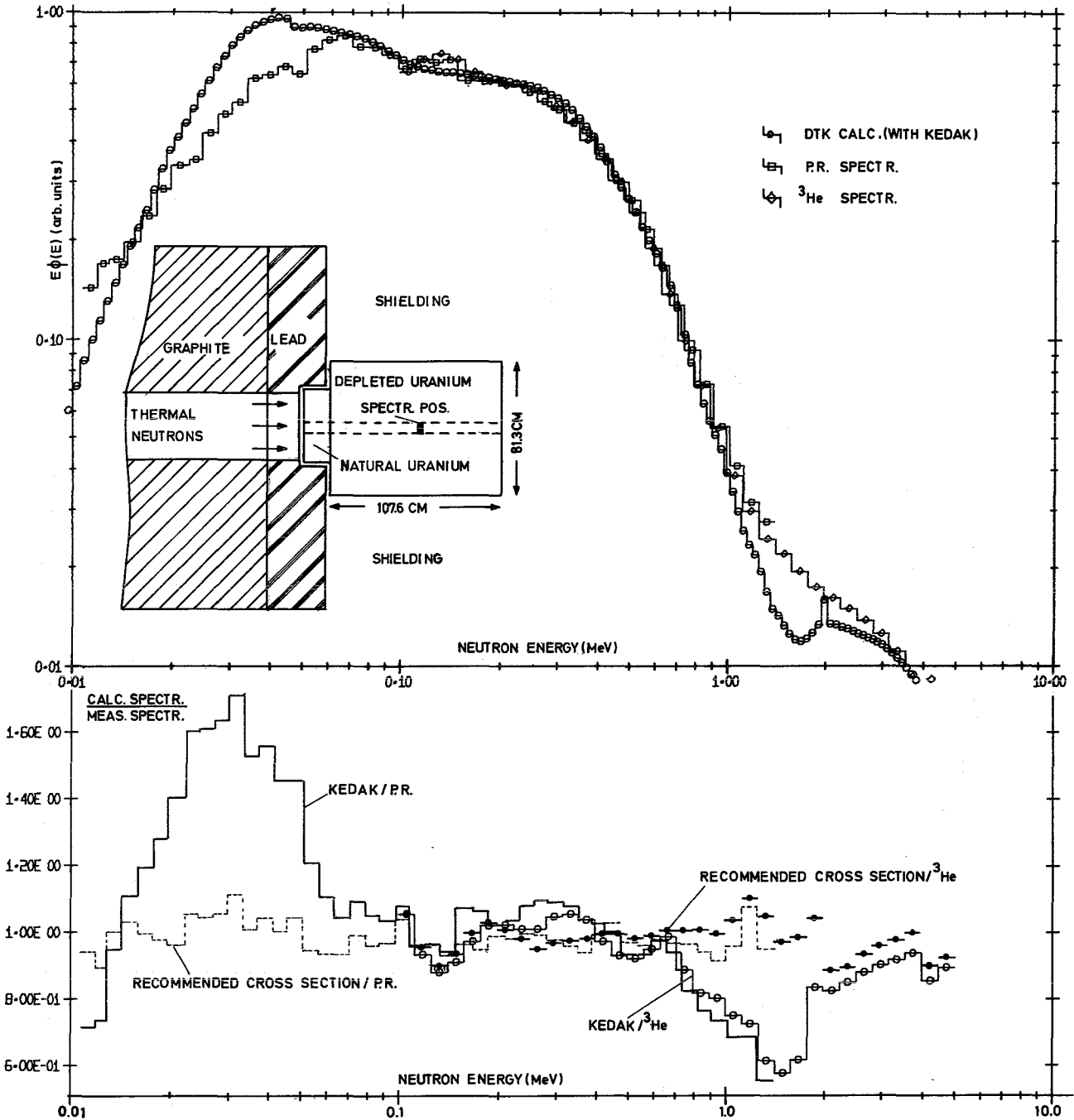


FIG. 5.21 SET-UP OF DEPLETED URANIUM PILE AND COMPARISON OF MEASURED AND CALCULATED SPECTRA

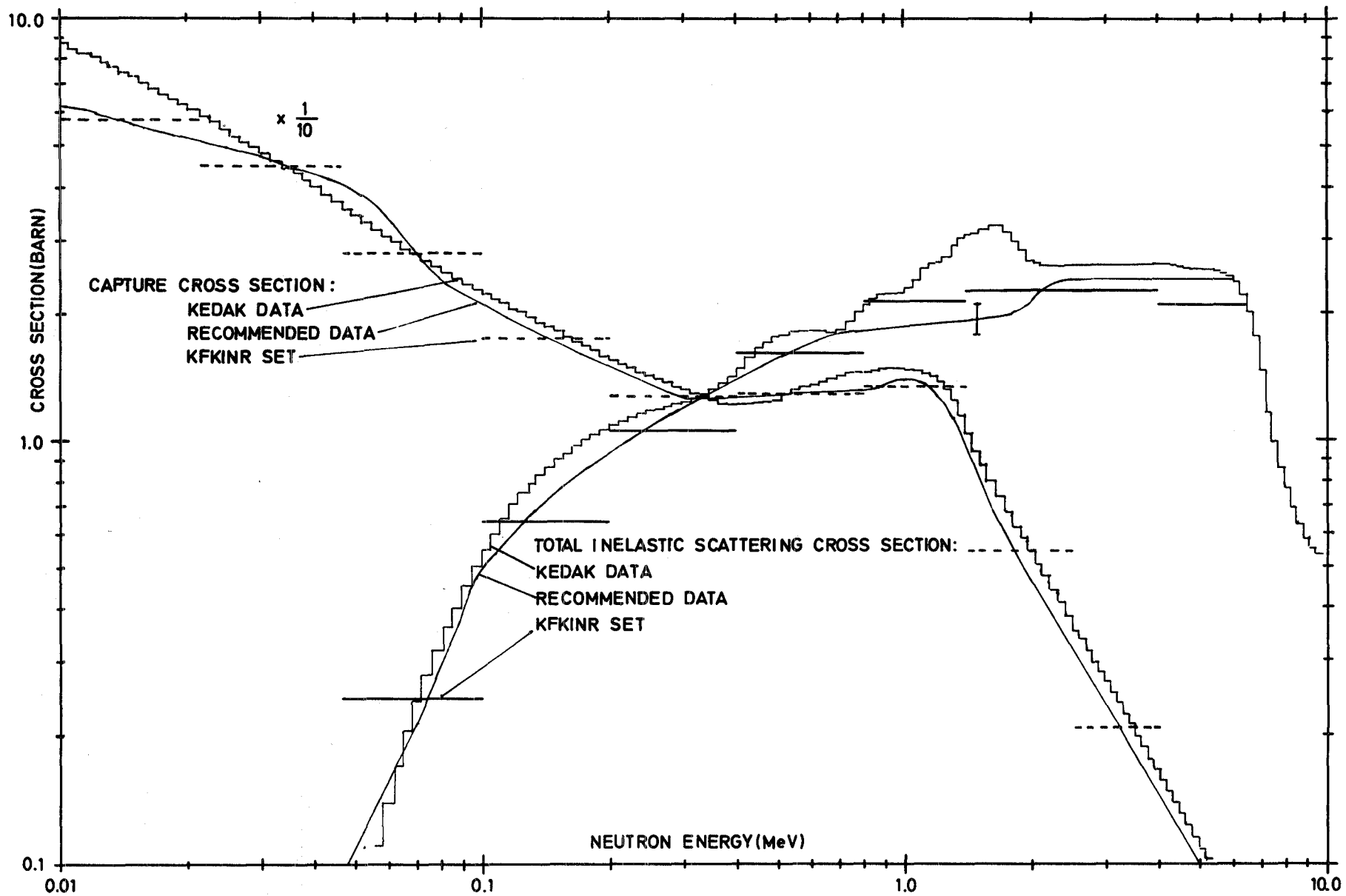
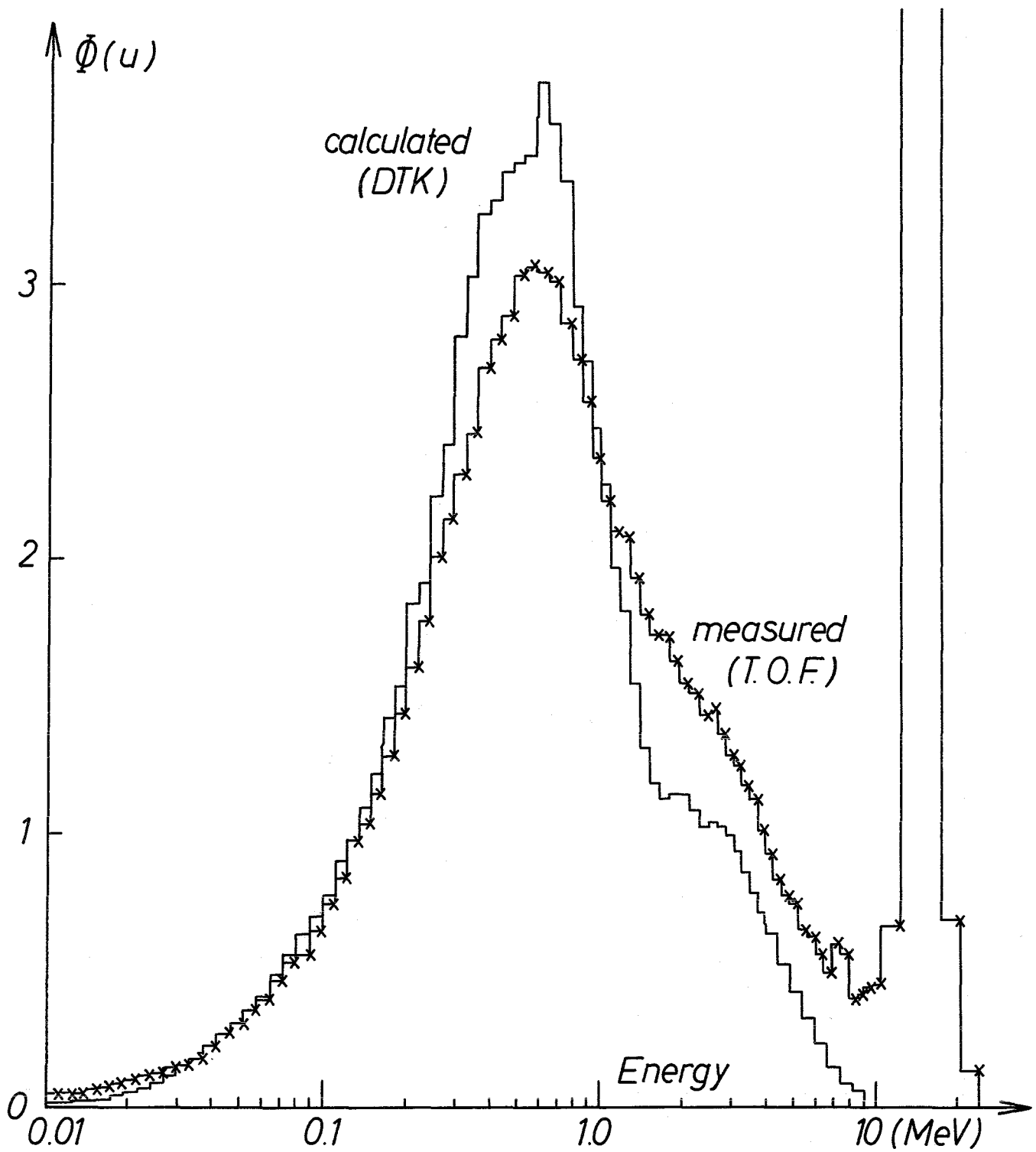


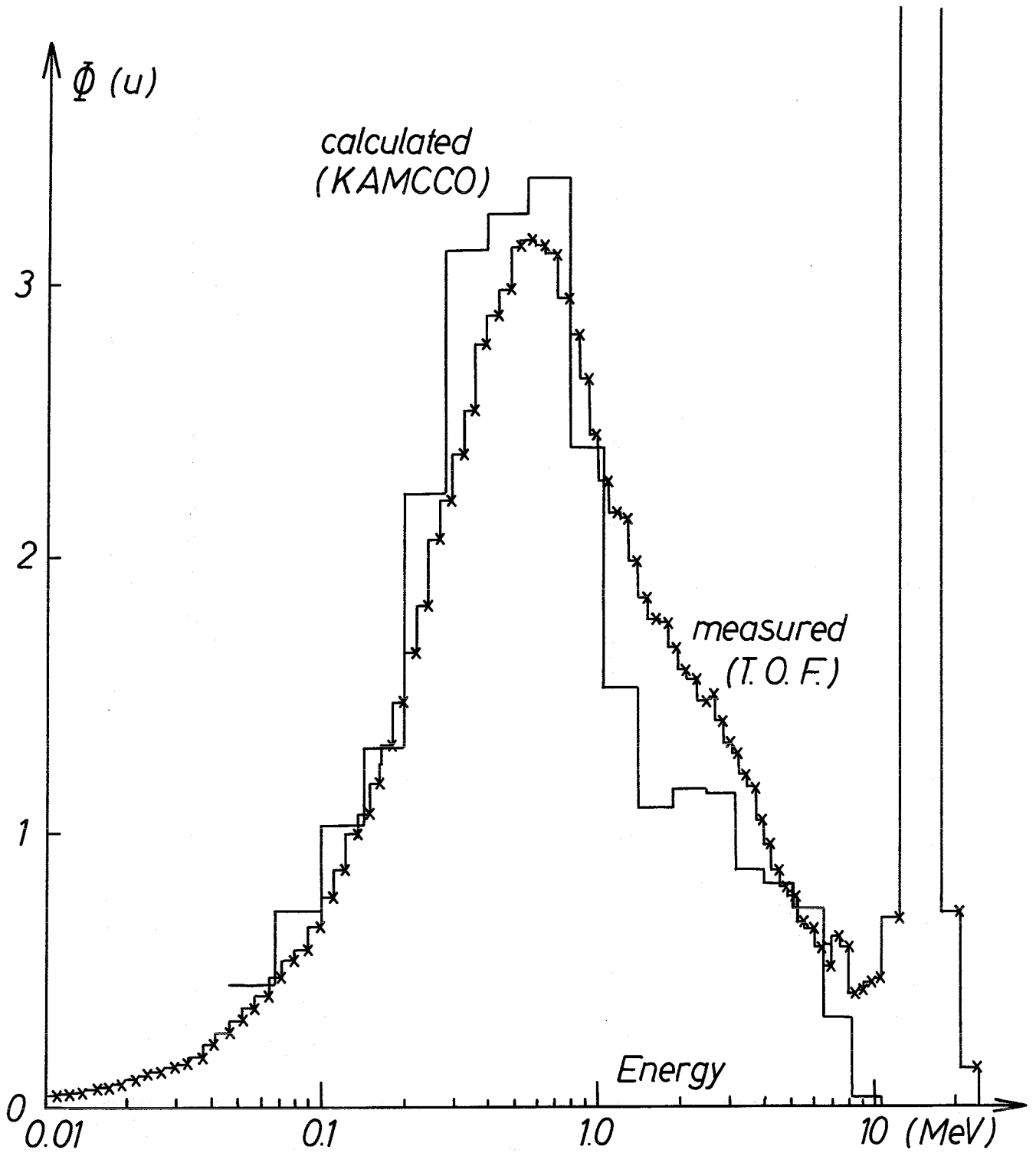
FIG. 5.22 URANIUM-238 CROSS SECTIONS



x measured spectrum by time-of-flight

┌ calculated spectrum by DTK - S8 -
normalized to equal total fluxes between 10KeV and 10MeV

Fig.5.23 Leakage spectrum of "UNAT" assembly



x measured spectrum by time -of - flight

┌ calculated spectrum by Monte-Carlo KAMCCO-code
└ normalized to equal total fluxes between 46.5 KeV and 6.5 MeV

Fig.5.24 Leakage spectrum of "UNAT" assembly

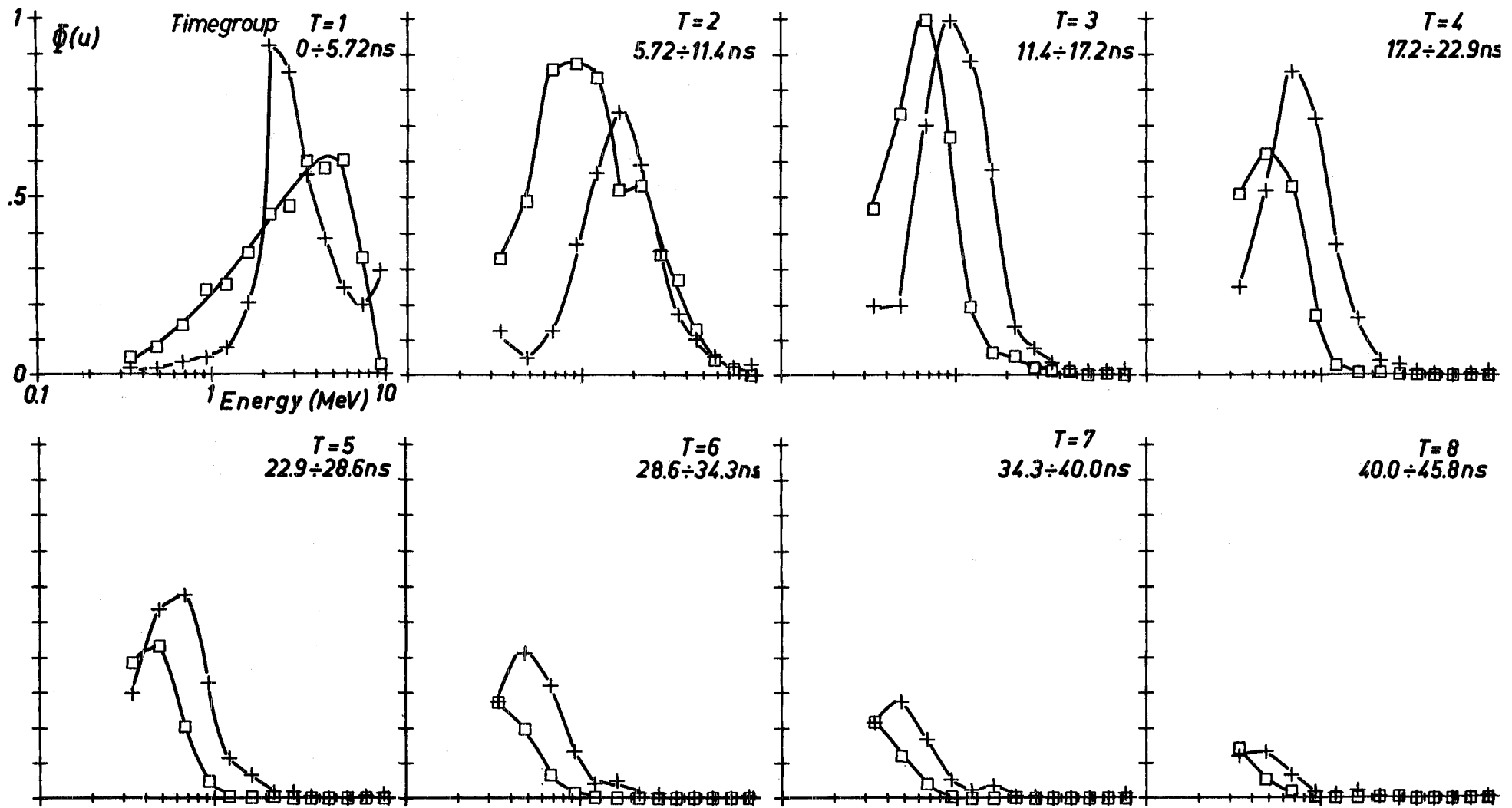


Fig.5.25 Time - dependent leakage spectra of "UNAT"

+ Measured by NE 213 - scintillator

□ Calculated by Monte - Carlo code KAMCCO

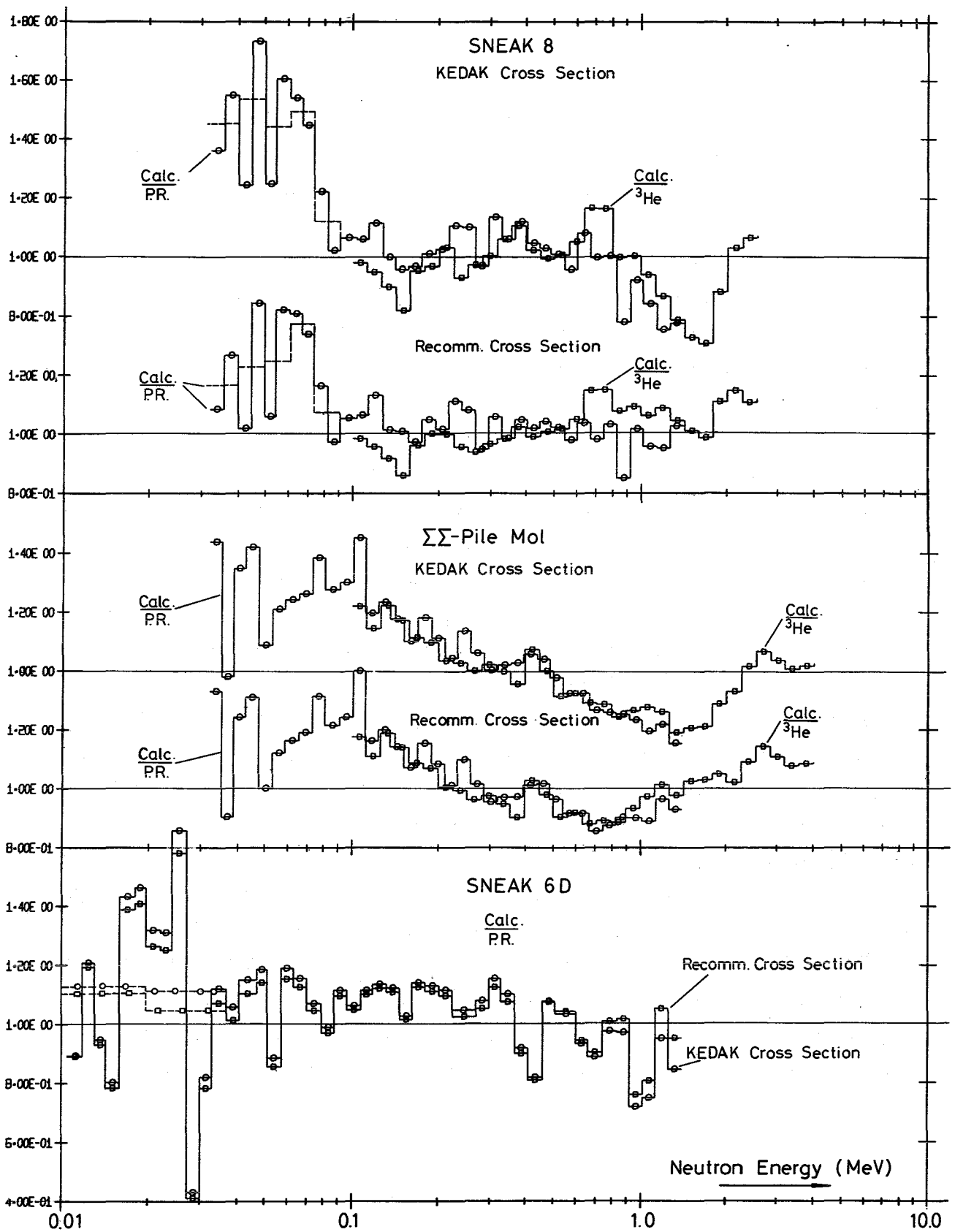


FIG. 5.26 COMPARISON OF MEASURED SPECTRA WITH CALCULATIONS USING THE KEDAK AND THE ADJUSTED U-238 CROSS SECTION SET

5.9. Measurement of prompt fission-neutron spectra

Recent studies of the thermal-neutron induced fission of ^{235}U and ^{239}Pu with activation detectors / 5.39 / indicate that 1) the average energy of ^{235}U fission neutrons is about 10 % higher and 2) the average energy of the ^{239}Pu fission neutrons is remarkable closer to that of the ^{235}U fission neutrons than previously deduced from differential spectrum measurements / 5.40 / These differences have noticeable influence on some important fast reactor parameters / 5.41 /. Therefore the fission neutron spectra of ^{235}U and ^{239}Pu have been remeasured using two independent methods, proton recoil proportional counters and the ^3He -semiconductor-sandwich-spectrometer with γ -n-discrimination / 5.42 /.

The measured spectra are shown in Fig. 5.27. Above 600 keV the spectra measured with both techniques agree rather well. The quite large discrepancies below 500 keV are mainly due to the large amount of wall-scattered neutrons which affects both methods in a different way.

The measured spectra have been fitted by a Maxwellian distribution $\chi(E) \sim \sqrt{E} \cdot e^{-E/T}$ ($T=E_M/1.5$). In a large part of the measured energy range the experimental spectra are quite well represented by Maxwellian distributions. Only above 6 MeV the measured spectra lie generally below the Maxwellian distribution. In Table 5.19 the Maxwellian energies E_M and their ratios deduced from the present measurements are compared with averages over a series of differential measurements / 5.40 / and with activation detector results / 5.39 /. The Maxwellian energies of the present investigation agree within 2 % with the differential average, whereas the 10 % discrepancy with the ^{235}U activation detector value is definitely larger than our experimental error (5 %). On the other hand for the $^{239}\text{Pu}/^{235}\text{U}$ ratio of Maxwellian energies the present results are not conclusive. Whereas the ^3He -ratio favours the low activation detector value, the proton recoil result confirm the differential average.

Table-5.19 Comparison of Maxwellian energies for fission-neutron spectrum

Isotope	Maxw. energy E_M (MeV)			Ratios		
	^{235}U	^{239}Pu	^{252}Cf	$\frac{^{239}\text{Pu}}{^{235}\text{U}}$	$\frac{^{252}\text{Cf}}{^{235}\text{U}}$	
Present investi- gation	Proton recoil	1.956	2.136	2.155	1.092	1.102
	^3He -spectr.	2.020	2.075	2.130	1.028	1.054
Differenttial average	1.979	2.084	2.189	1.084		
Activation detectors	2.20			1.039		

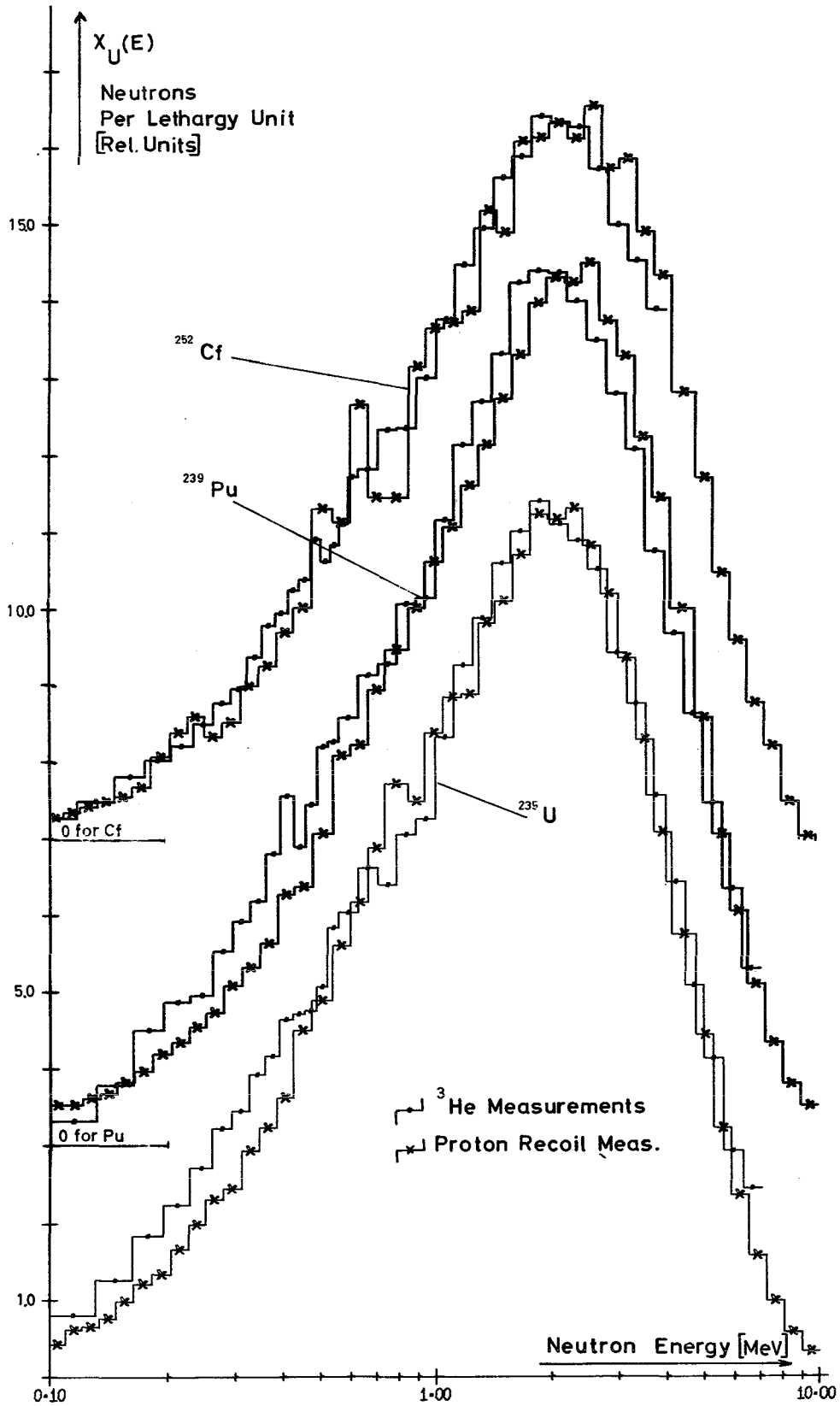


FIG. 5.27 PROMT FISSION-NEUTRON SPECTRA OF U-235, PU-239 AND CF-252

5.10. Measurement of delayed fission-neutron spectra

The delayed fission neutron spectra of ^{235}U , ^{238}U and ^{239}Pu were measured. 14 MeV neutrons and for ^{235}U , also thermal neutrons were used to induce fission. The conventional method of periodic irradiation of the sample was used. The irradiation was done with a 400 KV (d,t)-neutron generator. To induce fission by thermal neutrons both the 14 MeV neutron source and the sample were located inside of a polyethylene sphere ($\phi = 30$ cm).

The energy distribution of the delayed neutrons was determined with proton-recoil proportional counters. The counters were filled with various pressures of hydrogen and methane. The proton recoil distribution was evaluated by the method of BENJAMIN /5.43/. Below 200 keV the BENNETT- γ -n-discrimination method /5.44/ was applied.

From measurements with different irradiation and counting time intervals the spectra of the various half-live groups were extracted by the Gaussian iteration method. The systematic error of the isolated group spectra lies between 15 - 20 %.

The results of ^{235}U (thermal fission), Fig.5.28, agree for all groups within the error limits with the BATCHELOR-HYDER data /5.45/. Also the resonance structure is similar in both measurements.

As is seen from Fig.5.29 for ^{235}U the spectra are very similar for thermal and fast fission. This indicates that in both cases the same precursors are responsible for the different neutron groups.

In Table 5.20 the average neutron energies of the group and steady-state spectra are given for the isotopes investigated. In general the mean values for the corresponding spectra are within the error limits equal for different isotopes.

TABLE 5.20 Mean energies of group and steady-state spectra, relative error of the values $\pm 10\%$

Measurement	Mean Energies (keV)					Steady-State Spectra
	group 1	2	3	4	5	
U-235 (therm.)	277	484	447	432	-	435
U-235 (14 MeV)	286	458	432	480	-	451
U-238 (14 MeV)	278	468	443	425	382	445
Pu-239 (14 MeV)	296	481	411	430	-	425
BATCHELOR /5.45/ (U-235, therm.)	250 \pm 20	460 \pm 10	405 \pm 20	450 \pm 20	-	430
BURGY /5.46/ (U-235, therm.)	300 \pm 60	670 \pm 10	650 \pm 90	910 \pm 90	400 \pm 70	-

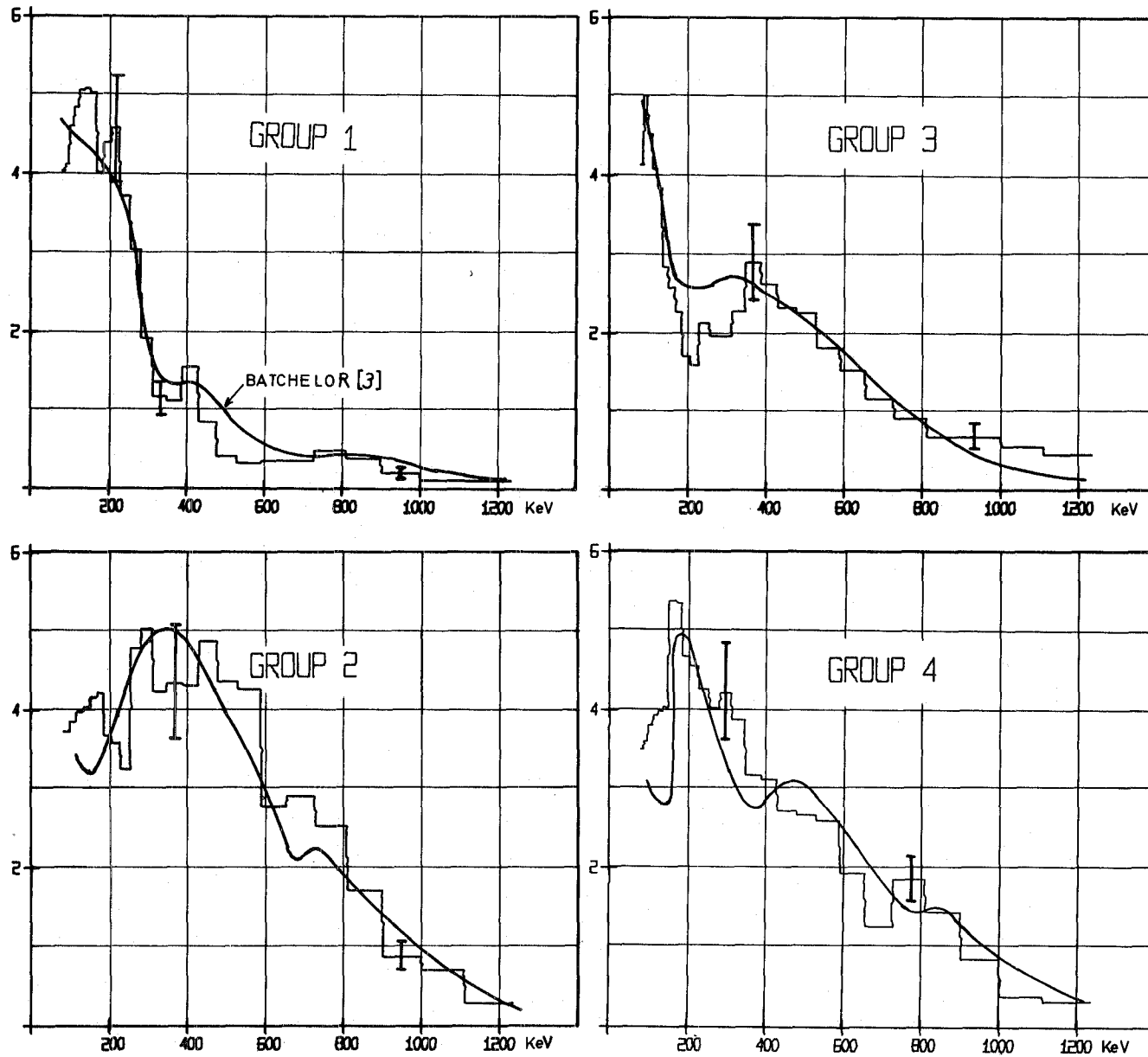


FIG. 5.28 DELAYED NEUTRON SPECTRA FOR U-235 (THERMAL FISSION) (NEUTRON PER ENERGY INTERVAL)

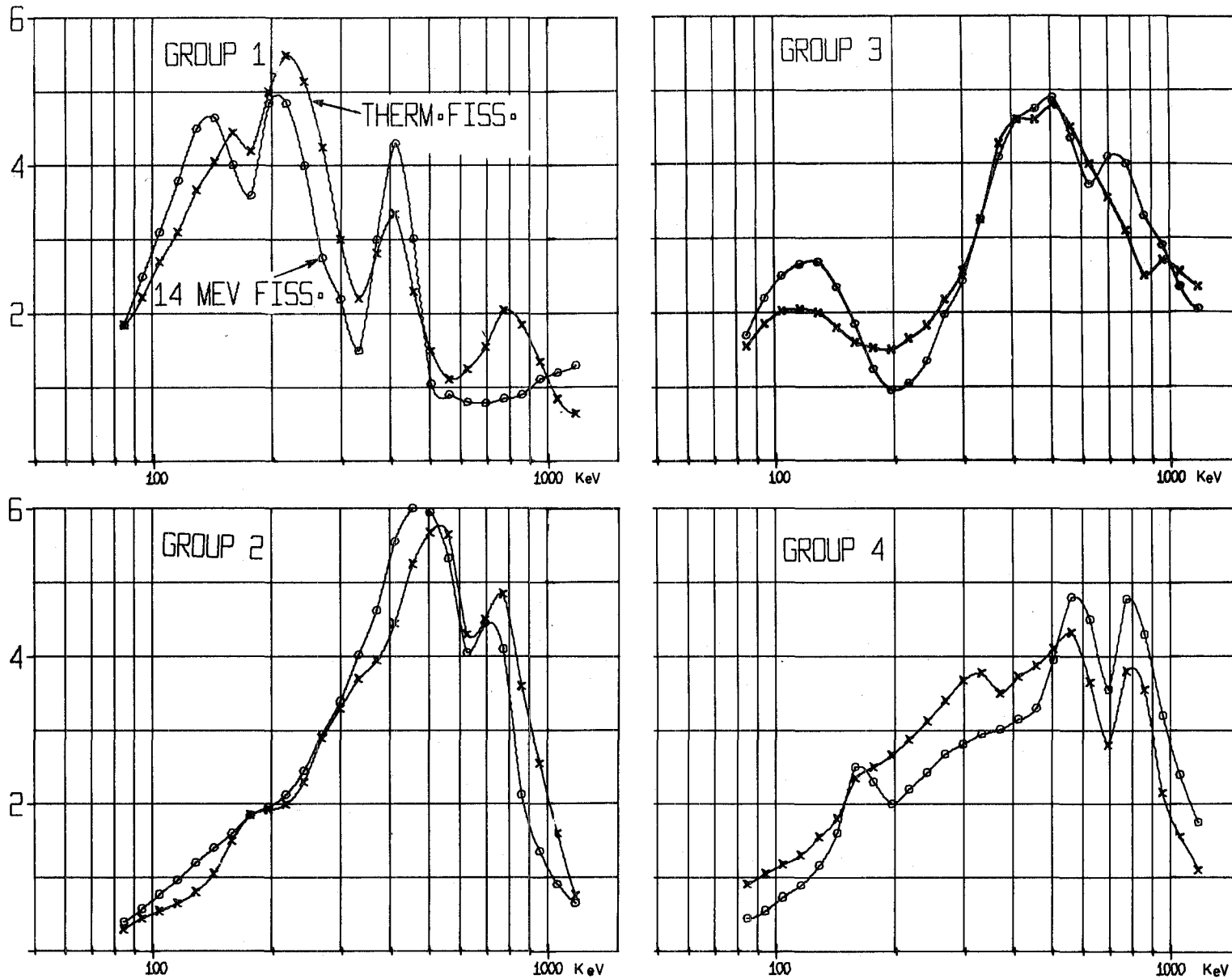


FIG. 5.29 COMPARISON OF DELAYED NEUTRON SPECTRA FOR U 235 AT THERMAL AND 14 MeV FISSION (NEUTRON PER LETHARGY INTERVAL)

5.11 Typical deviations for predicted physics parameters
in integral experiments, status 1972

As a conclusion to chapter 5, here we summarize the 1972 state of prediction of physics quantities for fast zero power facilities. With the improved calculational and experimental techniques, described in chapters 3 and 4, typical deviations of the predicted most interesting physical parameters from experiment, as given in Table 5.21, are obtained.

Table 5.21 Typical deviations for predicted physics parameters in integral experiments, status 1972.

k_{eff} (fresh core)	Peak to average power	Breeding ratio	Material worth		Control rod worth	Doppler coeff.	Na void coeff.
			heavy nuclei	medium nuclei			
$\pm 1\%$	2 - 3 %	5-10 %	5-10%	10-25%	5% (Bor) 10-15% (Follower)	10 %	10-20%

By comparing Table 5.21 with Table 2.1, which represents the status in 1969, the progress obtained in the past three years is clearly demonstrated. It should be noted that this Table 5.21 can not be compared directly with the target numbers in Table 1.1 of section 1.7.

The to Table 1.1 corresponding table will be evaluated in the following chapter 6.

References for Chapter 5

- /5.1/ E. Kiefhaber, D. Thiem KFK 1561 (März 1972)
- /5.2/ F. Helm et.al., KFK 1399, (June 1971)
- /5.3/ P. Hammer, F. Plum, CEA-N-1561, KFK 1581 (September 1972)
- /5.4/ G. Jourdan, F. Plum, H. Reichel, KFK 1612 (June 1972)
- /5.5/ J. Quenon et.al. Belgonucleaire, Internal Report (March 1969)
- /5.6/ M. Billaux et.al. BNES Conference, London (June 1969), paper 2.4
- /5.7/ M. Billaux, Belgonucleaire, Internal Report (January 1970)
- /5.8/ H. Gebhardt, Interatom, Internal Report
- /5.9/ S. Pilate, F. Plum, KFK 1633 (July 1972)
- /5.10/ A. Meyer-Heine et.al. BNES Conference, London (June 1969), paper 1.2
- /5.11/ P. Hammer, CEN de Cadarache, private communication, (1971)
- /5.12/ R. Keepin, The Physics of Nuclear Kinetics, Addison Wesley, New York (1965)
- /5.13/ S. Pilate et.al. Reaktortagung 1972, Hamburg, paper 127
- /5.14/ H. Huschke, KFK-770, (1968)
- /5.15/ E. Kiefhaber and J.J. Schmidt, KFK-969, (1970)
- /5.16/ P. Greebler et.al. "SEFOR Experimental Results and Application to LMFBR's" Intern. Conf. on Eng. of Fast Reactors for Safe and Reliable Operation, Karlsruhe, (Oct. 1972)

- /5.17/ G. Jourdan et.al., KFK-Report, SNEAK 9B, to be published
- /5.18/ A.E. Evans, M.M. Thorpe, M.S. Krick, Revised LASL Delayed Neutron Data, to be published
- /5.19/ K. Hornyik, KFK-799 (1968)
- /5.20/ D. Wintzer, KFK-743 (1969)
- /5.21/ TDC Interatom, Internal Report
- /5.22/ H. Werle et.al., Reaktortagung 1971, Bonn, Compacts p. 58 (1971)
- /5.23/ G. Jourdan et.al., KFK-1612 (1972)
- /5.24/ W. Bickel et.al., KFK-1271/3, p. 121-25 (1971)
- /5.25/ C. Günther and W. Kinnebrock, KFK-1381 (1971)
- /5.26/ C. Günther and W. Kinnebrock, unpublished
- /5.27/ Pitterle, Proc. Second Int. Conf. on Nucl. Data for Reactors, Vol. II, p. 687, IAEA (1970)
- /5.28/ J.G. Panitkin et.al., Proc. Second Int. Conf. on Nucl. Data for Reactors, Vol. II, p. 57 (1970)
- /5.29/ M.P. Fricke et.al., Proc. Second Int. Conf. on Nucl. Data for Reactors, Vol. II, p. 265 (1970)
- /5.30/ E. Kiefhaber, KFK 1572 (1972)
- /5.31/ D. Rusch and E. Wattecamps, KFK-1271/4, p. 121-3 (1971)
- /5.32/ D. Sanitz et.al., to be published

- /5.33/ J.J. Schmidt, KFK-120 (1968)
- /5.34/ Lalovic, private communication
- /5.35/ C.G. Chezem, Nucl. Sci. Eng. 8 (1960) 652
- /5.36/ J.L. Campan et.al., Report CEA No. 1997 (1961)
- /5.37/ E. Kiefhaber, private communication
- /5.38/ H. Meister, KFK-1271/3 (1971)
- /5.39/ J. Grundl, Nucl. Sci. Eng. 31 (1968) 191
- /5.40/ A.B. Smith, IAEA Consultants Meeting on the Status of Prompt Fission Neutron Spectra, Vienna (1971)
- /5.41/ E. Kiefhaber and D. Thiem, KFK-1561 (1972)
- /5.42/ H. Werle and H. Bluhm, J. Nucl. Energy 26 (1972) 165
- /5.43/ P.W. Benjamin et.al., AWRE Report NR 2/64 (1964)
- /5.44/ E.F. Bennett, Nucl. Sci. Eng. 27 (1967) 16
- /5.45/ R. Batchelor and H.R. Mck. Hyder, J. Nucl. Energy **3** (1956) 7
- /5.46/ M. Burgy et.al., Phys. Rev. 70 (1946) 104

6. RESULTS OBTAINED IN ZERO POWER FACILITIES AND THEIR
EXTRAPOLATION FOR USE IN FAST POWER REACTORS

The physics parameters of the Fast Breeder Prototype SNR-300 will be determined making extensive use of measurements carried out in the fast critical facility SNEAK. Supplementary information from the Dutch facility STEK is also available. These experiments were performed because the status of prediction on the basis of basic nuclear data and computer codes were not satisfactory, and could certainly not be used with confidence for a prototype design. However, for several reasons the experimental set up in SNEAK was different from the structure of the SNR. The main, and most severe differences are a) use of zoned techniques in SNEAK because of the limited Pu inventory, b) different isotopic composition of the Pu used in SNEAK, and c) different heterogeneity. Thus, the task to be accomplished by theory and calculation is the extrapolation of SNEAK results to the SNR, and also an assessment of the accuracy of the prediction based on this procedure. In Table 6.1 the important critical experiments for SNR-300 are listed. The SNEAK-assemblies 2C and 6A were planned as common experiments in collaboration with the MASURCA group at the French research center Cadarache. These assemblies contained about 100 kg of Pu from MASURCA, in addition to about 200 kg Pu from SNEAK.

The last column in the Table 6.1 lists the parameters of SNR-300 which are predicted on the basis of experiments, the second last column lists the corresponding measurements. Some of these measurements were described in more detail in earlier sections of this report. Most of this information refers to the initial loading of SNR only. The prediction of the burn-up behaviour has to rely mainly on calculations with basic nuclear data, and can be done only with a rather large uncertainty.

Table 6.1 Critical Experiments for SNR-300

Assembly	Short description	Measurements to be used for SNR-300	Parameters of SNR-300
SNEAK-2A	^{235}U fueled reference core	critical mass of the reference core	critical mass
SNEAK-2B	2 enrichment zones Pu-fueled sector substituted into 2A	sector substitution experiment	
SNEAK-2C	Buffer with MASURCA-Pu in 2B	radial reaction rate traverses, control rod worth (central and off-center)	radial power profile control rod worth (central and off-center)
SNEAK-6A	Pu-fueled central zone Pu (MASURCA) fueled buffer zone ^{235}U -fueled driver zone	axial reaction rate traverses, control rod worth with ^{10}B and Ta, small zone (17 liters) with high ^{240}Pu (22.4%)	axial power traverses control rod worth (use ^{10}B , not Ta), corrections for high ^{240}Pu
SNEAK-9B	Pu-fueled central zone ^{235}U -fueled driver zone	spectral indices, especially σ_{c8}/σ_{f9} axial reaction rate traverses	breeding ratio
		large Na-void configurations (up to 200 l)	maximum Na-void reactivity
STEK-Assemblies (1000, 2000, 3000, 4000)	central $^{235}\text{U}/\text{C}$ zone (different fast spectra) thermal driver zone	reactivity worth of fission product samples	fission product reactivity

The most important aspect of progress in fast reactor physics is the reduction of uncertainty for predicted integral parameters that are related to the economy and safety of fast reactors under consideration. The considerations of this chapter concentrate on estimated uncertainties for the SNR-300.

It is not always clear which technique should be used for the transfer of past experience (gained predominantly, but not exclusively by analysis of experiments in zero power assemblies) to predictions. A major channel for the flow of information is certainly the modification of cross section sets with the aim of improving the agreement between measured and calculated integral parameters for a wide class of benchmark type assemblies. The KFKINR cross section set is expected to contain more of this general experience than our older sets did (compare section 5.1).

A second and additional technique which often is used, is the normalization of predictions by E/C (experiment over calculation) ratios obtained in similar reactor configurations (physical or engineering mock-ups). The confidence level of the predictions is then limited by uncertainties due to:

- a) possible experimental errors and limited interpretability of experiments
- b) uncertainties in the extrapolation of mock-up results to the specific plant under consideration, which must rely on calculations.

The normalization technique is justified if the combination of these uncertainties is lower than the uncertainty estimated for the case without normalization. It should be pointed out that this is not always the case. One of the reasons is that unisotropic diffusion properties of plate or thick rod lattices in zero power assemblies are usually more pronounced than in a demonstration plant. Thus, corresponding methodical deficiencies may introduce larger uncer-

tainties if the normalization technique is used (interpretation of experiments is difficult), than they would do in the case of direct calculations for the demonstration plant.

We also have to consider that we know from analysis of quite a few assemblies that possible and to some degree probable errors in specific cross sections (see Table 6.2) and calculational methods tend to compensate each other for certain integral parameters like criticality. However, we do not know which ones do so. It is for this reason, that we think we should not be more optimistic in estimating uncertainties due to extrapolation of specific differences between a SNEAK-assembly and the SNR than the numbers of Table 6.2 imply.

Table 6.2 summarizes estimated uncertainties for integral parameters of some important materials if they are calculated with the KFKINR set. The numbers are to be understood for a confidence level of about 90%. All uncertainty considerations of this section refer to this confidence level. The estimates are not free from personal judgement. It was tried to base them on

- differences between recent differential cross section measurements
- estimated possible errors of the calculated neutron spectrum
- experience by direct and indirect measurements in SNEAK and other zero power assemblies.

Most of the uncertainty estimates described in the subsequent sections use the uncertainties listed in Table 6.2 as a common basis.

Table 6.2

Estimated Uncertainties for Material Specific Integral Parameters ⁺⁾

Material	Relative Uncertainty (%)		
	ν	σ_f/σ_{f9}	σ_c/σ_{f9}
^{239}Pu	1.7	-	20
^{240}Pu	1.7	20	30
^{241}Pu	1.7	20	35
^{238}U	1.7	10	12
SS, Na	-	-	35
Fission Products	-	-	40

⁺⁾ Estimated for calculated values based on the KFKINR cross section set.

6.1 CRITICALITY

The specification of the initial fuel enrichment for the prototype reactor requires criticality calculations for the cold and fresh core and for the reactor at full power and nominal burn-up before reloading.

Correction factors for these calculations are presently based on the analysis of SNEAK-2 experiments including successive substitution of uranium by plutonium.

The estimated uncertainty of criticality predictions for the SNR at full power and nominal burn-up is presently 1.8 percent in k_{eff} (with a confidence level of about 90%). Contributions to the uncertainty of different sources of error are listed in Table 6.3 and will shortly be discussed below:

Experimental uncertainties in SNEAK are mainly due to possible errors in the extrapolation of plutonium zone experiments to a fictitious full plutonium core and to possible errors in the actual composition of the assembly. Careful analyses of plutonium sector substitution experiments in SNEAK-2B have considerably reduced the uncertainty due to the limited amount of ^{239}Pu available for SNEAK. Essential reductions of these uncertainties are not expected for the next few years.

Possible errors due to a different plutonium vector in the SNR are expected to be reduced by the present series of SNEAK-9 experiments which includes zone experiments with a sufficiently high percentage of ^{240}Pu and ^{241}Pu . A certain reduction of the uncertainties was already achieved by some experiments in SNEAK-6A.

Other differences in material densities between the SNEAK-assemblies listed in Table 6.3 and the SNR (^{239}Pu density in the Pu zones, ^{238}U and steel densities) cause additional uncertainties. Past and future reduction of these uncertainties was and will be achieved by material weight measurements and supporting reaction ratio measurements.

Possible extrapolation errors due to methodical errors of the neutronics calculations still lead to a major contribution (+0.8% in k_{eff}) to criticality prediction uncertainties. Included are estimated uncertainties in the extrapolation of transport corrections, heterogeneity and streaming effects, REMO-corrections, resonance shielding effects near boundaries and errors due to the use of simplified geometrical reactor models. A major partial contribution is due to difficulties in the calculation of streaming effects in control rod followers. A significant reduction of this contribution is expected from absorber rod and sodium follower experiments in SNEAK-9A.

Table 6.3 Estimated Uncertainties for Criticality Predictions

Source of Uncertainty	Relative Uncertainty ¹⁾ (%)		
	1970	1972	1974 ²⁾
1) Experimental conditions in SNEAK	0.5	0.4	0.3
2) Errors due to uncertainties of extrapolation			
Different Pu vector	1.0	0.7	0.4
Different other material densities	0.7	0.5	0.4
Methodical errors of extrapolation	1.0	0.8	0.5
Subtotal 1) and 2) ⁴⁾	1.6	1.2	0.8
3) Uncertainties due to power and burn-up			
Temperature effects	0.6	0.4	0.3
Burn-up reactivity effects ³⁾	0.9	0.7	0.4
Swelling and bowing effects ³⁾	0.3	0.2	0.2
4) Fissile Mass Uncertainty	0.8	0.8	0.8
Total Uncertainty ⁴⁾	2.2	1.8	1.3
Comments: <ul style="list-style-type: none"> 1) Confidence level =90% 2) Target values 3) For 4 months operation at full power 4) Geometrical combination of uncertainties 			

The uncertainty in the prediction of temperature reactivity effects was reduced during the last two years mainly by the SEFOR Doppler experiments and their analysis. Uncertainties in the geometrical consequences of local thermal expansion under burn-up conditions are now the dominant ones. Little progress is expected during the next two years.

Uncertainties of burn-up reactivity effects were reduced during the last two years by the international progress of knowledge about the ^{239}Pu capture to fission ratio (it is related to the loss of ^{239}Pu during burn-up) and to increased confidence for ^{238}U capture rate prediction that was gained by σ_{c8}/σ_{f9} measurements in the SNEAK assemblies listed in Table 6.1. The present burn-up reactivity uncertainty is about 25% of the calculated reactivity loss. The expected reduction to about 15% in 1974 can be achieved by:

- application of correction factors to burn-up calculations for σ_{c8}/σ_{f9} and for the reactivity worth of ^{239}Pu which are based on past and future SNEAK measurements, and
- transfer of fission product reactivity experience from analysis of the related STEK experiments.

The fissile mass uncertainty is governed by specifications for manufacturing and can scarcely be reduced.

Reactivity losses due to swelling effects during burn-up are governed by the rather uncertain swelling of structural materials for fast neutron doses beyond the range of direct experience. No essential progress is expected in this respect during the next few years. Some progress, however can be expected for the relation between specified hypothetical local swelling and creeping conditions on one hand and consequences for geometry and density distribution for core and blankets on the other hand.

The geometrical combination of individual contributions to the total uncertainty is not completely justified since some of the possible

errors are correlated to a certain degree. Correlations are considered to be negligible except of those between possible burn-up errors and extrapolation errors due to different uranium and plutonium densities. However there are correlations and countercorrelations of similar importance so that the strictly geometrical combination still is expected to lead to about the same level of confidence ($\approx 90\%$) for the total uncertainty.

The subtotals of 1) and 2) in Table 6.3 were listed separately because these numbers are relevant if one asks for the advantage of the extrapolation procedure from a specific SNEAK-assembly (e.g. assembly 2B) over direct criticality calculations for the SNR. Uncertainty estimates for direct calculations can be based on the analysis of section 5.1: Typical deviations between criticality calculations and experiments are about $1\% \Delta k/k$ or less for a wide range of fast assemblies and about $2\% \Delta k/k$ for two rather exotic assemblies. This implies a 90% confidence uncertainty of about $1.5\% \Delta k/k$ for the direct criticality calculation of the SNR. Comparable numbers of Table 6.3 are 1.2% (presently) and 0.8% (as achievable target for 1974) for the cold and fresh SNR. The conclusion is that we have some more confidence in predictions that are based on normalization to SNEAK-2B results than on direct calculations.

6.2 REACTIVITY WORTH OF ABSORBER RODS

Increased confidence in ^{10}B control rod worth calculations was gained by the analysis of ^{10}B worth measurements in SNEAK-2C and SNEAK-6A. A rather consistent overestimation of 5 to 10 per cent was found for MOXTOT calculations (compare chapter 5.5), which justifies the normalization of SNR predictions for control rod worths.

^{10}B reactivity worth measurements planned for SNEAK-9A are aiming specifically at mutual shielding effects between several absorber

rods and at reactivity effects of dominantly sodium containing absorber rod followers.

Table 6.4 summarizes uncertainty estimates for 1970 and 1972 and target values for 1974. Some comments on specific contributions are given below.

Table 6.4 Estimated Uncertainties for ^{10}B Absorber Rod Worths

Source of Uncertainty	Relative Uncertainty ^{+) (%)}		
	1970	1972	1974
Experimental uncertainties	9	7	4.5
Uncertainties due to extrapolation			
Delayed neutron fraction	8	7	4
Different reactor composition	10	6	4
Mutual influence of rods	8	5	3
Methods of calculation	5	3	2
Actual rod content	1	1	1
Combination of all	18	13	8
+) Confidence level is =90%			

Experimental uncertainties are caused by possible errors of the reactivity measurements including errors in the delayed neutron parameters for the inhour equation. Included are interpretation difficulties due to specific features of the experiments such as flux and adjoint tilting in the sector experiments.

Contributions from uncertainties of the delayed neutron fraction are predicted to decrease after confirmation of recent β_{eff} measurements for ^{238}U and ^{239}Pu .

Progress concerning calculational methods since 1970 is essentially due to checks of the KASY program (compare section 5.5) with experiments and 3 dimensional diffusion calculations. Further improvements are expected both by analysis of absorber rod worth measurements in the SNEAK-9 assemblies and by theoretical investigation of transport and rod heterogeneity corrections for ^{10}B rod reactivity worths.

6.3 POWER DISTRIBUTION

The importance of the maximum to average power density ratio for reactor economy is well known. Estimated uncertainties of this ratio for the SNR-300 are shown in Table 6.5.

The main experimental uncertainties are caused by possible foil positioning errors in the case of fission rate traverse measurements with foils and by streaming effects in the case of fission chamber measurements. Progress since 1970 is mainly due to refinements of the foil technique (see section 4.1).

Uncertainties caused by calculational methods include interpretation difficulties for measurements in the plate lattices of SNEAK (fine structure and lattice streaming) and probable errors in the resonance shielding treatment near boundaries.

Uncertainties due to burn-up effects are essentially uncertainties in the time dependence of local concentrations of plutonium isotopes. It is expected that these uncertainties can be reduced by future reaction rate and material worth measurements parallel to the reduction of burn-up reactivity uncertainty.

There is not yet much experimental experience concerning the predictability of control rod influence on power distribution. Specific measurements in SNEAK-9A and a careful analysis of these experiments will hopefully improve the confidence in power distribution predictions in the case of partially inserted control rods.

Table 6.5 **Estimated Uncertainties for the Maximum to Average Power Density Ratio of the SNR Core**

Source of Uncertainty	Relative Uncertainty ¹⁾ (%)		
	1970	1972	1972 ²⁾
Possible experimental errors in SNEAK	1.5	1.0	0.8
Methods of calculation	2.5	1.0	0.8
Burn-up effects	3.5	3.0	2.0
Control rod influence	4.0	3.0	1.0
Gamma energy contribution	1.5	1.0	0.8
Combined uncertainty ³⁾	6.2	4.5	2.6
<p>Comments: 1) Confidence level ≈90%</p> <p> 2) Target values</p> <p> 3) Geometrical combination of uncertainties</p>			

6.4 BREEDING RATIO

Estimations yield a relative uncertainty of ±10% (confidence level ≈90%) for the breeding ratio of the SNR as calculated with the KFKINR cross section set. The dominant sources of error are:

- The ratio capture rate of ^{238}U over fission rate of ^{239}Pu in the core
- The number of neutrons per fission leaking into the axial and radial blanket (about 70% of them are captured by ^{238}U)
- Competing absorption in the blanket by steel and sodium and neutron leakage out of the blanket

- ^{239}Pu capture to fission ratio in the core.

A slight reduction of the uncertainty is presently possible by adjusting the calculated σ_{c8}/σ_{f9} ratio by E/C ratios of recent measurements in SNEAK. More progress in this direction is expected for the next two years by further measurements and by reduction of calibration uncertainties for σ_{c8}/σ_{f9} measurements. Progress is also expected by reduction of the uncertainty for the ^{239}Pu capture to fission ratio by further analysis of relevant experiments and by increased information for neutron leakage out of the blanket.

A target value of about $\pm 6\%$ for the combined uncertainty of the breeding ratio seems to be achievable by 1974.

6.5 POWER AND ENERGY COEFFICIENTS

Power and energy reactivity coefficients of the SNR are governed by the Doppler effect. The analysis of the SEFOR Doppler measurements has greatly improved the confidence in power and energy coefficient calculations for $^{239}\text{Pu} - ^{238}\text{U}$ mixed oxide fueled fast reactors. Possible errors of the thermal conductivity and heat capacity of the fuel in SEFOR are highly correlated to those of the SNR. The present relative uncertainty for predictions of both power and energy coefficients for the SNR is about $\pm 20\%$ if the calculations are normalized by SEFOR Doppler E/C ratios. No essential further progress is expected for the next two years.

6.6 SODIUM VOID REACTIVITY

The maximum sodium void reactivity is an important parameter for safety considerations. Accurate prediction is difficult because of the high degree of compensation of positive and negative partial effects. The best way to transfer experience from related SNEAK measurements to the SNR is presently the derivation of nor-

malization factors both for the positive reactivity component (by analysis of central Na worth measurements) and for the negative component due to increased leakage (by analysis of large zone void experiments). Unfortunately, a certain relative uncertainty in the positive component causes a relative uncertainty of the net value of the maximum void reactivity which is almost twice that much. An additional difficulty for the interpretation of void experiments in SNEAK is the anisotropic change of the neutron diffusion coefficient caused by removal of sodium from the plate lattice.

Different groups of physicists estimate different uncertainties for a 90% confidence level which vary between 20% and 30% for 1972 and between 15% and 20% for a realistic target for 1974.

Some of the experiments of the SNEAK-9 series are specifically aiming at the reduction of the present uncertainties.

7. GENERAL CONCLUSIONS

In this concluding chapter we summarize the progress in fast reactor Physics, made in Germany in the past three years, and its present 1972 status.

We start by comparing the corresponding results of the analysis of physics parameters in integral experiments, obtained in 1969 and in 1972. This is done in Table 7.1.

Table 7.1 Typical deviations for predicted physics quantities in integral experiments, status 1969 and 1972.

Quantity	Status 1969	Status 1972
k_{eff} (fresh core)	$\pm 2 \%$	$\pm 1 \%$
Peak to average power	5 %	2 - 3 %
Breeding ratio	10 %	5 - 10 %
Material worth	30 %	5 - 10 % (heavy nuclei) 10 - 20 % (medium nuclei)
Control rod worth	20 - 30 %	5 % (Bor) 10 - 15 % (Follower)
Doppler coeff.	15 %	10 %
Na-void coeff.	50 %	10 - 20 %

The progress obtained in last years, is evident. This success is based on the following facts:

1. A thorough investigation of calibration techniques and a comparison of various methods in measuring reaction rates and neutron spectra (4.1.2., 4.1.6., 4.2.4) has resulted in a much improved confidence in

experimental results. In addition, by a close cooperation between experimentalists and theoreticians most of the involved persons were aware of the various aspects and also difficulties connected with both the experimental performance and the theoretical analysis. Especially mentioned should be the integral measurements related to the problem of reactivity scale (5.4.1), which helped to bring some clarification especially in material worth measurements.

2. The current improvement in nuclear data and related group constant sets lead to the preparation of the KFKINR set (3.1.4). The merits of this set can best be expressed by the success that also those assemblies could be analyzed sufficiently accurate, which were built after the release of KFKINR set. Thus the strategy to consider differential nuclear data measurements and integral measurements as equally important, was made successful by the cooperating reactor physicists and nuclear data evaluators.
3. From the development of improved theoretical tools, the most important progress in the analysis of the heterogeneous fast zero power facilities was achieved by establishing the heterogeneity code KAPER (3.4.1). This code is thought to provide the relevant basis for the interpretation of measurements in fast assemblies. The successful application of the three dimensional synthesis code KASY (3.3.3) for the analysis of systems containing partially inserted and off center control rods, is also a big step forward. Finally, the current use of fine group calculations in zero and one dimensional geometry (3.1.3, also 5.8) has resolved many questions connected with coarse group calculations.

Only part of the aspects of fast reactor physics can be checked in critical facilities. From the problems related to the description of the time dependent reactor behaviour, the progress made in studying group collapsing schemes and the application of energy synthesis in reactor transient investigations (3.6.3) is worthwhile to be mentioned here. Large computer code systems for the analysis of severe accidents (3.6.1, 3.6.2) are well under way.

Having summarized the progress in fast reactor physics in Germany, it is necessary to consider the final question, whether with this progress the target accuracies for the physics parameters of a prototype reactor (chapter 1) are met already. Therefore in Table 7.2 the target accuracies are compared with the estimated uncertainties for the prediction of physics quantities, based on the experience in zero power facilities (chapter 6). All the numbers in Table 7.2 have a confidence level of about 90 %.

Table 7.2 Comparison of target accuracies and estimated uncertainties for the prediction of physics parameters of a prototype reactor.

Quantity	Target accuracy	Uncertainty 1969/70	Uncertainty 1972	Expected Uncertainty 1974
k_{eff} (end of life)	1.5 %	2.2 %	1.8 %	1.3 %
Peak to average power	3 - 5 %	6 %	4.5 %	2.6 %
Breeding ratio	5 - 10 %		10 %	6 %
Control rod worth	10 %	18 %	10 - 13 %	8 %
Doppler coefficient	10 - 20 %		20 %	20 %
Na-void coefficient	15 - 20 %		20 - 30 %	15 - 20 %

It is obvious that the numbers in Table 7.2 are not free from personal judgement and indeed different persons may evaluate other numbers. From this table it can be concluded that many targets are already met. An outstanding feature is the not satisfactorily solved problem of sodium

void reactivity. The difficulty is caused by the fact that the Na-void effect consists of partly compensating positive and negative contributions. Such it is influenced by many facts, as data uncertainties, methods and the presence of higher plutonium isotopes and control rods.

The expected uncertainties for 1974 in the last column are mainly based on the further analysis of experiments in SNEAK.

As a concluding remark, it should be noted that the required targets and the estimated uncertainties are related to a fast prototype reactor as SNR 300. They thus cannot be applied for large fast power plants as part of an entire reactor generation. An evaluation of the corresponding numbers has not yet been made.